DEVELOPMENT OF CARDIAC TROPONIN-T (cTnT) APTASENSORS FOR POINT-OF-CARE DIAGNOSIS OF MYOCARDIAL INFARCTION

by

Vinay B

Roll no. 156106040

A THESIS

Submitted in Fulfilment of the

Requirements for the Award of the Degree of

DOCTOR OF PHILOSOPHY

at the

Indian Institute of Technology Guwahati

Department of Biosciences and Bioengineering

Indian Institute of Technology Guwahati

Guwahati – 781039, Assam, India

August 2023

INDIAN INSTITUTE OF TECHNOLOGY GUWAHATI

Department of Biosciences and Bioengineering

Guwahati – 781039

STATEMENT

I do hereby declare that the matter embodied in this thesis entitled "**Development of cardiac troponin-T (cTnT) aptasensors for point-of-care diagnosis of myocardial infarction**" is the result of investigations carried out by me in the Department of Biosciences and Bioengineering, Institute of Technology Guwahati, Assam, India, under the guidance of **Prof. Pranab Goswami.**

In keeping with the general practice of reporting scientific observations, due acknowledgements have been made wherever the work described is based on the findings of other investigators.

August 2023

Vinay B

INDIAN INSTITUTE OF TECHNOLOGY GUWAHATI

Department of Biosciences and Bioengineering

Guwahati – 781039

CERTIFICATE

It is certified that the work described in this thesis, entitled "**Development of cardiac troponin-T (cTnT) aptasensors for point-of-care diagnosis of myocardial infarction**", done by Mr. **Vinay B** (Roll No. 156106040) for the award of degree of Doctor of Philosophy is an authentic record of the results obtained from the research work carried out under my supervision in the Department of Biosciences and Bioengineering, Indian Institute of Technology Guwahati, India.

The results embodied in this thesis have not been submitted to any other University or Institute for the award of any degree.

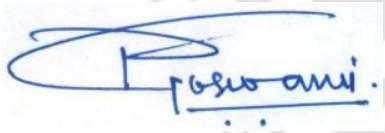

Prof. Pranab Goswami

(Thesis Supervisor)

Acknowledgments

I take this opportunity with much pleasure to express my sincere gratitude to all those who have supported me through the course of my journey towards producing this thesis. First, I am thankful to Indian Institute of Technology Guwahati for giving me the opportunity to carry out Ph.D. in this esteemed Institute. I would like to extend my deepest gratitude towards my thesis supervisor ***Prof. Pranab Goswami*** *for mentoring me to throughout this PhD journey and teaching me perseverance and patience in research work. His constant encouragement, time, ideas, and the freedom to do research work has helped me to propel my work in a fruitful direction. I would also like to thank him for the well-equipped laboratory, vast resources and dedicated work culture that has made working in his laboratory a pleasant experience. His optimism and down to earth and helpful nature make him one of the best teachers in my life.*

I am thankful to my doctoral committee members, members ***Associate Prof. Biplab Bose****,* ***Prof. Bithiah Grace Jaganathan,*** *and* ***Prof. Anil Kumar Saikia*** *for critically evaluating my research work and for their valuable suggestions which helped me produce better research work.*

I would like to thank CIF for FESEM, Laser Raman, ITC, BSBE, COE for providing the access to various instruments without which this study would not be feasible.

Special thanks to my past and present lab members, ***Babina, Priyamvada, Ankana , Lightson, Priyanki, Sharbani, Naveen, Santhosh, Abdul, Arup, Smita, Malaya, Nabajyoti, Rupinder, Rafiqul, Mrinal, Kangkana and Abhishek*** *who have shared their struggles and supported me in all my endeavours. A special thanks to my M. Tech juniors* ***Lekhashree*** *and* ***Khadija*** *and B. Tech juniors* ***Ayush, Lazmy, Jai Sardar*** *who helped me in my research work.*

I also express my profound debt to my family members, especially my late ***father*** *and* ***my mother*** *as well as my brother and all my other family members for their unconditional love, encouragement, sacrifices, and faith in my capabilities to fulfil this journey.*

Vinay B

Table of Contents

Abstract i

List of Abbreviations v

List of Symbols viii

List of Figures xi

List of Tables xvii

List of Scheme xviii

Introduction 1

Chapter 1: Review of Literature 5

1.1 Cardiovascular diseases 6

1.2 Myocardial Infarction 7

1.3 Clinical Diagnosis of MI 9

1.4 Cardiac biomarkers for MI 10

1.4.1 Cardiac Troponin 11

1.4.2 Biological function of cardiac troponin 12

1.4.3 Structure of cardiac troponin complex 13

1.4.4 Release kinetics of cTnT 17

1.5 Detection of cTnT 18

1.5.1 Analytical techniques for detection of cTnT 18

1.5.2 Biosensors and kits for MI 19

1.5.3 Electrochemical cTnT biosensors 20

1.5.4 Optical cTnT biosensors 22

1.5.4.1 Fluorescent biosensors 23

Table of Contents

1.5.4.2 Colorimetric Biosensors **24**

1.6 Aptamers as biorecognition element **26**

1.6.1. General process of SELEX **30**

1.6.2 Aptamer-target interaction studies **31**

1.6.3 Aptamer for cTnT detection **32**

1.7 Paper based biosensing platforms **34**

1.8 Significant gaps in research **36**

1.9 Objectives of the study **37**

Chapter 2: Generation of an aptamer Database "Aptabase" **40**

2.1 Overview **41**

2.2 Experimental procedures **43**

2.2.1 Data acquisition **43**

2.2.2 Data conversion **44**

2.2.3 Aptabase construction **45**

2.2.4 Website construction **45**

2.2.5 Plugins **47**

2.3 Results and discussion **50**

2.3.1 Data collection and data formatting **50**

2.3.2 Database Analysis **51**

2.4 Conclusion **56**

Chapter 3: An Ensemble insilico 3D Modelling of ssDNA aptamers **57**

3.1 Introduction **58**

3.2 Methodology **60**

3.2.1. Generation of 3D aptamer structure **60**

3.2.2. Web server for generation of 2D structure **61**

3.2.3. Web server for generation of 3D RNA structure **63**

3.2.4. VMD Plugins for 3D RNA to 3D DNA conversion **63**

3.3 Results and discussion **64**

3.3.1 Secondary structure generation and analysis **65**

3.3.2 Convertion of ssDNA secondary structure into 3D RNA structure **66**

3.3.3 3D RNA structures into 3D DNA structures **68**

3.4 Conclusion **73**

Chapter 4: Cloning , Expression, Purification and Charecterization of cTnT and sTnT **75**

4.1 Overview **76**

4.2 Experimental procedures **76**

4.2.1 Materials **76**

4.2.2 Bacterial cell culture **77**

4.2.3 Quantification of DNA **77**

4.2.4 Protein estimation **77**

4.2.5 Plasmid DNA isolation **78**

4.2.6 Agarose gel electrophoresis **78**

4.2.7 Polymerase chain reaction **79**

4.2.8 Restriction digestion of *cTnT, sTnT* **80**

4.2.9 Ligation of cTnT, sTnT into pGEMT easy vectors and pET-28a (+) vectors **80**

4.2.10 Competent cell preparation **81**

4.2.11 Transformation of competent cells **81**

4.2.12 Cloning of *cTnT, sTnT* **81**

Table of Contents

4.2.13 Expression of His-tagged cTnT, sTnT in *E. coli* BL21 (DE3) **82**

4.2.14 Purification of His tagged troponins **82**

4.2.15 Sodium dodecyl sulphate polyacrylamide gel electrophoresis **83**

4.2.16 Western Blot **83**

4.2.17 Circular dichroism study **84**

4.2.18 Matrix- assisted laser desorption ionization- mass spectroscopy **84**

4.2.19 Determination of Isoelectric point **84**

4.3 Results and discussion **85**

4.3.1 Cloning and expression of human cardiac troponin T, and slow skeletal troponin T **85**

4.3.2 Expression and purification of cTnT, sTnT **87**

4.3.3 Charecterization of the recombinant cTnT and sTnT **88**

4.4 Conclusion **89**

Chapter 5: Development of aptamers Specific for cTnT and its characterization **91**

5.1 Overview **92**

5.2 Experimental procedure **93**

5.2.1 Materials **93**

5.2.2 Invitro selection of aptamers using c-SELEX **93**

5.2.3 Cloning of enriched aptamer candidates **94**

5.2.4 Prediction of aptamer structure and G- quadraplex mapping **95**

5.2.5 Docking studies and generation of aptamer 3D structures **95**

5.2.6 Determination of dissociation constant (KD) of aptamer- cTnT interaction by CD spectroscopy and Isothermal Titration Calorimetry **95**

5.3 Results and discussion **96**

5.3.1 Development of specific aptamer against cTnT **96**

Table of Contents

5.3.2 Effect of pH and c-SELEX buffer on the aptamer structure **101**

5.3.3 Binding affinity and protein-aptamer interactions **103**

5.4 Conclusion **111**

Chapter 6: Conductive ink-based Electrochemical Paper Platform for cTnT Detection **113**

6.1 Overview **114**

6.2 Experimental Procedure **116**

6.2.1 Materials **116**

6.2.2 Conductive ink formulation **116**

6.2.3 Platform Selection **117**

6.2.4 Electrode design **117**

6.2.5 Screen printing technique optimization **118**

6.2.6 Fabrication of SPE **118**

6.2.7 Electrochemical analysis **119**

6.2.8 Statistical analysis of the data **120**

6.3 Results and discussion **120**

6.3.1 Conductive ink formulation **120**

6.3.2 Platform Selection **124**

6.3.3 Screen printing technique optimization **125**

6.3.4 Response Charecteristic of the aptasensor **126**

6.4 Conclusion **130**

Chapter 7: Electrochemiluminescence-Based LFA Assay for cTnT Detection **132**

7.1 Overview **133**

7.2 Experimental methods **134**

7.2.1 Materials **134**

7.2.2 Docking studies **135**

7.2.3 DC voltage supply device **135**

7.2.4 LFA platform design **135**

7.2.5 Fabrication of LFA **136**

7.2.6 Charecterization of luminol and lumidot **138**

7.2.7 Electrochemical charecterization of luminol and lumidot **138**

7.2.8 Aptamer lumidot linking **138**

7.2.9 Setup for ECL-LFA detection of cTnT **138**

7.2.10 Statistical analysis of data **139**

7.3 Results and discussion **140**

7.3.1 Aptamer selection for ECL-LFA **140**

7.3.2 Dimensional optimization of LFA strip **141**

7.3.3 Chreacterization of luminol and lumidot **142**

7.3.4 Electrochemistry of luminol and lumidot **143**

7.3.5 Detection of cTnT using LFA strips **144**

7.3.6 Quantitative detection of cTnT **144**

7.4 Conclusion **146**

Conclusion and Future directions **148**

Bibliography **152**

Publications in refereed journals **170**

Appendix **173**

Copyright Permissions **179**

Abstract

The main objective of this thesis is the development of aptasensors for cardiac troponin T (cTnT) for the diagnosis of myocardial infarction (MI). The thesis has been divided into six chapters, starting with a brief introduction expressing the motivation behind this work and outlining the work performed to address the primary objective defined for this thesis.

The first chapter described a detailed literature survey on the work, identified the research gaps based on the survey, and then defined the objectives to bridge a few critical gaps through the work described in this thesis.

The second chapter described the development of an aptamer database using 610 aptamer candidates for different targets reported in the literature. The database provides key information on the individual aptamers, including sequence, sequence length, GC%, buffer compositions, targets (general and specific), and target affinity. It has been created with an interactive user interface with options to update it for admin and end users. The front end of the database was designed using HTML, CSS, Bootstrap, and JavaScript. The database's backend or server-side was developed using Apache web server and MySQL database, and the scripting was performed with PHP. The Aptabase also hosts plugins like the GC calculator, which segregates the inserted sequence into its corresponding nucleotides for both ssDNA and ssRNA. The database was also equipped with google analytics to understand website traffic better.

Understanding the 3-D structure of nucleic acid aptamers is important for the rational design of aptamer-based constructs in various applications, including for developing aptasensors. The third chapter described a simple approach for 3D modelling of ssDNA aptamers through an ensemble of web applications. The procedure utilized 30 aptamers whose 3D XRD or NMR experimental structures are available for validation. As a first step, the primary sequences of ssDNA aptamers were transformed into 2D structures using six widely used web applications: RNA fold, Vector builder, RNA Structure, UNA fold, Centroid fold, and IP Knot. The generated 2D structures were then passed through the RNA composer web application to generate 3D RNA structure, which in turn was converted to 3D DNA structures using various Visual Molecular Dynamics plugins that also include conversion of ribose sugar into deoxyribose sugar backbone and uracil to thiamine. The energy-minimized generated 3D structures were matched well with high accuracy to their experimental counterparts. This study identified that the Guanine residues are crucial in the aptamer 3D structure prediction and in algorithms that

generate secondary structures. Further, the GC content (<50%), GC bond percentage (<60%), and G: C ratio (<1.12) act as limiting factors in predicting the 2D structures of aptamers. There were variations in the 2D structure predictions by the web applications, even though all these applications were a combination of the MFE, MEA, and McCaskill functions. Processing these structures through the web applications described above produced best-fit 3D structures with the experimental one, thus offering the present ensemble approach to predict the 3D structure of aptamers for various applications reliably.

The MI biomarker, cTnT, and the control protein for the experiment, smooth skeletal troponin T (sTnT), were cloned, expressed, purified, and finally, characterized through the work described in Chapter 4. The proteins were cloned and expressed into *E.coli* BL21 (DE3) pLysS bacterial cells. Various methods like CD spectroscopy, western blot, MALDI-TOF, and Zeta potential confirmed the structural integrity of the expressed proteins. We expressed these proteins with His-tag to facilitate their purification and immobilization, which is involved in some experiments in the latter chapters of this thesis work.

Chapter 5 describes the selection of ssDNA aptamers against cTnT following a centrifugal SELEX (c-SELEX) process, a variant of the conventional SELEX process. The c-SELEX works principally on centrifugation. The advantages of the c-SELEX over the conventional one are (a) less time consuming, (b) it requires less number of SELEX rounds, (c) the complete protein is exposed for interaction with the aptamer library, thereby increasing the chances of finding the best aptamer candidates, and (d) requirement of less amount of consumable items for the selection process. The cTnT protein purified in Chapter 4 was used as the target for the c-SELEX, whereas sTnT served as the control protein for the negative c-SELEX. Following the process of c-SELEX, we isolated four aptamer candidates, cT12, cT21, cT22, and cT33. The selected aptamers were then characterized for their specificity and binding affinity to the target. The sequences and free energy values determined by circular dichroism (CD) spectroscopy and Isothermal titration calorimetry (ITC) are presented in the table below.

Aptamer name	K_d value ITC	K_d value CD	Sequence (5' - 3')
cT12	14.42±1.5µM	0.4193±0.1561µM	CACCTAATACGACTCACTATAGACTTCGTATGCCAACAGCGAT CCTAGATCGCGCAAGCTTGTTCGAGCCAG
cT21	10.7±0.056µM	0.17±0.2877µM	CACCTAATACGACTCACTATAGACTTCGTATGCCAACAGCGCA CAGGGGACGCGCAAGCTTGTTCGAGCCAG
cT22	49.22±3.33µM	0.5888±0.2884µM	CACCTAATACGACTCACTATAGGCACAGGGGACGCACTTCGT ATGCCAACAGCGCAAGCTTGTTCGAGCCAG
cT33	13.1±21µM	2.6143±0.1091µM	CACCTAATACGACTCACTATAGGCACAGGGGACGCACGGCGT ATGCCAACAGCGCAAGCTTGTTCGAGCCAG

The tertiary structures of the selected aptamers were generated using the ensemble technique proposed earlier, and docking studies were performed as a shred of supporting evidence for the specific interactions between the aptamers and cTnT. The developed aptamers were utilized in two independent yet interlinked approaches for cTnT detection described in chapters 6 and 7, respectively.

Chapter 6 described a conductive ink-based electrochemical paper platform for cTnT detection. In this approach screen printing technique, sensing platform, and conductive ink were optimized for their performance in the integrated sensing platform. The aptamer cT22 was immobilized on the screen-printed electrodes (SPE) by physical adsorption. The electrodes and their performance were characterized by cyclic voltammetry (CV) and electrochemical impedance spectroscopy (EIS). The LOD of the sensor, discerned from the CV experiment, was 280.03 pM, and the linear detection range was 1 nM - 100 nM. Thus the fabricated sensor could detect cTnT within a clinically significant range at a much lower level. Notably, the cTnT level in a healthy individual is < 5 nM, and its physiologically significant range under the ailing condition is 5 nM to 10 µM.

Chapter 7 described electrochemiluminescence-based lateral flow assay (LFA) for cTnT. There has been a continuous strive to develop highly sensitive and low-cost detection systems for MI to meet the demand for effective screening of patients in developing countries where the cases are predominant. In the current chapter, a modified LFA platform was devised. The screen printing technique of the electrodes was adopted from the previous work where a paper-based electrochemical platform was generated. Lumidot (CdSe@ZnS) nanoparticles tagged with cT33 aptamer were used as the receptor molecules, whereas the aptamer cT22 immobilized on the LFA platform acted as the capture probe. The ECL signal was generated when cTnT was captured by cT22 and tagged by the cT33-lumidot at an applied potential of

0.6V. The ECL-LFA strips could detect very low levels of cTnT in the ECL-based sensors. The LOD of the system was 42.71 pM.

The thesis concluded with a section, Conclusions and future direction, at the end of the chapters, describing the key findings and the scope for future work on improving the developed biosensors against cTnT and translating the proof of concept for real-world applications.

List of Abbreviations

ACS	Atherosclerotic Plaque
AKD	Alkyl Ketene Dimer
AHA	American Heart Association
AMI	Acute myocardial infarction
ASSURED	Affordable, Sensitive, Specific, User-friendly, Rapid, Robust, Equipment-free, and Deliverable to the end users
AST	Aspartate aminotransferase
BSA	Bovine Serum Albumin
CA	Chronoamperometry
CD	Circular Dichroism
CDC	Centre for Disease Control
CE	Control Electrode
CHD	Coronary Heart Disease
CNT	Carbon Nano Tubes
CP	Chronopotentiometry
c-SELEX	Centrifugal-SELEX
CSS	Cascading Style Sheet
cTnC	Cardiac Troponin C
cTnI	Cardiac Troponin I
cTnT	Cardiac Troponin T
CV	Cyclic Voltammetry
CVD	Cardio Vascular Diseases
DAB	3,3'-Diaminobenzidine
DBMS	Database Management System
DPV	Differential Pulse Voltammetry
dsDNA	Double stand Deoxy Ribose Nucleic Acid
ECG	Electrocardiogram
ECL	Electrochemiluminescence
ED	Emergency Department
EDLC	Electrical Double-Layer Capacitance
EDTA	Ethylenediaminetetraacetic acid

List of Abbreviations

EIS	Electrochemical impedance spectroscopy
ELISA	Enzyme Linked Immune Sorbent Assay
EtBr	Ethidium Bromide
FET	Field Effect Transistor
FRET	Fluorescence Resonance Energy transfer
fTnI	Fast Skeletal Troponin I
fTnT	Fast Skeletal Troponin T
HAS	Human Serum Albumin
HRP	Horse Radish Peroxidase
Hs Trop T	High Sensitive Troponin T
HTML	Hypertext Markup Language
IPTG	Isopropyl β- d-1-thiogalactopyranoside
ITC	Iso Thermal Calorimetry
LAMP	Linux, Apache, MySQL, and PHP
LB	Luria Bertani
LFA	Lateral Flow Assay
LOD	Limit of Detection
MALDI-ToF	Matrix-assisted laser desorption/ionization- Time of Flight
MD	Molecular Dynamic
MEA	Maximize the expected accuracy
MFE	Minimum Free Energy
MI	Myocardial Infarction
MySQL	My Structured Query Language
Ni-NTA	Nickel-Nitrilotriacetic Acid
NMR	Nuclear Magnetic Resonance
OD	Optical Density
ORF	Open Reading Frame
PBS	Phosphate Buffer Saline
PDB	Protein Data Bank
PET	Positron Emission Tomography
PHP	Hypertext Pre Processor

List of Abbreviations

PI	Iso electric Point
PLIP	Protein Ligand Interface Profiler
PNIPAAm	N-isopropylacrylamide
POC	Point of Care
PVDF	polyvinylidene fluoride
QCM	Quartz Crystal Microbalance
QGRS	Quadruplex forming G-Rich Sequences
RDBMS	Relational Database Management System
RE	Reference Electrode
RET	Resonance Energy Transfer
SDS PAGE	Sodium dodecyl sulphate Polyacrylamide gel electrophoresis
SELEX	Systematic evolution of ligands by exponential enrichment
SPE	Screen Printed Electrode
SPECT	single-photon emission computerized tomography
SPR	Surface Plasmon Resonance
SQL	Structured Query Language
ssDNA	single stranded deoxyribonucleic Acid
ssRNA	single stranded Ribonucleic Acid
sTnI	Smooth Skeletal Troponin I
sTnT	Smooth Skeletal Troponin T
SWV	Square Wave Voltammetry
TnI	Troponin I
TnT	Troponin T
UV	Ultra Violet
VARCHAR	Variable Character
VMD	Visual Molecular Dynamics
WE	Working Electrode
WHO	World Health Organisation
XRD	X-Ray Diffraction

List of Symbols

%	Percent
~	Approximately
<	Lesser than
=	Equal to
>	Greater than
≥	Greater than equal to
°C	Degree Celsius
µA	Microampere
µg	Micro calorie
µg	Micrograms
µl	Microliter
µM	Micromolar
µmole	Micromole
2D	Two dimensional
3D	Three dimensional
A	Ampere

List of Symbols

Å	Angstrom
a.u.	Arbitrary units
bp	Base pair
cal	Calorie
cm	Centimetre
Da	Dalton
ε	Extinction coefficient
fM	Femto molar
g	Grams
hr	Hour
Hz	Hertz
Ka	Association constant
kcal	Kilocalorie
Kd	Dissociation constant
kDa	Kilodalton
kHz	Kilohertz
L	Liter

List of Symbols

M	Molarity
mdeg	Millidegree
mg	Milligrams
min	Minute
ml	Millilitre
mM	Millimolar
mm	Millimeter
ng	Nanograms
nM	Nanomolar
nm	Nanometer
Pg	Picograms
Pm	Picomolar
s	Second
T	Temperature
ΔG	Change in free energy
Ω	Ohm

List of Figures

Figure 1.1: Estimated human mortality data in India (WHO, 2015).

Figure 1.2: Cardiac biomarkers discovery timeline (Collinson et al., 2015).

Figure 1.3: Representation of the human thin filament containing human cTn, Tropomyosin, and actin: yellow for cTnT, blue for cTnI, red for cTnC, cyan for calcium ion, green/orange for overlapping Tropomyosin, and silver/grey for actin filament. (Manning et al., 2011).

Figure 1.4: Sequence alignment of various human Troponin I (TnI) isoforms: fast skeletal Troponin I (fTnI), Cardiac troponin I (cTnI), Smooth skeletal Troponin I (sTnI).

Figure 1.5 : Predicted cTNT protein structure with its structural position.

Figure 1.6: Sequence alignment of various human Troponin T (TnT) isoforms: fast skeletal Troponin T (fTnT), Cardiac troponin T (cTnT), Smooth skeletal Troponin T (sTnT).

Figure 1.7: Diagrammatic representation of the release of the troponins into the blood stream after ischemia and necrosis (Gaze and Collinson., 2008).

Figure 1.8: Elution curve of cTnT with time in the event of an ischemia or necrosis (Wu et al., 1998).

Figure 1.9: (a) Sensor with sputtered ZnO over gold electrode pattern; (b) assembled sensor for bio-sensing using EIS; (C) SEM of nano-textured ZnO thin film; (d) Immunoassay setup on the ZnO surface using DSP bound with troponin-T antibody; (e) Immunoassay setup on the ZnO surface using APTES bound with troponin-T antibody (Munje et al., 2013).

Figure 1.10: Schematic representation of the on-off sensor on a switchable bioelectrode (Ashaduzzaman., 2015).

Figure 1.11: Stepwise illustration of an on-chip chemiluminescent immunoassay with CNT photodetector (Shim et al., 2009).

Figure 1.12: (Left) High sensitive troponin diagnostic assays commonly used in current clinical practices. (Right) Roche CARDIAC Trop T Sensitive test (visual).

Figure1.13: (A) Human sTnT doped cTnT concentrations cross reactivity study. (B) Western blot of human sTnT at multiple concentrations probed with cTnT antibodies (Meex et al.,2018).

Figure 1.15: Number of research articles along with the citations over years on electrochemical paper platforms-based assays (Ataide et al., 2020).

Figure 2.1: Aptamer data processing flowchart.

Figure 2.2: Code generation for aptamer database "Users".

Figure 2.3: Screen shot of the SQL worksheet built for the aptamer database.

Figure 2.4: Screenshot of the homepage of Aptabase.

Figure 2.5: Screenshot of the aptamer search page of the Aptabase.

Figure 2.6: Screenshot of the update form.

Figure 2.7: Aptamers available in the database and their distribution based on their target molecules and also the type of aptamer molecules.

Figure 2.8: Screenshot of the aptamer information page of Aptabase.

Figure 3.1: (A) Aptamer 1AC7 with all six apps giving same secondary structure, (B) Aptamer 1AW4 with different apps generating different structures.

Figure 3.2: (A) Number of similar structures generated in different number of applications, (B) Pie chart of app wise similarity in different aptamer, (C) Instances of app vs app similarity in aptamer secondary structure generation, (D) Algorithms used by different secondary structure generation applications.

Figure 3.3: Top row: Generated 3D ssDNA aptamers in blue and the same energy minimized structures in red. Bottom row: generated aptamers and energy minimized structures overlapped of the aptamers corresponding to top row.

Figure 3.4: 3D DNA Structure overlap of dissimilar aptamers generated from different secondary structure generation applications. Aptamer IDs are on the left of each of the images.

Figure 3.5: overlap of set 1 and 2 structures with their experimental equivalents, blue being the experimental structures and red the generated structures.

List of Figures

Figure 4.1: (A) PCR amplification of *cTnT* (~1 kb) in L3 and *sTnT* (~1 kb) in L4 observed in 0.8% agarose gel stained with Ethidium Bromide (EtBr). (B) Insert release of cTnT in L2 and sTnT in L3 from pGEMT vector.

Figure 4.2: Confirmation of recombinant plasmids by restriction digestion of (A) *pET 28a_cTnT*: (L3) PCR amplicon of the recombinant plasmids: cTnT: 870 bp and sTnT, (L4) Restriction digestion of *pET 28a_cTnT*. (6.25 kb) (B) *pET 28a_sTnT*: (L2) Single restriction digestion of *pET 28a_sTnT* with Xho1 (6.2 kb) and (L3) insert release of *sTnT* (831 bp).

Figure 4.3: SDS PAGE (10 % gel stained with comassie brilliant blue). (A) IPTG optimization of sTnT induced at an IPTG concentration of 0.4 and 0.2 mM for 12 hr at 37^0 C. Lane L1: ladder, L2: sTnT 0.2mM Soup, L3: sTnT 0.2mM pellet, L4: sTnT 0.4mM soup, L5: sTnT 0.4mM pellet, L6: BL21 DE3 soup, L7: BL21 DE3 pellet. IPTG optimization of (B) cTnT induced at an IPTG concentration of 0.4 and 0.2 mM for 8 hr at 25^0 C. Lane L1: ladder, L2: cTnT uninduced pellet, L3: cTnT uninduced soup, L4: cTnT 0.2mM pellet, L5: cTnT 0.2mM soup, L6: cTnT 0.4mM pellet, L7: cTnT 0.4mM soup, L8: cTnT 0.6mM pellet, L9: cTnT 0.6mM soup.

Figure 4.4: The purified (A) sTnT and (B) cTnT expressed in *E.coli* with 0.2mM IPTG induction and an incubation temperature of 25^0 C and 37^0 C respectively. (C) Western blot of recombinant sTnT in L2 and cTnT in L3 with anti His antibody (1: 10,000 dilution) over PVDF membrane.

Figure 4.5: CD spectra of (A) sTnT and (B) cTnT 1mg/ml in 25mM sodium phosphate buffer. MALDI-MS analysis of (C) sTnT and (D) cTnT. Zeta potential of recombinant (E) sTnT and (F) cTnT at various PH range.

Figure 5.1: PCR amplified bands at the completion of each c-SELEX cycle L1−L15, respectively. Bands L1, L6, L9 and L14 are negative c-SELEX with control protein sTnT.

Figure 5.2: Screening of positive colonies by PCR amplification of the plasmids obtained from TA plasmid in *E. coli* DH5 α.

Figure 5.3: Grouping of aptamers on the basis of percentage similarity of sequences where, comparatively more similar sequences were grouped together.

Figure 5.4: Secondary structures of aptamers cT12, cT21, cT22 and cT33 predicted by RNA Fold webserver.

Figure 5.5: 3D structures of all four aptamers generated using 3D ensemble method.

Figure 5.6: CD spectra of (A) cT12, (B) cT21, (C) cT22, (D) cT33 in water and SELEX Buffer.

Figure 5.7: Effect of pH on the structure of (A) cT12, (B) cT21, (C) cT22, (D) cT33.

Figure 5.8: CD spectra of (A) cT12, (B) cT21, (C) cT22, (D) cT33 in the presence of the target protein cTnT (0-5µM).

Figure 5.9: Isothermal titration calorimetry analysis for binding of (A) cT12, (B) cT21, (C) cT22, (D) cT33 aptamer to cTnT protein.

Figure 5.11: Curve fitting plots for K_D (Binding affinity) calculation using data from CD measurements.

Figure 6.1: The electrode design along with their dimensions used for SPEs.

Figure 6.2: Resistance measurements of sonicated probes at different time intervals.

Figure 6.3: (A) Raman spectra of conductive ink at different periods of sonication. (B) FESEM from left to right: plain nitrocellulose, screen printed graphite electrode (no sonication) and screen-printed graphite electrode at 30 min sonication.

Figure 6.4: Resistance measurements of different composition of conductive ink.

Figure 6.5: Different PEG compositions of conductive ink printed on (A) Whatman paper, (B) nitrocellulose membrane, (C) AKD treated Whatman paper, and (D) AKD treated nitrocellulose membrane.

Figure 6.6: Resistance measurements for different screen-printing technique: (A) Number of layers that can be printed to generate working electrodes with least resistance. (B) Number of layers that can be printed to generate reference and counter electrodes with least resistance. (C) Incubation time after printing each layer of working electrode. (D) Study of the effect of the contact angle of the squeeze while screen printing. (E) Study of resistance

behaviour of same aliquot of conductive ink in terms of number of layers of prints made on the nitrocellulose membrane.

Figure 6.7: (A) CV spectra of bare SPE, at different fabrication steps and in presence of the control protein sTnT. (B) CV peak current values of SPE at different concentrations of cTnT.

Figure 6.8: Response curve of the decreasing peak current values with increasing cTnT concentration and the linear range used for calculating the LOD of the sensor.

Figure 6.9: 1/Nyquist plots on the response of the generated cT21-SPEs toward cTnT concentration.

Figure 7.1: Circuit design of the DC voltage supply device fabricated for potential generation.

Figure 7.2: aptamer-protein docking interactions. (A) cT21 interaction with cTnT protein, (B) cT21 and cT33 interaction with cTnT, (C) cT21 and cT12 interacting with cTnT, (D) cT21 and cT22 interaction with cTnT.

Figure 7.3: image of the ECL-LFA for detection of cTnT.

Figure 7.4: (A) UV-vis absorption spectra of luminol, lumidot, luminol + lumidot. (B) Fluorescence spectra of luminol, lumidot, luminol+ lumidot.

Figure 7.5: CV spectra of gold electrode bare, in presence of luminol and luminol+ lumidot.

Figure 7.6: The ECL response plot derived from the mean pixel intensity of luminol in presence of varying concentrations of cTnT (1pM to 10 µM).

List of Tables

Table 1.1: Different biochemical markers of cardiac necrosis along with their release kinetics, specificity and clinical relevance.

Table 1.2: Differential diagnosis of high sensitive cTnT (HsTrop T) levels and the possible clinical diagnosis.

Table 1.3: Performance comparison of various analytical and sensor techniques used to detect cTnT.

Table 3.1: List of aptamers considered for 3D ssDNA modelling and its characteristics.

Table 3.2: Secondary structures segregated into different sets on the basis of similarity of generated secondary structures.

Table 3.3: Experimental vs generated RMSD values of set1 aptamers.

Table 3.4: Experimental vs generated RMSD values of set 2 aptamers.

Table 5.1: G-Quadraplex Prediction of all aptamers from QGRS Mapper.

Table 5.2: Prediction of interacting residues at the aptamer cT12-protein interface.

Table 5.3: Prediction of interacting residues at the aptamer cT21-protein interface.

Table 5.4: Prediction of interacting residues at the aptamer cT22-protein interface.

Table 5.5: Prediction of interacting residues at the aptamer cT33-protein interface.

Table 5.6: Type and number of interactions for each of the aptamer from docking studies.

Table 5.7: Comparison of the binding affinities of the aptamers developed by c-SELEX process along with their sequences.

Table 6.1: D/G ratio data extracted from the Raman spectrum of conductive ink captured at different period of sonication.

Table 6.2: The distance between each of the electrodes and their respective current outputs.

List of Tables

Table 7.1: A comparison of performance of various aptamer-based sensors developed to detect cTnT.

List of Schemes

Scheme 2.1: Flowchart of the database generation.

Scheme 3.1: Schematic representation of ssDNA 3D modeling.

Scheme 4.1: Schematic representation of the cloning methodology adopted for the current work.

Scheme 5.1: Schematic representation of the c-SELEX protocol followed to develop aptamer against cTnT.

Scheme 6.1: The screen-printing technique adopted for preparation of SPEs.

Scheme 6.2: Schematic representation of the generated electrochemical signal from the SPEs.

Scheme 7.1: Schematic representation of the LFA strip designed for the ECL sensor. The nitrocellulose membranes were screen printed with Ag/AgCl ink as reference ink and Carbon ink as working electrode by adopting the screen-printing procedure mentioned in chapter 6.

Scheme 7.2: ECL-LFA strip developed and all its components.

Scheme 7.3: Schematic representation of the steps involved in the ECL-LFA assay.

Scheme 7.4: Reaction scheme of the ECL generation reaction occurring between luminol and lumidot on electrochemical oxidation of both the species.

Introduction

Introduction

Cardiovascular diseases (CVDs) are the leading cause of mortality all around the globe (WHO Report, 2021). More than 75% of deaths in developing countries are caused by CVDs (Krishnan, 2012). An analysis showed that in the last decade, 24.8% of all deaths in India were due to CVDs (Prabhakaran and Jeemon, 2016). A study by Ke et al. (2015) indicated an increasing trend of CVDs in both rural and urban India. The primary reason for CVD-led death is Myocardial Infarction (MI). The complete blockage of the coronary artery often causes MI due to the rupture of atherosclerotic plaques. It is estimated that at least one billion cardiac cells are lost in a typical MI in a short period. Hence, a rapid and reliable diagnosis method for MI is crucial to initiate timely therapeutic intervention and save life. The conventional laboratory-based analytical methods used for its diagnosis are time-consuming and involve sophisticated instruments. Moreover, these methods are difficult to perform onsite and in the point of care (POC) settings due to their bulky nature and require skilled manpower for operations. Hence, there is a serious urge to develop rapid, reliable, portable, simple, and inexpensive diagnostic tool for MIs. The biosensors may be the right choice to address this critical issue, as there are numerous success stories with these analytical tools in diverse sectors, including clinical and environmental applications. Some prominent examples of biosensors include glucometers, pregnancy strips, and malaria test strips. A biosensor is a portable and simple analytical device that can detect the target analyte of interest rapidly and sensitively at an affordable price. It uses a biorecognition element on the surface of a transducer to transduce the biochemical signal generated from the interaction between the element and the target entity to a signal proportional to the target concentration. Figure 1 depicts the general configuration of a biosensor along with widely used biorecognition elements and transducers.

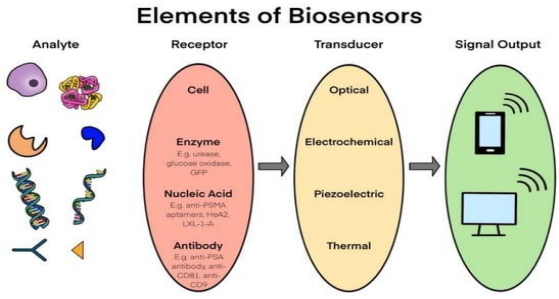

Figure 1: A general scheme of a biosensor device.

To develop a suitable biosensor, a reliable biomarker is essential for a proper and unambiguous diagnosis of the ailment. The research over the last few decades to explore such biomarkers for CVDs is astounding, as revealed by the plethora of publications available in the open literature. The emergence of cardiac biomarkers, specifically cardiac troponins, in the late nineties brings hope to meet the demands in MI diagnosis (O'Regan et al. 2003). Cardiac troponin T (cTnT) is now considered a gold standard biomarker for MI along with cardiac troponin I (cTnI). cTnT, the tropomyosin-binding subunit of troponin, plays a vital role in the Ca^{2+}-mediated regulation of the cardiomyocytes contractions. The release of troponins into the circulation from the myocardium occurs in the first few hours following the necrosis or ischemia conditions. The cytoplasm of the cardiomyocytes contains about 6-8% of cTnT and 2.8-4.1% of cTnI, which are released initially. This event is followed by the breakdown and release of the bound myofibrillar troponin components (Gaze and Collinson, 2008). A biphasic pattern of release is observed in the case of cTnT. The concentration rises at 4-6 hours following injury and attains optimal levels by 12-24 hrs. The level may remain stable for two weeks (Maynard, 2000).

There have been many reports of developing biosensors targeting troponins. However, most reported biosensors utilized antibodies as a biorecognition element. Incidentally, antibody-based sensors encounter many challenges, among which the low stability of these protein-based recognition elements and their cross-reactivity, batch-to-batch production variation, high cost of production, and long time-lag required for their development are some notable problems (Byrne et al. 2009). A recent trend in biosensor research is to replace antibodies with nucleic acid aptamers as recognition elements. Nucleic acid aptamers consist of short oligonucleotides that bind specifically to their targets. These nucleic acid-based recognition elements have many advantages over antibodies, such as their equal or superior affinity and specificity to the target, smaller in size, easier modification and immobilization on solid surface, and better stability.

Considering the importance of developing reliable and portable MI diagnostic tools in the global market and the positive traits of aptamers as recognition elements for biomarkers, we are motivated to generate aptasensors for POC-based detection of cTnT. A detailed literature survey was performed, and the objectives for the current thesis were identified. As a maiden step, an aptamer database was created to facilitate the quick extraction of aptamer-related

data available in scientific literature, including patents (https://www.iitg.ac.in/proj/aptabase/). The database was generated in three steps. The first step was a collection of all aptamer data from the literature. The second step was to convert all the data into SQL files. In the final step, a user-friendly interface was created for public use employing different coding languages. The literature survey also revealed the need for an in-depth understanding of the ssDNA aptamer-protein interaction for designing a suitable detection strategy for using aptamers in biosensors. Hence an ensemble approach was envisaged to generate 3D ssDNA aptamers. The approach was also analysed with different statistical tools to examine the authenticity of the approach. To develop biosensors for cTnT detection, a recombinant cTnT was prepared following standard molecular techniques. The as-prepared cTnT was then used as a target to develop selective aptamer following a new SELEX (Systematic Evolution of Ligands by EXponential enrichment) technique by introducing centrifugal steps to screen and enrich the desired aptamers. Finally, the isolated aptamers were used to develop an electrochemical biosensor with screen-printed electrodes specific to the MI biomarker. The biosensor relied upon the electrochemiluminescence (ECL) principle in a lateral flow assay (LFA) format. The selection of the ECL principle was prompted by its extreme sensitivity as guided by the current literature. The ECL-based detection was executed by introducing a new recognition strategy involving two aptamers, binding in different sites of the target, mimicking the sandwich assay format widely exploited in immunoassays. The chromatographic paper with nitrocellulose strips was used to develop the sensor platform that complies well with the ASSURED (Affordable, Sensitive, Specific, User-friendly, Rapid, Robust, Equipment-free, and Deliverable to the end users) mandate of the World health organization (WHO). The performance of the fabricated biosensors was analysed and presented in this thesis. In the end of the thesis, a critical analysis has been described, including the prospects of the presented work.

Chapter 1

Review of literature

Review of Literature

1.1 Cardiovascular diseases

Cardiovascular diseases (CVDs) are the leading cause of mortality around the globe. According to a report from the World Health Organization (WHO), an estimated 17.9 million deaths occurred from CVDs in 2019 alone, of which 85% were due to acute myocardial infarction (AMI) and stroke. Another WHO report in 2021 informed that CVD causes 38% of premature deaths globally. Middle and low-income countries account for 75% of CVD-related mortalities. In India, CVDs strike a decade early compared to the Western countries and registered 272 per 100000 deaths due to this ailment (Prabhakaran and Jeemon, 2016). A 2015 WHO report estimated that approximately 24 % of all the mortalities in India are due to CVDs (Figure1.1).

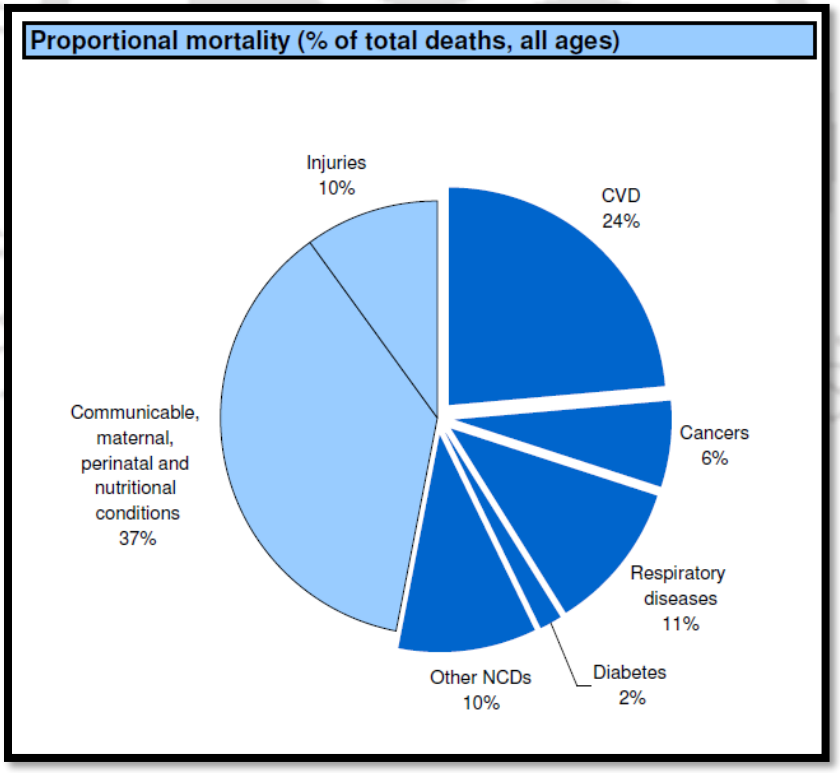

Figure 1.1: Estimated human mortality data in India (WHO, 2015).

There has been an exponential increase in the number of CVD cases in India, with particular concern for its early onset, rapid progression, and high mortality rate. The rate greatly upsurges in some states like Kerala, Punjab, and Tamil Nadu. India bears the highest number of acute coronary syndrome and ST-elevation myocardial infarction (MI) cases (Kumar and Sinha, 2020).

CVDs are the group of disorders of the blood vessels and the heart, generally occur due to the blockages caused in the blood vessels. These diseases may be classified into the following types based on the part of the body which they affect: (a) cerebrovascular diseases, which affects the vessels supplying blood to the brain, (b) coronary heart disease, which affects the blood vessels supplying blood to the heart muscle cells, and (c) deep vein thrombosis and pulmonary embolism, which affect the veins of the legs (AHA report). Heart attacks and strokes are the acute manifestation of the CVDs which are due to the blockage of the blood supply to the heart and brain, respectively. The arteries are generally smooth and allow easy passage of blood. An unhealthy lifestyle, occurrences of other diseases like diabetes and blood pressure, or the aging process usually lead to fatty acid and lipoprotein deposition on the arteries' walls and within the endothelium. Overtime, these depositions initiate a cascade of free radical reactions leading to the formation of macrophages, which deposit on the inner linings of the endothelium and eventually, produce foam cells with fibrous caps. This lesion is called atherosclerotic plaque (ACS). The rupture of the ACS, which can be hazardous, makes the ruptured plaque particles travel to smaller arteries blocking them. The complete blockage of an artery generally takes time and is an acute event that leads to stroke and heart attacks.

1.2 Myocardial infarction

Myocardial infarction (MI), commonly called a heart attack, is the leading cause of mortality among CVDs in countries across different economic statuses. In India alone, the MI has enhanced its stake from 1% in 2001-2003 to around 9-10% in 2010-2013 (Gupta et al., 2016). There has been a fourfold rise in the prevalence of coronary heart disease (CHD) in India in the past 40 years. More than 75% of deaths due to CVDs are in developing countries (Krishnan, 2012). The primary reasons are the lack of awareness and the unavailability of reliable, rapid, inexpensive test kits or sensors in the Indian market. The onset of symptoms in MI is usually gradual and occurs over

several hours. One billion cardiac cells are estimated to be lost in a typical MI. The study showed that deaths due to Acute Myocardial Infarction (AMI) in South Asians occurred 5-10 years earlier than Western population (Krishnan, 2012).

MI prognosis follows a similar template to the rest of the CVDs. One of the critical factors is the exposure to plaque. A tissue can be termed as ischemic when the tissue has deficient oxygen due to inadequate blood flow. The general myocardial ischemia is atherosclerosis of the coronary arteries. Atherosclerosis is the thickening of the coronary arteries' inner linings due to plaque build-up, causing an obstruction. An obstruction in the coronary artery may allow sufficient blood flow at rest. However, during excessive physical activity or increased mental stress condition, the increased activity of the sympathoadrenal system causes the heart rate and blood pressure to rise, increasing the work of the heart and thereby increasing the heart's oxygen requirements. Myocardial cells are adapted to respire aerobically and cannot respire for more than a few minutes without oxygen. If ischemia and anaerobic respiration prolong, this may lead to necrosis in regions of cardiac muscle tissue that are deprived of oxygen. Sudden, irreversible necrosis of this kind leads to myocardial infarction (Mendis et al., 2011). MI manifests as chronic CVDs developed due to several medical conditions and lifestyle choices. High blood pressure, high cholesterol, and smoking are key risk factors for heart disease. Several other medical conditions and lifestyle choices can also put people at a higher risk for heart disease, including diabetes, overweight and obesity, poor diet, physical inactivity, excessive alcohol use and mental stress. Early identification of manifestations of MI can allow patients to report to emergency department (ED) where one can undergo early treatments to prevent the necrosis. MI manifestations are very important for clinical diagnosis and treatment of MI. Even in countries like USA, 47% of cardiac deaths occur outside the hospitals. This clearly suggests that many people with heart diseases fail to recognise the early symptoms. According to the Centre for Disease Control (CDC), the Symptoms of MI are:

- Chest discomfort: It is one of the major symptoms of heart attack. The sensation of burning or pinching in the heart or experience of pressure in the chest region.

- Feeling tired: Sudden fatigue feeling for reasons unknown.

- Long lasting cold conditions: Persistent cold condition as the heart struggles to pump with consistent pressure and which in turn may result in the blood to get back into the lungs. This is clearly indicated by white or pink mucus which comes out on the cough.
- Swelling: As the heart fails to pump the body with blood, the veins of the legs start swelling.
- Dizziness: Due to lack of sufficient supply of oxygen to the brain.
- Shortness of breath.

1.3 Clinical diagnosis of MI

The conventional methods of diagnosis of MI are based on simple principles of good patient history, physical examination, and early and complete 12 lead Electrocardiogram (ECG). ECG is an easy and quick test documenting the electrical signals from the heart. Any aberrations in the general ECG are indicative of some heart-related conditions. Traditional ECG is called a 12 lead ECG, but of late, a number of variants like 5 lead, 3 lead, and 1 lead ECG are available. Following are some other techniques/methods used to diagnose MI: Echocardiography, Myocardial perfusion imaging, Angiogram with coronary catheterization to look for the areas of blockage in arteries, and Estimation of the size of the infarct, duration since the onset of the process.

An echocardiogram is an ultrasound of the heart. It works on the principle of the Doppler effect by using ultrasound waves, which show how the blood flows in the heart and the sounds made by the heart valves. The test is usually used to diagnose patients with known heart issues. It is one of the most prevalent imaging modalities in cardiology, capable of detecting MI at an earlier phase. Myocardial perfusion imaging is another non-invasive imaging technique that falls under nuclear medicine. A tracer molecule that is essentially a nuclear material like thallium-201 and technetium-99m isotopes is introduced into the bloodstream. The technique works on the principle of single photon emission computed tomography (SPECT) and positron emission tomography (PET). The techniques discussed above require trained personnel and expensive

equipment, and the instruments are bulky, making it not a favourable choice for POC-based detection of MI which is the need of the hour in developing and underdeveloped economies.

1.4 CARDIAC BIOMARKERS FOR MI

An ideal cardiac biomarker should be specific and found abundantly in cardiac tissue. The biomarker should be absent in the non-myocardial tissue. It should have rapid-release kinetics and an extended half-life for identification in the complete diagnostic window. Diagnosis of MI has to be made in the early stages since mortality occurs within first few hours and benefits of all interventions are greater once these are instituted early. Hence the need for an improved diagnostic which relies upon biomarkers becomes prominent. The first account of the use of a biochemical marker in the study of myocardial injury was published by La Due and colleagues in the journal Science in 1954. They measured serum glutamate oxaloacetic transaminase activity (Collinson et al., 2015).

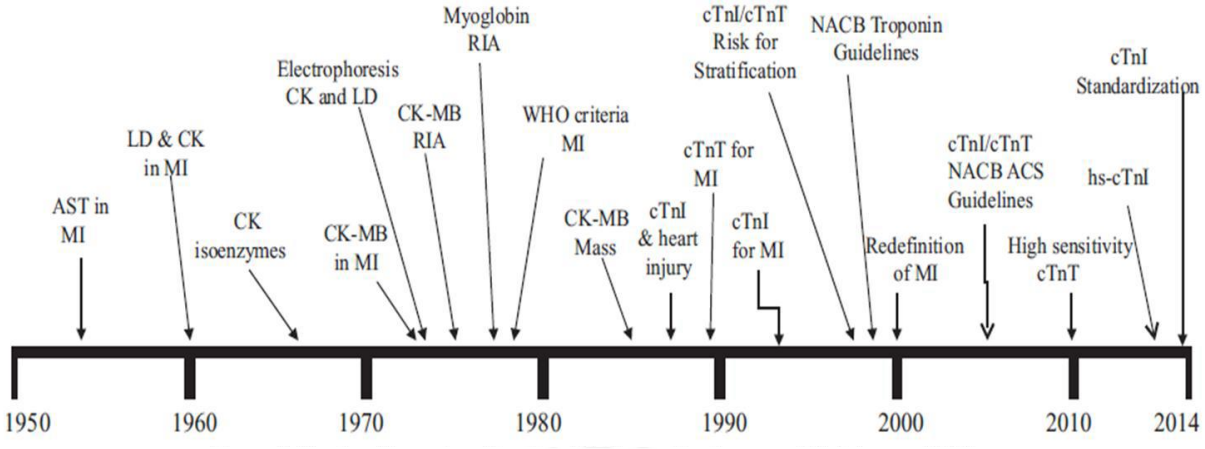

Figure 1.2: Cardiac biomarkers discovery timeline (Collinson et al., 2015).

Initially, a number of Cardiac Biomarkers were identified, and a few significant ones being are Aspartate aminotransferase (AST), Lactate dehydrogenase, Creatine kinase, Hydroxybutyrate dehydrogenase, CK-MB, Myoglobin, Glycogen phosphorylase BB, Heart fatty acid binding protein, Myosin light chains (Kemp et al., 2004). Biomarkers for CVD were discovered in the early 1950's

with AST being the first biomarker and since then a number of biomarkers were discovered (Figure 1.2). All the biomarkers mentioned above have their own limitations. Table 1.1 depicts some important biomarkers of cardiac necrosis and their characteristics.

1.4.1 Cardiac troponin

The myofibrillar protein called "troponin" was reported by Ebashi in 1963. The protein is involved in calcium ion-mediated muscle contraction. troponinis essential in the Ca^{2+}-induced regulation of skeletal and cardiac muscle contraction. Cardiac troponinis a complex of three proteins, namely cardiac troponinC (cTnC), cardiac troponinI (cTnI), cardiac troponinT (cTnT), and together with tropomyosin, it is located on the Actin thin filament (Takeda et al., 2003). Each protein is under individual genetic control, and they have specific isoforms for each muscle type. The cTnI and cTnT are distinctive in cardiac muscles compared to skeletal muscles; hence, they are considered biomarkers for cardiac injury. cTnC binds to Ca^{2+}, and cTnT links the complex to tropomyosin (Yang et al., 2014).

Biomarker	Specificity	Stability	Time of detection	Peak	Duration of elevation
CK-MB	Lacks Tissue specificity	Highly unstable	4-6 hr	12-24 hr	2-3 days
H-FABP 3	Highly specific	Moderately stable	2-3 hr	8-10 hr	1-1.5 days
Myosin light chains	Less specific	Stable	3-6 hr	4 days	10-14 days
Myoglobin	Less specific	Moderately stable	2-3 hr	6-12 hr	24-48 hr
cTnT	Highly specific	Highly stable	4-6 hr	12-24 hr	7-10 days
cTnI	Highly specific	Highly stable	4-6 hr	12-24 hr	6-8 days

Table 1.1: Different biochemical markers of cardiac necrosis along with their release kinetics, specificity and clinical relevance.

troponinis the first biomarker reported for MI, which later became a gold standard for this ailment (Memoriam, 2008). The structure of cardiac troponincomplex along with tropomyosin and actin in its native biological form is depicted in the figure 1.3.

1.4.2 Biological function of cardiac troponin

troponin-tropomyosin controls muscle contraction by blocking and unblocking the myosin-binding sites on actin. The ratio of troponin: tropomyosin: actin in thin filaments is 1:1:7(Takeda, 2005). Ca^{2+} ion concentration in the cardiomyocytes regulates muscle contraction. The regulation is carried out by the thin filamentous regulatory proteins tropomyosin-troponin(Tobacman 1996; Gordon et al., 2000; Szczesna et al., 2002), along with the actin and myosin filaments. tropomyosin is composed of two α-helical coils, which are noncovalently bound to each other from the head of one coil to the tail of the other (Li et al.,2002). The tropomyosin complex is wound around the actin filaments regulating the activation of actin.

Cardiac muscle cells remain relaxed in the absence of Ca^{2+} ions. The Ca^{2+}, when released from the sarcoplasmic reticulum, binds to the Ca^{2+} -specific sites of cTnC. The binding triggers a change in conformation, exposing a patch of hydrophobic residues in the N-terminal domain of cTnC that interact with cTnI and cTnT. These internal changes allow the translocation of the tropomyosin-troponincomplex to shift from the outer layers of the actin filaments enabling the cyclic interaction between actin and myosin heads, resulting in cardiac muscle contraction. Upon removal of Ca^{2+} ions, the cardiac troponincomplex reverts to its native conformation, which blocks the interaction between actin filaments and myosin heads, resulting in the relaxation of the cardiac muscle tissue (Gomes et al., 2002). The complete interaction occurs in three states called the blocked state, where the Ca^{2+} ions are still in the sarcoplasmic reticulum, and the troponin-tropomyosin still covers the outer domain of the acting heads. Upon release of Ca^{2+} ions, the blocked state of cardiomyocytes moves into the next phase called the closed state, where the troponin-tropomyosin complex moves from the outer domain and allows the myosin and actin interaction. The interactions are incomplete as all the actin filaments are not activated in this state. The closed state is a transition phase that leads to the last phase, called the open phase, where all the actin heads and myosin filaments are exposed, allowing them to interact, and hence the muscle contraction takes place.

1.4.3 Structure of cardiac troponincomplex

Cardiac troponincomplex is a complex of three proteins namely cTnC, cTnI, cTnT. troponincomplex is a 265 Å long; the cTnI, cTnC and C- terminal region of the cTnT forms a globular region while the rest of the cTnT forms a rod like structure which is 160 Å in length. This rod like structure is called as the tail region of the troponincomplex as it resembles a tail. The tail region interacts with the tropomyosin from center to bottom of the protein.

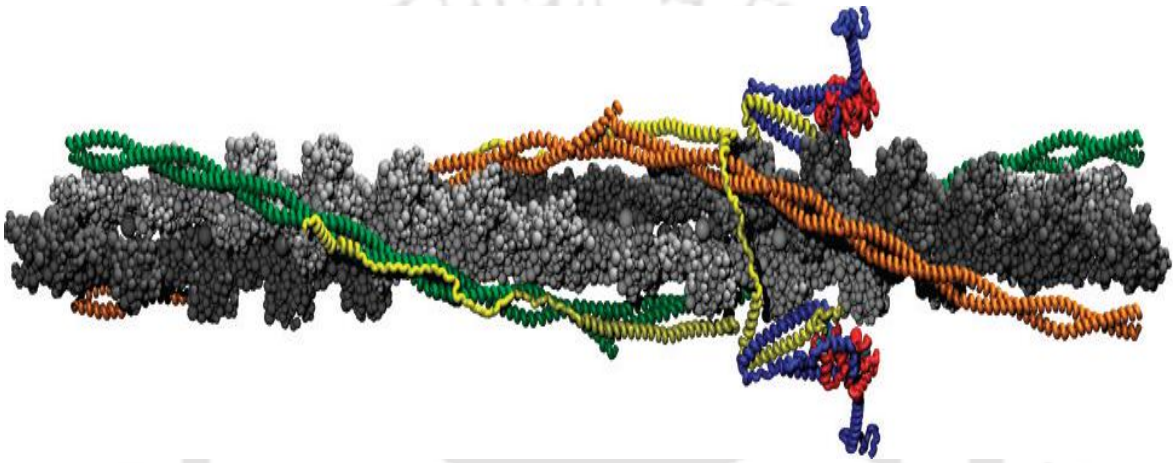

Figure 1.3: Representation of the human thin filament containing human cTn, tropomyosin, and actin: yellow for cTnT, blue for cTnI, red for cTnC, cyan for calcium ion, green/orange for overlapping tropomyosin, and silver/grey for actin filament. (Manning et al., 2011).

There are three types of muscle cells i.e., cardiomyocytes, smooth skeletal muscle cells and fast skeletal muscle cells. cTnC protein is same in all the three types of muscle cells and has a molecular weight of 18 kDa. cTnC is the Ca^{2+} binding subunit of the troponincomplex and its interaction with the rest of the complex varies markedly in the presence and absence of the Ca^{2+} ions. The change in interaction due to the conformational changes due to Ca^{2+} ions with the rest of the troponincomplex is the key for the muscle contraction and relaxation. The cTnC is a globular protein which is a dumbbell shaped molecule. The cTnC has two globular domains which are linked by a central helical linker which does so by linking the N-terminal of one globular structure with the C-terminal end of the other. Both the globular domains have a EF hand motif which is generally evident in the Ca^{2+} binding protein family (Kretsinger., 1980). The N-terminal of the

cTnC has two Ca^{2+} binding sites which are selective and of low affinity while the C-terminal of the cTnC has two high affinity binding sites for Ca^{2+} which also allows binding of the Mg^{2+} ions competitively.

cTnI is the inhibitory subunit of the troponincomplex. cTnI inhibits the actin-myosin Mg^{2+} -ATPase activity. It is a 32 kDa protein. In the presence of Ca^{2+}, cTnC changes its conformation and enhances the interaction with cTnI. The Amino acid regions of 96-116 are dissociated from the actin filaments during the interaction with cTnC. cTnI has two actin binding sites which acts as molecular switch and depend on Ca^{2+} concentration. It is regulated by three independent genes which codes for cardiac, smooth skeletal and fast skeletal proteins. The alignment analysis of all three isoforms of cTnI represented in figure 1.4. All three proteins are homologous in nature barring 39 amino acids which are unique in each of the cases.

```
CLUSTAL O(1.2.4) multiple sequence alignment


fTnI      ------------------------------MGDEEKRNRAITARRQHLKSVMLQIAATE  29
cTnI      MADGSSDAAREPRPAPAPIRRRSSNYRAYATEPHAKKKSKISASRKLQLKTLLLQIAKQE  60
sTnI      ------------------------------MPEVERKPKITASRKLLLKSLMLAKAKEC  29
                                         . ::: :  ::*:  **:::*  *

fTnI      LEKEESRREAEKQNYLAEHCPPLHIPG-SMSEVQELCKQLHAKIDAAEEEKYDMEVRVQK  88
cTnI      LEREAEERRGEKGRALSTRCQPLELAGLGFAELQDLCRQLHARVDKVDEERYDIEAKVTK  120
sTnI      WEQEHEEREAEKVRYLAERIPTLQTRGLSLSALQDLCRELHAKVEVVDEERYDIEAKCLH  89
           *:* ..*..** . *: :   *.  * .:: :*:**::***::: .:**:**:*.:  :

fTnI      TSKELEDMNQKLFDLRGKFKRPPLRRVRMSADAMLKALLGSKHKVCMDLRANLKQVKKED  148
cTnI      NITEIADLTQKIFDLRGKFKRPTLRRVRISADAMMQALLGARAKESLDLRAHLKQVKKED  180
sTnI      NTREIKDLKLKVMDLRGKFKRPPLRRVRVSADAMLRALLGSKHKVSMDLRANLKSVKKED  149
          .  *: *:. *::********* *****:*****::****:: * .:****:**.*****

fTnI      TEKERDLRDVGDWRKNIEEKSGMEGRKKMFESES-----       182
cTnI      TEKEN--REVGDWRKNIDALSGMEGRKKKFES-------       210
sTnI      TEKERP-VEVGDWRKNVEAMSGMEGRKKMFDAAKSPTSQ       187
          ****.   :*******::  ******** *::
```

Figure 1.4: Sequence alignment of various human troponinI (TnI) isoforms: fast skeletal troponinI (fTnI), Cardiac troponinI (cTnI), Smooth skeletal troponinI (sTnI).

The human cTnT is composed of 288 amino acids and has a molecular mass of 35 kDa with a pI of 5.15. It has a molar extinction coefficient of 16500 $M^{-1}cm^{-1}$ at 280 nm. cTnT lacks cysteine residues and hence has no disulfide bonds present. The protein also has no *β*- sheet structures and has

only α-helices and random coils. cTnT is split into two sub-fragments cTnT1 and cTnT2, by mild treatment with chymotrypsin. Even though both fragments interact with tropomyosin, cTnT1 has a very high binding affinity towards tropomyosin than cTnT2. This fact infers that cTnT binds to tropomyosin predominantly by cTnT1. The α-helical residues (71-150) form a stable triple-stranded binding structure with tropomyosin's two coiled α-helix structures, while the cTnT1 might be binding to tropomyosin, but cTnT2 only regulates the activity. The predicted structure of cTnT is illustrated in the figure 1.5.

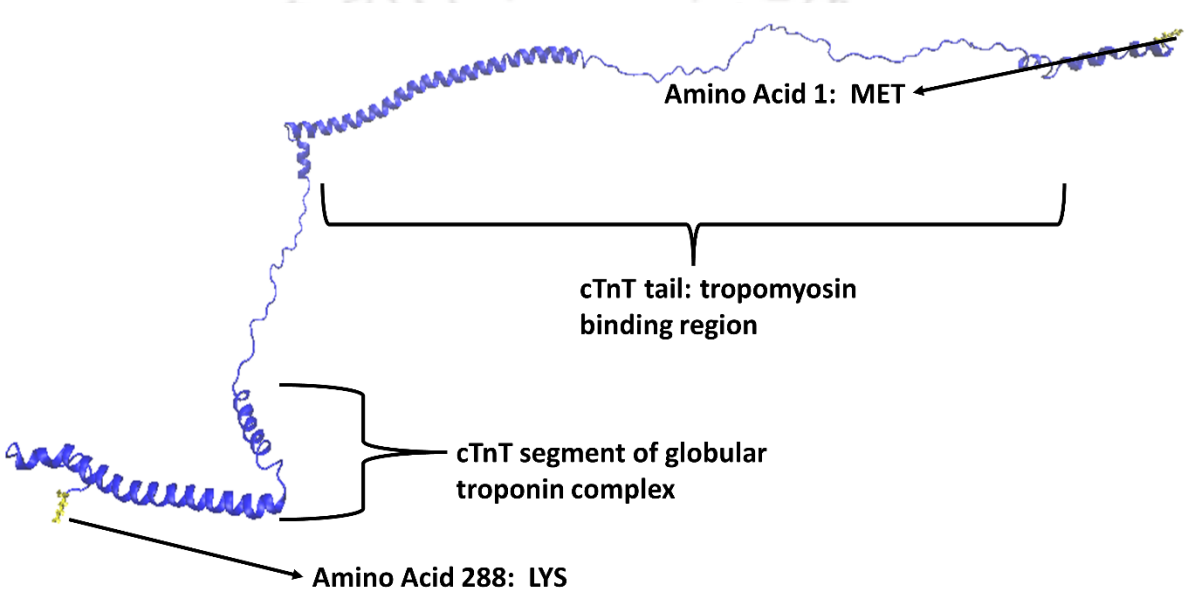

Figure 1.5 : Predicted cTnT protein structure with its structural position.

A small patch of 17 residues near the C-terminal end of $cTnT_2$ forms the main binding tropomyosin binding region, which in presence of Ca^{2+} ions interact with tropomyosin and hence confers the contraction function by perturbing the position on actin filaments. A highly conserved region comprising of residues 222-227 is critical for binding of cTnI and cTnT although a large portion of $cTnT_2$ interacts weakly. The interaction between cTnC and cTnT is however uncertain(Ohtsuki, 1999). cTnT binds to tropomyosin in an antiparallel manner, with its C terminal domain situated to the 190th residue of tropomyosin (Wu et al., 1998).

Like troponin I, troponin T have three isoforms and the amino acid sequence of all the three isoforms varies along with the size and the overall charge. All the three structures are homologous

and are α-helical in nature. The variation in the isoforms is due to the different splicing of the exons of cTnT during protein translation. The alignment analysis of all three isoforms of cTnT represented in figure 1.6. It has also been reported that all the three isoforms have different sensitivity to Ca^{2+}.

```
CLUSTAL O(1.2.4) multiple sequence alignment


fTnT      MESPPMGLFRGSSVTITERLFHACMFAELYSQSPPTGSSL--------------------  40
cTnT      -------------MSDIEE------VVEEYEEEEQEEAAVEEEEDWREDEDEQEEAAEED  41
sTnT      -------------MSDTE------------------------EQEYEEEQ----------  13
                       ::  *

fTnT      ------PSAFRVSKSTFNMSDTEDIEQHFEEEKPKF-----KPTAPKIPDGEKVDFDDIQ  89
cTnT      AEAEAETEETRAEEDEEEEEAKEAEDGPMEESKPKPRSFMPNLVPPKIPDGERVDFDDIH  101
sTnT      ------PEEEAAEEEEEAPEEPEPVAEPEEERPKPSRPVVPPLIPPKIPEGERVDFDDIH  67
                 .   ..:.    .  *      **              ****:**:******:

fTnT      KKRHNKDTLELQCLIDAHFEHRQKEEEELIALRERIEKRRSERAEQQRIRTEQEKERHAR  149
cTnT      RKRMEKDLNELQALIEAHFENRKKEEEELVSLKDRIERRRAERAEQQRIRNEREKERQNR  161
sTnT      RKRMEKDLLELQTLIDVHFEQRKKEEEELVALKERIERRRSERAEQQRFRTEKERERQAK  127
          :** :**  *** **:.***:*:******::*::***:**:*******:*.*:*:**: :

fTnT      REEERLRKEEADAKKKAEEDAKKKSALSSMGSNYSSYLQKADSKKGGKKQTEREKKKKIL  209
cTnT      LAEERARREEEENRRKAEDEARKKKALSNM-MHFGGYIQKTERK-SGKRQTEREKKKKIL  219
sTnT      LAEEKMRKEEEEAKKRAEDDAKKKKVLSNMGAHFGGYLVKAEQK-RGKRQTGREMKVRIL  186
            **: *:** : :::**::*:**..**.*  ::..*: *:: *  **:** ** * :**

fTnT      AERRKQLNIDHLNEDKLRDKAQELYEWIKTLESEKFEHMERLKRQKYEVTTLRRRVEELS  269
cTnT      AERRKVLAIDHLNEDQLREKAKELWQSIYNLEAEKFDLQEKFKQQKYEINVLRNRINDNQ  279
sTnT      SERKKPLDIDYMGEEQLREKAQELSDWIHQLESEKFDLMAKLKQQKYEINVLYNRISHAQ  246
          :**:* * **::.*::**:**:** : *  **:***:   ::*:****:..* .*:.. .

fTnT      KFSKKGAAARRRK---      282
cTnT      KVSKTRGKAKVTGRWK      295
sTnT      KFRKGAGKGRVGGRWK      262
          *. *  . .:
```

Figure 1.6: Sequence alignment of various human troponin T (TnT) isoforms: fast skeletal troponin T (fTnT), Cardiac troponin T (cTnT), Smooth skeletal troponin T (sTnT).

Due to their presence as different isoforms in different muscle cells, both cTnI and cTnT are considered cardiac biomarkers for detecting MI. The cardiac troponins T and I (cTnT and cTnI) have been found to have excellent sensitivity and specificity and are superior to creatine kinase-MB (CK-MB) as indicators of myocardial necrosis. Both cTnI and cTnT are considered gold-standard

cardiac biomarkers. Nevertheless, cTnT has a few advantages over cTnI, making it a better indicator of MI. The following are the advantages of cTnT over cTnI:

- The cytosol has 6-8% cTnT and 2.8-4.1% cTnI which are released during initial stages of cardiac injury into the blood stream, hence cTnT is released at a higher concentration than cTnI.
- cTnI is released in both reduced and oxidised forms and also contains serine residues which are phosphorylated in the cardiac tissue making it hard to generate aptamer or antibodies against cTnT as the number of structural conformations increases.
- In case of neonatal cardiac abnormalities, cTnT has been found to be a highly reliable biomarker while the same for cTnI is not yet established (Gaze and Collinson, 2008).
- cTnT levels remain stable even after two weeks of cardiac injury while cTnI remains elevated only for 6-8 days, making cTnT a biomarker of choice for late diagnosis.
- cTnI is released into the serum in multiple forms, whereas, free cTnT in single predominant form is released.

1.4.4 Release kinetics of cTnT

The release of troponins into the circulation from the myocardium occurs in the first few hours after the necrosis or ischemia. The cytoplasm of the cardiomyocytes contains about 6-8% of cTnT and 2.8-4.1% of cTnI, which are released initially (Figure 1.7). This release is followed by the breakdown and release of the bound myofibrillar troponin components (Gaze and Collinson 2008). Different levels of cTnT indicate a different level of cardiomyocyte damage. The higher the necrosis higher is the cTnT released into the bloodstream. The release of cTnT into the blood stream in the event of a necrosis or ischemia is represented in the figure 1.8 in the form of an elution curve. Healthy individuals are expected to have cTnT levels less than 5 ng/L, and a 14 ng/L is set as the 99th percentile value; cTnT value above this is considered a case of heart tissue damage. In the event of a large AMI, more than a billion cardiomyocytes die, releasing cTnT levels of more than 10,000 ng/L at its peak (Table 1.2).

cTnT is released rapidly in the initial phase followed by the bound form. Hence a biphasic pattern of release is observed in case of cTnT. The concentration begins to rise at 4-6 hours following injury and reaches optimal levels by 12-24 hrs. The levels can remain stable for two weeks(Maynard, 2000).

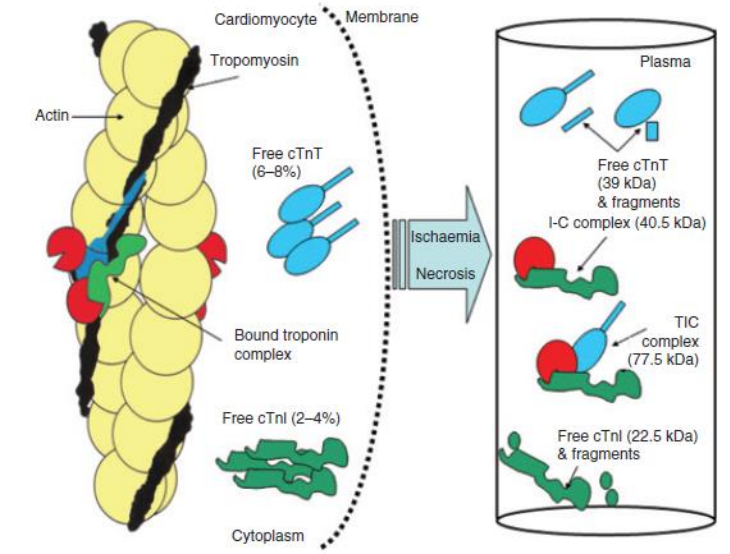

Figure 1.7: Diagrammatic representation of the release of the troponins into the blood stream after ischemia and necrosis (Gaze and Collinson., 2008).

1.5 Detection of cTnT

1.5.1 Analytical techniques for detection of cTnT

Over the last decade, much importance has been given to develop a new method for rapid, affordable, user-friendly, reliable POC diagnosis for MI. In this context, biosensors have captivated the attention of researchers due to their function's compliance with the desired performances. The broad acceptability of biosensing techniques depends mostly on how well they perform the daunting task of rapidly identifying extremely rare analytes in complex biological samples (Liu and Yobas, 2014). As discussed in the following sections, several reports have been published concerning biosensor-based diagnostic assays for cTnT.

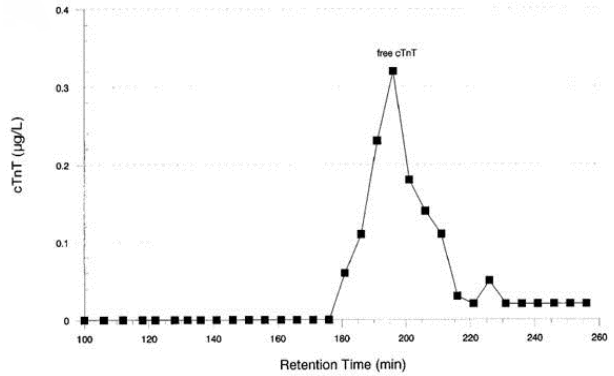

Figure 1.8: Elution curve of cTnT with time in the event of an ischemia or necrosis (Wu et al., 1998).

Hs Trop T (ng/L)	Possible clinical consequences
10,000	Very large AMI, myocarditis
1000	Large AMI, myocarditis, pulmonary embolism (PE), critical illness
100	Congestive cardiac failure, early large AMI, small AMI,
50	Micro AMI, early large AMI, myocarditis, PE shock, hypertensive crisis
14	----------99th Percentile----------
10	Stable angina, CCF, left ventricular hypertrophy (LVH), subclinical heart disease
5	Healthy individuals

Table 1.2: Differential levels of cTnT (Hs Trop T) and their potential clinical consequences.

1.5.2 Biosensors and kits for MI

A biosensor is an analytical tool consisting of biologically active material (biorecognition element) used in close conjunction with a device that converts a biochemical signal into a quantifiable electrical signal. Various biorecognition elements are used in developing biosensors, among which aptamers have recently received broad interest due to their advantages over conventional

bioreceptors such as enzymes and antibodies (Bhalla et al., 2016). Optical and electrochemical techniques are two of the most extensively used transducers for cTnT detection.

1.5.3 Electrochemical cTnT biosensors

Electrochemical biosensors are known for their high sensitivity, low cost, simple operation, requirement of very low sample volume, and easy to miniaturize. A wide range of detection techniques, such as voltammetry (including DPV, SWV, etc.), impedance spectroscopy, chronoamperometry, potentiometry, and capacitance measurement, could be utilized to develop these biosensors. Integrating nanomaterials and nanostructures assists miniaturization and improve the sensitivity of electrochemical biosensors. In the case of a solid-liquid interface, the measure of surface potential is critical. Hsueh et al. (2015) proposed a planar nano-gap structure that can monitor variations in surface potential. The authors proposed an architecture where the difference in the surface potential variance was determined by the electrical double-layer capacitance (EDLC) between the nano-gap electrodes. Cyclic voltammetry was used to measure the variance in the EDLC upon chemical modification on the electrode surface. The proposed planar nano-gap device can detect the cTnT up to 1 µg/ml even with 10 µg/ml interference. Several novel approaches are explored for cTnT detection. Munje et al., (2013) proposed one such proof-of-concept, where a non-faradaic label-free electrochemical sensor for cTnT detection was employed. Nanotextured zinc oxide thin film was fabricated on the electrode surface by cross-linking two different polymers dithio-bis-succinimidyl propionate and 3-aminopropyl triethoxysilane, and a comparative analysis was performed to study the effect of the cross-linking polymers on the metal oxide thin film (Figure 1.9). The performance of both cross-linking polymers on zinc oxide thin film was studied using EIS technique. The sensor performance was analyzed based on parameters like the LOD and the dynamic range of the systems. Of the two types of linkers used in this work the linker utilizing zinc surface terminations, displayed a wider dynamic range. The zinc surface termination extended the dynamic range from 26% to 54% in phosphate-buffered saline and from 21% to 65% in human serum. The dynamic concentration range was from 10 fg/mL to 10 ng/mL of cTnT. The current assay can potentially be explored as a POC for CVDs.

An innovative immunosensor was designed where a temperature regulated interaction of the N-isopropylacrylamide (PNIPAAm) biofunctionalized cTnT-anti cTnT complex detected the cTnT levels (Ashaduzzaman., 2015). The PNIPAAm was covalently linked with anti cTnT which displayed switch on and off properties. The reported sensor can be regenerated upto 97% after 7 cycles for further utilization of the sensors. PNIPAAm provides a lipophilic micro environment around the electrode surface with reduction in the specific volume and making the space available for cTnT binding and facilitating analyte recognition. The experiment was backed by computational studies where the structural changes occurring at the electrode was evident. A schematic representation of the entire work is depicted in the figure 1.10.

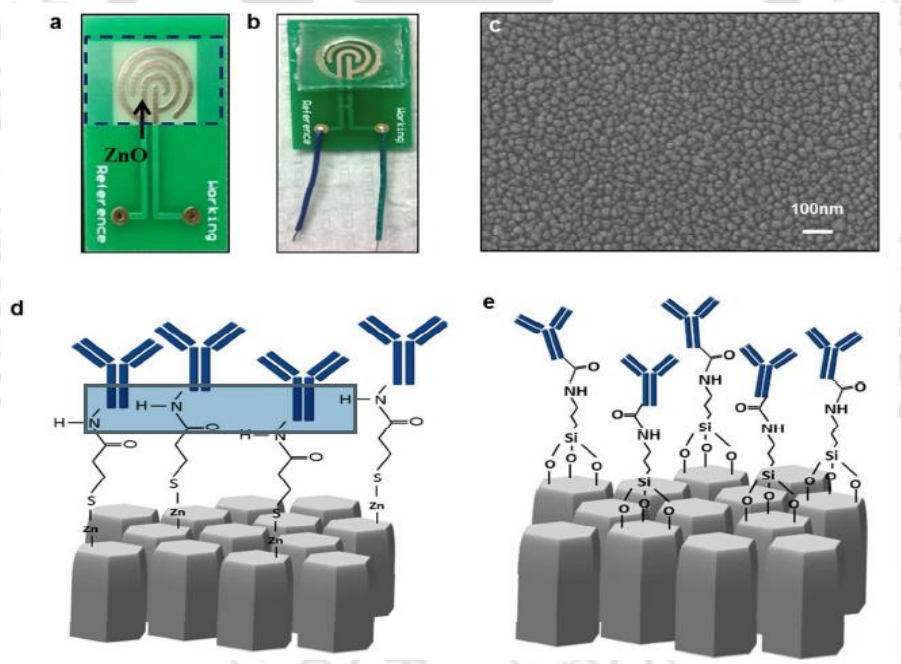

Figure 1.9: (a) Sensor with sputtered ZnO over gold electrode pattern; (b) assembled sensor for bio-sensing using EIS; (C) SEM of nano-textured ZnO thin film; (d) Immunoassay setup on the ZnO surface using DSP bound with troponin-T antibody; (e) Immunoassay setup on the ZnO surface using APTES bound with troponin-T antibody (Munje et al., 2013).

Despite electrochemical sensors possessing many advantages, a few challenges, such as difficulty in fast analytical evaluation, high cost, and low portability, still exist in their application to detect cTnT.

1.5.4 Optical cTnT biosensors

Optical biosensors offer a significant advantage compared to conventional analytical assays as they offer visual, real-time target detection with specificity and sensitivity. Optical biosensors have translated into many lateral flow assays (LFA) commercially available for diagnosing diseases like malaria and typhoid. These biosensors mainly employ three different sensing principles: Colorimetric, Fluorometric, and Electrochemiluminescence (ECL).

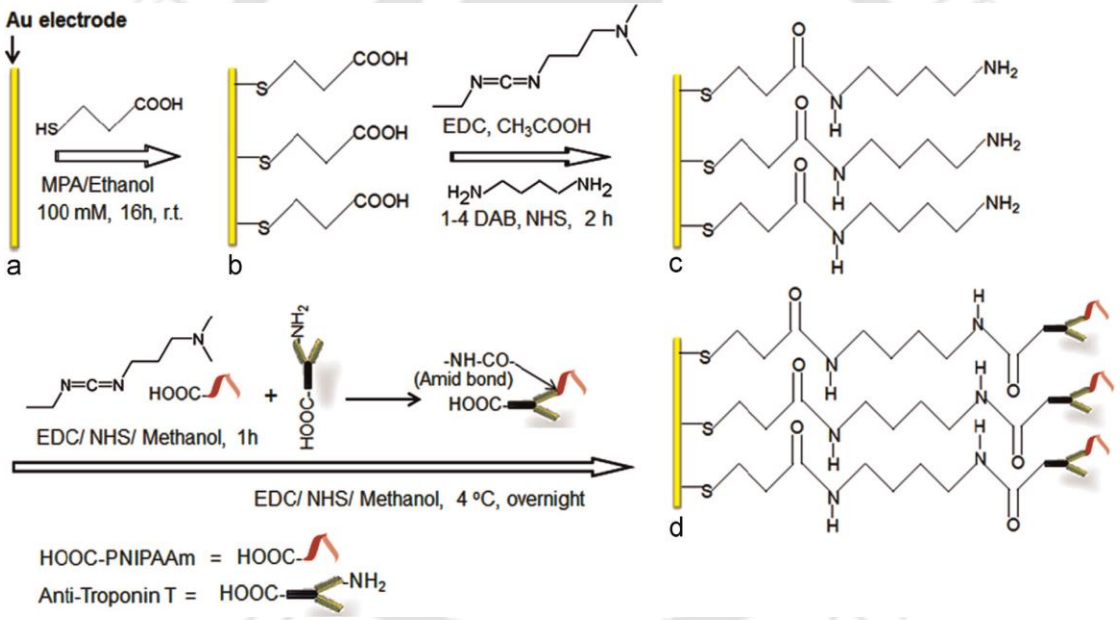

Figure 1.10: Schematic representation of the on-off sensor on a switchable bioelectrode (Ashaduzzaman., 2015).

1.5.4.1 Fluorescent biosensors

Fluorescence-based optical biosensors are gradually gaining popularity due to their high sensitivity and the emergence of portable hand-held fluorescence transducers (Malic and Kirk, 2006). Moreover, the number of highly efficient fluorophores for biological applications is

increasing in the market (Zheng and Lavis., 2017). However, the study on fluorescence-based MI biosensors is limited. A novel optical Förster resonance energy transfer (FRET) platform has been developed for detecting cTnT. One of the widely used photophysical techniques for developing a fluorescence-based detection system is FRET, which is based on energy transfer between the fluorophores. Fluorophores were conjugated with the cTnT antibody-protein A complex and silanized on the optical fibers. The distance between the donor and acceptor pairs was utilized to detect the conformational changes when the anti-cTnT antibody interacts with cTnT protein. In the presence of cTnT, the antibody underwent conformational change yielding fluorescence. The proposed proof-of-concept had an LOD of 75 nM (Grant et al.,2005).

1.5.4.2 Colorimetric biosensors

Colorimetric biosensors are primarily based on color change, which can be visualized through the bare eye making it highly attractive for PoC detection. Most of the colorimetric biosensors work on the principle of chemiluminescence. Chemiluminescence is the emission of light due to the chemical reaction that generates electronically excited states, which on its return to the ground state, produces luminescence in the visible region. A carbon nanotube (CNT) based optical immunosensor with a photovoltaic polymer coating was developed to detect cTnT. CNT was assembled on a titanium electrode and then coated with a photovoltaic polymer (Figure 1.11). This chemiluminescent immunoassay had an LOD of 12pg/ml (Shim et al., 2009).

Enzyme-linked immune sorbent assay (ELISA) is a biochemical assay that employs antibodies as a biorecognition element. The signal is generated from the enzyme tagged to the antibody, effecting a color change due to the color based chemical reaction. The first and second generation of the commercial kits were based on ELISA principle. A highly sensitive first-generation one-step sandwich ELISA for troponin T using two monoclonal antibodies was developed (Katus et al.,1992). The assay was completed at room temperature in 90 minutes, offering an LOD of 100ng/L. However, the assay plagued with cross-reactivity in the cases of skeletal muscle injury resulted in some false positive results (Muller-Bardorffetal.,1997). To overcome the problem, the antibody 1B10, which was the reason for cross-reactivity, was replaced by a more specific antibody M11.7. This change substantially improved the specificity and response time of the

assay. The new LOD of the assay 12 ng/L with a reduction assay time of 45 minutes could be achieved. However, the assay produced a variation of results up to 5.8%.

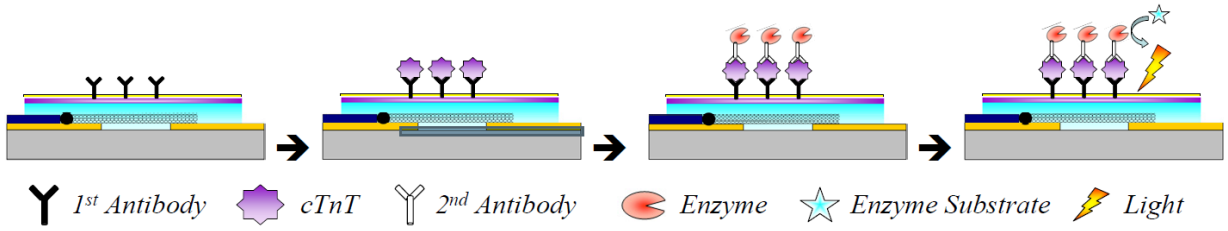

Figure 1.11: Stepwise illustration of an on-chip chemiluminescent immunoassay with CNT photodetector (Shim et al., 2009).

Commercially available troponin assays	99th percentile cut-off (ng/ml)
cTnT	
Roche Elecsys, third generation	0.01
cTnI	
Abbott AxSYM	0.30
Bayer ACS: Centaur	0.15
Bayer ACS: 180	0.07
Beckman Access, second generation	0.04
DPC Immulite	0.40
Abbott Architect	0.04
Siemens: Dimension Vista	0.05

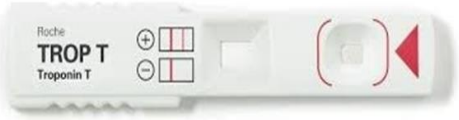

Figure 1.12: (Left) High sensitive troponin diagnostic assays commonly used in current clinical practices. (Right) Roche CARDIAC Trop T Sensitive test (visual detection).

Currently, only one cTnT assay kit is commercially available by Roche Diagnostics (Figure 1.12). This assay has undergone several improvements and is currently in its third-generation stage. The assay works on an immune-electrochemical technique using two cardiac-specific antibodies targeting two epitopic sites in the cTnT protein. The test offers a shelf life of 12 weeks once opened and a response time of 15 min. The accuracy of the assay was ~ 90%, with an intra-batch variation of 3 – 6.4% (Wang et al., 2017). The assay, however, could provide only a Yes/No format and cannot identify the extent of ischemia or necrosis. The assay is not economical to use and

requires 2 – 6^0 C storage conditions and a humidity-free environment. Meex et al., (2018) reported that the assay exhibits cross reactivity with skeletal troponins (figure 1.13).

As stated earlier, not many cTnT biosensors are reported in literature. Some of the prominent POC products presented by different research groups till date are tabulated in the table 1.3 along with the LOD, measurement range, sensor type and sensor platforms.

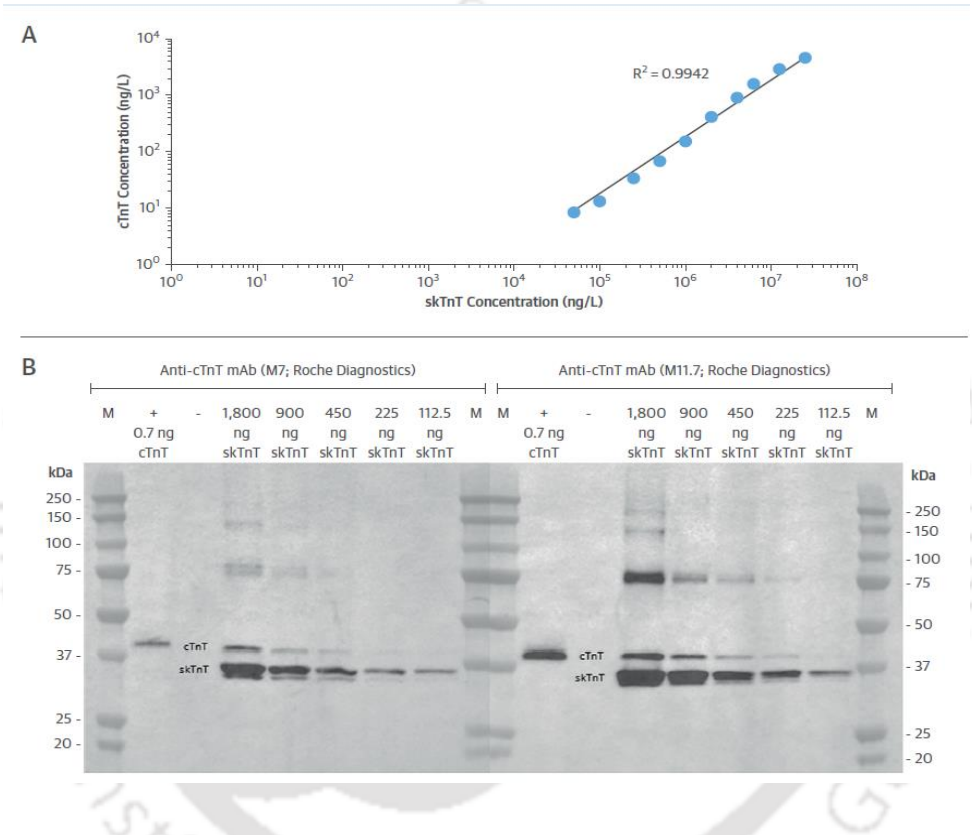

Figure1.13: (A) Human sTnT doped cTnT concentrations cross reactivity study. (B) Western blot of human sTnT at multiple concentrations probed with cTnT antibodies (Meex et al.,2018).

1.6 Aptamers as biorecognition element

The word "aptamer" was derived from the Latin words "Aptus," meaning "to fit," and Greek "meros," meaning "region." Since its independent inception by Ellington et al., Tuerk et al., and Robertson et al. in the year 1990, nucleic acid aptamers have caught the attention of researchers as emerging molecular recognition probes in diagnostic and therapeutic applications. Aptamers are developed against a wide range of target molecules ranging from proteins to small organic

molecules, whole cells, and even metal ions [Yang et al., 1998; Stoltenburg et al., 2012; Marangoni et al., 2015; Radom et al., 2013].

The process conventionally used to identify aptamers specific to a given target molecule is called SELEX (Systematic Evolution of Ligands by Exponential enrichment), which is generally an iterative process wherein a large library of ssDNA ligands are utilized for in vitro selection followed by amplification processes. The aptamers generated from SELEX have the ability to fold into their distinctive 3D structure based on the ssDNA sequence and then bind to the target, like antigen-antibody interaction. The affinities of the aptamer to its receptor are mostly in the nanomolar to picomolar ranges [Kimoto et al., 2013; Kraemer et al., 2011; Parekh et al., 2013]. The major interactions between an aptamer and its receptor are π-π stacking, van der Waals and electrostatic interactions between charged groups, hydrophobic interactions, and hydrogen bonding. Aptamers undergo conformational changes while binding to their target. ssDNA aptamers can differentiate targets even when their structural differences are minimal. [Xiong et al., 2014; Cho et al., 2009; Ng et al., 2006; Jenison et al., 1994]. One such example is the theophylline binding aptamer. This aptamer has a 10,000-fold higher binding affinity to its ligand than the caffeine molecule, structurally very similar to the theophylline molecule, with the contrast being the presence of the methyl groups at the nitrogen atom N7. Similarly, in the case of the isomers L-Arginine and D-Arginine, the aptamer developed against L-Arginine has a 120,000-fold higher affinity than with D-Arginine. Other advantages of aptamers are their nontoxic and non-immunogenic properties [Eyetech Study., 2002; Ireson et al., 2006]. Aptamers, due to their chemical properties, can penetrate the tissues and cells more efficiently than antibodies, which are more structurally complex than aptamers. This property also infers that aptamers can be used in therapeutics. They have fast renal clearance rates and a short half-life in blood circulation [Martinez et al., 2014; Melancon et al., 2014]. Other properties of aptamers that make them promising commercial synthetic ligands are their thermal stability, low cost of production, rapid synthesis, chemically modifiable, and no batch-to-batch variations [Sun et al., 2015; Potyrailo et al., 2015].

The thermal stability of the aptamers makes it possible to denaturation them at higher temperatures and then renature them to their intact structure by cooling them. Aptamers can also be produced in large quantities by chemical synthesis, using a thermocycler, and performing a polymerase chain reaction. Aptamers are also chemically versatile and easy to modify. Some of the modifications are linking the aptamers with probe molecules, with fluorophores, and with a number of functional groups on both the phosphate group and the ribose sugar moiety. Aptazymes are modified aptamers where the nucleotide bases are chemically modified to imbibe aptamers with enzymatic activity. Chemical modifications are also performed on aptamers to enhance their resistance to nuclease degradation [Kool *et al*., 1997; Ramzaeva *et al*., 2000; Tung *et al*., 2000; Williams *et al*., 2001; Niemeyer *et al*., 2002; Ito *et al*., 2003; Schoetzau *et al*., 2003; Tennilä *et al*., 2008; Kricka *et al*., 2009]. Attempt has also made to generate aptamers in vivo by transforming the cells with plasmids that encode aptamer sequence [Famulok *et al*., 2001; Burke *et al*., 2002; Famulok *et al*., 2002; Choi *et al*., 2006; Kwak *et al*., 2009].

Sensor platform/ Materials	Sensor type	Recognition element/substrate	Measurement range and LOD	Reference
Nanostructured CNTs-PEI on an AuE	Electrochemical (CV)	Antibody/AuE	0.1–10 ng mL^{-1} (PBS) LOD–0.033 ng mL^{-1} 0.02–0.32 ng mL^{-1} (Serum)	gomes et al., 2013
Nanofluidic diode	Electrochemical (FET)	Antibody	10 $fgmL^{-1}$,10pg/ml (Serum)	Liu and Yobas., 2014
Polyaniline derivative poly-o-ABA modified electrode	Electrochemical (Chronoamperometry)	Antibody/GCE	0.05–10 ng mL^{-1} (PBS) LOD–0.016 ng mL^{-1} 0.025–7.5 ng mL^{-1} (Serum) LOD–0.088 ng mL^{-1}	Mattos et al., 2013
MWCNTs modified with artificial Abs	Electrochemical (Potentiometry)	MIP	1.41–20.86 µg mL^{-1} LOD–0.16 µg mL^{-1}	Moreira et al., 2011
N-MIP with co-polymer matrix rGO electrode surface	Electrochemical (DPV)	MIP/SPE	0.01–0.5 ng mL–1 (PBS) LOD–0.006 ng mL–1 0.017–0.28 ng mL–1 (Serum)	Silva et al., 2016
Nanostructured ZnO electrodes	Electrochemical (EIS)	Antibody/Polyimide	0.0001 ng mL^{-1} 100 ng mL^{-1} LOD–1 pg mL^{-1} (Serum)	Shanmugam et al., 2017
Two planar Al electrodes	Capacitance measurement	Antibody/SiO2/Si	0.01–5 ng mL^{-1} (PBS), 0.07–6.83 ng mL^{-1} (Serum)	de Vasconcelos et al., 2009
Gold substrate functionalized with SAM layer	SPR	Antibody/AuE	0.1–50 µg mL^{-1} LOD–100 ng mL^{-1}	Liu et al., 2011
Sandwich immunoassay with AuNPs	Fluorescence	Antibody	0.25–14 nM LOD–0.02 nM (0.7 ng mL^{-1})	Mayilo et al., 2009
cTnT-labeled MBs with the micro-fluxgate sensor	Magnetic	Antibody/ Glass	0.01–10 ng mL^{-1} LOD–0.01 ng mL^{-1}	Guo et al., 2017
AuNPs immobilized on dithiol-modified surface	QCM	Antibody/ Quartz	0.003–0.5 ng mL^{-1} LOD–0.0015 ng mL^{-1}	Fonseca et al., 2011.
CMOS-compatible SiNW array	Electrical	Antibody/ SOI	0.000001–1 ng mL^{-1} LOD–1 fg mL^{-1} (PBS), LOD–30 fg mL^{-1} (Serum)	Chua et al., 2014
SPR sensor on a commercially available SPRAUTOLABSPIRITs	SPR	BiotinylatedMAb-cTnT	50 ng/L	Dutra et al., 2017

Table 1.3: Performance comparison of various analytical and sensor techniques used to detect cTnT.

Aptamers have long been promised as a substitute for antibodies and other ligands. In the last few years, several aptamers have entered the clinical trials pipeline, and several of them have cleared the clinical trials barrier and made it to the commercial scene. Pegaptanib [Ruckman et al., 1998] sodium is a 27 nucleotide pegylated RNA aptamer. Pegaptanib was the first aptamer approved for therapeutic application by the US FDA in 2004 and is now approved in Europe, Canada, Brazil, and Australia. Other aptamers in clinical trials or cleared clinical trials are E10030 [Burg et al., 1999] and ARC1905 [Biesecker et al., 1998] by Ophthotech, NOX-A12 [Rocarro et al., 2014], NOXE-36 [Oberthu et al., 2015] from Noxon Pharma, ARC1779 [Duerschimed et al., 2009] from Archemix and many others.

1.6.1. General process of SELEX

SELEX is a complete in vitro process which starts with a randomized nucleotide aptamer library, which is a random combination of the nucleotides forming unique sequences. An aptamer library generally consists of approximately $10^{12\text{-}15}$ different aptamer sequences. The number of different aptamer sequences is determined by the length of the aptamer library. The aptamer library sequence has two segments a random library segment regions where the different aptamer sequence is present. This random region is flanked on both the ends with primers. The random region length varies from 10-90 nucleotides. The primer region helps in PCR amplification. SELEX works on four basic stages binding, partition, elution and amplification. The first step in any SELEX is the incubation of the aptamer library with the target or control molecule which is either in free form or is immobilized on to a surface. The bound aptamer-target molecules are then partitioned from the unbound aptamers. The unbound aptamers are washed through several washing steps. The bound aptamers are now eluted and then amplified by PCR. These amplified aptamers are used for next round of SELEX. A conventional SELEX has 15-20 such iterations which helps to find out the aptamers which bind specifically to a given target molecule. In the final step all the last round aptamers are cloned and sequenced for further analysis.

1.6.2 Aptamer-target interaction studies

Aptamer interaction with the target is of immense interest as it determines the efficacy and specificity of the interaction. Thus, in-depth knowledge of the interaction is essential, for which the knowledge of the aptamer tertiary structures is equally important. Most interaction studies on the aptamer with its target are limited to binding affinity studies. The X-Ray and NMR structures of the aptamer-target complex crystals generally provide detailed information about the interactions. The synthesis of a crystal is a tricky process adopted by some groups (Ruigrok *et al*., 2012; Jarvis *et al*., 2015). Even though much progress has been made to predict the 3D structures for RNA molecules, no single app or method is available to generate authentic 3D ssDNA structures. Hence, there is a pressing need to explore a working approach, software, or application in this direction.

A few studies attempted to generate a 3D aptamer structure through modeling. However, the generated 3D structures through these approaches agree with only sequences that can generate hairpin loop structures. A first-of-its-kind utilized UNAfold, which was previously called Mfold, DNA server to generate 2D structures, which were then converted into 3D coordinates in Chimera/ assemble, and then the 3D RNA was converted into 3D DNA with VMD Auto PSF and VMD molefacture. Then Auto IMD plugin was used to run MD simulations [Jeddi and Siaz., 2017]. A second effort from Sabri et al., (2020) is nearly similar to the first work [Zulkeflee et al., 2020]. The group modified the initial method by changing the 3D RNA structure generation by RNA Composer and then converting them into 3D DNA with Pymol. The latest effort to generate 3D ssDNA generation is by Zhang et al., (2022), which combines DNA and RNA template libraries to generate the ssDNA 3D structures. Then MD simulations were performed to verify the validity of the strategy. There is a need for a better modelling approach that can predict the 3D structure with better accuracy. The current techniques are suitable only for aptamers with a secondary hairpin loop structure. All these issues hamper the ability of MD simulations with aptamer and its target molecules to discern the interactions. Another approach to generate tools for computational studies of the aptamer target interactions is by creating databases of aptamers and all possible data related to the aptamer and the target structure. The collected data from the

databases can be used in the artificial intelligence/ machine learning platforms to create models which can successfully predict the interactions.

1.6.3 Aptamer for cTnT detection

In the last few decades, there has been a constant effort to substitute antibodies with other biorecognition elements, which have the advantages of an antibody-based sensor but can negate the lacunae the antibody-based sensors demonstrate. Synthetic ligands are explored extensively to substitute antibodies in developing various diagnostic and detection devices (Thiviyanathan and Gorenstein., 2012). One such synthetic ligand is aptamers, which have emerged as an efficient and viable alternative to antibodies (Yang et al., 1998; Stoltenburg et al., 2012; Marangoni et al., 2015; Radom et al., 2013). Over the last few years, aptamer-based sensors have been developed against cTnT. Two different aptamers have been reported that are specific to cTnT. The first reported aptasensor was a multiplex assay that could detect cTnI, cTnT, and myoglobin. All three are critical biomarkers for MI diagnosis. The multiplex assay is an ECL-based assay fabricated on a gold electrode by self-assembling thiolated aptamers that behave like a capture probe. Once the aptamer captures the target molecules, a corresponding biotinylated antibody specific for the biomarkers is introduced, which in the presence of ruthenium, emits a versatile ECL signal. The method displayed high sensitivity with very low detection levels of .30 ng/mL for cTnT. The proof-of-concept developed had both the imaging modality and PMT-based detection (Yang et al., 2017). The aptamer sequence used in the current study is 5’-HS-(CH2)6-ACGTACCGACTTCGTATGCCAAC AGCCCTTTATCCACCTC-3’. The aptamer was generated by Sangon Biotech (Shanghai) Co., Ltd.

POCT-based assays have generated significant interest in disease diagnosis as this assay is generally quick, accurate, inexpensive, and does not require skilled staff. Electrical immunosensors generally have several advantages, including simple measurements, easy miniaturization, and no need for complex instrumentation units (de Morales and Kubota., 2016). However, in the case of cTnT, electrochemical immunosensors have received limited attention (Livi et al.,2015; Chua et al., 2009; Li et al., 2014). One such effort is the development of an aptamer-based electrical sensor which was achieved using a dielectrophoretic assembly of

graphene oxide. The graphene oxide undergoes reduction for the detection of cTnT. The electrochemical immunosensor developed in the current work has an LOD of 1.2 pg/mL (Sharma and Jang, 2019). cTnT specific aptamer used in the study was developed by OTC Biotech Canada, and the aptamer is a 70-nucleotide long ssDNA aptamer whose sequence is presented below.

5'-
ATACGGGAGCCAACACCAGGACTAACATTATAAGAATTGCGAATAATCATTGGAGAGCAGGTGTGACGGA
T.-3'.

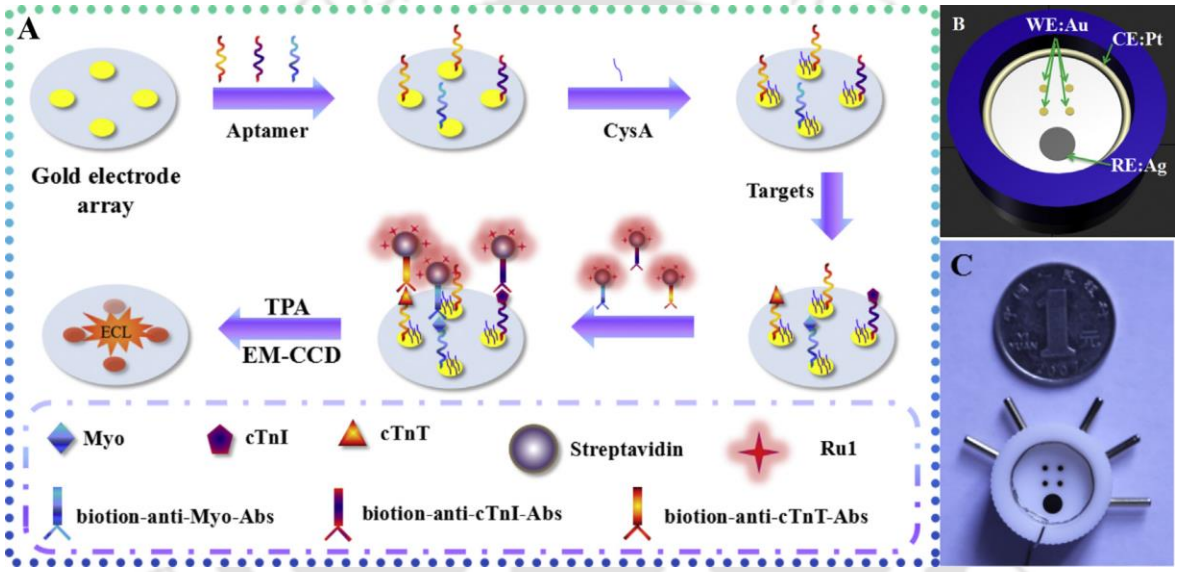

Figure 1.14: (A) Schematic diagram of the ECL biosensor array for the detection of three targets. (B) Diagram and (C) photograph of gold electrode array (Yang et al., 2017).

Another electrochemical platform was demonstrated by Agarwal et al. (2018) by bio functionalizing the same cTnT-specific aptamer on a ZnO thin film surface, which was used as an active semiconducting channel material. The biofunctionalization was established with atomic force microscopy and X-ray photoelectron spectroscopy. To understand the efficiency of the interaction between cTnT and its aptamer Kelvin Probe Force Microscopy was performed, and effective contact potential difference was monitored. Then a thin film transistor microdevice was fabricated using the ZnO as a channel material. The fabricated device demonstrated qualitative detection of 10ng/L. No other aptasensors are known to develop against cTnT until writing this

thesis. Aptamer-based sensing cTnT is still in its infancy, and there is a vast scope for developing aptasensors for detecting MI.

1.7 Paper based biosensing platforms

An important step in generating a low-cost biosensing diagnostic device for developing and underdeveloped countries is to explore a biosensing platform that compiles well the ASSURED (Affordable, Sensitive, Specific, User-friendly, Rapid, Robust, Equipment-free, and Deliverable to the end users) mandate of WHO. Chromatographic paper is an exciting addition to this mission as it has the following advantages: (i) inexpensive, portable, easily accessible [Macek et al., 1971], (ii) compatible with biological samples [Pelton et al., 2009], (iii) can be easily modified to immobilize different biomolecules like protein, DNA, small molecules, etc. [Zhao et al., 2008; Giddings et al., 1965], (iv) ease of storage, transport and disposal [Martinez et al., 2010], (v) paper absorbs liquids through capillary motion and evaporation, which eliminates the need for external pumps to drive fluid movement [Martinez et al., 2010], (vi) it serves as a good medium for colorimetric tests, providing a strong white contrast against the colored substrate [Martinez et al., 2010]. Due to the above advantages, paper is growingly used in Lateral flow immunoassays (LFI), which is based chiefly on the microfluidic principle. LFIs are portable, require no skilled personnel, and are cost-effective. These require significantly less sample volume for detection. However, LFIs have certain disadvantages as the test zones of the conventional LFIs are composed of nitrocellulose membrane. The problems with nitrocellulose membranes are their shelf life, low tensile strength, and protein incompatibility with surfactants used during pretreatment, and inconsistencies in the flow patterns due to desiccation [Yetisen et al., 2013]. At the same time, the conventional microfluidic device needs external pumps and detectors for identifying sample molecules. Paper-based microfluidic devices like the LFIs circumvent this major drawback with their inherent capillary force, which acts as a pump for the flow of liquids. Hence, paper-based assays are considered the key platform material for ASSURED criteria advocated by the WHO [Peeling et al., 2006].

Paper-based microfluidic surface can be patterned to generate devices of quantitative analysis. The transducing principle for paper-based quantitative assays includes colorimetric,

chemiluminescence, electrochemiluminescence, and electrochemical methods. Paper microfluidic devices are used to detect diseases with biomarkers specific to them. Some of the examples are carcinoembryonic antigen, alpha-fetoprotein, prostate-specific antigen etc., for cancer (Wu et al., 2014, Li et al., 2013), glucose for diabetes (Ornatska et al., 2011), and food-borne pathogens (Li et al., 2010). Paper-based electrochemical devices have developed into established tools for sensing. The techniques for the fabrication of the devices have simultaneously developed. For the first time, a paper-based printed electrode was demonstrated in 1992 to detect heavy metals by voltammetry. In paper-based electrochemical sensor devices, electrodes are printed on the paper substrate. The most commonly used inks for printing electrodes are Ag/AgCl for the reference electrode and carbon ink for the worker and counter electrode (Ding et al., 2021). Irrespective of the type of electrochemical detection method used, the fabrication process remains mostly identical. The paper device requires patterning of its surface with different zone, including reaction, sample applications and adsorbent zones. This patterning to generate hydrophilic microfluidic channels could be created following different techniques such as photolithography, wax printing, and ink-jet printing (Ataide et al., 2020). There is an exponential increase in interest among scientific community for harnessing the excellent microfluidic properties and also its hydrophobicity to generate paper based electrochemical sensors (Figure 1.15).

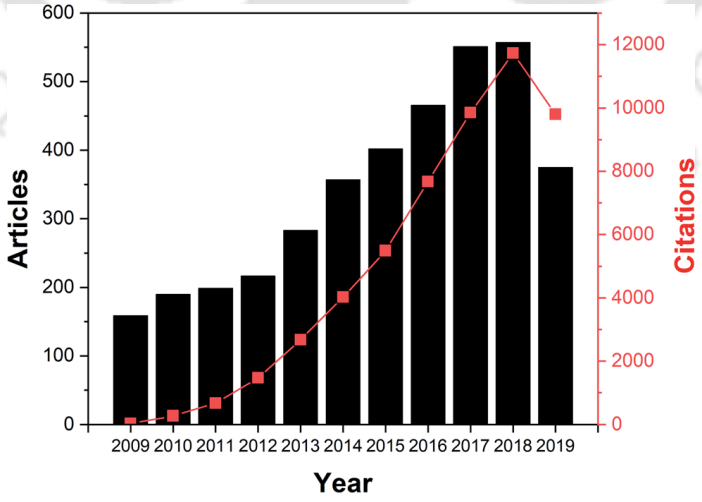

Figure 1.15: Number of research articles along with the citations over years on electrochemical paper platforms-based assays (Ataide et al., 2020).

1.8 Significant gaps in research

The importance of developing rapid, reliable, portable and inexpensive MI biosensors is extremely high in the modern society as unequivocally revealed from the vast literature available on the subject. At the same time, the literature also established cTnT as the gold standard biomarker for early detection of MI. However, proportionate to the volume of research, the proof-of-concept developed for MI detection is limited. Among these limited reports, majority have explored antibody as biorecognition element even though, false positive results due to cross reactivity with skeletal troponins in case of severe muscle injuries the antibodies fail to predict MI accurately. Antibody based sensors are not the best candidates for low cost POC based assays. Antibodies have disadvantages like increased chances of cross reactivity as observed with sTnT, high cost of synthesis of antibodies, temperature sensitivity and their massive structures are smaller than that of antibodies. Aptamers are known to be a great substitute for antibodies. Unfortunately, only a few cTnT based POCs detection of MI are available, thus opening an avenue to create aptamer based cTnT sensors. In order to develop a rational design for sensing mechanism using the aptamers as recognition elements, an understanding of the aptamer-target (protein here) interactions is essential, which is ironically, a grey area of research in the current literature. The study of interaction at a molecular level may be possible with molecular dynamic (MD) simulation studies. However, to perform MD simulation, the primary requirements are the 3D spatial coordinates of the molecules under study. This can be realized through a PDB file. The PDB files are obtained by generating crystal structures which are realized through NMR and X-Ray studies. These conventional methods are time consuming and require a lot of resources. A lot is known about the basic biomolecules like proteins, nucleic acids. Hence researchers have made significant strides in the development of modelling techniques for creating PDB files. A lot of this focus has been on the proteins and RNA and to some extent on dsDNA. There are limited tools and resources available for ssDNA molecules. There is a great need for generating applications and algorithms capable of generating ssDNA 3D molecules which can be used to create 3D aptamer model. This can be achieved by two strategies. The first method is to create a tool solely on the knowledge available on ssDNA folding and its tertiary structure formation. This requires a great detailed algorithms and is very hard to make. The alternative to the same method is to

utilize all the tools available currently for RNA and dsDNA modelling and then generate ensemble procedures to create 3D ssDNA PDB files. The second approach is by ab initio modelling. This relies mainly on the available and established structures. The data obtained from the existing models is extrapolated to make 3D models. For ab initio method to be successful, complete data set of all the available structure is a must. Hence there is need for generating databases which are specific to aptamers only. A few efforts were made in this regard but maintaining a database requires constant upgrading of the interface along with updating the new reported aptamers. This is a tedious procedure and so the database made in the past are either defunct or not specific to aptamers alone. Hence there is also a need for an aptamer database.

For detection of MI, a highly sensitive sensing method is important considering the fact that the level of cTnT biomarker are very low even in cases of cardiac problems, cTnT is considered as a marker of choice due to its specificity to the cardia tissue. Also, the levels of cTnT in the blood stream also indicates the extent of cardiac damage. Moreover, the current sensors (proof-of-concept etc) do not cover the complete range for cTnT detection. So, it is important for the sensor to not only detect low levels a sensor that is specific but also cover the entire clinical range of cTnT for accurate and sensitive detection of the biomarker and its linked accurate diagnosis of MI. In this aspect, electrochemical biosensors would be a right choice due to their extreme sensitivity and other advantages such as low sample volume and reproducibility. The other approach is by exploiting the positive traits of the electrochemical sensors and then incorporating them in an optical sensor by producing an ECL assay based POC for cTnT detection. We have made efforts to bridge all these research gaps by formulating the objective as outlined below.

1.9 Objectives of the study

Considering the importance of developing biosensors for the early diagnosis of MI and the suitability of the marker cTnT to this effect, the main objective defined for the thesis is “Aptasensing cardiac troponin-T (cTnT) for point of care diagnosis of myocardial infarction”. The following sub-objectives were set following a detailed literature survey and identified the research gaps to address the main objective. Each sub-objective has been addressed in an individual chapter of this thesis.

1. **Creation of an aptamer database:** The need for an aptamer database is clearly explained in the literature review section. The aim of this objective is to create database which is exclusively for aptamers. All the steps involved in a database generation along with all the coding languages used are explained. The methods used for the collection of all aptamer data is also described. Performance of the generated database along with the working modality the plugins are also elaborated.

2. **3D modelling of ssDNA aptamers:** The aptamer-protein interaction is critical in designing aptamers highly specific to a given target. In this objective ssDNA sequences of a list of selected aptamers are converted into 3D ssDNA structures. The whole ensemble process adopted is explained and detailed analysis is performed to understand the significance of each of the step and all the six secondary structure generation app.

3. **Cloning and expression of cTnT and sTnT:** To develop an efficient MI sensor, cTnT as marker protein and its skeletal counterpart sTnT as control protein were cloned, expressed purified and characterized. The cloned ORFs were confirmed through restriction digestion and electrophoresis. The purity and integrity of expressed proteins were validated through various techniques such as, western blot, circular dichroism spectroscopy, Zeta potential studies. A detailed account on the basic findings is incorporated in this chapter.

4. **Producing aptamers specific for cTnT by a modified SELEX procedure:** Development of specific ssDNA aptamers against cTnT was accomplished by the process of c-SELEX, including counter c-SELEX against sTnT. The c-SELEX procedure is a modified version of SELEX where in the cutoff filters are used for separation of bound and unbound aptamer candidates. The secondary and 3D structures of the evolved aptamer candidates were determined through computational and spectroscopic study. The selected candidates were further investigated to explore their specificity using different tools and techniques such as CD, ITC and docking studies.

5. **Paper based electrochemical platform for cTnT sensing:** Here in, we report a paper-based screen-printed electrode (SPE) system for the detection of cTnT. Conductive ink is

formulated for screen printing as working electrode. A screen-printing technique is optimized along with the platform selection for screen printing. The generated SPEs are fabricated with cT22 aptamer developed in the objective 4 and the efficiency of the sensor platform is determined with cTnT.

6. **Paper based electrochemiluminescence assay with lateral flow assay principle for cTnT detection:** A novel ECL-LFA platform developed for cTnT detection. The ECL-LFA platform was characterized by cyclic voltametric studies. A Device was made to supply potential to the platform for the ECL to occur. The design, fabrication and screen printing of the electrodes are mentioned in detail. Finally, the ECL luminescence is recorded by capturing the images and measuring the blue colour intensity of the images to determine the cTnT concentrations and in turn the efficiency of the generated platform.

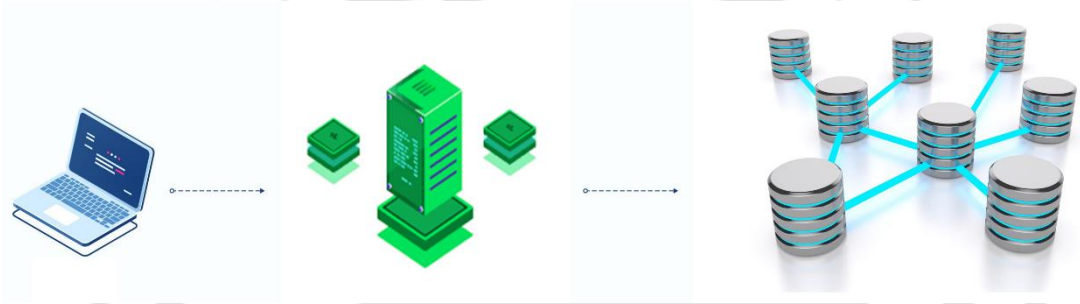

Chapter 2

Generation of an aptamer Database "Aptabase"

Chapter 2

Generation of an aptamer Database “Aptabase”

2.1 Overview

Nucleic acid aptamers are synthetic ligands composed of short single-stranded oligonucleotide sequence. These are mainly used as recognition element in biosensors and as therapeutic agents in medical sciences. Conventionally, these aptamers are synthesized through a chemical approach, termed SELEX (Systematic Evolution of Ligands by Exponential Enrichment)(Ellington and Szostak, 1990)(Tuerk and Gold, 1990). It is a repetitive in-vitro process which selects aptamer molecules specific for a target biomarker through selection, amplification and elimination steps. Aptamers are considered a substitute for antibodies as they exhibit all the positive characteristics of an antibody with additional advantages like high stability, insignificant batch-to-batch variation, broad target ranges, low production cost, and easy chemical synthesis process (Mi Song et al., 2012). These positive traits fueled the aptamer research since its invention in the 1990s across different areas of biology and interdisciplinary sciences such as sensors and therapeutics to reap the benefits of their specific target recognition functions and other advantages mentioned above (Hydrogels *et al.*, 2020) (Ulrich and Wrenger., 2009)(Ding et al., 2017). With time, the number of aptamer candidates reported in the literature has been exponentially increased and many of these are entering the clinical trials, while some of these are already cleared the trial phase (Kaur *et al.*, 2020), Pegaptanib sodium (Ruckman *et al.*, 1998), E10030 (Burg *et al.*, 1999), ARC1905(Biesecker *et al.*, 1999), NOX-A12 (Roccaro *et al.*, 2014), NOXE-36 (Oberthu *et al.*, 2015), NOXH-94 (Schwoebel *et al.*, 2013), ARC1779 (Duerschmied, Merhi and Tanguay, 2009).

The immensely increased aptamer candidates in the literature demand for a suitable aptamer database for a ready reference of the scientists to intensify their aptamer research. There have been a few efforts in this direction one such being the "The Aptamer Database" which contained sequences drawn from 239 published articles(Lee *et al.*, 2004). This site was hosted online in 2003 and is currently defunct. "RiboaptDB" is another database consisting of a total of 4212 sequences but seems to be lacking in updating aptamer sequences as the main focus of the site is on ribozymes sequences (Thodima et al., 2006). Hence, the current scenario demands a comprehensive aptamer database which provides

users with extensive aptamer data, gets updated continuously, and allows the users with multiple aptamer analysis tools and datasets.

Databases are the collection of data usually stored electronically in a computer in an organized manner. These can be handled by a database management system (DBMS). Both spreadsheets and databases store information and are similar in their structure. However, spreadsheets are for a single person's use whereas databases perform more complex operations and can hold large collections of data in a dynamic fashion making large data sets accessible to a wider audience. Also, databases can be used as a base for the generation of several machine learning and artificial intelligence-based simulation and computational models. Databases are vaguely classified into two types namely relational databases and non-relational databases (Oracle.com). The concept of databases started to come into existence in the 1960s. The initial models of databases were not flexible but could store data. In 1980 the concept of relational databases was developed where data are compartmentalized and stored in the form of rows and columns making them effective, flexible, and easy to use.

Structured query language (SQL) is used for writing a database and it predominantly uses programming language in the construction of relational databases and maintaining them. Since its inception in the late 1970s and early 1980s, SQL has transpired as an absolute medium for programming relational databases(Tutorials point). There are several open-source and proprietary relational databases built with the SQL framework. Some of the products which have successfully captured the market include Microsoft SQL Server, Oracle MYSQL, Oracle databases, IBM Db2 and SAP Adaptive Server. Even though all the above-mentioned products are based on SQL, their development is proprietary in nature; hence different variants of the SQL are not compatible with one another. MySQL is the most popular open-source Relational Database Management Systems (RDBMS) which works on different operating systems like macOS, Windows, Solaris and Linux. MySQL is programmed in C and C++ coding languages and its latest stable version was release in 2022 by Oracle Corporation(Oracle Corporation).

MySQL is used by many popular websites for construction of their databases and it is a part of LAMP software stack. LAMP is a very popular stack composed of the Linux, Apache, MySQL, and PHP/Perl/Python (LAMP) Software. A software stack is a set of components

which work together to run a complete application. LAMP is the basis of many web applications(IBM.com, 2022). Linux is an open-source operating system which is based on Linux Kernel(Linux.com). Some of the popular Linux distributions include Ubuntu(Ubuntu.com), Fedora(Fedoraproject.org), and Debian(Sheldon, 2022). The distributions intended for the server side do not include graphics and usually is a component of the solution stack. Apache is another free source server platform which is released under the terms of Apache license 2.0(Apache.org). It works on Unix-like operating systems and also on Windows(Hernandez, 2023). PHP (Hypertext Pre-processor), the first stable release of which was in the year 1995, is a server-side scripting language, created for web development(STechies). It is a secure and widely used for interaction with the server to execute commands and retrieve data. The current stable release is PHP version 8.1.4(PHP.net).

Herein, a new aptamer database termed "APTABASE" has been reported. It is an effort to compile the entire aptamers developed worldwide under one website. Aptabase is a dynamic interactive database with secured login features for the admin to update it regularly and contains PHP forms for the users to list their aptamer data into the Aptabase to dynamically update the aptamer information. The Aptabase also hosts plugins like the GC calculator for both ssDNA and ssRNA. The detailed technical feature of the developed database has been reported in this thesis.

2.2 Experimental procedures

Aptabase is a complete database which is equipped with additional plugins and security features. The construction of Aptabase is accomplished through a standard website generation procedure. The complete procedure adopted in the construction of the generated “Aptabase” is revealed in a sequential method with the following steps:

- Data acquisition
- Data construction
- Database Construction

2.2.1 Data acquisition

Aptamer data in journal publications were explored and collected using Web of Science, Pubmed, SciFinder, and Google Scholar search engines. Search engines Patentpak, Pubcrawler, and Google Patents were utilized to explore and collect patent information. All the available data were collected and segregated in a table in a Microsoft Excel spreadsheet. Data were tabulated into categories: aptamer name, target (general and specific), length, affinity, buffer, GC content, sequence, and references. The complete process adopted for database generation is represented in figure 2.1. All the aptamers sequence were passed through the developed GC calculator and the GC percentage was recorded in the excel sheet and also the length of the sequence were recorded.

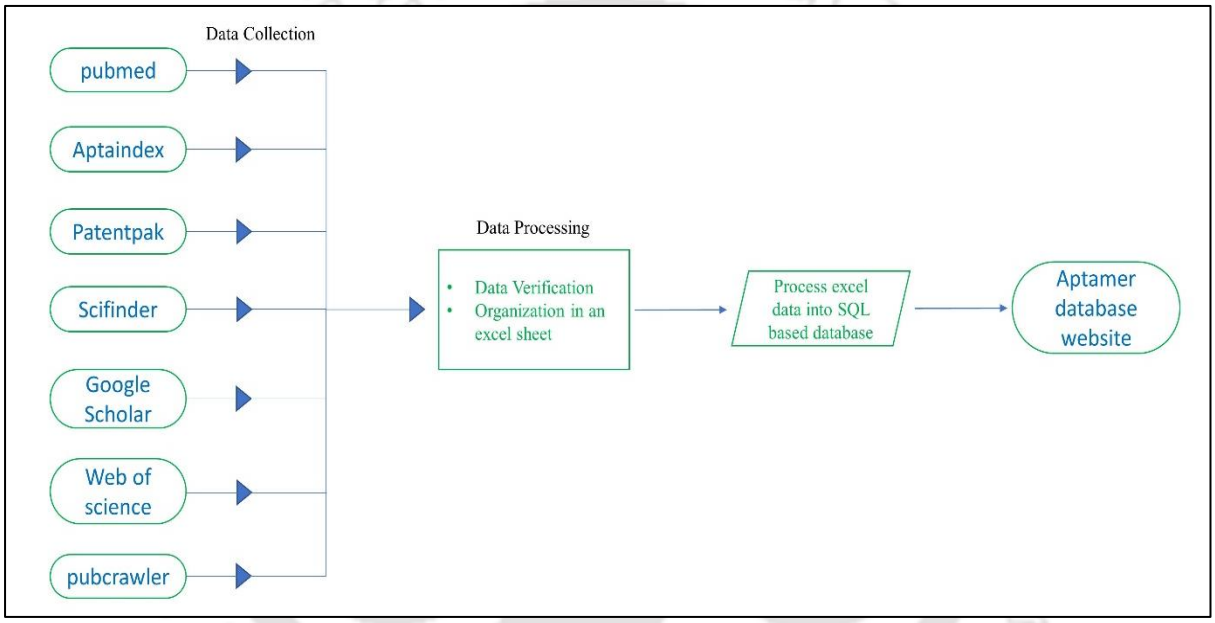

Figure 2.1: Aptamer data processing flowchart.

2.2.2 Data conversion

A database called "Apta" was created in phpMyAdmin software [29], with the fields matching the segregated data in a spreadsheet. All the databases generated in PhpMyAdmin are based on MYSQL and PHP, enabling the graphical interface instead of a command line to create, edit, and update the generated databases. These databases can also be linked via PHP, HTML, and CSS to receive external commands from users outside the PhpMyAdmin workbench and outside the server. Several parameters were selected to create the database. Variable character (Varchar) was used as input type with an auto-defined collation for all fields/columns except the ID (serial number) column. The ID field was marked as the primary key with selecting an auto-increment option. The Excel sheet

with aptamer data was converted into a ".xml" file format and saved. The Excel data were uploaded to the APTA using the Import function. The following options were set as base parameters to upload the Excel file: Import function was executed with the file character set as "utf-8"import file formatted to "XML" enabling the foreign key checks. Another database called "users" was generated for secured admin login and up-gradation of the website. "Users" was generated using the SQL query window. The code defining the table structure is depicted in figure 2.2.

2.2.3 Aptabase construction

Databases are the collection of data which is stored in a server in an organised manner. Aptamer database is a database which falls under the category of LAMP stack. LAMP is a software stack which is used to generate website or database. The LAMP stack is constructed with Linux, Apache, MySQL, PHP/Perl/Python. The database constructed in the current work explored PHP as the server-side scripting language which communicates with the Apache webserver where the database is stored. The database was constructed with MySQL. The construction of database can be divided into two parts:

- Server-side scripting and backend code
- Website construction

2.2.4 Website construction

The Aptabase was constructed using open-source platforms. MySQL 8.0 version was used as a relational database while PHP (Hypertext preprocessor) was used as a server-side scripting language and also to generate dynamic and interactive webpages. PHP, the most versatile server-side language is embedded with HTML. HTML and CSS along with Bootstrap were used to create the website. To script all the coding, the notepad++ 8.1.4 version was used. Notepad++ is an open-source text editor capable of supporting many computer scripting languages. It has a faster speed of execution and a smaller program size. All the necessary code and platforms for the generation of the database were open source. Homepage of the website, a web counter from HitWebCounter, was used to assess the web traffic. To further analyze the visitor metrics which provide information for future upgradation of the website a google analytics script was incorporated. Google Analytics is a free open-source analytics service offered by Google. The initial testing of the created database and the webpages

were performed by converting the host laptop (HP pavilion power 15-cb0xx) into a local server.

```
SET SQL_MODE = "NO_AUTO_VALUE_ON_ZERO";
SET AUTOCOMMIT = 0;
START TRANSACTION;
SET time_zone = "+00:00";


/*!40101 SET @OLD_CHARACTER_SET_CLIENT=@@CHARACTER_SET_CLIENT */;
/*!40101 SET @OLD_CHARACTER_SET_RESULTS=@@CHARACTER_SET_RESULTS */;
/*!40101 SET @OLD_COLLATION_CONNECTION=@@COLLATION_CONNECTION */;
/*!40101 SET NAMES utf8mb4 */;

--
-- Database: `test_db`
--

-- --------------------------------------------------------

--
-- Table structure for table `users`
--

CREATE TABLE `users` (
  `id` int(11) NOT NULL,
  `user_name` varchar(255) NOT NULL,
  `password` varchar(255) NOT NULL,
  `name` varchar(255) NOT NULL
) ENGINE=InnoDB DEFAULT CHARSET=latin1;

--
-- Dumping data for table `users`
--

INSERT INTO `users` (`id`, `user_name`, `password`, `name`) VALUES
(1, 'test', '202cb962ac59075b964b07152d234b70', 'test'),
(2, 'test1', '202cb962ac59075b964b07152d234b70', 'test1');

--
-- Indexes for dumped tables
--


--
-- Indexes for table `users`
--
ALTER TABLE `users`
  ADD PRIMARY KEY (`id`);

--
-- AUTO_INCREMENT for dumped tables
--


--
-- AUTO_INCREMENT for table `users`
--
ALTER TABLE `users`
  MODIFY `id` int(11) NOT NULL AUTO_INCREMENT, AUTO_INCREMENT=5;
COMMIT;

/*!40101 SET CHARACTER_SET_CLIENT=@OLD_CHARACTER_SET_CLIENT */;
/*!40101 SET CHARACTER_SET_RESULTS=@OLD_CHARACTER_SET_RESULTS */;
/*!40101 SET COLLATION_CONNECTION=@OLD_COLLATION_CONNECTION */;

```

Figure 2.2: Code generation for aptamer database "Users".

This was achieved by the use of a mock server called "Apache webserver" and database table generation by phpMyAdmin open-source software. Once tested successfully the

database was hosted in the IITG server. The complete scheme adopted for the generation of Aptabase is represented in scheme 2.1.

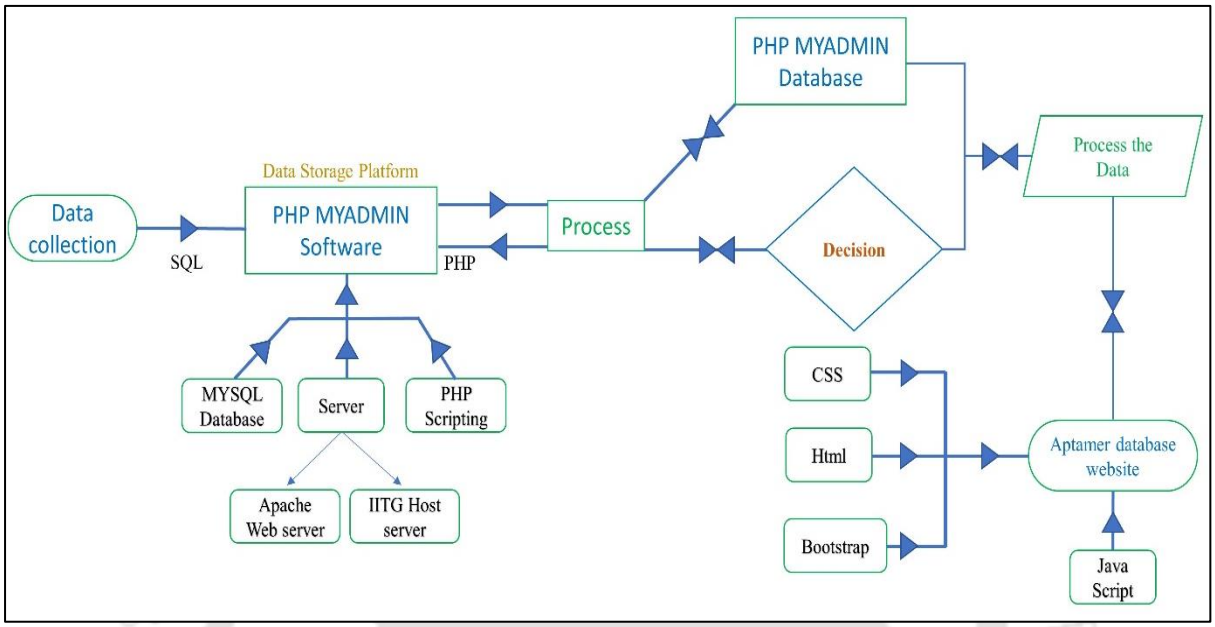

Scheme 2.1: Flowchart of the database generation.

2.2.5 Plugins

An additional plugin GC Calculator were also integrated with the website to assist the viewers for performing basic aptamer analysis operations. The designed GC% calculator plugin is a hybrid of HTML, CSS and JavaScript. Java script enables the GC calculator to work. The additional plugin generated was based on JavaScript, the most explored web programming language. It was used as the client-side web coding language for the plugin GC Calculator. The source code for the GC calculator is a modified version of the oligo calc (https://sites.pitt.edu/~rsup/OligoCalc.html). This enhanced version is capable of identifying RNA as well as the DNA sequence. Our GC calculator can also provide the GC content of the Hybrid molecules which consists of both DNA and RNA residues in their sequences. The calculate function of the javascript along with the string, count char and variable function forms the core of the plugin. JavaScript is embedded in Html by form element. This makes the plugin render results in a web browser. The complete GC calculator code was a mixture of HTML and javascript. The concept of loops, logic and arithmetic operations were used as part of the javascript in order to make the calculator work. The code used to run is mentioned in the script box 2.1.

```
 <body>
<div class="gccal">


<form action="get">

  <!-- PS: This code is modified version of an existing code of the Oligonucleotide
  Properties Calculator which can be found at
  http://www.pitt.edu/~rsup/OligoCalc.html.-->
  <table  style="padding:10px; border-style:outset; background-color:none">
      <tr>
         <td><table>
               <tr>
                  <td style="width:20% text-align:justify" ><h2>GC Calculator</h2><br>
                  Aptamer sequences without nucleotide modification.<br>
                     <textarea cols="30" onchange="Calculate(this.form)" name="apt_Box"
                     rows="7" placeholder="Enter Aptamer Sequence here" style=
                     "text-align:left; white-space: nowrap; overflow: auto; "
                     ></textarea></td>
                  <td>
                     <input name="Calbutton" onclick="Calculate(this.form)" value=
                     "Submit" type="button">
                     <br>
                     <br>

                     <input value="Reset" type="reset"></td>
               </tr>
            </table>
            <table style="padding:5px; text-align:left">
               <tr>
                  <td>Aptamer Sequence Length:</td>
                  <td><input size="3" name="lengthBox" onfocus="Disallow(this.form)"
                  ></td>
               </tr>
               <tr>
                  <td >Adenine (A):</td>
                  <td><input size="3" name="aBox" onfocus="Disallow(this.form)" ></td>
               </tr>
               <tr>
                  <td>Thymine (T):</td>
                  <td><input size="3" name="tBox" onfocus="Disallow(this.form)"></td>
               </tr>
               <tr>
                  <td>Guanine (G):</td>
                  <td><input size="3" name="gBox" onfocus="Disallow(this.form)"></td>
               </tr>
               <tr>
                  <td>Cytosine (C):</td>
                  <td><input size="3" name="cBox" onfocus="Disallow(this.form)"></td>
               </tr>
               <tr>
                   <tr>
                  <td>Uracil (U):</td>
                  <td><input size="3" name="uBox" onfocus="Disallow(this.form)"></td>
               </tr>

                  <td>GC Content (%)</td>
                  <td><input size="3" name="gcBox" onfocus="Disallow(this.form)"></td>
               </tr>


            </table></td>
      </tr>
   </table>
</form>
```

```
<script type="text/javascript">

   function Calculate(form) {
      newnuc_Count = new nuc_Count(form.apt_Box.value);
      form.apt_Box.value = newnuc_Count.Sequence;
      form.lengthBox.value = newnuc_Count.Sequence.length;
      form.aBox.value = newnuc_Count.aCount;
      form.tBox.value = newnuc_Count.tCount;
      form.gBox.value = newnuc_Count.gCount;
      form.cBox.value = newnuc_Count.cCount;
      form.uBox.value = newnuc_Count.uCount;
      form.gcBox.value = newnuc_Count.GC();
   }

   function nuc_Count(theString) {
      this.Sequence = RemoveNonBase(theString);
      this.aCount = CountChar(this.Sequence, "A");
      this.cCount = CountChar(this.Sequence, "C");
      this.gCount = CountChar(this.Sequence, "G");
      this.tCount = CountChar(this.Sequence, "T");
      this.uCount = CountChar(this.Sequence, "U");
      this.GC = GC;
   }

   function GC() {
      if (this.Sequence.length > 0) {
         // Multiply by 10, then divide by 10 to get one DP
         return Math.round((100 * (this.gCount + this.cCount) / this.Sequence.length) *
         10) / 10;
      } else {
         return "";
      }
   }

   function RemoveNonBase(theString) {
      var returnString = "";
      theString = theString.toUpperCase();
      messageDisplayed = 0;
      for (var i = 0; i < theString.length; i++) {
         if ((theString.charAt(i) == "A") || (theString.charAt(i) == "G") || (
         theString.charAt(i) == "C") || (theString.charAt(i) == "U") || (theString.charAt
         (i) == "T")) {
            returnString += theString.charAt(i);
         } else if (i == 0 && theString.charAt(i) == ">") {
            // This is a FASTA format sequence.  Skip ahead to a CR/LF.
            while (i < theString.length && !(theString.charAt(i) == '\r' ||
            theString.charAt(i) == '\n'))
               i++;
         } else if (messageDisplayed == 0 && theString.charAt(i) != ' ' &&
         theString.charAt(i) != '\r' && theString.charAt(i) != '\n') {
            // Allow space, CR, and LF, otherwise delete non-Base characters and notify
            the user.
            messageDisplayed = 1;
            sb.ui.showMessage("Your DNA sequence contains characters other than A, T, G,
            U and C.  These characters will be deleted.");
         }
      }
      return returnString;
   }

   function CountChar(theString, theChar) {
      var returnValue = 0;
      theString = theString.toUpperCase();
      for (var i = 0; i < theString.length; i++) {
         if (theString.charAt(i) == theChar) {
            returnValue++;
         }
```

```
        }
        return returnValue;
    }

    function Disallow(form) {
        form.apt_Box.focus();
    }

</script>
</div>

<div id= "counter">
      <!-- hitwebcounter Code START -->
<a href="https://www.hitwebcounter.com" target="_blank">
<img src=
"https://hitwebcounter.com/counter/counter.php?page=7874434&style=0001&nbdigits=7&type=page&initCount=0" title="Free Counter" Alt="web counter"   border="0" /></a>


</div>

</div>
<script>


</div>

  </body>
</html>
```

Script box 2.1: Complete Html and Css code used in GC calculator plugin generation.

2.3 Results and Discussion

2.3.1 Data collection and data formatting

All the aptamer data were collection from different websites and tabulated in Microsoft excel sheet. Once all the data collections were completed, these were refined by eliminating all the duplicate entries. Further data cleaning was performed by updating the original citation instead of any other sources which had reported the aptamer. The excel sheet acts as a database. However, in order to create a web-based database for masses, the excel were was converted into SQL format in a MYSQL workbench (figure 2.3).

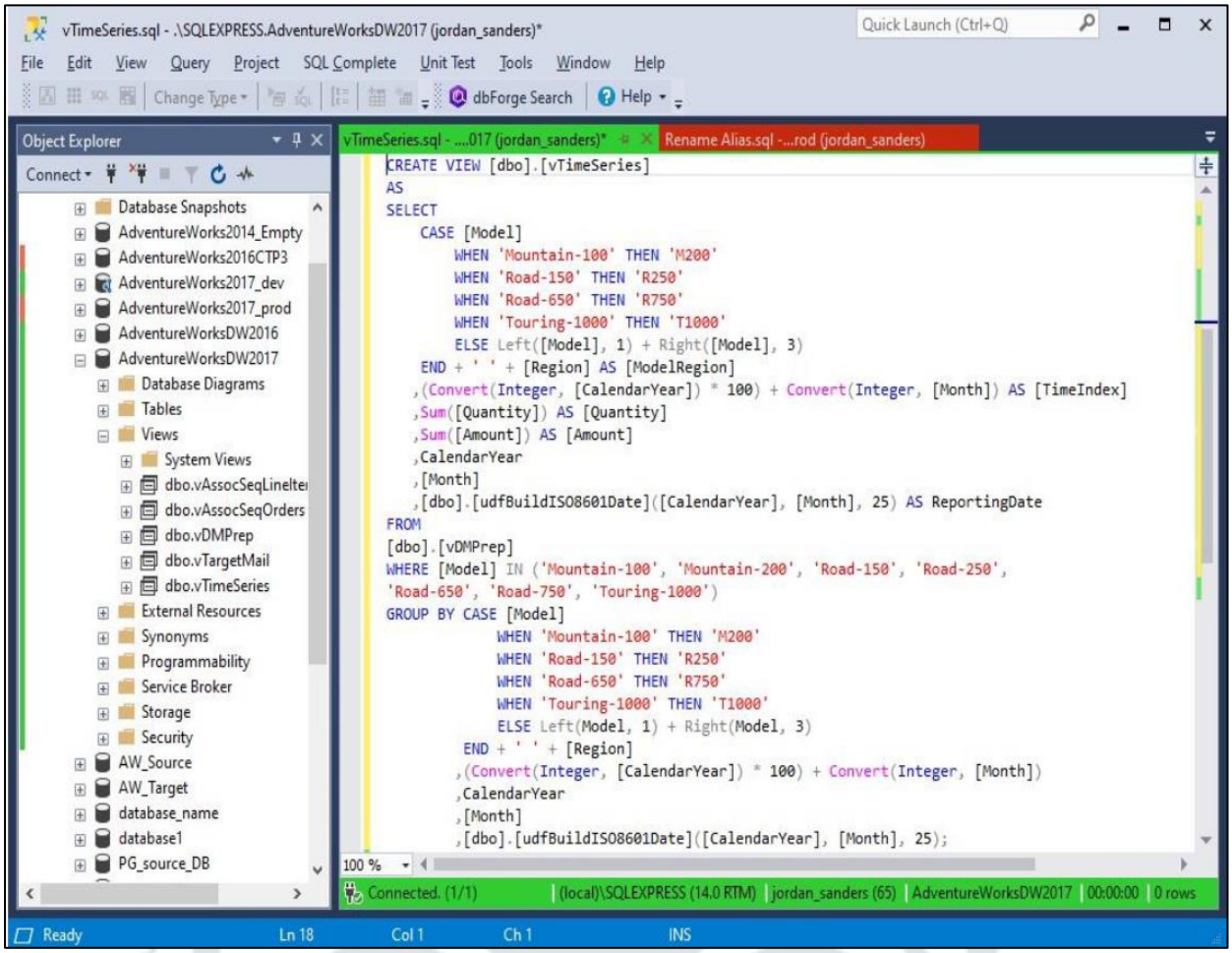

Figure 2.3: Screen shot of the SQL worksheet built for the aptamer database.

2.3.2 Database Analysis

The size of aptamers varies depending on the size of the random libraries from which the SELEX is performed. Hence the size varies from as small as 10 to up to 155 nucleotides long. The current version of Aptabase hosts 605 aptamers and the homepage of the site contains an additional plugin called a GC Calculator. The GC calculator plugin works on JavaScript and is capable of identifying the length of nucleotide sequence entered, along with the type and number of nucleotides for both RNA as well as DNA. The plugin also calculates the GC percentage of the entered nucleotide sequence. GC content dictates the tertiary structure of the aptamer, the formation of G-quadruplex structures and also plays a vital role in the aptamer-target interaction.

Considering the changing landscapes of the internet-accessible devices and their screen variable sizes the entire Aptabase is made responsive. HTML and CSS web designs were generated for all devices like desktops, Laptops, Tablets and Mobile phones to

accommodate viewers of all categories and to make the website easy to use regardless of the mode of access. Future versions of the Aptabase will be designed to be more user-friendly by utilizing the data obtained from Google Analytics matrices. Google Analytics helps the administrator to track and also observe several crucial matrices like the geographical location of the user, time spent by the user and also the type of device used for viewing. All these matrices enable the creation of a more interactive website in upcoming versions. The homepage of the website has a navigation bar linking all the web pages (figure 2.4). The home page also hosts the GC calculator plugin.

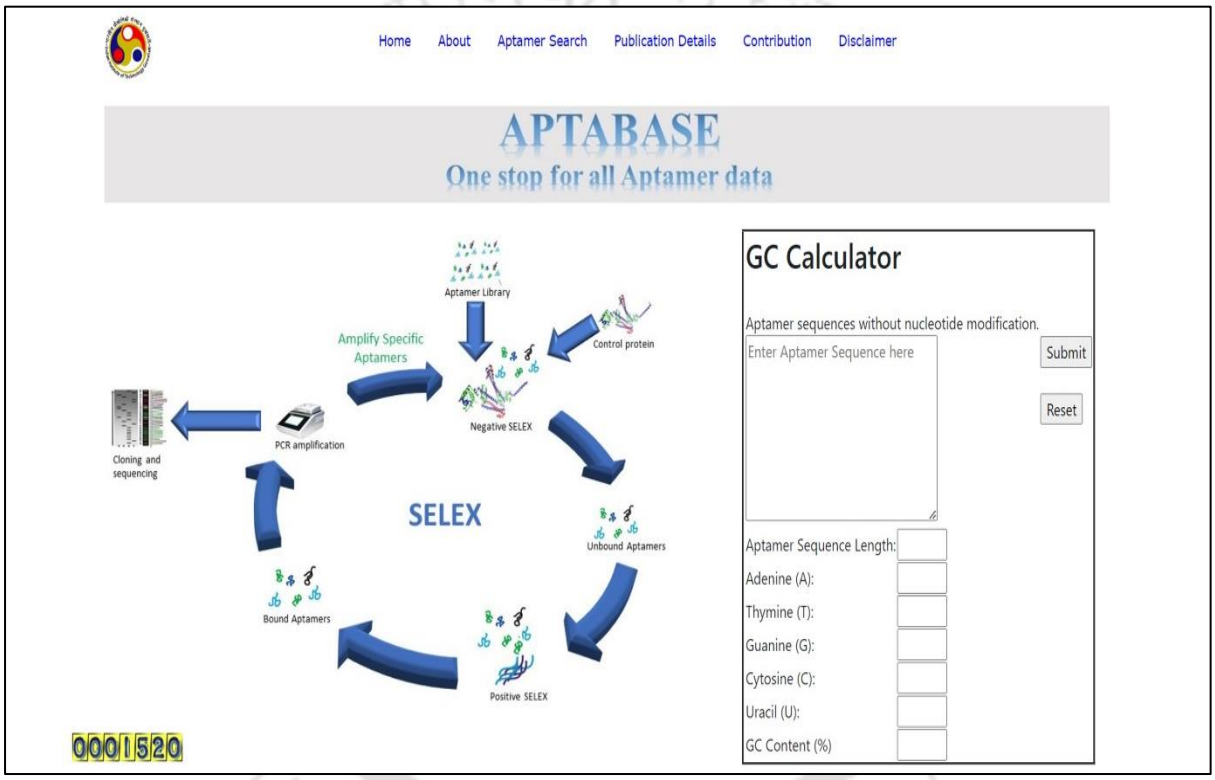

Figure 2.4: Screenshot of the homepage of Aptabase.

The webpage called "Aptamer search" accommodates all the aptamer-related search and selection operations. The Aptamer search page also consists of an update form enabling researchers worldwide to update their Aptamer data in our database (figure 2.5).

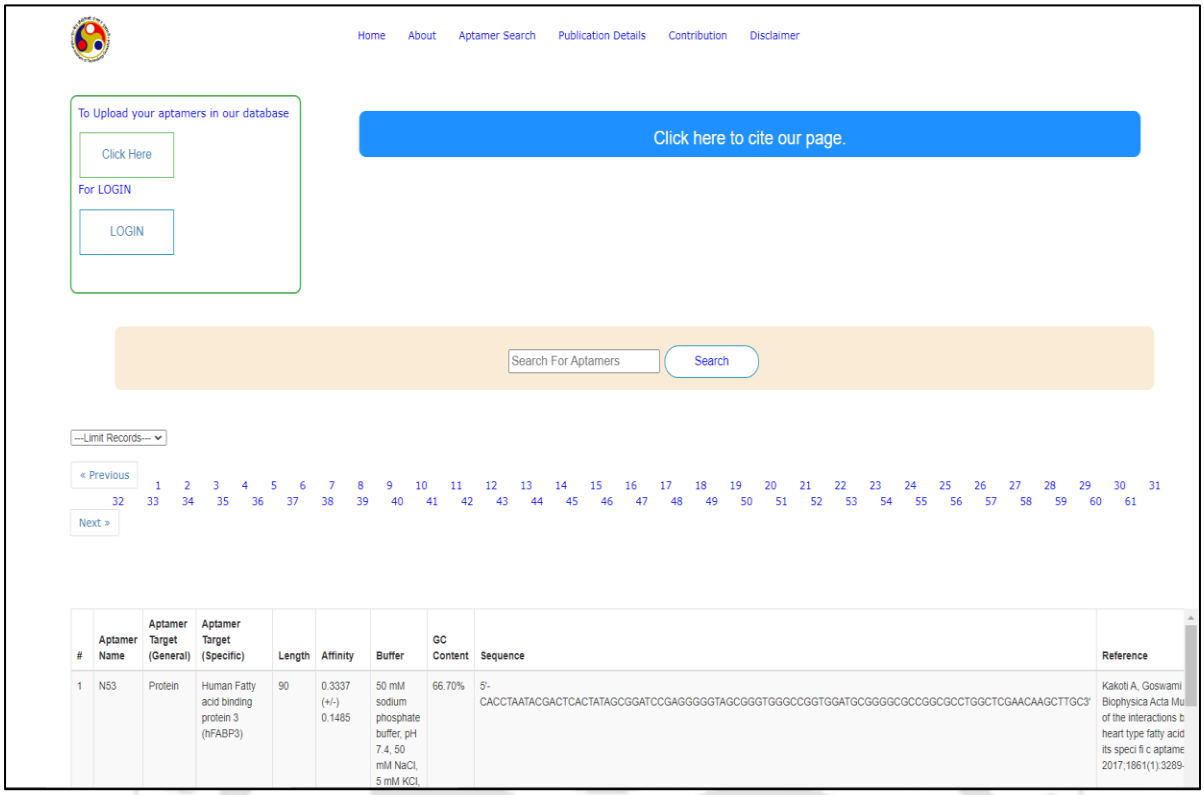

Figure 2.5: Screenshot of the aptamer search page of the Aptabase.

The updated form facilitates users to update data which is further scrutinized by mandatory information to ensure the rightness of the data which will be further verified with the reference provided by the author. An updated form is a Google form which is a two-part form (figure 2.6). Part 1 requires the data of the person uploading the information and part 2 collects the aptamer information with optional as well as mandatory fields and the last entry being the reference (https://docs.google.com/forms/d/e/1FAIpQLSdZ24RzM-a4BaqVJ9gzTzXglOfWI_MObOeUSZDj-avhvaV6nQ/viewform).

Aptamer Search page also contains login option for the administrator to add, edit, delete and also create new admin user along with their passwords. To ease the search for aptamers from the database a PHP-Bootstrap-enabled search bar is also created. The database hosts a total of 605 aptamers which are paginated with PHP limiting the number of aptamer records as per the user's choice.

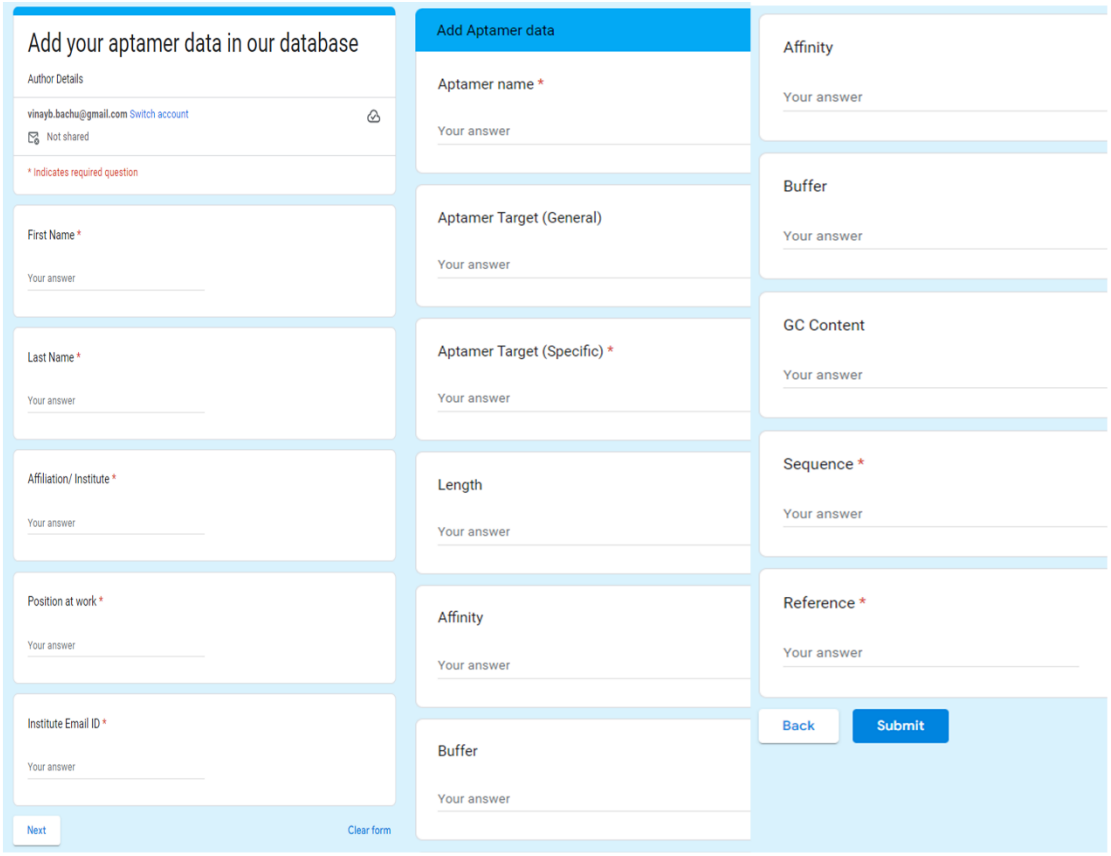

Figure 2.6: Screenshot of the update form.

A breakdown of the database records generates information for a variety of studies and also for an AI mediated/ machine learning-based analysis for further understanding of the scope and future prospects of aptamer research. Aptabase records entries of aptamers targeting different categories like proteins, small organic molecules, cells/tissues, RNA, DNA, polypeptides and other smaller subcategories. The complete breakdown of the aptamer entries is depicted in figure 2.7. Aptamers may be oligonucleotides or polypeptides which recognize and bind to a specific target. The Aptabase has entries for varied kinds of aptamers. The different categories of aptamers include DNA, RNA, polypeptide, DNA and RNA combined and modified aptamers.

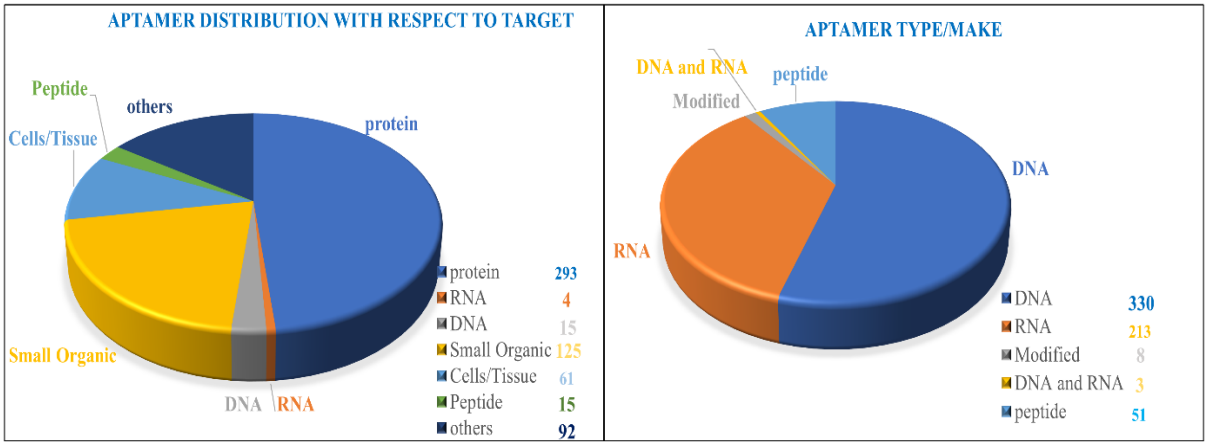

Figure 2.7: Aptamers available in the database and their distribution based on their target molecules and also the type of aptamer molecules.

The website also hosts other web pages like a details page with a basic introduction to the readers about aptamers and also about the Aptabase website (Figure 2.8). Other web pages include a publication page with a list of all the aptamer-related patents and publications from our lab and a contribution page to list all contributors and also provide contact information. The website also consists of a disclaimer page to clarify the claims and rights of the website. The current version of the database is available for viewers at https://www.iitg.ac.in/proj/aptabase/index.html.

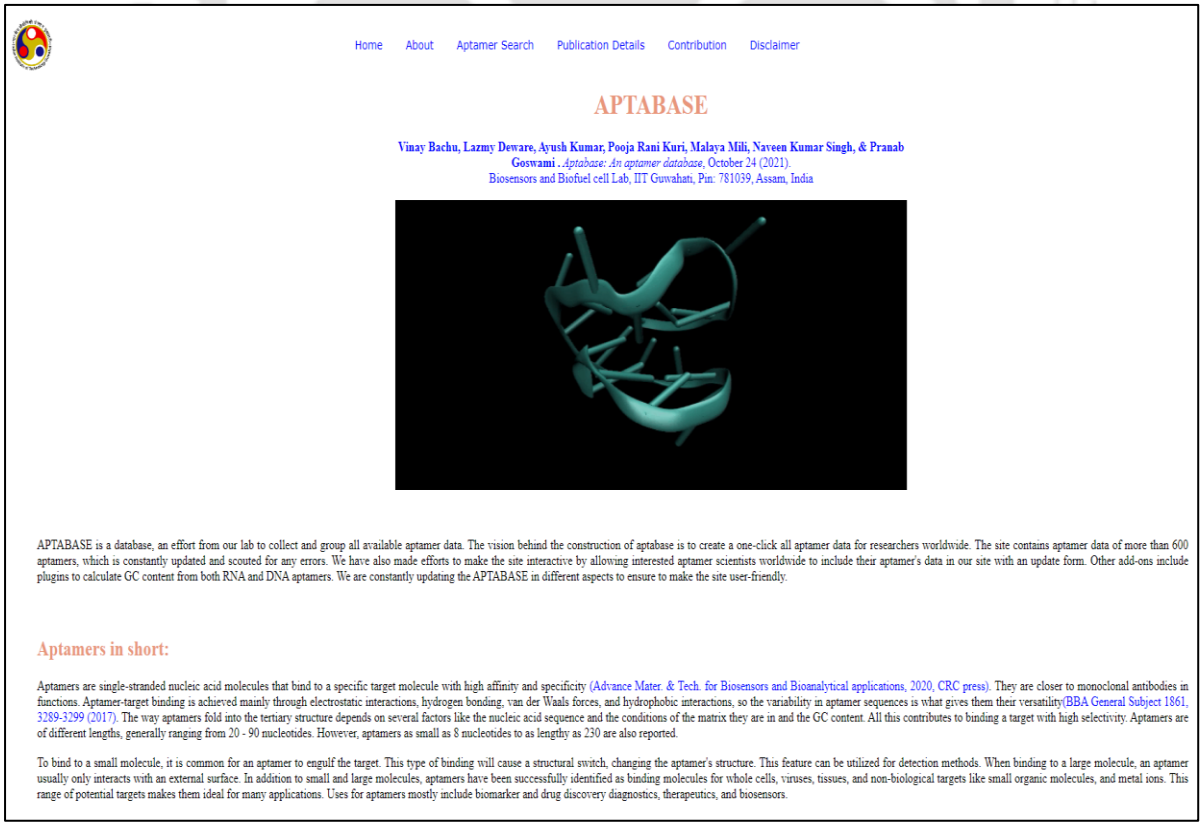

Figure 2.8: Screenshot of the aptamer information page of Aptabase.

2.4 Conclusion

There is a growing interest on aptamers among the research fraternity with respect to aptamers. Once more and more aptamers make it through the clinical trial barrier, an exponential research avenue will be explored for aptamer applications. All these factors make it extremely necessary to have a database solely focusing on aptamers. The database should be a comprehensive information platform where all aptamer related functions like GC calculations, G quadruplex identifier and other analysis can be performed. The ultimate goal of "Aptabase" is to generate interactive, user-friendly, frequently updated, multiple analytics tools-based websites. The current version of the Aptabase hosts a GC calculator, aptamer data of more than 600 aptamers and is equipped with google analytics to evaluate the traffic and also understand the user base of the site.

The Aptabase is a unique aptamer database due to its following qualities:

- Unlike its predecessors, the current database is amenable to being constantly updated.
- The database uses Google Analytics to understand the user traffic and improve the website.
- The database is equipped with an admin dashboard with a secure login; this property helps in uploading new aptamer information without any need for coding skills.

However, this current version is an initial attempt to create a one-stop access point for aptamer scientists. The future versions of the Aptabase should be equipped with a G quadruplex finder, a secondary structure generation plugin, and also an aptamer 3D structure predictor which will adequately meet the user experience and interest. Moreover, advanced curation strategies like data cleaning and automatic data ingestion process will enrich the function and maximize the usefulness of the database.

Chapter 2

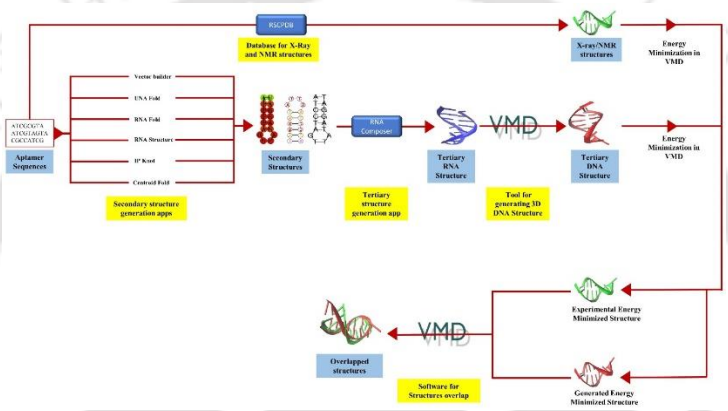

Chapter 3

An Ensemble insilico 3D Modelling of ssDNA aptamers

Chapter 3

An Ensemble insilico 3D Modelling of ssDNA aptamers

3.1 INTRODUCTION

Nucleic acid aptamers, which were first introduced in 1990 (Ellington and Szostak, 1990), are synthetic single-stranded oligonucleotides that can assume a three-dimensional shape by virtue of intra-strand base pairing, and thereby exhibit conformational specificity and high affinity to a target or a cognate ligand. Conventionally, these oligonucleotide molecules are generated in vitro by a process called SELEX (Systematic Evolution of Ligands by EXponential enrichment). Aptamers are capable of interacting with a wide variety of targets viz. metal ions, simple inorganic and organic molecules, proteins, and microorganisms. The binding process involves various non-covalent interactions such as van der Waals force, hydrogen bonds, base stacking and electrostatic interactions between the binding pockets in their organized three-dimensional structure with that of its corresponding target (Kakoti and Goswami, 2017). Intra-strand base pairing between nucleotides causes the formation of aptamer secondary structures including stems and loops. The nucleotide regions of stems and loops further undergo sequence-dependent complementarity with nucleotide regions of other stems and loops of the same aptamer, resulting in the formation of tertiary structure (Santosh and Yadava, 2014). Aptamers bind to their specific targets with high selectivity and affinity the way antibody does (Nimjee et al., 2017). Owing to its molecular recognition property and several advantages over antibodies, the application of aptamers has been intensively studied in biomedicine and analytical technologies including biosensors (Zhang, et al., 2019)

Aptamer interaction with the target biomarker/biomolecule is of immense interest as it determines the efficacy and specificity of the interaction. Thus, an in-depth knowledge on the interaction is important, for which the knowledge on the aptamer tertiary structures is equally important (Seelam, et al., 2019)(Ilgu et al., 2019). Even though a lot of progress has been made to predict the 3D structures for RNA molecules, there is no single app or method available to generate authentic 3D ssDNA structures. Hence, there is a pressing need to explore a working approach or software or application in this direction.

A few studies attempted to generate a 3D aptamer structure through modeling. However, the generated 3D structures through these approaches are in agreement with only sequences which can generate hairpin loop structures. A first of its kind utilized UNAfold which was previously called as Mfold, DNA server to generate 2D structures which were then converted into 3D coordinates in chimera/ assemble and then the 3D RNA was converted into 3D DNA with VMD Auto PSF and VMD molefacture. Then Auto IMD plugin was used to run MD simulations(Jeddi and Saiz, 2017). A second effort was from Sabri et al. (2020) that is nearly similar to the first work. The group came up with a few modifications to the initial method by changing the 3D RNA structure generation by RNA Composer and then converting them into 3D DNA with Pymol. The latest effort till date to generate 3D ssDNA generation is by Zhang et al., which combines DNA and RNA template libraries to generate the ssDNA 3D structures (Zhang, et al., 2022). Then MD simulations were performed to verify the validity of the strategy.

Current efforts in ssDNA aptamer modelling can generate 3D structures mostly for hairpin loop structures. Another limitation of the current methods is their accuracy is proportional to the accuracy of secondary structure application used in the method. In our initial search for secondary structure generation apps reveals there are six different widely used working applications namely RNA Structure (Hofacker et al., 1994), RNA Fold (Hofacker et al., 1994), Centroid Fold (Hamada et al., 2011), Vector Builder (Zuker and Stiegler, 1981), IP knots (Sato et al., 2011), and UNA fold (Zuker, 2003). It is imperative to know the exact mechanism adopted to generate a secondary RNA structure in each of these applications as it helps to understand the specific application for a given type of aptamer to predict an accurate 3D structure. The apps UNA fold, RNA Fold, RNA Structure, Vector builder are founded on minimum free energy (MFE) algorithm while, RNA fold relies on maximize the expected accuracy (MEA) function. The McCaskill function, an algorithm on which centroid fold works, is another method for generating 2D structures. McCaskill function works on the folding problem by calculating the full equilibrium partition function for generation of secondary structure and also for all the substructures (McCaskill, 1990). IP Knot also works on McCaskill and MEA function. The secondary structures acts as a fingerprint for generation of the 3D structures as the .ct files generated from these applications are the input files for RNA composer to generate 3D RNA structures. RNA composer

is a completely automated online application which is capable of converting the Vienna format 2D structure data into 3D .pdb format (Antczak et al., 2016). The application also enables the user to select the format in which the 2D structure was generated and converts accordingly.

Herein, we propose an ensemble approach to generate ssDNA 3D structures from its primary sequence. The approach explored six widely available 2D structure generation applications as mentioned above, and gives a comparative account on the accuracies of each app and also the plausible reasons of variations in the generated structure. Our strategy also highlights the need for better functional algorithms that can precisely predict ssDNA aptamer 3D structures universally.

3.2. Methodology

3.2.1. Generation of 3D aptamer structure

Initially aptamer names and their sequences were collected from Aptabase (Bachu, et al., 2021). The collected aptamers are then submitted in the RSCPDB database. Aptamers with X-ray/NMR structures were downloaded in .pdb file format. The total number of structures obtained was 60. Statistical sampling methods were followed for the selection of aptamer sequences whose 3D is to be generated. 30 aptamer candidates were finally selected randomly from the available 60 candidates.

The 30 aptamers were categorized into two classes by stratified random sampling method. Class one aptamers, which were eventually considered for the current study, consist of conventional DNA sequences, some of these contain modified nucleotides. The sample subset understudy consists of aptamers sequence length ranging from 10 to around 30 nucleotides. The class one aptamers were further divided into two sub categories on the basis of their secondary structures. The apps that were used to generate the secondary structure are RNA Structure, RNA Fold, Centroid Fold, Vector Builder, IP knots, and UNA fold. Similar secondary structures of the aptamers generated by using above six apps are categorized into first subcategory. These six available functional webservers convert the DNA and RNA sequence into its secondary RNA

structures. Apps like RNA Structure and Vector builder can also generate secondary DNA structures. However, the tertiary structure generation app considers only RNA sequences for its structure generation; hence we restricted the functions only for the RNA structures. Each of the webservers exploits a given set of algorithms like MEA, MFE or McCaskill function or a combination of the three which compute the nucleotide sequence into a predicted secondary structure. The predicted structure is only as good as the accuracy of the algorithm which is applied to generate the 2D structure. 2D structures of all 30 aptamers were generated with all 6 applications and the structures were compared by analyzing the number of bonds, the bonded pairs and the structures formed.

3.2.2. Web server for generation of 2D structure

3.2.2.1 RNA Structure Web servers

It predicts the secondary structure based on MFE and MEA. The calculations are on the basis of parameters like minimum free energy of the structure, pseudoknot prediction, partition function and the maximum predicted accuracy function. Each of the sequence is converted to 2D structures by uploading the sequence in RNA structure. All the fields were set as default and Fold DNA was attempted. The results were obtained in .ct format.

3.2.2.2 UNA fold

All possible secondary structures are approximated based on Watson-Crick base pairing and the most thermodynamically stable structures are selected. The initial sequences were selected as linear at a temperature of 37 °C and ionic concentration of 1 M of Na^+, 0 M of Mg^{2+}, computing only fold configurations within 5% from the MFE, and considering a maximum number of 50 folds with no limit to the maximum distance between paired bases. In addition to the predicted secondary structure of the ssDNA this step provides the minimum free energy of the fold.

3.2.2.3 RNA fold web server

It predicts the secondary structure on the basis of MFE function. The application also allows the user to select MFE and also MFE with partition function. Other functions include selection to omit isolated base pairs and also to have or not have GU pairs at the end of the helices. MFE and partition function along with GU base pairs were selected as input parameters for folding.

3.2.2.4 Vector builder

It is reasonably a simple application which works on MFE function. DNA sequences were inserted in FASTA format and secondary structures were obtained.

3.2.2.5 Centroid fold web application

It works on McCaskill function for generation of secondary structures. DNA sequences were inserted in FASTA format and secondary structures were generated.

3.2.2.6 IP Knot

It provides the secondary structure by MEA function using integer programming with threshold cut. IP Knots provides several adjustable parameters on the basis of the sequences. The app allows the user to select the level of prediction which is on the basis of extent of pseudoknot formation and is segmented into three levels. Level 2 prediction was selected as this option considers pseudoknots generation moderately. The applications also allow the user to select the scoring model and McCaskill scoring method was selected to generate the secondary structures.

From here on all the six applications are represented in the tables and images as ABCDEF, where in A is RNA Fold, B is Vector Builder, C is RNA Structure, D is UNA Fold, E being Centroid Fold and F being IP Knot. The predicted 2D structures were used as template for the generation of dot bracket confirmation. Dot bracket notation is a binary format of paired and unpaired DNA bases. The paired are represented in the open bracket and close bracket confirmations and the on

paired bases are represented by dots. This notation is used as the upload format for the RNA composer application.

3.2.3. Web server for generation of 3D RNA structure

The 3D RNA structures are generated by RNA composer tool, which initially converts the .ct file secondary structure data into dot bracket (Vienna format). Thus, obtained data were entered in the RNA Composer modelling server which works in two modes namely interactive mode and batch mode. The interactive mode is selected as the mode to generate the 3D structures along with option to choose the method with which the secondary structure was generated as this increases the accuracy of the generated 3D structure. In case of apps like Vector builder and RNA structure where 2D DNA structure is generated, the RNA Composer can auto convert it to 2D RNA and then generate 3D RNA structure.

The pdb files of 3D RNA structures are downloaded and launched in VMD application (Humphrey, et al., 1996). VMD is a molecular graphics program which is dedicated for molecular dynamics study and also for molecule display, analysis and modelling. VMD is equipped with several plugins which enhances the modelling capabilities. Two important VMD plugins for the current work are VMD molefacture and VMD auto PSF.

3.2.4. VMD Plugins for 3D RNA to 3D DNA conversion

i. Molefacture VMD plugin: It edits the structures and change the molecules and also the special orientation of both complex and simple molecules. The uracil molecules are converted into thymine molecules by replacing the C5 linked hydrogen atoms with methyl groups.

ii. AutoPSF VMD plugin: It is used to convert the ribose sugar backbone into deoxyribose sugars there by generating 3DssDNA structures.

iii. QwikMD VMD plugin: It is used to energy minimize all the generated ssDNA aptamer structures as well as experimentally obtained aptamers. Advanced run was selected as the method for simulation with explicit solvent conditions with 0.5mol/L salt concentration.

Minimization was performed for 10,00,000 steps or 2 ns in constant NPT ensemble condition at 370 C and 1 atm pressure with no restraints. The ensemble protocol proposed consists of different secondary structure generation applications. The data obtained in .ct format is uploaded into RNA Composer where the data is converted in Vienna format. The Vienna format notation acts as an input to the RNA composer. The generated 3D RNA structures are then converted into 3D DNA aptamers and energy minimized. The generated energy minimized structures are then overlapped over each other by VMD RMSD tool. The whole ensemble protocol is depicted in scheme 3.1.

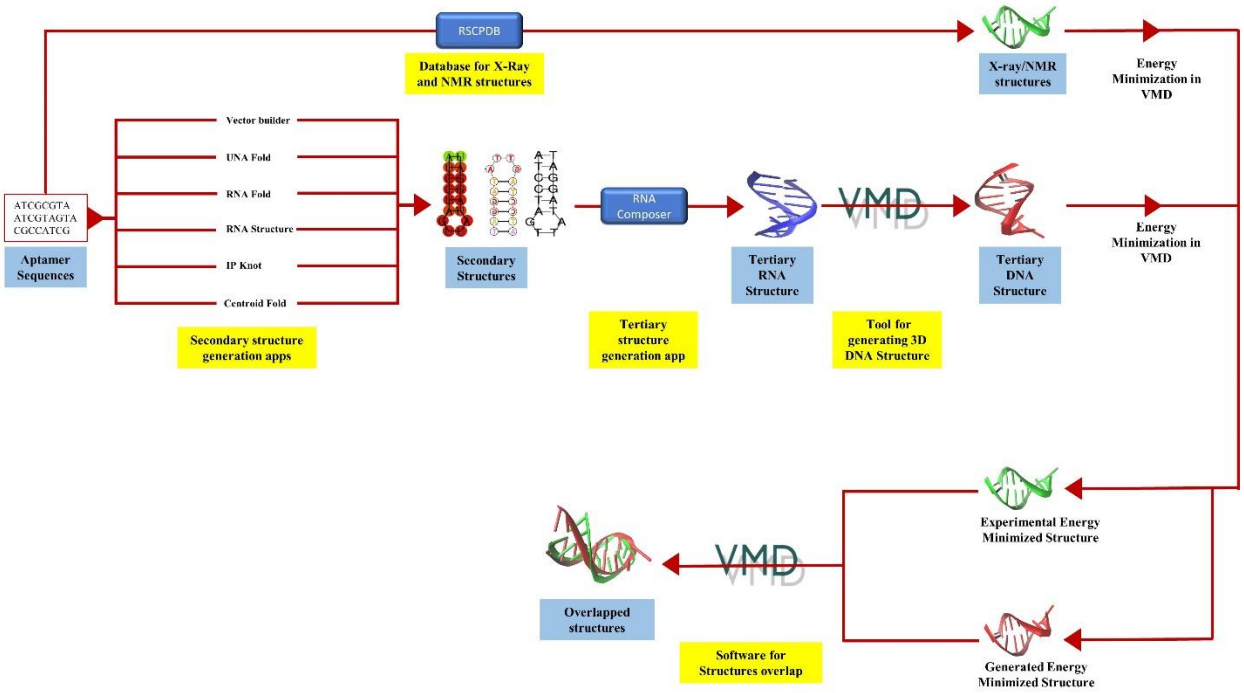

Scheme 3.1: Schematic representation of ssDNA 3D modeling.

3.3 Results and discussion

Aptamer database "Aptabase" was used to pick the aptamers. A list of aptamer was chosen for the study whose experimental pdb structures are available. After adopting the random sampling method, a list of 30 aptamers (Table 3.1) was considered for the current study. All the aptamers were analyzed based on the nucleotide sequence and the GC content, GC bond to AT bond ratio and percentage of guanine residues.

3.3.1 Secondary structure generation and analysis

Secondary structures for all 30 DNA aptamers were generated in all six applications and the generated structures were saved in .ct format and images in png format. All six different structures generated for each of the 30 were manually compared (Table 3.2) and segregated into similar structures and dissimilar structures. The secondary structures are illustrated in figure 3.1. All structures were evaluated with the initial tabulation which already had several aptamer parameters. The structures were also categorized based on the algorithms the applications used. A total 13 out of the 30 structures had the same secondary structures in all of the six applications. In all of the 30 cases, at least 2 apps generated the same secondary structure. On a cursory glance not much of a pattern emerges, but on careful examination of Tables 3.1 and 3.2 reveals few patterns. Guanine residues act as the key hindrance in the prediction accuracy of the algorithms. A higher percentage of GC content, Guanine to cytosine ratio and GC bond percentage yielded different secondary structures in different applications.

Sl/No	ID	Length	Sequence	GC%	G:C Ratio	GC bond %
1	1AC7	16	ATCCTAGTTATAGGAT	31.3	1.5	33.33333333
2	1BJH	11	GTACAAAGTAC	36.4	1	50
3	1EN1	18	GTCCCTGTTCGGGCGCCA	72.2	0.857142857	75
4	1JVE	27	CCTAATTATAACGAAGTTATAATTAGG	25.9	1.333333333	50
5	2GKU	24	TTGGGTTAGGGTTAGGGTTAGGGA	50	0.5	0
6	2L5K	23	CAGTTGATCCTTTGGATACCCTG	47.8	0.833333333	57.14285714
7	2O3M	22	AGGGAGGGCGCTGGGAGGAGGG	77.3	7.5	100
8	2M53	25	TGTGGGGGTGGACGGGCCGGGTAGA	72	5	100
9	1A8N	12	GGGCTTTTGGGC	66.7	3	100
10	1AO9	13	GAGAGAXTCTCTC	46.2	1	60
11	1AW4	27	ACCTGGGGGAGTATTGCGGAGGAAGGT	59.3	4.333333333	100
12	1CS7	13	GUTTTGXCAAAAC	30.8	1	20
13	1D16	16	CGCGCGTTTTCGCGCG	75	1	100
14	1DB6	22	CGACCAACGTGTCGCCTGGTCG	68.2	0.875	62.5
15	1DGO	18	AGGATCCTUTTGGATCCT	44.4	1	57.14285714
16	1ECU	19	GCGCGAAACTGTTTCGCGC	63.2	1	62.5
17	1EZN	36	CGTGCACCCGCTTGCGGCGACTTGTCGTTGTGCACG	66.7	1	83.33333333
18	1FV8	11	TATCATCGATA	27.3	0.5	25
19	1IDX	18	AGGATCCTTUTGGATCCT	44.4	1	57.14285714
20	1JU0	23	CTTGCTGAAGCGCGCACGGCAAG	65.2	1.142857143	57.14285714
21	1L0R	14	ACGAAGTGCGAAGC	57.1	1.666666667	100
22	1LA8	13	CGCGGTGTCCGCG	84.6	1.2	100
23	1NGO	27	CTCTTTTTGTAAGAAATACAAGGAGAG	33.33	2	27.27272727
24	1NGU	27	CTCTCCTTGTATTTCTTACAAAAAGAG	33.33	0.5	33.33333333
25	1P0U	13	GCATCGACGATGC	61.5	1	60
26	1QE7	22	CTAGAGGATCCTTTUGGATCCT	45.5	1	57.14285714
27	1SNJ	36	CGTGCAGCGGCTTGCCGGCACTTGTGCTTCTGCACG	66.7	1	84.61538462
28	1XUE	17	GTGGAATGCAATGGAAC	47.1	3	100
29	2ARG	30	TGACCAGGGCAAACGGTAGGTGAGTGGTCA	56.7	2.4	50
30	2F1Q	42	GCACTGCATCCTTGGACGCTTGCGCCACTTGTGGTGCAGT GC	61.9	1	66.66666667

Table 3.1: List of aptamers considered for 3D ssDNA modelling and its characteristics.

Different statistical methods were applied and the available data was segregated based on similarity in all apps. The initial analysis revealed the different combinations of apps generating similar structures. On further analysis based on the correlation between all three parameters, we found that a GC content of less than 50% gave similar structures in all 6 apps and above 50% resulted in different structures in different applications. This held true in 80% of cases. Further, in the remaining cases, the structures were analyzed on the G: C ratio and a ratio of 1.12 was determining factor for structural similarity and this held true in 42.85% of the remaining cases. The remaining cases were scrutinized based on GC bond percentage. In 40% of the remaining cases, a 60% GC Bond was the limit below which the structures were similar in all 6 apps. Overall, by examining all the structures first by GC content followed by G: C ratio and then by GC bond percentage the chances of similarity in all apps can be predicted by 96.67% accuracy. The structure prediction similarity in all six apps does not validate the authenticity of the generated structure.

3.3.2 Convertion of ssDNA secondary structure into 3D RNA structure

Even though all the applications work on three algorithms, the app vs app similarity (Figure 3.2) varied greatly and hence algorithm wise comparison would have also been debatable. The similarity in all six apps does not confirm the structure similarity with the experimental structures. Hence, further examinations of the generated secondary structures were carried out by generating their 3D ssDNA aptamer structures and then comparing with the experimental structures and also with each other.

The first steps in converting the secondary structures into the 3D structures involved creating the 3D RNA structures. The .ct files of all the 30 aptamers were uploaded in the tools page of the RNA composer and the file data were converted into Vienna notation which is uploaded into the RNA composer home page where the 3D RNA pdb files are generated. The generated pdb files are downloaded. The minimized structures were then edited in VMD molefacture.

Sl/No	ID	Length	Set 1	Set 2	Set 3	Set 4	Set 5
1	1AC7	16	ABCDEF				
2	1BJH	11	ABCDEF				
3	1EN1	18	ABDE	CF			
4	1JVE	27	ABCDEF				
5	2GKU	24	ABEF	C	D		
6	2L5K	23	ABDE	C	F		
7	2O3M	22	AF	B	C	D	E
8	2M53	25	ABDE	C	F		
9	1A8N	12	ABCDE	F			
10	1AO9	13	ABCDEF				
11	1AW4	27	AB	C	D	E	F
12	1CS7	13	ABF	DE	F		
13	1D16	16	ABCDEF				
14	1DB6	22	ABEF	CD			
15	1DGO	18	ABCDEF				
16	1ECU	19	ABCDEF				
17	1EZN	36	AB	CD	E	F	
18	1FV8	11	ABF	CDE			
19	1IDX	18	ABCDEF				
20	1JU0	23	ABCDE	F			
21	1L0R	14	CDEF	AB			
22	1LA8	13	ABCDEF				
23	1NGO	27	ABCDEF				
24	1NGU	27	ABCDEF				
25	1P0U	13	ABCDEF				
26	1QE7	22	ABCDEF				
27	1SNJ	36	ABF	CDE			
28	1XUE	17	ABEF	C	D		
29	2ARG	30	AB	CF	DE		
30	2F1Q	42	AB	CD	E	F	

Table 3.2: Secondary structures segregated into different sets on the basis of similarity of generated secondary structures.

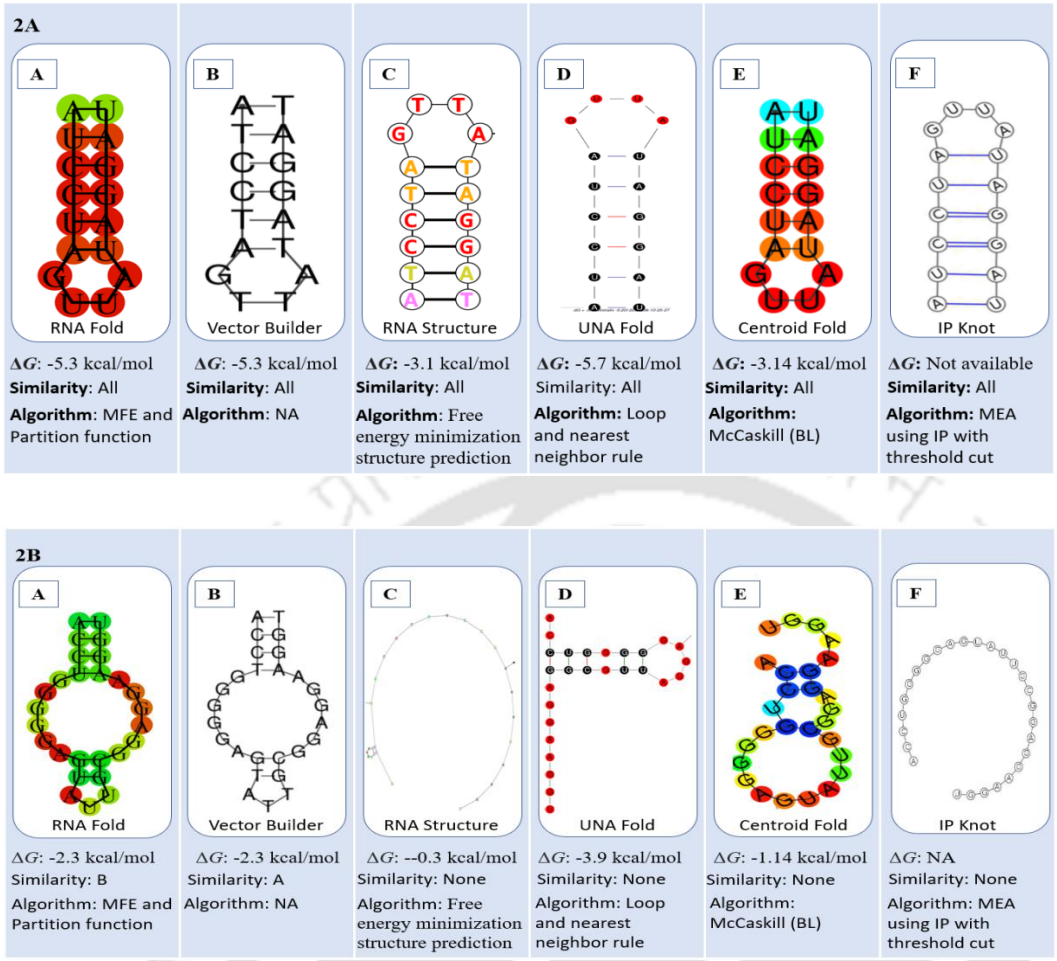

Figure 3.1: (A) Aptamer 1AC7 with all six apps giving same secondary structure, (B) Aptamer 1AW4 with different apps generating different structures.

3.3.3 3D RNA structures into 3D DNA structures

The pdb files were opened in word pad and all the hydrogen (H5) of C5 residue of the nitrogen base of the thymine residues were identified. In molefacture the H5 residue were replaced with methyl group. The altered molecules were saved in pdb format. In VMD AutoPSF plugin the above mentioned pdb files were uploaded and all the sugar moieties were converted from ribose to deoxy ribose back bone. Pdb files of the 3D ssDNA aptamers are stored and structures of all the pdb files are energy minimized in QwikMD VMD. The energy minimized structures were initially overlapped in VMD RMSD alignment tool. Both the minimized and the generated structures were

overlapped with 100 % similarity (Figure 3.3). Similarly, even the experimental structures were energy minimized.

A

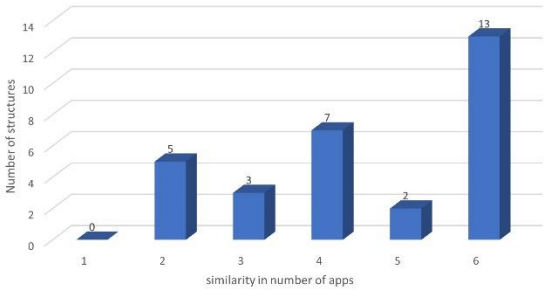

B

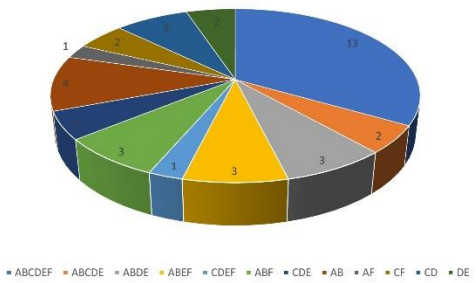

C

	A	B	C	D	E	F
A	30					
B	28	30				
C	15	15	30			
D	18	18	21	30		
E	21	21	18	23	30	
F	20	19	16	14	17	30

D

	App name	Algorithm
A	RNA fold	MFE, MEA
B	Vector Builder	MFE
C	RNA structure	MFE
D	UNA fold	MFE
E	Centroid fold	McCaskill
F	IP Knot	McCaskill, MFE

Figure 3.2: (A) Number of similar structures generated in different number of applications, (B) Pie chart of app wise similarity in different aptamer, (C) Instances of app vs app similarity in aptamer secondary structure generation, (D) Algorithms used by different secondary structure generation applications.

In case of aptamers where dissimilar secondary structures were generated, 3D RNA structures were overlapped over each other to study if there is any similarity in their 3D confirmation (Figure 3.4). The overlapping revealed in some structures (1CS7, 1EZN, 1DB6, 2ARG, 1EN1) even though the base pair formation varied, the three-dimensional orientation remained the same. This clearly illustrates as to why the secondary structure-based analysis of aptamer modelling reveals only partial information. The overlapping did not yield any significant outcome. So, we continued and moved on to the next step.

In the final step both experimental and generated structures were overlapped to check the accuracy of the ensemble method adopted in the current work (Figure 3.5).

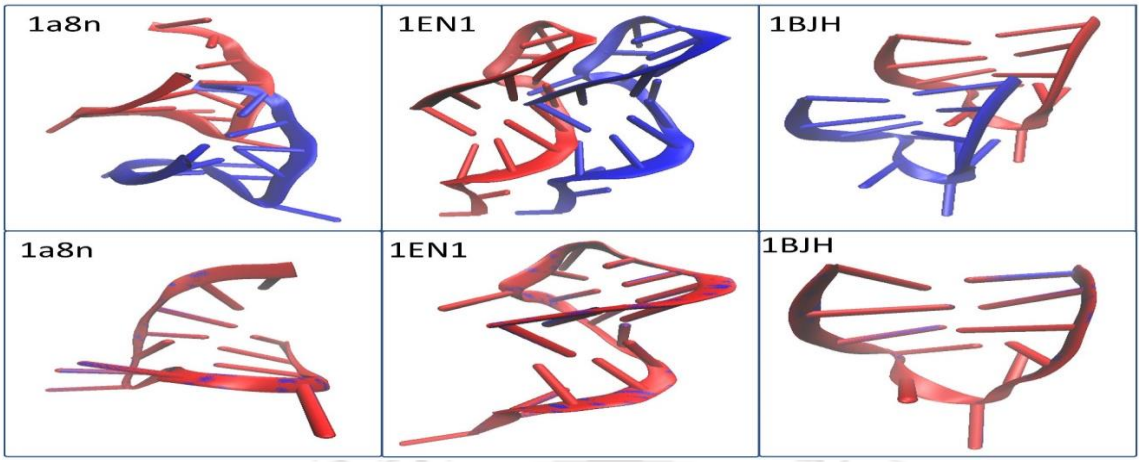

Figure 3.3: Top row: Generated 3D ssDNA aptamers in blue and the same energy minimized structures in red. Bottom row: generated aptamers and energy minimized structures overlapped of the aptamers corresponding to top row.

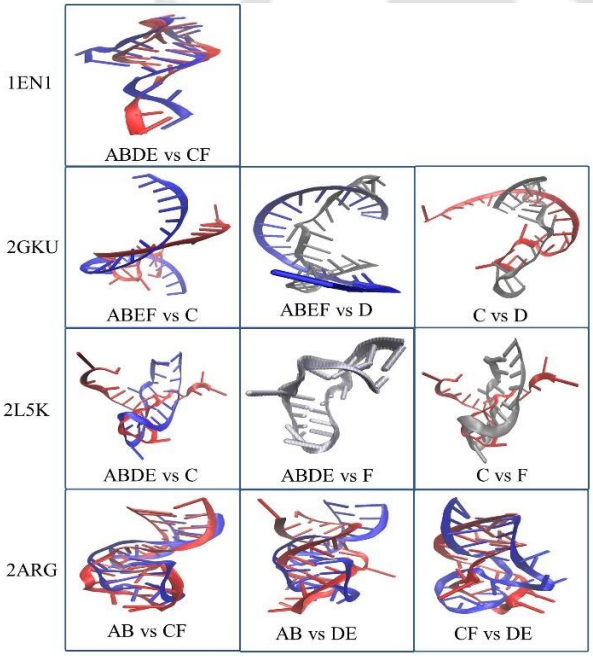

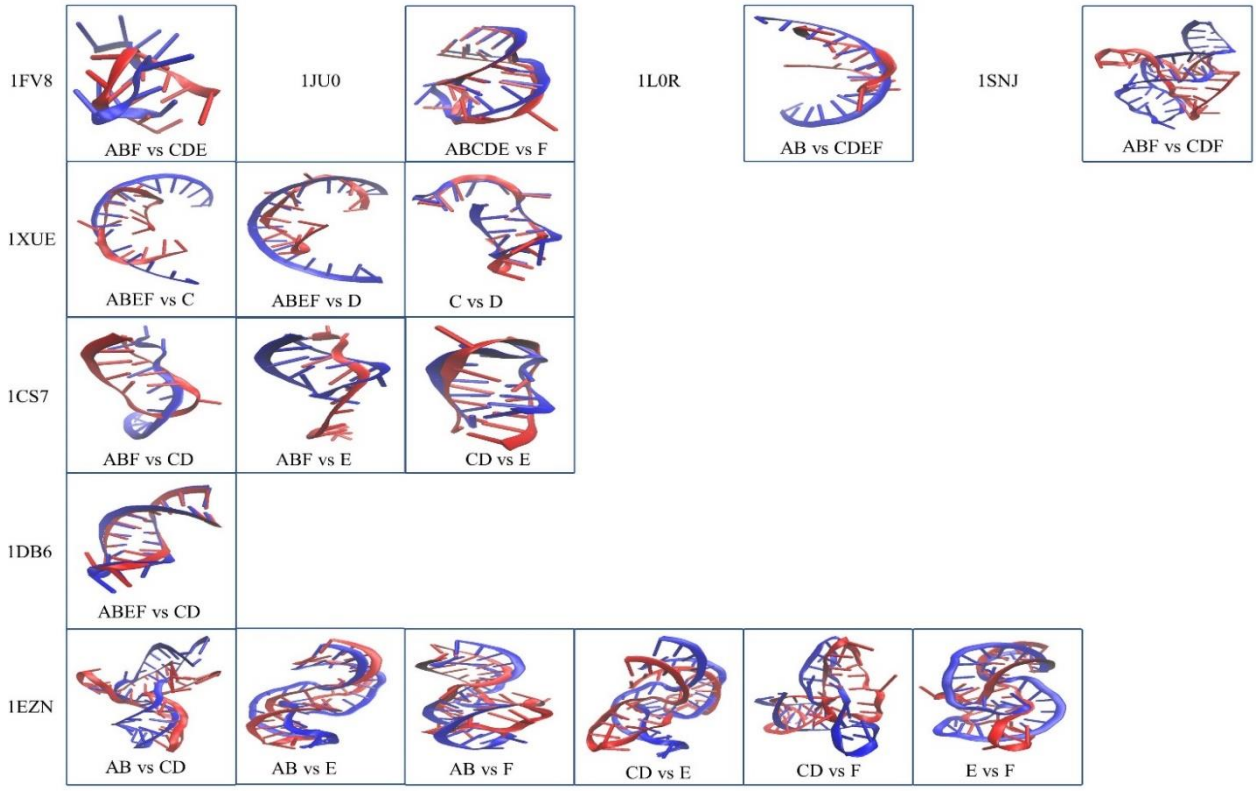

Figure 3.4: 3D DNA Structure overlap of dissimilar aptamers generated from different secondary structure generation applications. Aptamer IDs are on the left of each of the images.

The screening of the 3D DNA structures of the dissimilar apps reduced the number of overlaps to be performed for analysis. The aptamers selected for the study also includes modified aptamers like 1AO9 and our ensemble strategy could faithfully predict a structure similar to the available NMR structure. 1AO9 is a modified ssDNA aptamer which includes a modified nucleotide base at nucleotide sequence number 7 where a oct) -O-(CH2)8-O-PO2-O-(CH2)8-O-PO2- is present (Bartley et al. 1997).

Once all the 3D structures were generated from the experimental ones, the aptamers were classified into four categories based on their 3D confirmations namely hairpin, globular, helical chains and stem loop structures. This classification assists to further streamline the secondary structure generation app to be applied in the proposed ensemble process. On segregating all the 30 structures it was observed that there were four globular, three stem-loop, five helical chains and 18 hairpin structures.

After the overlap of the structures was completed the RMSD values were generated in the RMSD calculator and tabulated (Table 3.3 and 3.4). The higher the RMSD value higher is the deviation from the experimental structures. For hairpin structures generally all the apps can generate 3D structures which are acceptable. However, the RNA Structure and UNA Fold yields correct structures in 94.4% of the 18 aptamers and for stem loop structures in all of the 3 aptamers.

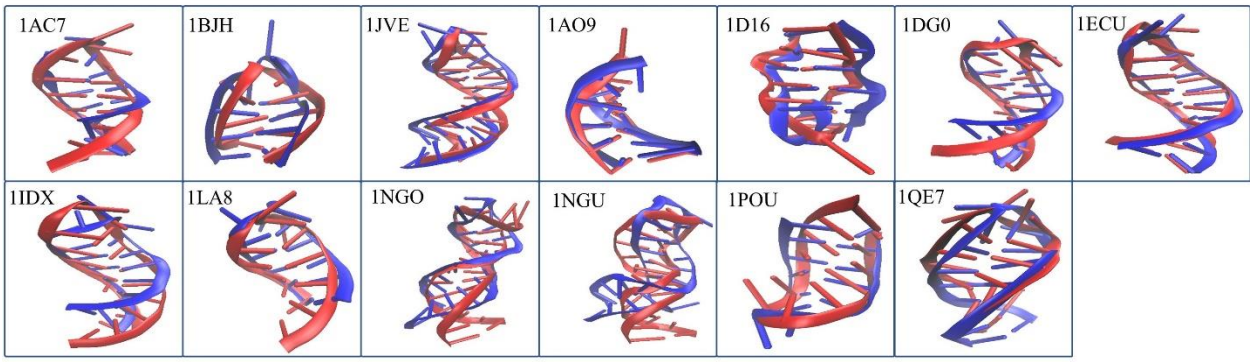

Figure 3.5: overlap of set 1 and 2 structures with their experimental equivalents, blue being the experimental structures and red the generated structures.

In case of globular structures Vector builder generated the correct structure in all 4 cases and RNA fold generated correct structures in 4 out of 5 cases in helical chain structures.

serial number	PDB ID	RMSD	Type	Sequence Length
1	1AC7	3.0781	hairpin	16
2	1BJH	3.0193	hairpin	11
4	1JVE	5.5373	hairpin	27
10	1AO9	3.482	hairpin	13
13	1D16	5.309	hairpin	16
15	1GD0	3.19	hairpin	18
16	1ECU	3.0194	hairpin	19
19	1IDX	4.055	hairpin	18
22	1LA8	2.495	hairpin	13
23	1NGO	6.8926	Helical Chain	27
24	1NGU	6.8477	Helical Chain	27
25	1P0U	3.8773	hairpin	13
26	1QE7	3.5642	hairpin	22

Table 3.3: Experimental vs generated RMSD values of set1 aptamers.

Serial number	PDB ID	RMSD						Type	Sequence Length
		RNA Fold	Vector Builder	RNA Structure	UNA Fold	Centroid Fold	IP Knot		
3	1EN1	6.85027	6.85027	**6.5549**	6.85027	6.85027	**6.5549**	Hairpin	18
6	2L5K	**5.073302**	**5.073302**	8.07522	**5.0733**	**5.0733**	**5.0733**	Hairpin	23
9	1A8N	**3.4851**	**3.4851**	**3.4851**	**3.4851**	**3.4851**	6.4208	Hairpin	12
12	1CS7	13.0178	13.0178	**2.11087**	**2.11087**	**2.11054**	13.0178	Hairpin	13
18	1FV8	4.7396	4.7396	**2.2029**	**2.2029**	**2.2029**	4.7396	Hairpin	11
20	1JU0	**7.9432**	**7.9432**	**7.9432**	**7.9432**	**7.9432**	**7.1762**	Hairpin	23
28	1XUE	10.5726	10.5726	**8.3998**	**8.88757**	10.5726	10.5726	Hairpin	17
5	2GKU	**12.72699**	**12.72699**	**12.6312**	15.5179	**12.727**	**12.727**	Globular	24
7	2O3M	16.0406	**10.2426**	14.8728	14.1211	11.8747	16.0406	Globular	22
8	2M53	**12.60003**	**12.60003**	12.7027	**12.6**	**12.6**	**12.6**	Globular	25
21	1LOR	**5.8412**	**5.1482**	6.535	6.535	6.535	6.535	Globular	14
11	1AW4	**8.1148**	**8.1148**	14.5483	13.4186	13.9711	19.0018	Helical Chain	27
14	1DB6	**7.906**	**7.906**	8.1115	8.1115	**7.906**	**7.906**	Helical Chain	22
29	2ARG	11.86272	11.86272	11.7398	**6.61905**	**6.61905**	11.7398	Helical Chain	30
17	1EZN	15.829	15.829	**10.0742**	**10.0742**	15.5727	**10.779**	Stemloop	36
27	1SNJ	15.3229	15.3229	**9.9403**	**9.9403**	**9.9403**	15.3229	Stemloop	36
30	2F1Q	15.2237	15.2237	**13.9996**	**13.9996**	19.4844	22.1612	Stemloop	42

Table 3.4: Experimental vs generated RMSD values of set 2 aptamers.

3.4 Conclusion

The approach presented here successfully gives an ensemble approach which is not only capable of generating a 3D ssDNA aptamer but also predict it with best possible accuracy. One has to adopt to increase the probability of getting an accurate 3D ssDNA aptamer which can be part of a bigger pipeline of study. We postulate here the probable reasons for the current bottleneck in aptamer modeling. The current approaches realistically predict the structures of only hairpin loop forming aptamers. The following three are believed to be the major reasons: (i) Guanine residues play a key role in the aptamer tertiary structure and also in the algorithms which generate secondary structures. (ii) There was a clear limiting factor in the GC content (50%), GC bond percentage (60%) and G:C ratio (1.12). In majority of the case sequences that crossed this barrier had dissimilar secondary structures. (iii) Even though all the apps in this study were a combination of the MFE, MEA and McCaskill functions, there was a marked variability in the structures generated.

This chapter also illuminates the relationship of the secondary structure generation apps and RNA Composer. In some of the aptamers the secondary structures predicted dissimilar structures

whereas the RNA composer generated structures with 100% similarity. The similarity of the algorithms used is the predominant reason for the observed discrepancies. It also indicates the need for better algorithms which can yield appropriate structures in cases where the current algorithm fails. Better understanding of the role of guanine residues may help in creating algorithms which are suited for such instances. We have successfully classified the 3D aptamer structures in to different categories based on their 3D confirmation and based on which we have successfully adopted a dynamic ensemble strategy which filters out the secondary structure generation app which needs to be harnessed for generating the 3D aptamer structure. “RNA Structure” and “UNA Fold” web applications works best for hairpin and stemloop structures while “RNA fold” works best for helical chains and “Vector builder” works best for globular structures. The study also used structures which had modified aptamers like 1AO9 and 1CS7 whose structures were generated easily with the VMD plugins mentioned in our ensemble approach.

A few other applications, like Contrafold and Contextfold, have attempted different approach for secondary structure generation. Contrafold generates secondary structures on the basis of conditional log-linear models (CLLMs), which is a probabilistic method comes under stochastic context-free grammars (SCFGs) (Do at al. 2006). These kind mechanisms are predicted using predominantly MEA function. However, these methods work on machine learning (ML), which requires a huge data set to train the model and thus a laborious and uncharted task. Other applications, like Contextfold, have stimulated interests among aptamer scientists. Contextfold also depends on a ML approach for generating secondary structures and is also based on SCFG method (Zakov et al., 2011). These two applications tend to avoid all the physics-based parameters such as thermodynamic parameters. A reliable 3D ssDNA aptamer construct is essential for an in depth understanding of aptamer-ligand interactions, usually studied by molecular dynamics (MD) simulations approach. Hence, the analyses presented herein will greatly help the scientist in the field to design aptamers for various applications.

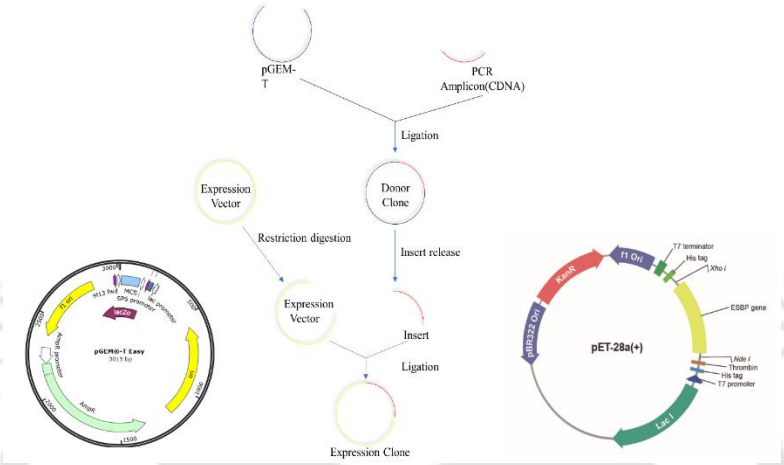

Chapter 4

Cloning , Expression, Purification and Charecterization of cTnT and sTnT

Chapter 4

Cloning , Expression, Purification and Charecterization of cTnT and sTnT

4.1 Overview

Cardiac troponin T (cTnT), I (cTnI) and c (cTnC) are part of the troponin complex. Among these troponins, cTnT and cTnI are unique to cardiomyocytes, while the cTnc is similar to the ones present in smooth skeletal (sTnT) and fast skeletal muscle cells (fTnT). cTnT is a structural protein and is unique in its structure and amino acid sequence in comparison to its skeletal muscle counterparts. sTnT has a 64% DNA sequence similarity and a 53% amino acid similarity with cTnT projecting it as an ideal control protein for studies of cTnT. cTnI has a DNA similarity of 51% and amino acid sequence similarity of 13.89% with cTnT. cTnT is released into the blood serum in the event of necrosis making cTnT an ideal biomarker for acute myocardial infarction (AMI).

This chapter describes cloning, purification, and characterization of cTnT protein and its control protein sTnT. We have expressed both these proteins with Histidine-tag with an aim to simplify their purification and immobilization, which aids the process of extracting the proteins involved in some experiments in the later chapters of this thesis work.

4.2 Experimental procedures

4.2.1 Materials

pANT-cGST clones of human cardiac troponin(*cTnT*) and smooth skeletal troponin (*sTnT*) were purchased from the DNASU Plasmid Repository (USA). Primers were synthesized from Bio serve Biotechnologies India Pvt. Ltd. BioMix™ Red PCR kit was obtained from Sigma Aldrich. Luria-Bertani (LB) agar/broth, ethidium bromide (10 mg/mL), calcium chloride ($CaCl_2$), magnesium chloride ($MgCl_2.6H_2O$), magnesium sulphate ($MgSO_4.7H_2O$), potassium chloride (KCl), tris base, ethylene diamine tetra acetic acid (EDTA), lysozyme, buffer saturated phenol were obtained from HiMedia® , Bengaluru, India. The SYBR Gold (10000X) was procured from Invitrogen (USA). pGEMT easy vector was purchased from Promega (USA). The pET28a and pCOLD-II vector were procured from Novagen (India), and Clontech (USA), respectively. Ni-NTA Hi-Trap column procured from GE healthcare (India). PVDF membrane (Hybond P) was procured from Amersham. Anti-His primary antibody and HRP tagged secondary antibody were purchased from bibiotech India. The 3,3'-diaminobenzidine (DAB) was from Amresco based in USA. The quick ligation kit

and Gel extraction kit was purchased from New England Biolabs and Sigma Aldrich, respectively. The TA cloning kit which contains the pGEMT vector along with DNA ligase, ligation buffer was obtained from Promega (USA). All other chemicals used in this chapter for experiments were of analytical grade and the sources of these chemicals have been cited under the methodology, wherever necessary.

4.2.2 Bacterial cell culture

E. coli DH5α and *E. coli* BL21 strains were cultured and cell lines were maintained for cloning and expression of recombinant clones, respectively in the present study. The clones as well the cells were stored as glycerol stocks at -80^0 C. LB broth and LB agar were used for the culturing and plating in which antibiotic (kanamycin: 50µg/mL, ampicillin: 100 µg/mL) was included when required. The culturing conditions were 37^0 C and a constant rocking at 180 rpm in a shaker incubator. The strains used and the media compositions are mentioned in table 1.1 and 2.1 in the appendix section.

4.2.3 Quantification of DNA

DNA was spectrophotometrically quantified using UV-Visible nanodrop spectrophotometer (Implen nanophotometer). Samples were prepared in water and the optical densities (O.Ds) were measured at λ_{260nm} and at λ_{280nm}. Prior to which, blank was set in the instrument with nuclease free water at λ_{260nm} and λ_{280nm} followed by sample measurements at aforesaid wavelength. Concentrations of DNA samples were calculated from the optical densities obtained after using suitable dilution factors.

4.2.4 Protein estimation

Bradford assay was followed for the protein estimation considering Bovine serum albumin (BSA) as the standard (Bradford., 1976). The concentrations were determined at λ_{595nm} using Coomassie Brilliant Blue (CBB) G-250.

4.2.5 Plasmid DNA isolation

A single bacterial colony was picked up from the plate and inoculated into 5 mL of LB broth and incubated for 16 to 18 hr at 37^0 C with vigorous agitation. The cells were then recovered by centrifugation at 8000 rpm for 5 minutes. The supernatant was then decanted, and the pellet was re-suspended in 100 µL of alkaline lysis solution 1 (table 3.1 in appendix). To the above, 200 µL of freshly prepared alkaline lysis solution 2 (table 3.1 in appendix) was added and mixed by inverting the microfuge tubes, which were then stored at 25^0 C for 5 minutes. To the above solution, 150 µL of ice-cold solution 3 (table 3.1 in appendix) was added and homogenized by inverting. The mixture was then stored in ice for 5 min. The solution was centrifuged at 12000 rpm, for 5 minutes at 4^0 C. The supernatant was transferred to a fresh tube and, to it RNase (A) was added to make a final concentration of 100 µg/ml and incubated at 37^0 C for 1 hr. Equal volumes of tris saturated phenol: chloroform was added and inverted the mix until the phases mixed properly. The solution was then centrifuged at 13000 rpm, for 5 minutes at 4^0 C. The aqueous phase was transferred to a fresh tube and an equal volume of isopropanol was added to it. The solution was mixed by inversion to precipitate DNA and incubated at -20^0 C for at least an hr. The solution was then centrifuged at 13000 rpm, for 5 minutes. Ethanol was discarded and blotted over paper to remove traces of ethanol. Pellet was air dried and suspended in 30 µl of autoclaved milli Q water. The preparation was checked by agarose gel electrophoresis (table 3.2 in appendix) and absorption spectroscopy.

4.2.6 Agarose gel electrophoresis

DNA samples were analyzed in agarose gel (0.8-1.5% containing 0.5 µg/ml of ethidium bromide) by electrophoresis. The electrophoresis was performed at 80 V in 1x TAE buffer till the desired resolution was achieved. The gel was then visualized on a UV transilluminator to observe the DNA bands and then documentation was done by a gel documentation system (ChemiDoc XRS+ Imaging System, BIO RAD) for future reference. The elution of DNA from the gel was carried out by gel extraction method using GenElute Gel Extraction kit (Sigma Aldrich, USA) following the manufacturer's protocol.

4.2.7 Polymerase Chain Reaction

4.2.7.1 Primer designing

Nucleotide sequences of *cTnT*, *sTnT* retrieved from NCBI were used to design primers with the help of Serial Cloner v2.6.1 to amplify the corresponding genes. Primers were flanked with Bam HI and Xho 1 for *cTnT,* Xho 1 and EcoR 1 for *sTnT* to generate restriction sites for creating cohesive ends. The primer sequences are depicted in the table 4.1 (appendix).

4.2.7.2 PCR

PCR was performed to amplify the genes for cloning into TA vector. Based on the average optimum melting temperatures (T_m) of both forward and reverse primers an annealing temperature was set for each of the gene. The following reaction mixture was set in a sterile 0.2 µL PCR tubes. The PCR cycling conditions were set as mentioned in table 5.1 in the appendix. PCR amplicons were resolved on 0.8 % agarose (w/v) at 80 V for 60 minutes.

4.2.7.3 Purification of PCR amplicons

Sigma PCR clean up Kit was used to purify the insert in order to remove the enzymes and buffers that may interfere with the downstream process. To one volume of the PCR product, 5 volumes of binding buffer was added and mixed thoroughly. A column was placed in a 2 ml collection tube and the suspension prepared previously was added to this setup. The column was centrifuged at 11,000 rpm for 30 seconds at room temperature. The flow through was discarded and the column was washed by adding 250 µl of Wash Buffer and centrifuging at 11,000 rpm for 30 seconds at room temperature. The flow through was discarded and diluted Wash Buffer II (1 volume of wash buffer II with 4 volumes of absolute ethanol) was added to the column and the column was centrifuged at 11,000 rpm for 30 seconds at room temperature. It was then kept open for 2 minutes at 70 ˚C for ethanol to evaporate. Purified PCR was eluted into a fresh vial with 15 µl of molecular grade water and the eluted amplicon was stored at -80 ˚C.

4.2.8 Restriction digestion of *cTnT, sTnT*

cTnT was double digested using Bam HI and Xho 1 to create cohesive ends complimentary to the vector, while *sTnT* was double digested with Xho 1 and EcoR 1 to create cohesive ends complimentary to the vector. The following reaction mixture was set and incubated at 37 °C for 1 hr. The reaction compositions for *cTnT* and *sTnT* are depicted in the table 6.1 (appendix)

4.2.9 Ligation of *cTnT, sTnT* into pGEMT easy vectors and pET-28a (+) vectors

4.2.9.1 Ligation into pGEMT easy vectors

The PCR extraction solutions of all three troponins were ligated into the pGEMT easy vectors following the reaction composition mentioned in table 6.2 (appendix). The reaction was carried out at 4^0 C overnight for maximum ligation efficiency. About 50ng of the ligation mixture was mixed with competent cells *E.coli* DH5α and then cells were plated onto LB agar with ampicillin as the selection marker. The positive clones were selected and then confirmed by restriction digestion.

4.2.9.2 Ligation into pET-28a (+) vectors

Vector and inserts were activated by digesting with the restriction enzymes specific for each of the troponin. The digested DNA fragments were extracted from the agarose gel by gel extraction kit. Vector and insert were used in the ratio of 1:3, 1:5 and 1:7 respectively for ligating into pET-28a (+). The multiple ratios were attempted as it increased the probability of ligation. Based on the size and concentration of the vector and insert, reaction volumes were prepared as mentioned in table 6.3 (appendix). The reaction mixture was made up to 20 µL with nuclease free water. Control tubes with only vector and vector with ligase was also set to omit non-recombinant background. The reaction tubes were kept at 16 °C overnight. After ligation 1 µl of ligated mixture was transformed into competent cells and plated on LB kanamycin plates. The plates were incubated at 37 °C for 12 – 16 hr.

4.2.10 Competent cell preparation

E.coli DH5α cells were revived on an LB plates and incubated overnight for 16-18 hr at 37 °C. A bacterial colony was picked up from the plate and inoculated into 5 mL of LB broth (primary culture) and incubated for 16 to 18 hr at 37 °C with vigorous agitation. A secondary inoculation was performed with 1 mL of the above culture (primary culture) into 100 mL of LB broth in a conical flask and incubated at 37 °C for about 3 hr. Optical density (OD_{600nm}) was constantly monitored till it reaches OD 0.25-0.3. The bacterial cells were then transformed to sterile, disposable, ice cold 2mL Eppendorf tubes and cooled to 4 °C by storing on ice for 10 minutes. Cells were then recovered by centrifuging at 1000 g for 5 minutes at 4 °C. Discard the supernatant and resuspend the pellet in $1/10^{th}$ volume of TSS solution (table in 3.3 appendix) and make a suspension. Aliquot of the cells were prepared and stored at – 80 °C till further use.

4.2.11 Transformation of competent cells

The competent cells collected from -80^0C microfuge were kept on ice for 10 minutes. To the 100 µL of the competent cells, 10-50 ng of DNA was added (in a volume of 10 µL or less) and mixed by swirling and incubated on ice for 30 minutes. The cells were given a heat shock at 42 °C (for 45 seconds for *E. coli* DH5 α and 90 seconds for *E. coli* BL21) in a water bath. The tubes were then immediately transferred onto ice and incubated on ice for 2 minutes. LB broth (900 µL) was added to the transformed cells and incubated at 37 °C for 1 hr. Required aliquots of the transformants were taken and plated on LB agar plates containing kanamycin (50 µL) and incubated at 37 °C for 12 – 16 hr.

4.2.12 Cloning of *cTnT, sTnT*

The complete strategy used for cloning *cTnT* and *sTnT* is depicted in Figure 4.1. The troponins ORF were amplified by PCR from the cDNA obtained from DNASU in pANT-cGST clones which were non-expression vectors. Primer sets were designed with restriction sites to facilitate the cloning. The amplified PCR cDNA fragments were cloned in to into pGEMT easy vector through TA cloning kit as describe earlier. The positive clones were isolated and restriction digestion was performed to release from the pET-28a (+) vector. The vector was also digested with the same

restriction enzymes mentioned earlier, followed by ligation of the insert and the vector performed. The ligation mixture was transformed into *E. coli* DH5 α competent cells. The transformed cells were selected over selective LB agar plate containing (Kanamycin for pET28a) antibiotics after overnight incubation at 37 °C. The recombinant clones were further confirmed with restriction digestion resulting in release of appropriate size of insert and vector. The single isolated colony of selected clones for *cTnT, sTnT* were confirmed by sequencing and the recombinant plasmids (insert+ vector) were further transformed to *E.coli BL21* cells for higher expression yield of the recombinant proteins.

4.2.13 Expression of His-tagged cTnT, sTnT in *E. coli* BL21 (DE3)

A fresh colony of *E. coli* BL21 with pET 28 a (+) cTnT, sTnT each were inoculated in 5 ml of LB media containing kanamycin (50 mg/L) as primary inoculum and incubated at 37^0 C overnight. This was further subcultured in 100 ml of LB media as a secondary inoculum with the same concentration of kanamycin till an O.D. of 0.6-0.8 is achieved. Expressions of the recombinant proteins were induced with Isopropyl *β*-D-thiogalactopyranoside (IPTG) of 0.2 mM for sTnT for 8 hr at 25^0 C and for cTnT 0.4 mM incubated for 12hr at 37^0 C with a shaking at 180 rpm. Cells were harvested by centrifugation at 10000 x g and resuspended in 50 mM sodium phosphate buffer, pH 7.4. The cells were then subjected to sonication using an ultrasonic processor (Hielscher) at 25 % amplitude with 0.5 cycles at 4^0 C till the lysate appeared translucent. The homogenate was clarified by centrifugation at 12,000 x g for 40 mins at 4^0 C. The supernatant was collected and stored at 4^0 C for further processing.

4.2.14 Purification of His tagged troponins

The supernatant was passed through Ni-NTA column at a rate of 0.5 ml min^{-1} then column was washed with 20 bed volumes of washing buffer for all three troponins. The elution of bound recombinant proteins from column was achieved at a flow rate of 0.5 ml min^{-1} with elution buffer for troponins. The purified recombinant cTnT was dialyzed against 50 mM Tris, pH 7.4 for overnight, where urea concentration was step-down from 8 M to 0 M in a step of 1 M difference. The composition of solutions used for protein purification have been listed in table appendix 3.4.

4.2.15 Sodium dodecyl sulphate polyacrylamide gel electrophoresis (SDS-PAGE)

The protein purified with Ni-NTA (nickel-nitrilotriacetic acid) affinity chromatography was analyzed through SDS PAGE electrophoresis (Laemmli, 1970). The 1-2 µg of recombinant protein or crude cell lysate was mixed with 5X SDS loading dye and denatured by heating in boiling water bath for 5 min. The denatured sample along with pre-stained protein ladder (Broad range NEB ladder, USA) was loaded into SDS-PAGE gel. The electrophoresis was performed over a discontinuous buffer system with a 5 % stacking gel on top of a 10 % separating gel, with a thickness of 0.75 mm at a constant voltage of 100 V in a MiniVE vertical electrophoresis unit (GE Healthcare). The separated protein bands were visualized over gel by using "Blue silver staining" protocol of Candiano *et al.,* 2004, where colloidal Coomassie G-250 (Sigma Aldrich, USA) (Table A3, appendix) was the staining dye.

4.2.16 Western Blot

Western Blot analysis was performed to check the recombinant protein expression in bacterial systems. Recombinant proteins were resolved by SDS-PAGE (12% gel) in the MiniVE vertical electrophoresis unit at 100 V. The electrophoresed protein gels were transferred to PVDF (Poly vinylidene fluoride)) membrane at a fixed voltage of 25 V, 300 mA for 3-4 hr at 4^0 C in Blot module (GE Healthcare). The membrane was carefully taken out from the electro-blotting module and transfer of proteins on membrane was confirmed by Ponceau S staining (Sigma). Membranes were then washed with sodium phosphate buffer, pH 7.4 (PBS) containing 0.1 % Tween 20 (PBS-T) for 10 mins to remove the Ponceau S stain. The buffer was discarded, and the membrane was washed again with PBS on a shaker.

The membrane was then blocked with blocking buffer (Table 3.6 in appendix) supplemented with 5 % BSA overnight to prevent non-specific adsorption. The blot was then washed with an excess of PBS-T three times for 10 min each. The wash buffer was discarded, and the membranes were then incubated with monoclonal anti-His antibody as the primary antibody (Sigma) using an optimized concentration in PBS containing 1 % BSA for 2 hr at room temperature. The membrane was washed three times with PBS-T for 10 mins each. This was followed by incubation with secondary antibody (HRP modified anti-rat IgG) from R&D systems (USA) appropriately diluted in

PBS (1 % BSA) for 1 hr at room temperature with slow shaking. Thereafter the membrane was thoroughly washed with PBS for three times. Finally, the blot was developed using 3, 3'-Diaminobenzidine (DAB) tetrahydrochloride hydrate (Amresco, USA) at a concentration of 4 mg per 10 ml of PBS and charged with 10 µl 30 % hydrogen peroxide (Sigma Aldrich, USA) followed by imaging with a gel documentation system (ChemiDoc XRS+ Imaging System, BIO RAD).

4.2.17 Circular dichroism study

Circular dichroism (CD) spectra of the proteins were recorded using a spectropolarimeter (J-815, Jasco, Japan) calibrated with 0.06 % (w/v) aqueous solution of (±)–10– camphorsulfonic acid. The spectrum was recorded in the wavelength range of 190-240 nm, in 0.1 cm path length suprasil quartz cuvette at 25^0 C, at a scan rate of 100 nm/min, 1 nm bandwidth resolution, with a time constant of 2 s and the scans were performed five times and average of them were considered. The spectrum was corrected for baseline and smoothed by Savitsky–Golay filter using Jasco spectral analysis software. The secondary structure analysis was performed using the Dichroweb web server.

4.2.18 Matrix- assisted laser desorption ionization- mass spectroscopy (MALDI-MS)

The molecular mass of the recombinant cTnT and sTnT proteins was confirmed by MALDI-MS (4800 plus MALDI TOF/TOF (time of flight) Analyzer, AB SCIEX, USA) analysis. The expected molecular weight of cTnT and sTnT protein were ~35 kDa and ~32 kDa, which are in a suitable range for the matrix (Sinapinic Acid - 10 to 150 kDa) for MALDI analysis. The as prepared content with the monomeric form of the protein was mixed with saturated solution of sinapinic acid and then the spectra were collected in a positive mode with each spectrum being an averaged for 100 shots.

4.2.19 Determination of Isoelectric point (p*I*)

The p*I* of the purified recombinant cTnT and sTnT was measured by zeta potential study on Zetasizer nano series (Malvern Instruments limited, U.K). The zeta potential was measured in 50 mM appropriate buffers covering pH range from 2 to 10 in capillary cell (DTS1070 - Malvern instruments limited) equipped with a gold platted Beryllium/Copper electrode. A graph was

plotted between the measured zeta potential values and the corresponding pH values. The p*I* of *cTnT* and *sTnT* was identified from the pH scale at which zeta potential is zero.

4.3 Results and discussion

4.3.1 Cloning and expression of human cardiac troponin T (*cTnT*), and slow skeletal troponin T (*sTnT*)

The strategy used for cloning has been illustrated in the scheme 4.1. Plasmids for *cTnT, sTnT* were purchased from DNASU Plasmid Repository in the form of pANT-cGST clones. The plasmids however were non-expression vectors and hence the genes had to be sub cloned initially into pGEM-t easy vector system and then into pET- 28a (+) expression vector.

The gene fragments of *cTnT, sTnT and* were initially augmented from the pANT-cGST clones by specific primer sets which were designed with specific restriction sites to aid cloning. The DNA fragments were amplified by PCR using specific primers for respective genes (Figure 4.1 A). The amplification conditions were standardized, and then the PCR product was extracted by gel elution kit of Sigma. The amplified fragments were first cloned into pGEM-t easy vector system (Figure 4.1 B). The reaction composition and conditions were stated earlier. The recombinant clones were confirmed by insert release. The results of which are shown in the figure 4.1. The released inserts were extracted by gel elution. pET- 28a (+) vector was activated by digesting the vector with restriction enzymes specific for the *cTnT, sTnT* fragments.

The *cTnT and sTnT* genes which were eluted from gel were then ligated with pre-digested pET-28a (+) vector followed by transformation into DH5 α by heat treatment. The recombinant clones were confirmed by insert release and PCR. The results of which are shown in the figure 4.2. Plasmids were extracted from the recombinant *E.coli* DH5 α and were transformed into *E.coli* BL21 for the purpose of expression.

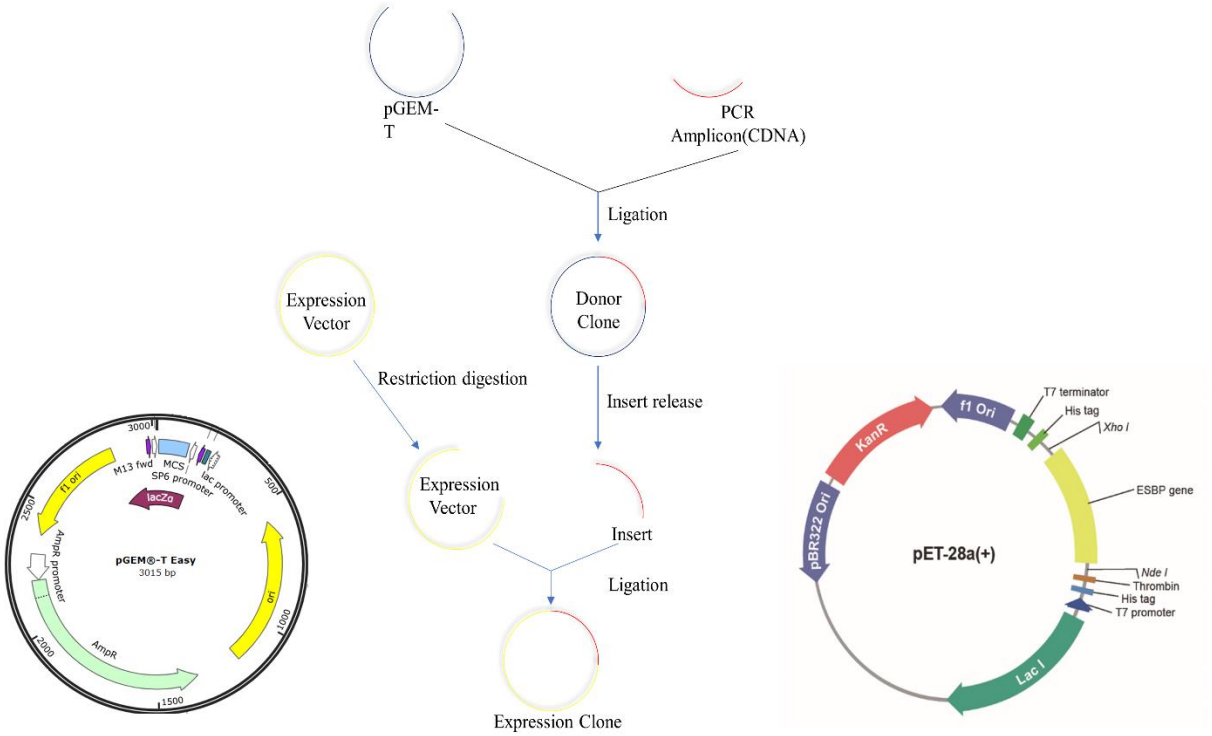

Scheme 4.1: Schematic representation of the cloning methodology adopted for the current work.

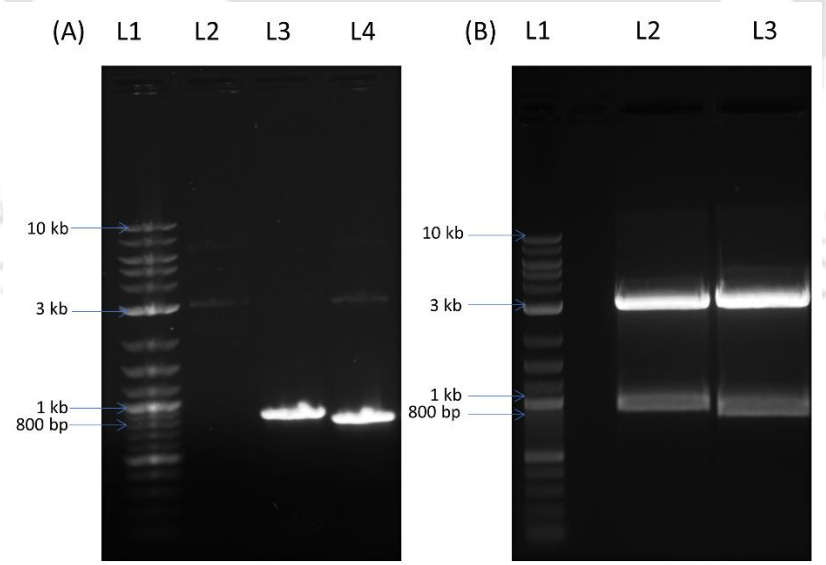

Figure 4.1: (A) PCR amplification of *cTnT* (~1 kb) in L3 and *sTnT* (~1 kb) in L4 observed in 0.8% agarose gel stained with Ethidium Bromide (EtBr). (B) Insert release of cTnT in L2 and sTnT in L3 from pGEMT vector.

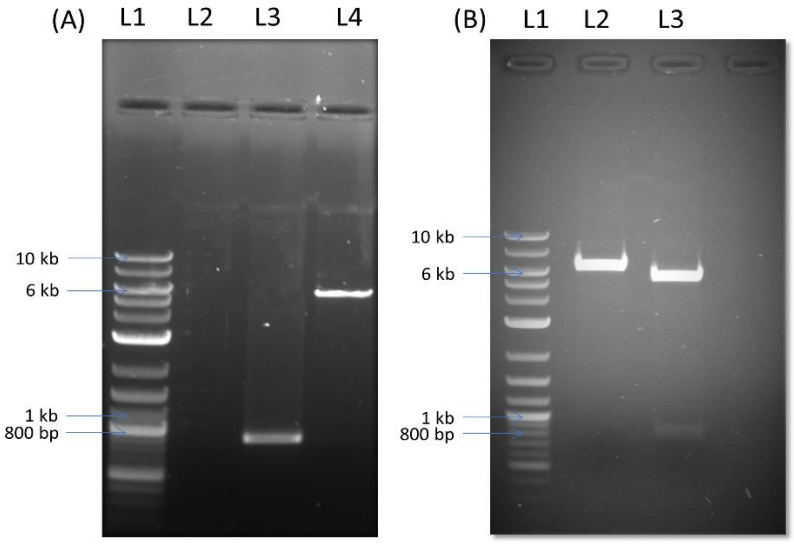

Figure 4.2: Confirmation of recombinant plasmids by restriction digestion of (A) *pET 28a_cTnT*: (L3) PCR amplicon of the recombinant plasmids: cTnT: 870 bp and sTnT, (L4) Restriction digestion of *pET 28a_cTnT*. (6.25 kb) (B) *pET 28a_sTnT*: (L2) Single restriction digestion of *pET 28a_sTnT* with Xho1 (6.2 kb) and (L3) insert release of *sTnT* (831 bp).

4.3.2 Expression and purification of cTnT, sTnT

The expression profile of these recombinant proteins was studied in soluble supernatant fraction of lysed recombinant *E. coli* cells (Figure 4.3). The optimum temperature and incubation time study were performed for both the proteins for maximum expression. The study revealed the average incubation time for sTnT was 8 to 10 hr and for cTnT it was 12-14 hr and optimum temperature for high yield of cTnT, sTnT *w*ere 30^0 C, 25°C with 0.2mM IPTG, respectively. The 6X His tagged recombinant sTnT was purified through Ni-NTA affinity chromatography. cTnT his tagged protein was purified with glutathione affinity column. For both the protein, cell lysate along with elute fractions were analyzed by SDS PAGE. The purification yield for cTnT and sTnT were ~1.2 mg L^{-1} and ~ 2 mg L^{-1}, respectively as calculated from Bradford assay.

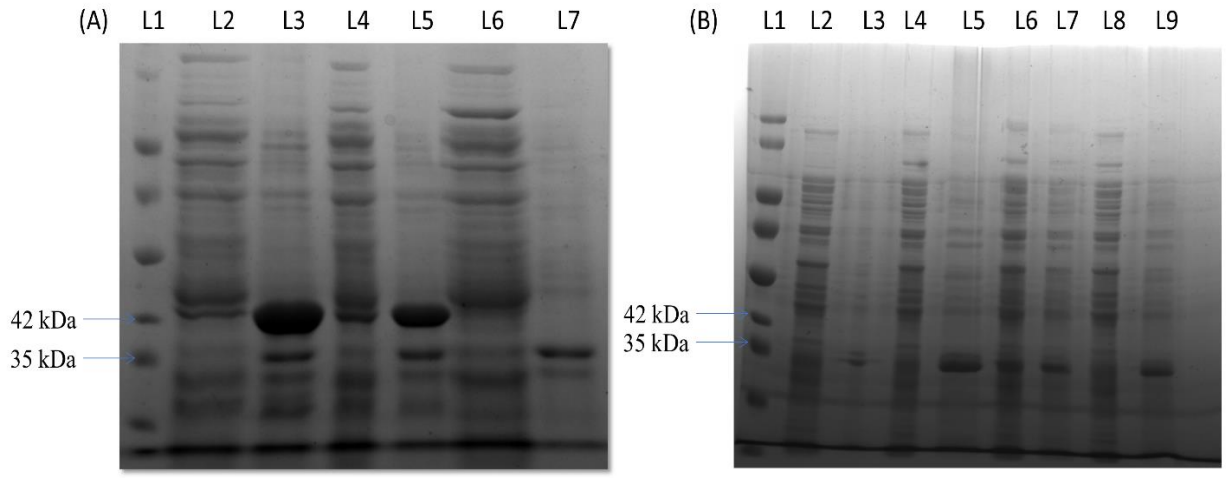

Figure 4.3: SDS PAGE (10 % gel stained with comassie brilliant blue). (A) IPTG optimization of sTnT induced at an IPTG concentration of 0.4 and 0.2 mM for 12 hr at 37^0 C. Lane L1: ladder, L2: sTnT 0.2mM Soup, L3: sTnT 0.2mM pellet, L4: sTnT 0.4mM soup, L5: sTnT 0.4mM pellet, L6: BL21 DE3 soup, L7: BL21 DE3 pellet. IPTG optimization of (B) cTnT induced at an IPTG concentration of 0.4 and 0.2 mM for 8 hr at 25^0 C. Lane L1: ladder, L2: cTnT uninduced pellet, L3: cTnT uninduced soup, L4: cTnT 0.2mM pellet, L5: cTnT 0.2mM soup, L6: cTnT 0.4mM pellet, L7: cTnT 0.4mM soup, L8: cTnT 0.6mM pellet, L9: cTnT 0.6mM soup.

4.3.3 Characterization of the recombinant cTnT and sTnT

To establish the precise structure of the recombinant proteins, initially western blot (Figure 4.4 C) and CD studies (Figure 4.5 A, B) were performed. Western blot was performed to identify recombinant protein with an anti-His antibody. The CD spectra of both the proteins were recorded and revealed major *α*-sheet content and no *β* framework, which complies with theoretical values and reported data. cTnT has 67% α helix and 33% random coils, while sTnT has 63% α helix and 37% random coils. To determine the molecular weight of the recombinant protein MALDI-TOF spectrometry was performed (Figure 4.5 C,D). The obtained molecular weight of both sTnT and cTnT agreed with the molecular weight predicted theoretically based on encoded amino acid sequence. The p*I* of sTnT and cTnT were discerned from the equation obtained by plotting zeta potential values against corresponding pH values. The zeta values of cTnT and sTnT were 4.82 and 5.34, respectively (Figure 4.5 E,F).

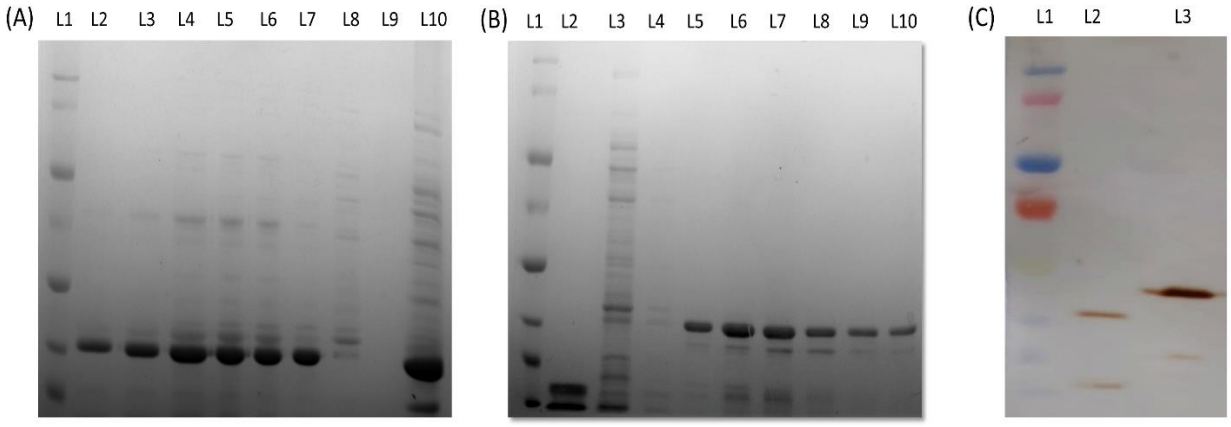

Figure 4.4: The purified (A) sTnT and (B) cTnT expressed in *E.coli* with 0.2mM IPTG induction and an incubation temperature of 25^0 C and 37^0 C respectively. (C) Western blot of recombinant sTnT in L2 and cTnT in L3 with anti His antibody (1: 10,000 dilution) over PVDF membrane.

4.4Conclusion

The target *cTnT* and *sTnT* genes were successfully cloned into a suitable expression vector and confirmed the clones through restriction digestion and PCR amplification. The expression conditions for the proteins were optimized. The recombinant proteins were purified through Ni-NTA chromatography and characterized the purified proteins for their structural integrity through different techniques such as CD and zeta potential studies. The molecular weight of the proteins was determined through MALDI MS and western blot. This study proves that both the proteins were successfully cloned, expressed and purified in appropriate structural, functional active form.

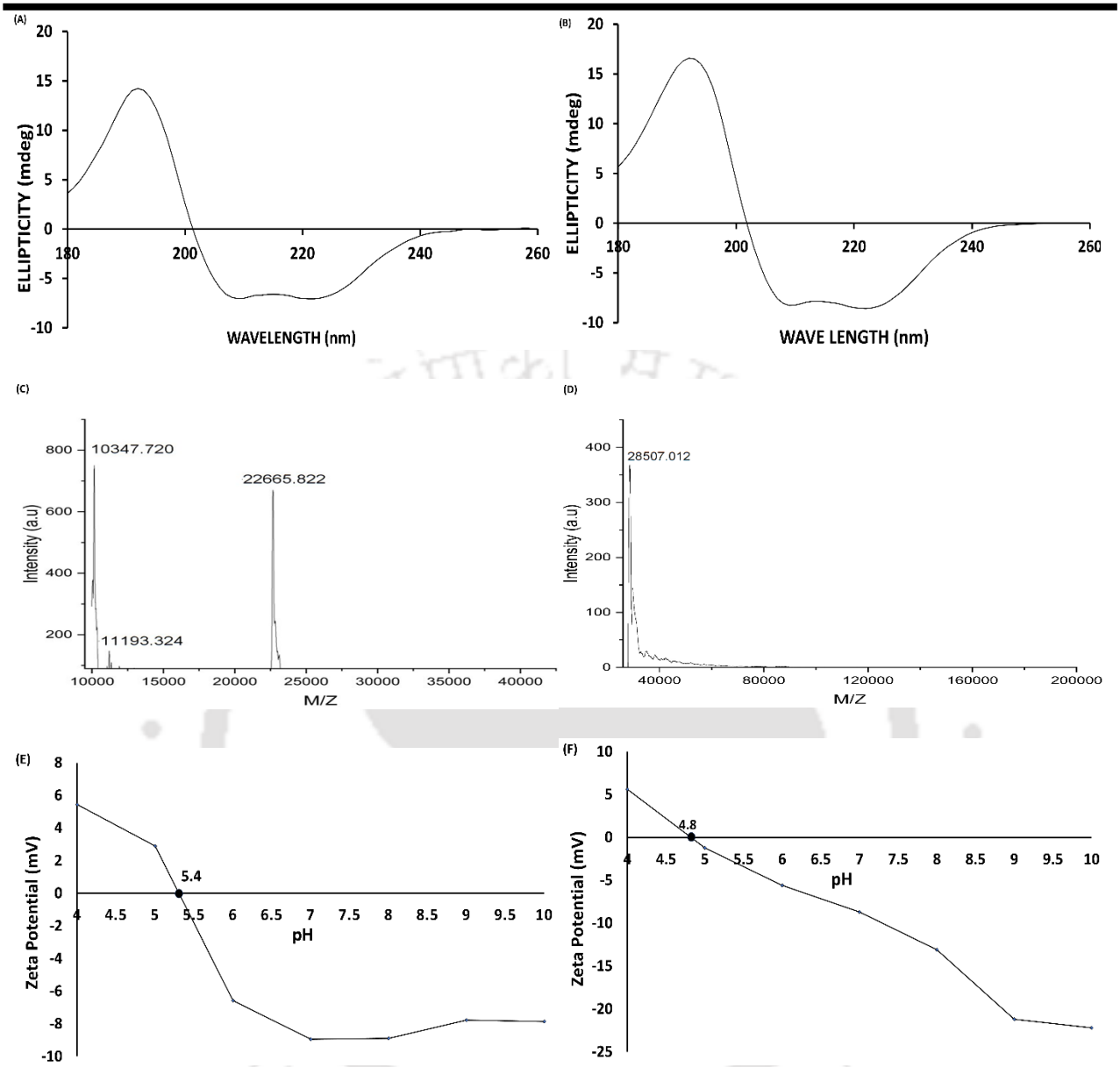

Figure 4.5: CD spectra of (A) sTnT and (B) cTnT 1mg/ml in 25mM sodium phosphate buffer. MALDI-MS analysis of (C) sTnT and (D) cTnT. Zeta potential of recombinant (E) sTnT and (F) cTnT at various PH range.

Chapter 5

Development of aptamers specific for cTnT and their characterization

Chapter 5

Development of aptamers Specific for cTnT and their characterization

5.1 Overview

Nucleic acid aptamers are synthetic ligands which are short single stranded oligonucleotides (DNA, RNA or modified RNA, DNA). Aptamers against a specific target is selected through a process called Systematic evolution of ligands by exponential enrichment (SELEX). The developed aptamers possess the ability to fold in to three dimensional (3D) shapes and bind to their targets via a combination of hydrogen bonding, π-π system stacking, van der Waals forces, and electrostatic interactions (Kakoti and Goswami, 2016). Aptamers boast of several advantages over antibodies as biorecognition elements: high thermal stability, low cost of production, non-immunogenicity, nontoxicity, lower batch to batch variability, and rapid large-scale synthesis to name a few. Aptamers have thus evolved as an attractive tool in the fabrication of diagnostic devices.

Although theoretically simple, the conventional SELEX procedures are time consuming, cost intensive and are plagued by a lot of uncertainties. Target immobilization often complicates the selection procedure particularly in the case of small molecules which eliminates the sites for aptamer to bind. Furthermore, the washing steps to remove unbound bound aptamers after every round of SELEX increase the overall number of steps and cause random losses of the selective aptamer candidates. Hence, these uncertainties compound to affect discrepancies which hamper the probability of successful selection (Spill et. al, 2016). Hence, there is an urge to explore more effective method to develop aptamers.

This chapter describes the selection of ssDNA aptamers against cTnT following the centrifugal SELEX (c-SELEX) process. The c-SELEX is a variation of conventional SELEX attempted in the current study. The c-SELEX works on the principally of separation of interacting and non-interacting aptamers by centrifugation process. The advantages of the present SELEX variant are as follows: (a) the time required to complete the SELEX is less than the conventional SELEX procedure, (b) the number of rounds of SELEX is also less than the conventional SELEX procedure, (c) the complete protein is exposed for interaction with the aptamer library there by

increasing the chances of finding the best aptamer candidates, (d) there is a significant reduction in the amount of consumable items for the c-SELEX. The cTnT protein purified in Chapter IV was used as the target for the c-SELEX whereas sTnT served as control proteins for negative-c-SELEX. Following the process of c-SELEX, we isolated four aptamer candidates, which were then characterized for their specificity, and affinity of binding to the target. A detailed account of the work is included in this chapter.

5.2 Experimental procedures

5.2.1 Materials

ssDNA aptamer library (10^{14} - 10^{15}) was acquired from IDT technology (USA). The library was composed from random oligonucleotide sequences with a region of random 30-nucleotides (**N30**) (5'-CACCTAATACGACTCACTATAGCGGATCCGA-**N30**-CTGGCTCGAACAAGCTTGC-3') flanked by a conserved primer binding site on either side for amplification. The primer sequences used for the PCR amplification are listed in the appendix table 4.2. All the buffer compositions used in the current chapter are listed in the appendix table 3.7. The primers used for the current study were procured from Bioserve (India). Restriction enzymes were purchased from New England Biolabs. Starting blocking buffer, H_2SO_4 and Top 10 competent cells were procured from Thermo Fisher. Dibasic/mono basic phosphate buffer, $MgCl_2$, NaCl, KCl, PCR kit, streptavidin magnetic beads and Bovine serum albumin (HSA) were procured from Sigma Aldrich. The molecular weight cutoff filters from Sartorius and pGEMT easy vector from Promega were purchased.

5.2.2 *In vitro* selection of aptamers using c-SELEX

SELEX was performed to select aptamers which are specific to *cTnT* protein. 5 nmol of ssDNA from the library was suspended in 1 ml of the binding buffer and the solution was heated for 10 min at 95 °C, followed by rapid cooling to room temperature. The first step of c-SELEX is a negative SELEX where the control protein *sTnT* is allowed to interact with the aptamer library for 1hr at room temperature followed by separation of bound and unbound aptamers by

centrifugation at 1210 RPM for 10 min of the reaction mixture in a cut off filter of 30 kDa. The hydrodynamic radius of all the aptamers in the aptamer library is approximately 21 kDa. The sTnT-aptamer complex has a hydrodynamic radius of approximately 50 kDa and upon centrifugation only the unbound aptamers from the aptamer library passed through the filter and gets collected in the flowthrough. The flowthrough is considered for further rounds of c-SELEX as it does not contain *sTnT* or *sTnT*-aptamer complex. The potential aptamer candidates in the collected flow through were amplified by using Taq Red DNA polymerase (Sigma) and the aptamer primers. The initial denaturation at 95 ^{0}C for 10 min, followed by 20 cycles of 95^{0}C for 15 s, 68^{0}C for 15 s, 72^{0}C for 3 s, and final extension at 72 ^{0}C for 3 s were used in the PCR. The PCR amplicons are then incubated with 25 µl of streptavidin magnetic beads in binding buffer at room temperature for 1hr. The beads are then washed with coupling buffer and ssDNA strands were separated from the magnetic beads by denaturing the dsDNA PCR amplicons in 100 µl of 150 mM NaOH. The separated strands were used for the next rounds of c-SELEX cycle. The second round of the c-SELEX was a positive SELEX where *cTnT* is made to interact with the ssDNA amplified from round one for 1hr at room temperature. The duration of interaction is increased incrementally in negative SELEX from 60 min to 90 min and decreased progressively in positive SELEX from 60 min to 15 min. The progressive reduction in the time was carried out after round 6. A total of 15 cycles were carried out with 4 negative cycles with sTnT (1st, 6th, 9th, 14th cycle) and 11 positive SELEX with cTnT. The PCR amplicons of the 15th cycle were used for cloning.

5.2.3 Cloning of enriched aptamer candidates

After completion of the 15 rounds of c-SELEX the probable aptamer candidates were cloned into pGEMT easy vector and transformed into *E. coli* DH5α cells. The transformed cells were selected by blue-white screening. Plasmids were isolated from the positive clones and sent for sequencing. The sequencing results of the candidates were analysed through Clustal omega alignment software for comparison.

5.2.4 Prediction of aptamer structure and G-quadruplex mapping

The aptamer secondary structure was generated in RNA Structure online application. The prediction conditions were at 310 K, MEA, MFE maximum percentage energy difference of 10, the number of iterations for prediction being 5 and minimum helix length for pseudoknot prediction at 3 nucleotides. The QGRS (Quadruplex forming G-Rich Sequences) mapper software was used for prediction of quadruplex forming region based on sequence analysis (Kikin et al., 2006). The default parameters were used with the parameters being maximum 30 sequences of QGRS length, minimum G-group of 2 and loop size between 0 - 36 nucleotides. The predicted aptamer structures were confirmed experimentally.

5.2.5 Docking studies and generation of aptamer 3D structures

The 3D ssDNA aptamer structures were generated following the protocol discussed in the chapter 3. Docking was performed in patch dock web server in default conditions. The pdb file of the aptamer protein complex obtained from patch dock after docking were uploaded into PLIP (Protein Ligand Interaction Profiler) server for easy identification of non-covalent interactions between biological macromolecules and their ligands.

5.2.6 Determination of dissociation constant (K_D) of aptamer- cTnT interaction by CD spectroscopy and Isothermal Titration Calorimetry (ITC)

ITC experiments were performed with 20 µM of aptamer and 5 µM of cTnT protein in 50mM sodium phosphate buffer (pH 7.5) on a GE Healthcare UK, iTC 200 microcalorimeter. Aptamer solution was prepared in MQ water. Both the aptamer and protein solutions were degassed for 10 min before introducing the solutions into the instrument. Following the first injection of 0.4 µl aptamer solution, subsequent injections of 1.2 µl each were administered by the ITC syringe to the reaction cell in 20 titrations, at 180 s intervals, at 25 °C, and a stirring speed of 450 rpm. Control experiment without aptamer was performed to correct for heat of dilution. Analysis of ITC data was performed by Origin v 7.0 (OriginLab, USA).

CD studies was performed to determine the binding affinity of the aptamers with the target protein in the solution state. The Binding affinity is usually measured as dissociation constant (K_D). The CD spectra were recorded on Jasco J-815 spectropolarimeter (Japan) at room temperature in 1 cm path length cuvette. The spectra were recorded in continuous mode with bandwidth of 1 nm and resolution of 1nm between λ_{200} to λ_{300} nm at a scan rate of 100 nm min^{-1}. Induced CD (ICD) spectra were recorded for K_D measurement of the aptamers after their binding with cTnT protein at increasing concentration. The buffer influence was removed from the recorded spectra and smoothened by Savitsky-Golay algorithm through Origin 8.0 software. The K_D value of the aptamer was calculated by plotting a graph of peak intensity versus concentration gradient of cTnT and fitted in single ligand binding model of Sigma plot. 10 µM of the aptamer was heated to 95^0 C for 10 min and then incubated at room temperature for 30 min in a thermocycler. The solutions are then incubated with cTnT solution for 1hr at room temperature.

5.3 Results and discussion

5.3.1 Development of specific aptamer against cTnT

Aptamer candidates specific to cTnT were enriched from the aptamer library by c-SELEX process. The schematic representation of the complete c-SELEX is depicted in the scheme 5.1.

A total of 15 rounds of c-SELEX were performed, out of which 4 cycles negative cycles and rest were positive cycles. After the second negative cycle, the duration of interaction between aptamer library and the cTnT protein had to decrease to increase the enrichment of aptamer candidates with high affinity to the target protein; whereas the duration of interaction between the control protein (sTnT) and the aptamer had to increase to extricate the aptamer candidates with any level of affinity to the control protein. After each positive cycle, a gradual enrichment of aptamers with affinity to cTnT occurred and after each cycle PCR was performed and bands were generated in the gel. After every negative cycle a drop in band intensity was observed (Figure 5.1) due to the disposal of non-specific aptamers. The enriched aptamers were PCR amplified and the amplicons were cloned. The clones were transformed into *E. coli* DH5α

competent cells and blue white screening was performed to screen all the positive candidates. The positive clones were digested with *EcoR1* and then confirmed the corresponding band in gel after performing the PCR (Figure 5.2).

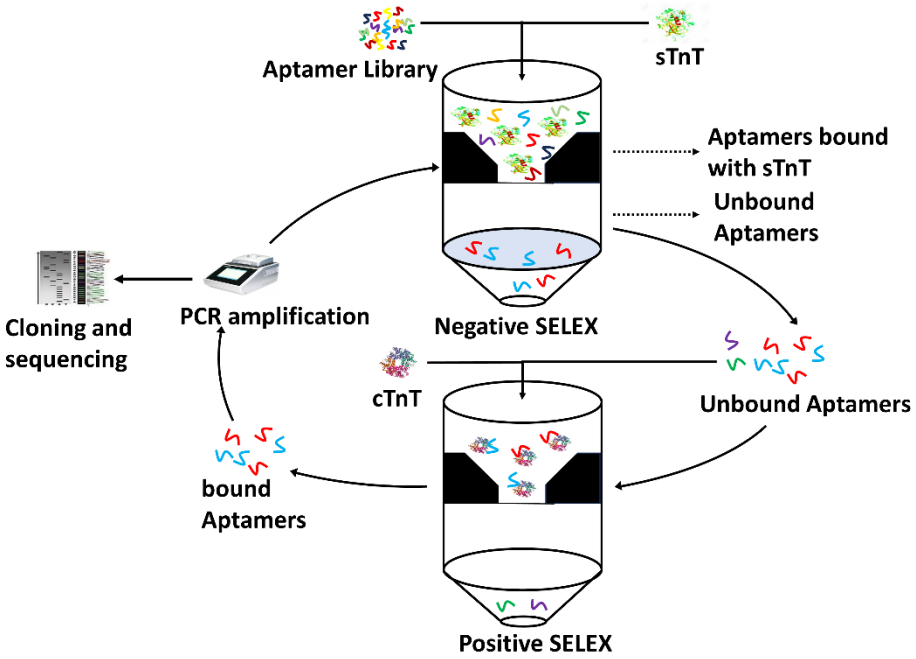

Scheme 5.1: Schematic representation of the c-SELEX protocol followed to develop aptamer against cTnT.

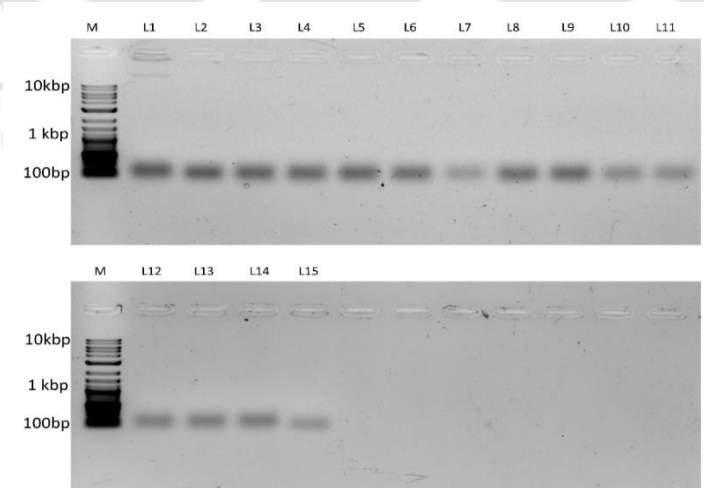

Figure 5.1: PCR amplified bands at the completion of each c-SELEX cycle L1−L15, respectively. Bands L1, L6, L9 and L14 are negative c-SELEX with control protein sTnT.

The amplicon bands are seen at ~100 bp with positive control bands (from aptamer library) are seen at L1, L13, L23 and L24. The positive colonies were then isolated, plasmids were extracted and sequenced. The sequencing results revealed 34 out of 35 colonies carried proper aptamer insert. All the colonies were named cT and its colony number to denote the aptamer specific for cTnT. Analysis of the 34 aptamer candidates were accomplished by Clustal omega, which showed four sets of aptamers based on sequence similarity and out of them aptamers cT12, cT21, cT22 and cT33 were selected for further studies (Figure 5.3).

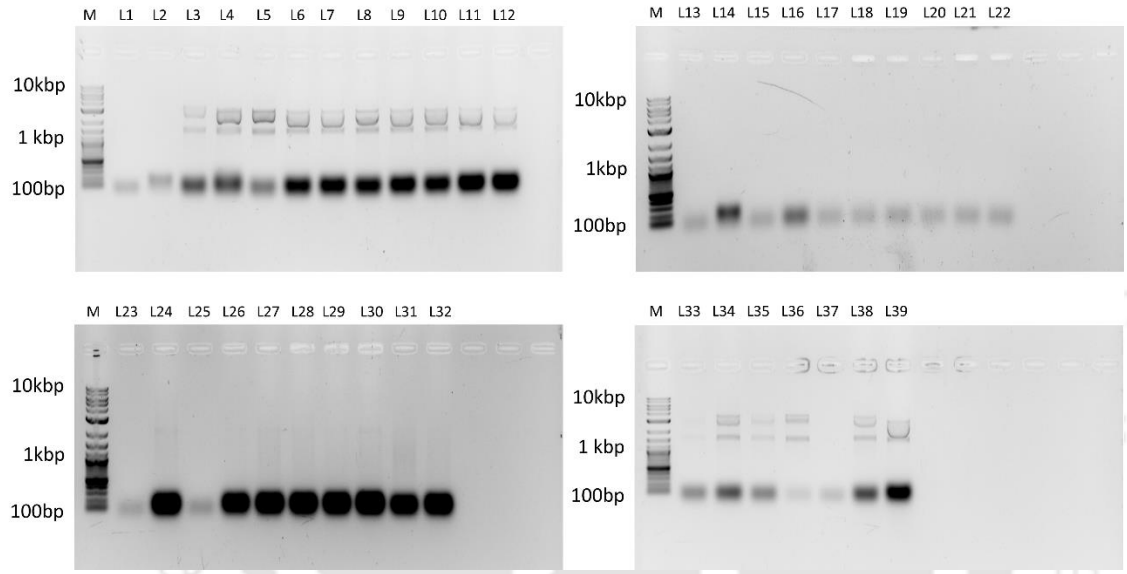

Figure 5.2: Screening of positive colonies by PCR amplification of the plasmids obtained from TA plasmid in *E. coli* DH5 α.

cT12 and cT21 has one big loop and four small loops. The central big loop structure is connected by three chain structures to three of the four loops. cT22 has a smaller loop structure which connects the bigger loop by a small chain and two long chains connect two other loops. cT33 is a straight loop and chain structure which has one big loop and three small loops (Figure 5.4). The aptamers were further analysed for the presence of G-quadraplex structures. The QGRS mapper analysis predicted the presence of one quadruplex forming regions in cT33 (Table. 5.1), while it was absent in the other aptamers.

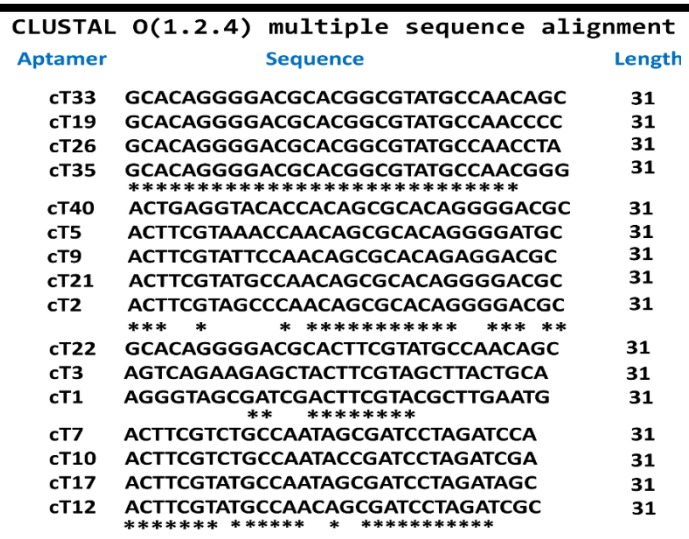

Figure 5.3: Grouping of aptamers on the basis of percentage similarity of sequences where, comparatively more similar sequences were grouped together.

Aptamer	Position	Length	QGRS	G-Score
cT12	0	0	NA	NA
cT21	0	0	NA	NA
cT22	0	0	NA	NA
cT33	22	18	GGCACAGGGGACGCACGG	15

Table 5.1: G-Quadraplex Prediction of all aptamers from QGRS Mapper.

Tertiary structures of all four aptamers were predicted using the ensemble strategy described in chapter 3. The aptamer 3D structures so generated are shown in figure 5.5. Based on the 3D structure classification mentioned in chapter 3, all the four aptamers were classified. Aptamers cT12, cT22, cT33 belongs to the class of helical chain while cT21 belongs to the class of hairpin structures.

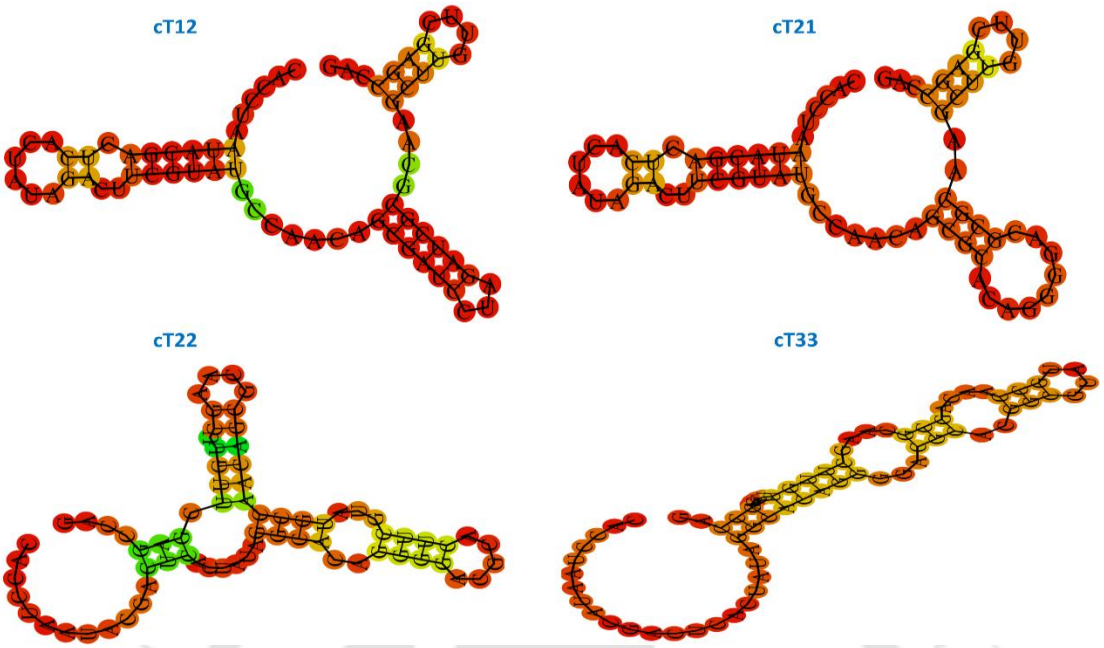

Figure 5.4: Secondary structures of aptamers cT12, cT21, cT22 and cT33 predicted by RNA Fold webserver.

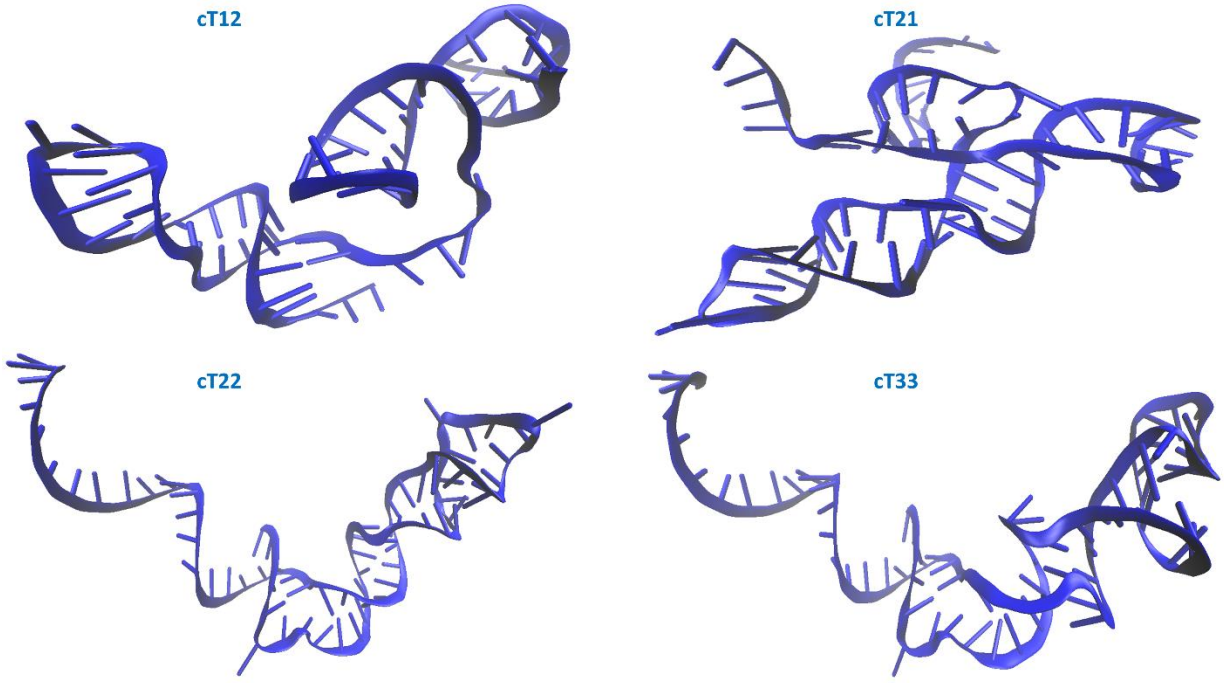

Figure 5.5: 3D structures of all four aptamers generated using 3D ensemble method.

5.3.2 Effect of pH and c-SELEX buffer on the aptamer structure

To confirm the predictions of QGRS mapper, CD spectra of all the aptamers were studied in both water and c-SELEX binding buffer. All the four aptamers exhibited signature peaks corresponding to duplex B DNA with a positive peak at $\lambda_{260nm - 280nm}$ and a negative peak at $\lambda_{240nm - 250nm}$. This clearly suggested that the aptamers hybridized to form regions of double strands which is also evident from the generated structures (Figure 5.6). The hybridized double stranded portions of all four aptamers can also be observed in the predicted 3D structures as indicated in the CD studies. In case of aptamer cT33 the peaks evident for a G-quadraplex is observed with positive peaks at λ_{264nm} and λ_{220nm} and a negative peak at λ_{245nm}.

The stability of aptamers is greatly affected by pH which is known to affect the 3D structures of the aptamers. Hence the effect of the pH on the natural conformation of the aptamers was studied in the presence of the binding buffer used for c-SELEX (Figure 5.7). The four aptamers behaved differently under different conditions but at pH 4 all of them displayed smaller peaks.

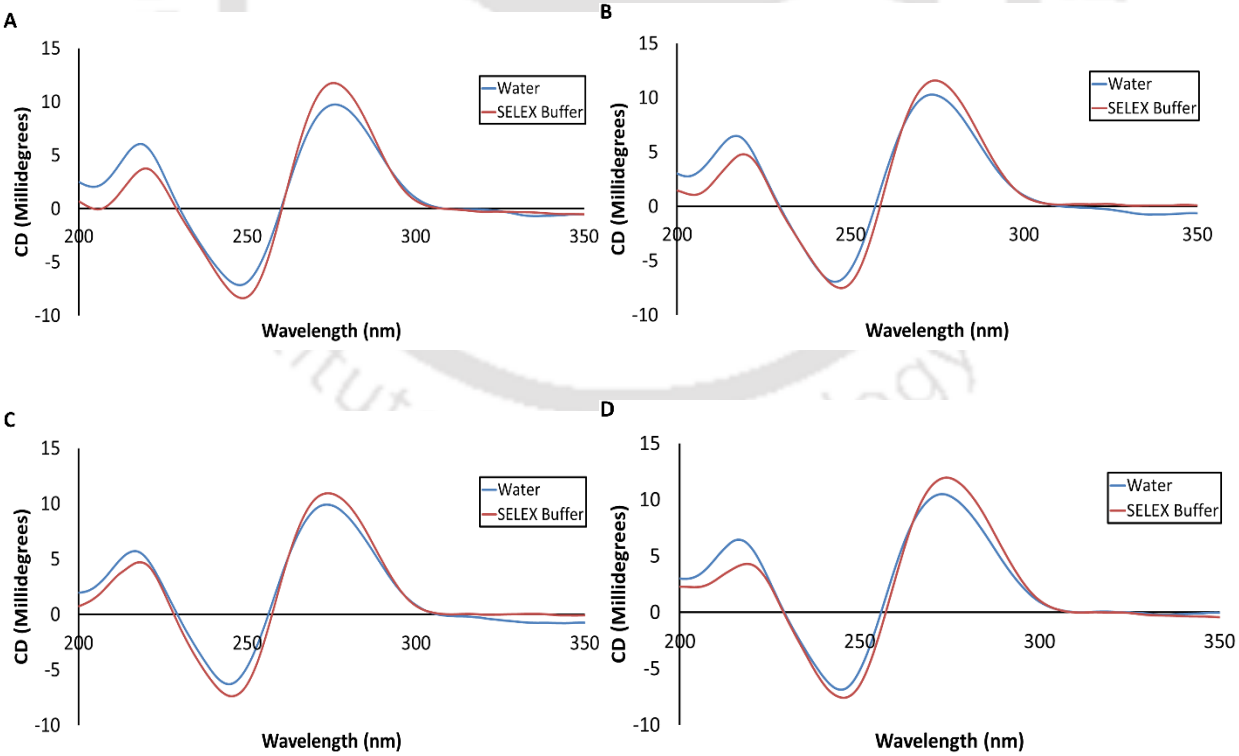

Figure 5.6: CD spectra of (A) cT12, (B) cT21, (C) cT22, (D) cT33 in water and SELEX Buffer.

For aptamer cT12, the peak intensity at 272nm and 245nm increased against pH conditions in the following order: pH 4 < pH 7 < pH 9 <pH 8 < pH 5< pH 6, with no apparent peak shift at all pH with the exception at pH 4. For aptamer cT21, the peak intensity at 272nm and 245nm were increased in the following order: pH 4 < pH 9 < pH 7 <pH 8 < pH 5 < pH 6, and a peak shift was observed at pH 5 by 5nm. In case of aptamer cT22, the peak intensity at 272nm and 245nm were increased in the following order: pH 4 < pH 7 < pH 6 <pH 8 < pH 5 < pH 9, and a peak shift of 1nm was observed when pH was shifted from 4 to 9; the aptamer was least stable at pH4 as evident from the CD studies (Figure 5.7 C). For aptamer cT33, the peak intensity at 272nm and 245nm were increased in the following order: pH 9 < pH 4 < pH 8 <pH 7 < pH 5 < pH 6. This study reveals the characteristic spectral behaviour of aptamers at different pH conditions. On the basis of the peak intensities, it can be said that all the four aptamers are relatively stable at a pH range of 6-8.

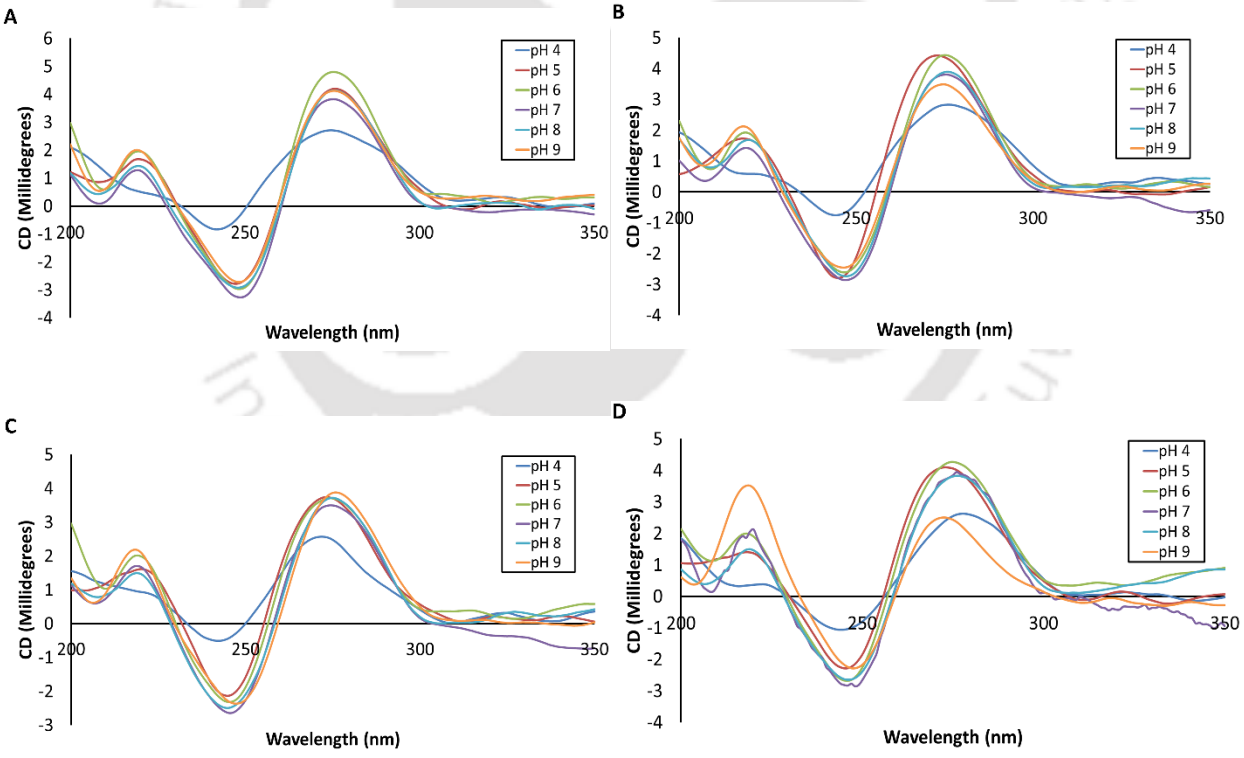

Figure 5.7: Effect of pH on the structure of (A) cT12, (B) cT21, (C) cT22, (D) cT33.

5.3.3 Binding affinity and protein-aptamer interactions

The generated aptamer 3D structures and the pdb structure of the cTnT were docked in web server. The results obtained were analysed in PLIP. All four aptamer interactions with cTnT were mainly hydrogen, hydrophobic interactions and salt bridges. Other interaction includes π-cationic interactions which is however, less frequent. All the interactions are tabulated in the tables 5.2 to 5.5. In depth analysis of the interactions reveal very high number (16) of salt bridges in case of cT21 indicating a higher affinity of the aptamer towards cTnT protein (Table 5.6). A high number (10) of salt bridge was observed in case of cT33. Additionally, highest number (16) of hydrophobic patches observed for the aptamer cT33. The docking interaction studies highlighted that cT33 which forms a G-quadraplex structure has the best affinity for the target protein.

The binding affinity and specificity of all the four aptamer candidates with the target protein (cTnT) and control protein (sTnT) were investigated by CD spectroscopy (Figure 5.8). There was an apparent change in ellipticity indicating their avid interaction with cTnT. An inverse relation was observed in all four aptamer cases where an increase in cTnT concentration resulted in a decrease in peak intensity in the CD spectra; this phenomenon was exploited to discern the binding affinity of the individual aptamers with the target protein. Unlike the target protein, the control protein cTnT did not produce any significant ellipticity change upon their interactions with the aptamers, indicating specificity of the selected aptamers towards the target protein.

Nucleotide	Nucleotide Number	Amino Acid Number	Amino Acid	Type of Bond	Number of bonds
Adenine	2	122	Serine	Hydrophobic	1
		125	Aspartic Acid	Hydrogen	1
		126	Arginine	Hydrogen	1
	35	142	Asparagine	Hydrophobic	1
		142	Asparagine	Hydrogen	1
	38	148	Arginine	Hydrogen	1
	56	163	Glutamine	Hydrogen	1
		159	Arginine	Salt bridge	1
	57	156	Arginine	Hydrogen	2
	71	156	Arginine	Hydrogen	2
Cytosine	1	129	Arginine	Hydrogen	2
	3	126	Arginine	Hydrogen	1
	4	126	Arginine	Hydrogen	3
	33	131	Arginine	Hydrogen	2
		134	Arginine	Hydrogen	1
		134	Arginine	Hydrophobic	1
		137	Glutamine	Hydrogen	1
		134	Arginine	Salt bridge	1
	34	135	Alanine	Hydrophobic	1
		138	Glutamine	Hydrophobic	1
		138	Glutamine	Hydrogen	1
	37	148	Arginine	Hydrogen	2
	51	144	Arginine	Hydrophobic	1
		144	Arginine	Hydrogen	1
		147	Glutamine	Hydrogen	1
		141	Arginine	Salt Bridge	1
	53	148	Arginine	Hydrogen	2
		155	Glutamine	Hydrogen	1
	55	155	Glutamine	Hydrogen	1
		159	Arginine	Hydrogen	1
		159	Arginine	Salt bridge	1
	59	176	Lysine	Pi-cation	1
	65	165	Arginine	Hydrogen	2
		165	Arginine	Salt bridge	1
	69	153	Alanine	Hydrophobic	1
		153	Alanine	Hydrogen	1
		156	Arginine	Hydrogen	1
	70	156	Arginine	Hydrogen	2
Guanine	32	134	Arginine	Hydrophobic	1
		131	Arginine	Hydrogen	1
		133	Glutamine	Hydrogen	1
		134	Arginine	Hydrogen	1
		130	Arginine	Salt Bridge	1
	39	148	Arginine	Hydrogen	1
	52	144	Arginine	Hydrogen	3
		147	Glutamine	Hydrogen	1
	54	155	Glutamine	Hydrogen	1
	58	156	Arginine	Hydrogen	2
	66	165	Arginine	Salt Bridge	1
	68	150	Asparagine	Hydrogen	1
Thymine	5	126	Arginine	Hydrogen	1
	50	141	Arginine	Salt bridge	1
	60	176	Lysine	Hydrophobic	1
		176	Lysine	Salt bridge	1
	61	176	Lysine	Hydrophobic	2
		179	Serine	Hydrogen	2
	63	173	Arginine	Hydrogen	1

Table 5.2: Prediction of interacting residues at the aptamer cT12-protein interface.

Nucleotide	Nucleotide Number	Amino Acid Number	Amino Acid	Type of Bond	Number of bonds
Adenine	12	216	Arginine	Salt bridge	1
	16	217	Lysine	Hydrophobic	1
		222	Aspartine	Hydrogen	2
	2	258	Lysine	Hydrophobic	1
	21	214	Glutamine	Hydrogen	1
		215	Arginine	Salt bridge	1
	23	210	Lysine	Hydrogen	1
		210	Lysine	Salt bridge	1
	38	196	Arginine	Hydrogen	1
	45	204	Glutamine	Hydrogen	2
		208	Lysine	Hydrogen	1
	50	200	Lysine	Hydrophobic	2
		200	Lysine	Hydrogen	2
		197	Lysine	Salt bridge	1
		199	Glycine	Hydrogen	1
	9	206	Glutamine	Hydrogen	2
		209	Lysine	Hydrogen	1
Cytosine	1	261	Iso leucine	Hydrophobic	1
	10	210	Lysine	Hydrogen	1
		209	Lysine	Salt bridge	1
	13	236	Leucine	Hydrophobic	1
		232	Lysine	Salt bridge	1
	17	222	Aspartine	Hydrogen	1
	27	243	Leucine	Hydrophobic	1
		244	Glutamine	Hydrogen	1
		247	Lysine	Salt bridge	1
	3	254	Phenyl alanine	Hydrophobic	1
	4	258	Lysine	Salt bridge	1
	44	208	Lysine	Salt bridge	1
	51	201	Arginine	Hydrophobic	1
		202	Glutamine	Hydrophobic	1
		201	Arginine	Hydrogen	2
		205	Arginine	Hydrogen	1
		205	Arginine	Pi-cation	1
		205	Arginine	Salt bridge	1
Guanine	11	216	Arginine	Salt bridge	1
	22	214	Glutamine	Hydrogen	1
	28	247	Lysine	Salt bridge	1
	39	196	Arginine	Salt bridge	1
	46	201	Arginine	Hydrogen	1
		204	Glutamine	Salt bridge	1
	47	199	Glycine	Hydrogen	1
	48	197	Lysine	Salt bridge	1
	49	200	Lysine	Pi-cation	1
	52	205	Arginine	Hydrogen	1
Thymine	14	217	Lysine	Hydrophobic	2
	20	215	Arginine	Salt bridge	1
	26	247	Lysine	Hydrogen	1

Table 5.3: Prediction of interacting residues at the aptamer cT21-protein interface.

Nucleotide	Nucleotide Number	Amino Acid Number	Amino Acid	Type of Bond	Number of bonds
Adenine	12	205	Arginine	Salt bridge	1
	19	253	Lysine	Hydrogen	2
	32	225	Asparagine	Hydrogen	1
	43	228	Glutamine	Hydrogen	1
		242	Asparagine	Hydrophobic	1
		239	Glutamine	Hydrogen	1
	7	200	Lysine	Hydrogen	1
	9	197	Lysine	Salt bridge	1
Cytosine	10	200	Lysine	Hydrophobic	1
	13	209	Lysine	Hydrophobic	2
		209	Lysine	Salt bridge	1
	40	232	Lysine	Hydrogen	1
	65	246	Glutamine	Hydrophobic	1
	70	210	Lysine	Salt bridge	1
Guanine	11	201	Arginine	Hydrogen	1
		202	Glutamine	Hydrogen	1
		205	Arginine	Hydrogen	1
	28	235	Glutamine	Salt bridge	1
	29	235	Glutamine	Salt bridge	1
	30	224	Leucine	Hydrophobic	1
		228	Glutamine	Hydrophobic	1
	31	224	Leucine	Hydrophobic	1
		228	Glutamine	Hydrophobic	1
		225	Asparagine	Hydrogen	2
		227	Aspartic acid	Hydrogen	1
		228	Glutamine	Hydrogen	1
	62	253	Lysine	Hydrogen	1
	66	243	Leucine	Hydrophobic	1
		244	Glutamine	Hydrogen	1
	68	209	Lysine	Hydrogen	1
		216	Arginine	Hydrogen	2
Thymine	14	209	Lysine	Salt bridge	1
	18	254	Phenyl alanine	Hydrophobic	1
	39	220	Alanine	Hydrophobic	1
	63	250	Leucine	Hydrophobic	1
		253	Lysine	Salt bridge	1
	8	196	Arginine	Hydrogen	1
		197	Lysine	Hydrogen	1

Table 5.4: Prediction of interacting residues at the aptamer cT22-protein interface.

Nucleotide	Nucleotide Number	Amino Acid Number	Amino Acid	Type of Bond	Number of bonds
Adenine	12	184	Phenyl alanine	Hydrophobic	1
		186	Glycine	Hydrophobic	1
		185	Glycine	Hydrogen	1
	16	181	Methionine	Hydrophobic	1
	19	174	Lysine	Salt bridge	1
	21	165	Arginine	Hydrogen	3
		173	Arginine	Hydrogen	1
		173	Arginine	Salt bridge	1
	48	131	Arginine	Salt bridge	1
	49	131	Arginine	Hydrogen	1
	67	171	Glutamine	Hydrophobic	1
Cytosine	10	187	Tyrosine	Hydrogen	1
	15	180	Aspartamine	Hydrogen	1
	17	178	Leucine	Hydrophobic	1
		181	Methionine	Hydrophobic	1
	24	157	Alanine	Hydrophobic	1
		157	Alanine	Hydrogen	1
		156	Arginine	Pi-cation	1
	33	138	Glutamine	Hydrogen	1
	47	131	Arginine	Hydrogen	2
	59	149	Glutamine	Hydrogen	1
	65	156	Arginine	Hydrogen	2
	69	176	Lysine	Hydrophobic	1
		172	Alanine	Hydrogen	1
		175	Lysine	Salt bridge	1
	70	176	Lysine	Hydrophobic	2
Guanine	11	186	Glycine	Hydrophobic	1
		187	Tyrosine	Hydrophobic	1
		185	Glycine	Hydrogen	1
		189	Glutamine	Hydrogen	1
		190	Lysine	Salt bridge	1
	22	173	Arginine	Hydrogen	2
		165	Arginine	Hydrogen	3
		165	Arginine	Salt bridge	1
	66	156	Arginine	Hydrogen	2
		160	Glutamine	Salt bridge	1
		170	Aspartamine	Salt bridge	1
	68	175	Lysine	Salt bridge	1
Thymine	14	184	Phenyl alanine	Hydrophobic	1
	18	178	Leucine	Hydrophobic	1
		174	Lysine	Hydrogen	1
		174	Lysine	Salt bridge	1
	20	177	Alanine	Hydrophobic	1
		164	Aspartamine	Hydrogen	1
		169	Glutamine	Hydrogen	2
	60	149	Glutamine	Hydrophobic	1
		149	Glutamine	Hydrogen	1

Table 5.5: Prediction of interacting residues at the aptamer cT33-protein interface.

A change in ICD signal upon increase in protein concentration is a direct indication of protein aptamer interaction (Garbett *et al.,* 2007). The binding affinities of 0.4193±0.1561µM for cT12, 0.17±0.2877µM for cT21, 0.5888±0.2884µM for cT22 and 2.6143±0.1091µM for cT33 were discerned. Isothermal Calorimetric titration of all four aptamers to cTnT resulted in a linear curve that yielded a dissociation constant of 14.42±1.5µM for cT12, 10.7±0.056µM for cT21, 49.22±3.33µM for cT22, 13.1±21µM for cT33 (Figure 5.9). These values are in close agreement with the K_D determined by CD study (Figure 5.10) and also indicated by docking analysis where the number of salt bridge, hydrophobic interactions and π cationic interactions were indicative of the strong interaction (table 5.6).

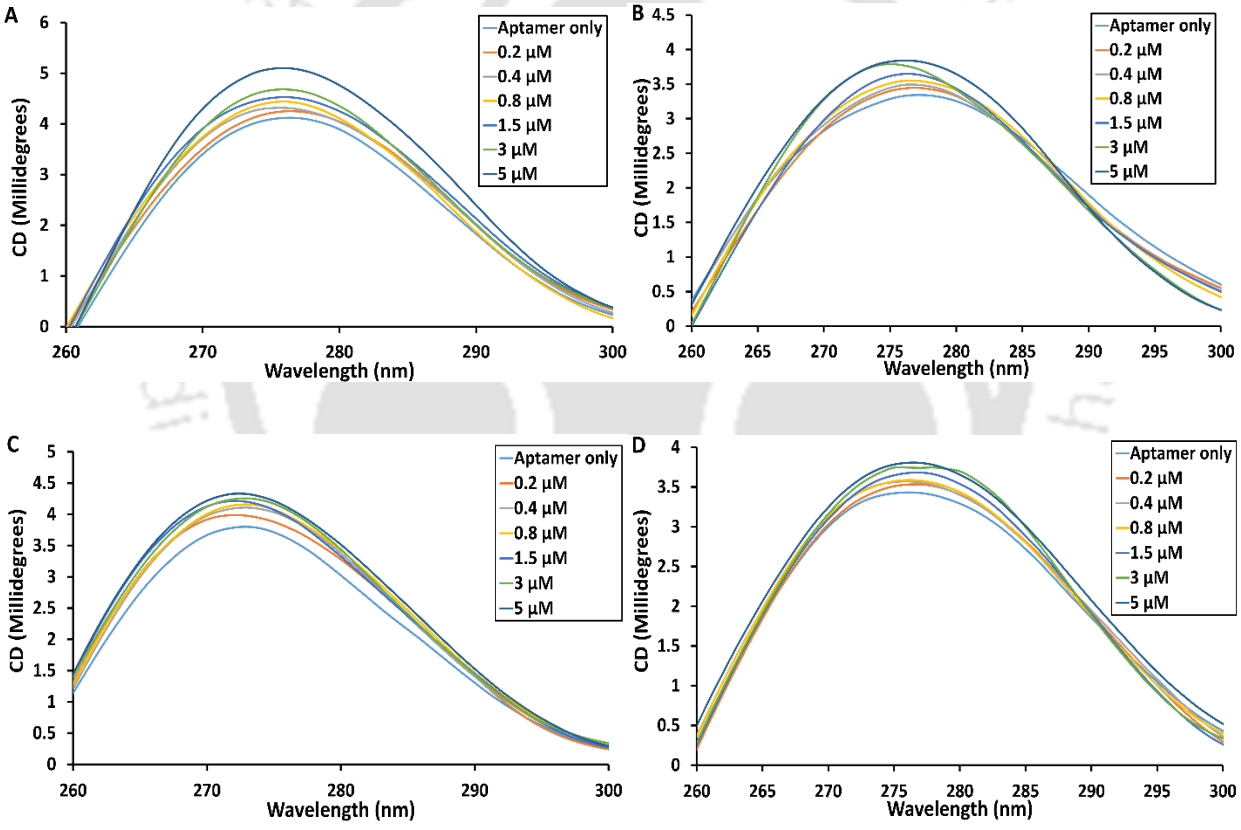

Figure 5.8: CD spectra of (A) cT12, (B) cT21, (C) cT22, (D) cT33 in the presence of the target protein cTnT (0-5µM).

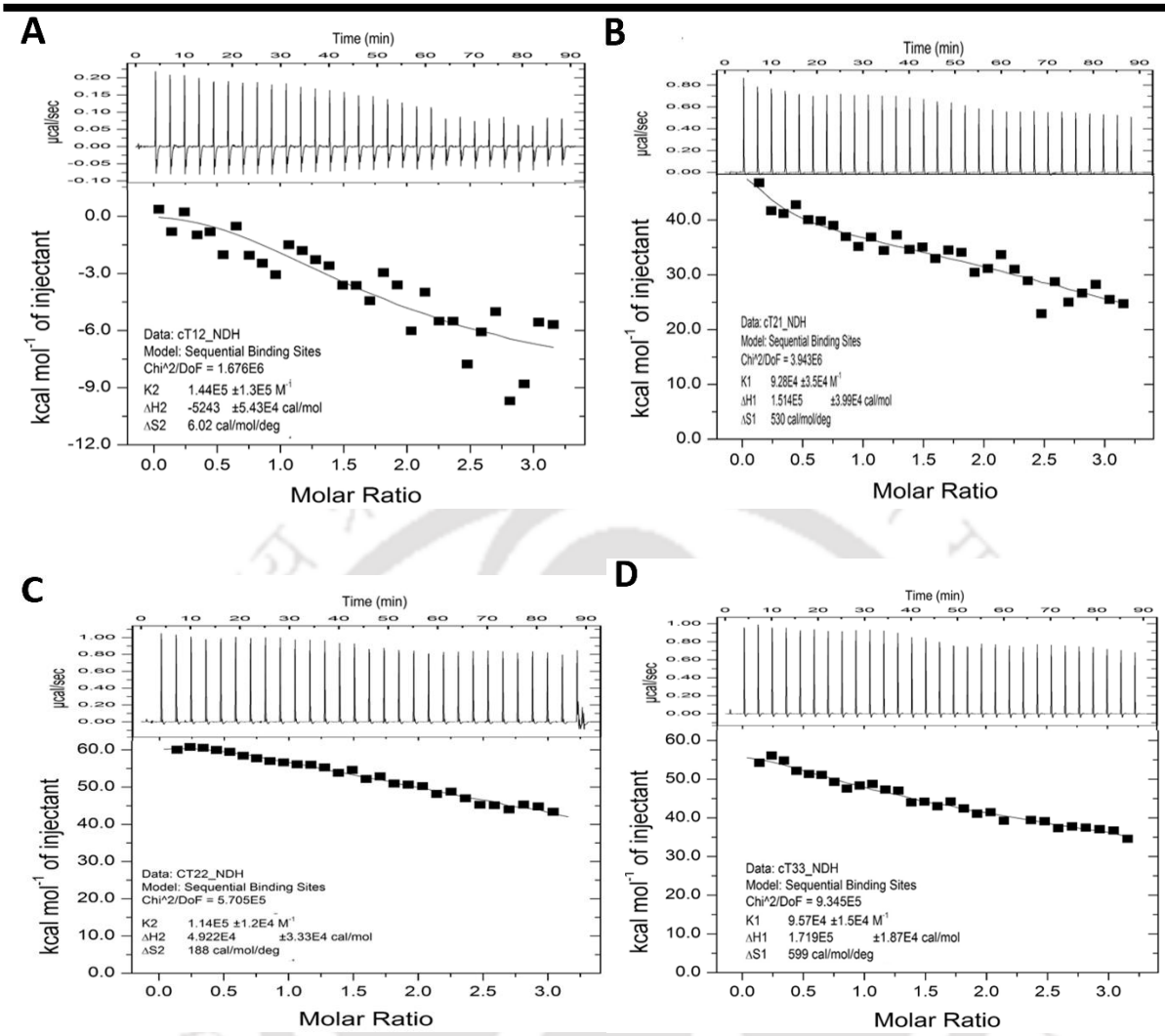

Figure 5.9: Isothermal titration calorimetry analysis for binding of (A) cT12, (B) cT21, (C) cT22, (D) cT33 aptamer to cTnT protein.

Aptamer	Hydrogen bond	Hydrophobic interaction	Π-cationic interaction	Salt bridge
cT12	51	11	1	9
cT21	25	12	2	16
cT22	21	13	0	8
cT33	30	16	1	10

Table 5.6: Type and number of interactions for each of the aptamer from docking studies.

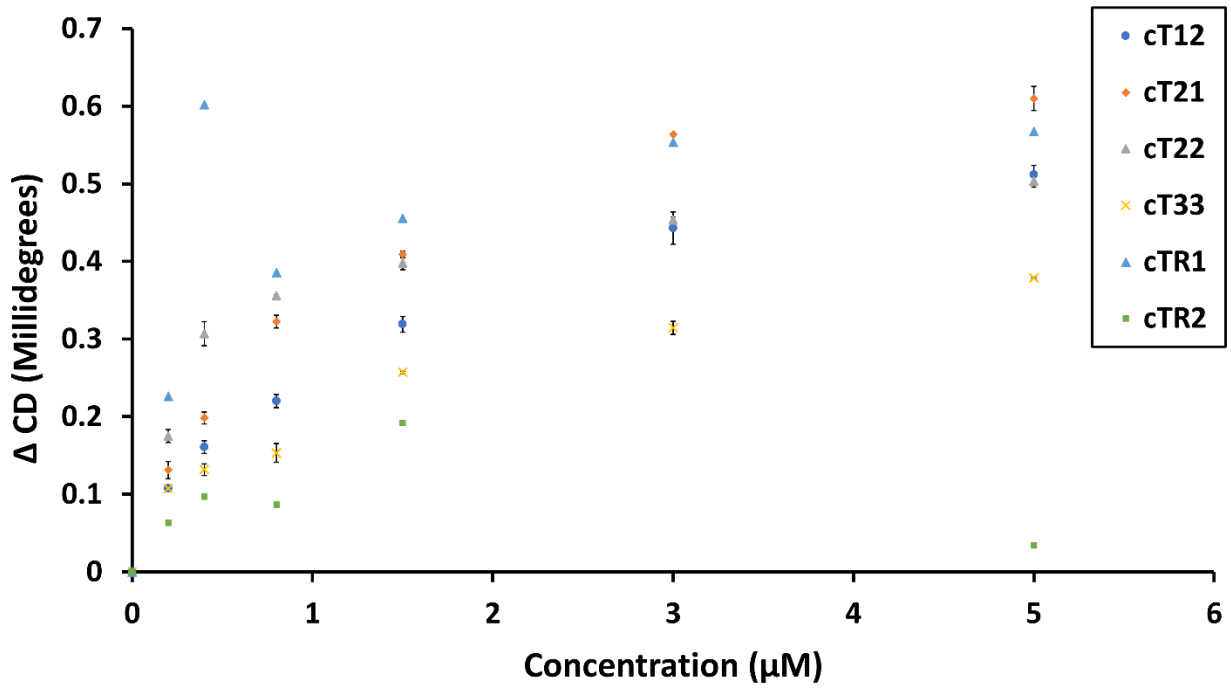

Figure 5.10: Curve fitting plots for K_D (Binding affinity) calculation using data from CD measurements.

5.4. Conclusion

A modified SELEX technique, termed c-SELEX, has been designed and operated to successfully select specific aptamers against the cTnT. The technique offered less time (each c-SELEX cycle takes 4.5 hr) and simplicity than the conventional SELEX techniques. A total four aptamers were enriched and subsequently identified through the steps of c-SELEX (including negative c-SELEX), cloning, and molecular sequencing processes. Stabilities of the identified aptamers were analysed under different pH and c-SELEX binding buffer conditions. The target binding affinity of the generated aptamers was analysed through in-silico docking studies and finally, the affinity was confirmed by CD and ITC studies. The binding affinities and the sequence of the finally selected aptamers are mentioned in the table 5.7.

Aptamer name	K_d value ITC	K_d value CD	Sequence (5' - 3')
cT12	14.42±1.5μM	0.4193±0.1561μM	CACCTAATACGACTCACTATAGACTTCGTATGCCAACAGCGATCCTAGATCGCGCAAGCTTGTTCGAGCCAG
cT21	10.7±0.056μM	0.17±0.2877μM	CACCTAATACGACTCACTATAGACTTCGTATGCCAACAGCGCACAGGGGACGCGCAAGCTTGTTCGAGCCAG
cT22	49.22±3.33μM	0.5888±0.2884μM	CACCTAATACGACTCACTATAGGCACAGGGGACGCACTTCGTATGCCAACAGCGCAAGCTTGTTCGAGCCAG
cT33	13.1±21μM	2.6143±0.1091μM	CACCTAATACGACTCACTATAGGCACAGGGGACGCACGGCGTATGCCAACAGCGCAAGCTTGTTCGAGCCAG

Table 5.7: Comparison of the binding affinities of the aptamers developed by c-SELEX process along with their sequences.

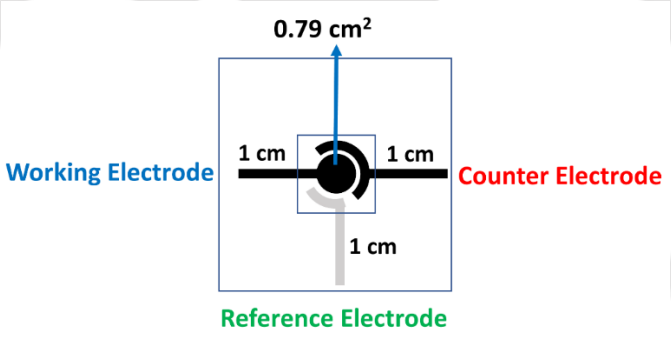

Chapter 6

Conductive ink-based Electrochemical Paper Platform for cTnT Detection

Chapter 6

Conductive ink-based Electrochemical Paper Platform for cTnT Detection

6.1 Overview

Point of care (POC) diagnosis for diseases like CVDs is extremely important especially in case of CVDs like strokes and AMI as they may results in either mortality or lead to serious health problems (Kakoti and Goswami 2013). However, commercial biosensors on POC and home diagnostics for such diseases are limited. Hence, a considerable attention has been paid recently for the development of such POC devices for AMI. The POCs devices for healthcare applications should be easy to handle, inexpensive, user-friendly and most importantly, these should be highly sensitive and complied well the ASSURED guideline of WHO. In this direction, the electrochemical biosensors are the potential candidates as they could meet the aforesaid requirements, provided the detection reactions are properly crafted and suitable disposable and environmentally friendly sensing platforms are designed.

Paper is one of the most widely used disposable platform for developing biosensors (Bordbar et al., 2021). It allows simple, cost-effective and large-scale production of the device. Paper has mechanical flexibility, hydrophilicity, and desirable dielectric properties. Moreover, the paper microstructure allows fluid transport through capillary action; hence no external pumping device for fluid flow on the platform is required. Paper also possesses surface properties that can easily be modified by some chemical or physical treatments to add flexibility to designs and applications of the resulting structures. Lightweight, renewable, and biodegradable are additional suitable properties that facilitated its commercial applications.

For developing paper based devices, various other membranes are also coupled to the platform to achieve some functionality such as filtration and support structures. Nitrocellulose and PVDF membranes are the most commonly used materials for these constructions. There are two general parameters for membrane design, physical dimensions and chemical composition. The physical structure generally concerns parameters like surface area, surface roughness, pore size (if any) and distribution and membrane thickness. The physical structure of the membrane is more critical for filtering applications, while the chemical composition is more critical for structural support applications (van den Hurk and

Evoy, 2015). Nitrocellulose is widely used in lateral flow immunoassays such as western blot as well as in screen printed electrodes (SPE).

SPE's are simple electrochemical system manufactured by printing different types of ink on different substrates. Sensitivity of such system are also contributed by conductive inks, which are deposited on them. A conductive ink generally consists of a conductive material such as silver flakes, silver nanoparticles, silver nanowires, Graphene, Carbon nanotubes etc., a surfactant to provide surface tension and a solvent to disperse all the materials. A screen-printed module with three electrodes contains a working electrode, auxiliary electrode (counter electrode), and reference electrode. Electrochemical event of interest is carried out on working electrode. The applied potential on the working electrode is controlled by potentiostat as a function of reference electrode potential. It is composed of redox inert material in the potential range of interest. Since the event of interest happens on the working electrode, its surface should be well defined and clean to ensure proper measurement. The reference electrode provides a well-defined and stable equilibrium potential. It is used as a reference point against which the potential of other electrodes can be measured in an electrochemical cell. The counter Electrode is used to complete the circuit. When the potential is applied the flow of electrons happens through the working and the counter electrode. To ensure that the kinetics of the reaction occurring at the counter electrode do not inhibit those occurring at the working electrode, the surface area of the counter electrode is made greater than the surface area of the working electrode. (Elgrishi et al., 2018).

The SPEs are generally made from carbon, gold, platinum, silver, or carbon nanotube inks. These are single use devices, inexpensive, specially designed to work with sample microvolumes, and they can be subjected to electrochemical analysis by various methods, such as cyclic voltammetry (CV), differential pulse voltammetry (DPV), square wave voltammetry (SWV), chronoamperometry (CA), and chronopotentiometry (CP). They are used successfully in the most varied fields that involve electrochemical analysis methods, such as quality control, research, detection of a wide range of analytes (i.e., antigens, enzymes, and heavy metal ions, high degree of efficiency) for its sensitivity. SPEs confer many advantages in comparison to the conventional diagnostic methods where detection of different analytes using immunological methods (ELISA) or even diseases and

microorganisms by molecular analysis (PCR, real-time PCR, LAMP, etc.) as they are easily convertible to POCs, they require very less sample and are easy to operate (Mincu et al., 2020). Although SPEs are suitable candidates for rapid diagnosis, they have limitations. For instance, cross reaction with other non-target products can occur, which leads to poor selectivity of the method.

In the current chapter a disposable paper based electrochemical biosensing platform for cTnT detection has been developed. The electrodes are printed on a nitrocellulose membrane by an in-house screen printing technique and the compositions in the electrode has been optimized during the printing keeping in mind the required functionality for the sensors. The working electrode of the SPEs is prepared by a pencil led (Graphite) conductive ink which exhibits good conductance for the ink to function as an electrode material. Aptamer cT21 prepared in chapter 5 is immobilized over the SPEs for detection of cTnT, which is the gold standard biomarker for AMI detection.

6.2 Experimental procedures

6.2.1 Materials

The screen-printing process used in this chapter was performed manually. The screen-printing apparatus requires wooden frame, squeeze, polyvinylidene fluoride (PVDF) membrane, and nylon mesh for its crafting. cT21 ssDNA aptamer was purchased from IDT technologies (USA). Sodium lauryl Sulfate (SLS), Sodium dodecyl sulphate (SDS), Polyethylene glycol (PEG), KCl, NaCl, NaH_2PO_4, Na_2HPO_4, Nitrocellulose blotting membrane (0.45µm) were purchased from HiMedia Laboratories Pvt. Ltd. Alkyl ketene dimer 1840 (AKD) was purchased from Flourish Paper and Chemicals Limited (Mumbai, India). pencil led (graphite) for the preparation of conductive ink was purchased from Faber castle. Silver/silver chloride ink, milliQ water, acetone, isopropyl alcohol for printing reference electrode and carbon ink for control electrode was procured from sigma Aldrich.

6.2.2 conductive ink formulation

The conductive ink formulated in the current work consists of a conductive element, surfactant and a solvent. The surfactant gives the consistence for the ink which helps to

print it. Different surfactants like SLS, SDS and PEG at different concentrations were tested. The surfactants were dissolved in different solvents like milliQ water, acetone, isopropyl alcohol. The final ingredient for the generation of the conductive ink is a conductive material which has good electrochemical behaviour. For which pencil led is used that composed of graphite, clay and binder (wax, resins or polymers). Graphite is used extensively as an electrode material as it has great electrical properties and also is chemically stable. The pencil led was grinded into find powder in a mortar. The powder was then passed through a sieve to filter larger pieces. Different percentages of the fine graphite powder were mixed with surfactants and solvents. The mixture was then sonicated with a probe at 4^0 C for 30 min. The ssDNA electrical properties were also studied to understand the behaviour of the aptamers when combined with the conductive ink.

6.2.3 Platform selection

The platform for developing a screen-printed electrode needs to be considered for its cohesion, hydrophobicity and electrical permittivity. PVDF membrane, Whatmann filter paper grade 4 were also tested for screen printing. The membranes were also tested by increasing their hydrophobicity by treating them with AKD. The membranes were soaked in 1% (W/V) AKD solution in *n*-heptane and then heated on a hot plate at 100^0 C for 5 min and cured for 30 min at 60^0 C before use.

6.2.4 Electrode design

The electrodes were designed in way to withstand strains generated during the clip connections. The nitrocellulose membrane is not sturdy to withstand the strain applied by three clips in a single portion. A directional approach for the printing to minimize the strain on the membrane was developed. This approach also ensure that the platform is stabilized and also prevents any fluctuation due to shaking of the platform on addition of sample analyte. A single geometry design with three different dimensions were chosen for the construction of the electrodes. The length and width of the electrodes were 1cm and 0.1cm, respectively. The working electrode has a circular portion with an area of 0.79 cm^2 where the aptamer will be immobilized. The electrode designs are illustrated in the figure 6.1.

6.2.5 Screen printing technique optimization

A wooden frame with mesh along with vinyl sheets, squeeze and transfer tape was purchased from amazon. The stencil-cut of the electrodes designed was made on to the vinyl sheet using a vinyl cutter. The obtained vinyl sheet with desired designs was then allowed to paste on to the wooden frame with the help of the transfer tape. The frame was then placed on the nitrocellulose membrane (substrate). The conductive ink was poured on to the frame over the stencilled vinyl sheet and then spread using a squeeze, which forces the ink (graphite-PEG) pass through the screen and transferred onto the nitrocellulose membrane to produce conductive paths for electrode connection, working and counter electrodes. The coated ink was air dried at room temperature. Later, Ag/AgCl paste was forced through the reference electrode design to obtain the reference electrode print. The adopted screen-printing technique is illustrated in scheme 6.1.

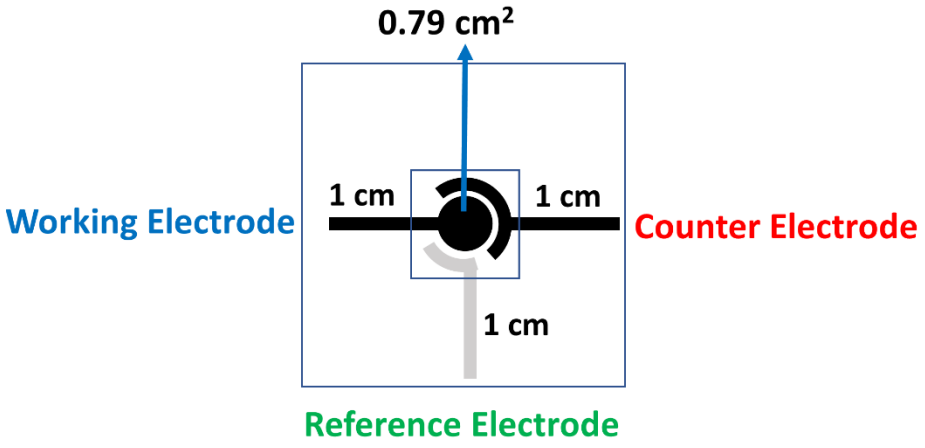

Figure 6.1: The electrode design along with their dimensions used for SPEs.

6.2.6 Fabrication of SPE

The distance between each electrode (WE-RE, RE-CE and CE-WE) was optimized by performing the CV measurements. The SPEs were printed according to the optimized dimensions. The printed SPEs are tested for the conductance each electrode separately and only the ones which fall within the top of the bell curve are selected for further processing. The finalized SPEs are then immobilized with aptamer cT21 by physical adsorption. 2 nM

cT21 was immobilized on the circular WE by drop casting and then incubating the SPEs in a desiccator at 37^0 C for 4 hr to dehydrate the membrane.

6.2.7 Electrochemical analysis

Cyclic voltammetry (CV) and electro chemical impedance spectroscopy (EIS) measurements were performed in a Zahner Zennium Photo electrochemical workstation (Zahner-elektrik, Germany). All the measurements were performed with the potentiostat mode turned on and by selecting the 3-electrode system for the study. All the measurements were made in 100 mM KCl in PBS. The CV studies were performed within a potential range of -0.5 V to 0.5 V at a slew rate of 50 mVs^{-1}.

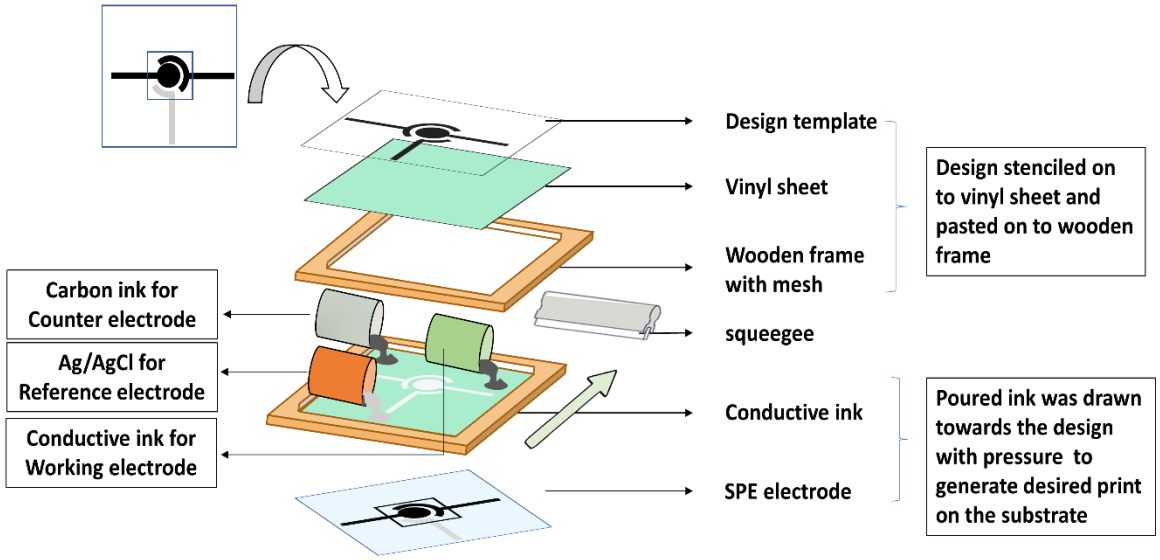

Scheme 6.1: The screen-printing technique adopted for preparation of SPEs.

The EIS experiments were performed within kHz to mHz and the amplitude of the alternate voltage was 10 mV. All the measurements were performed in a dust free environment inside a faraday's cage to prevent any external interference. cTnT samples of varying concentration (100 µl) were introduced on the WE of the SCP. The SCPs were incubated for 5 min for cTnT to interact with cT21 aptamer. The SCPs were then washed gently by dipping in a beaker with MQ water thrice. The SCPs are then connected to the PECC workstation and 100µl of the reaction buffer is introduced and the measurements were carried out as mentioned above.

6.2.8 Statistical analysis of data

All the CV and EIS experiments were performed in triplicates and the measurements were recorded. The limit of detection (LOD) was calculated from the slope of the calibration curve for the cTnT detection by using the relation, LOD= Limit of blank (LOB) + 1.65 X SD of lowest concentration, where LOB = Mean of blank + 1.65 X SD of blank.

6.3 Results and Discussion

The purpose of the current chapter is to produce a proof-of-concept of a paper based electrochemical sensor to detect cTnT. A three-electrode system was generated on a paper by the screen-printing technique. An indigenously prepared conductive ink was used to print the working electrode. The inks to print counter and the reference electrodes were commercially available carbon and silver/silver chloride ink, respectively. cT21 aptamer with best binding affinity that was selected in chapter 5 through SELEX, was immobilized on the working electrode by physical adsorption. Upon adsorption of the aptamer the resistance of the electrode system was increased. On introduction of the cTnT protein the resistance of the electrode system was increased further due to the binding of the cTnT protein to cT21 aptamer. The concentration of the bound cTnT was directly proportional to the increase in the resistance of the system as revealed from the CV and EIS experiments. The above concentration dependent increased resistance phenomenon was used to calculate the LOD of the system. The procedure adopted in the current work is depicted in scheme 6.2.

6.3.1 Conductive ink formulation

The conductive ink components were screened by investigating the solvent solubility of surfactants, the effect of solvent on the paper platform, the percentage solubility of the surfactant, and the ability of the led powder to disperse in the solution. Based on the above factors it was observed that the dissolution characteristics of SDS in all the three solvents i.e., acetone, isopropyl alcohol and MQ water resulted in excess frothing and could not be a suitable surfactant. PEG was soluble in isopropyl alcohol only up to 20 %. An ideal surfactant percentage for a conductive ink is above 60%. PEG was 100% soluble in MQ water. Hence, PEG in MQ along with led powder was finalized as the components for the conductive ink.

However, the percentage of PEG from 70 to 100 % generates highly viscous solutions and hence was not ideal for dispersing led powder. To overcome this problem, the components were sonicated at 4 ^{0} C. The duration of sonication was optimized initially only to uniformly disperse the led powder in the PEG solution. However, later it was observed that increase in the duration of sonication led to decrease in the resistance of the conductive ink making it more conductive. The effect of duration of sonication on resistance of the printed electrodes was measured (Figure 6.2) and found that a maximum of 40 min of sonication was sufficient as after 40 min the water is vaporised due to the generation of heat generated during the process.

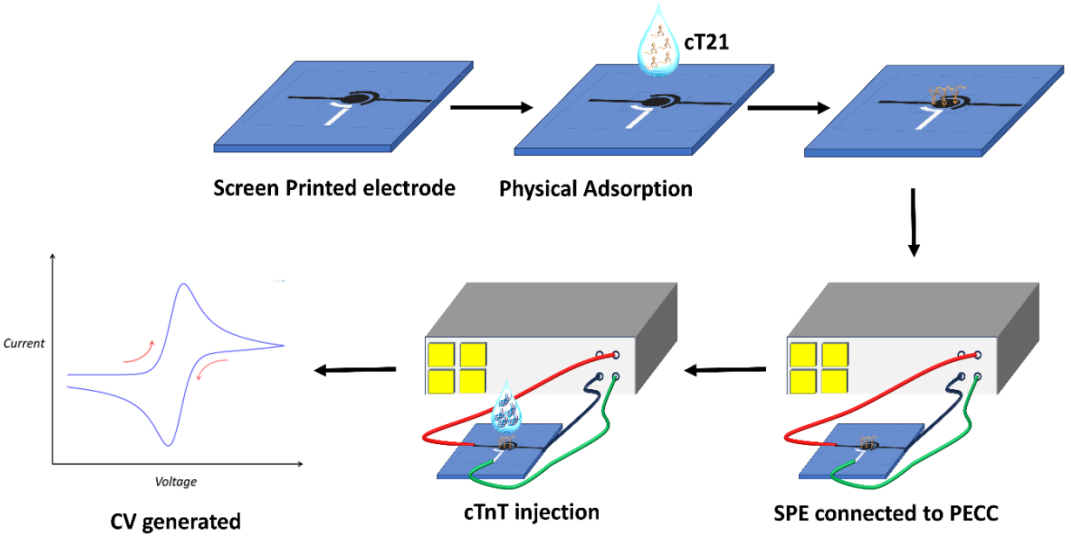

Scheme 6.2: Schematic representation of the generated electrochemical signal from the SPEs.

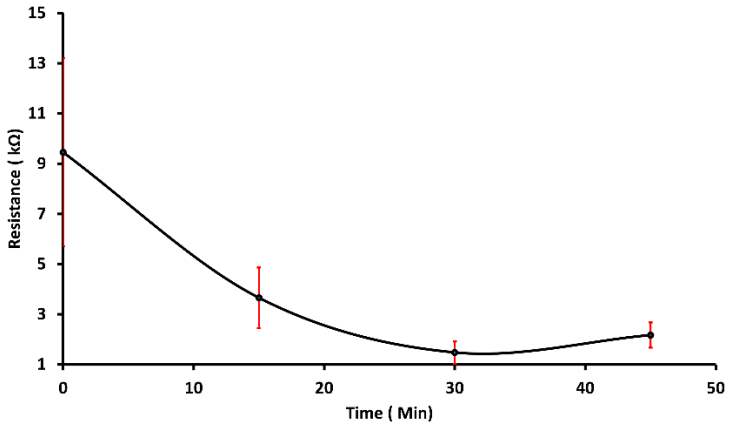

Figure 6.2: Resistance measurements of sonicated probes at different time intervals.

Scanning Electron Microscopy (SEM) and laser Raman spectroscopy studies revealed the interactions occurring in the conductive ink solution especially between the PEG molecules and the graphite of the led powder. Raman spectroscopy is an efficient and informative method to characterize the graphite (Kim et al., 1992). Graphite displays peaks at 1350 cm^{-1} called "D band" and 1580 cm^{-1} called as "G band". Both the bands are the resultant of the SP^2 carbon bonds. The G band is due to the in-plane vibrations of the SP^2 hybrid bonds while the D band is due to the structural defects in the graphite structure. A high D/G ratio means high conductivity. The experiments exhibited peaks at 1350 cm^{-1}, 1580 cm^{-1}, 2670 cm^{-1} which are characteristic of graphite (Figure 6.3 A). The Raman spectra of the conductive ink were measured after different period of sonication (0 min, 15 min, 30 min). The D/G ratio at 0 min was 0.1283, which was increased to 0.1774 at 15 min and to 0.707 at 30 min of the sonication (Table 6.1).

The increase in D/G ratio was due to the SP^2 molecules of the graphite which causes an increase in the D band following the reaction with the polyethylene functional groups of PEG molecules. The PEG molecule has a characteristic peak at 2845 and 2880 which were reduced drastically on sonication indicating the reduction in the number of polyethylene groups. The polyethylene groups interacted with SP^3 carbons resulting in the decrease in the SP^3 hybrid carbon molecules, which increased the conductance of the ink. Raman spectroscopy studies were complimented by the results of the SEM studies, which showed the polymer formation for 30 min sonication and formation of particulate matter conductive ink with no sonication (Figure 6.3 B).

To further enhance the conductivity of the ink, it was doped with single walled carbon nanotubes and iron nanoparticles. Different compositions of the PEG (80 – 100 %) were tried and the resistance was measured (Figure 6.4). A 30 min sonicated ink with void dopants was selected for printing the working electrode as it yields best electrochemical properties as in case of 100% PEG with no dopants gave least resistance with 1.1894 kΩ.

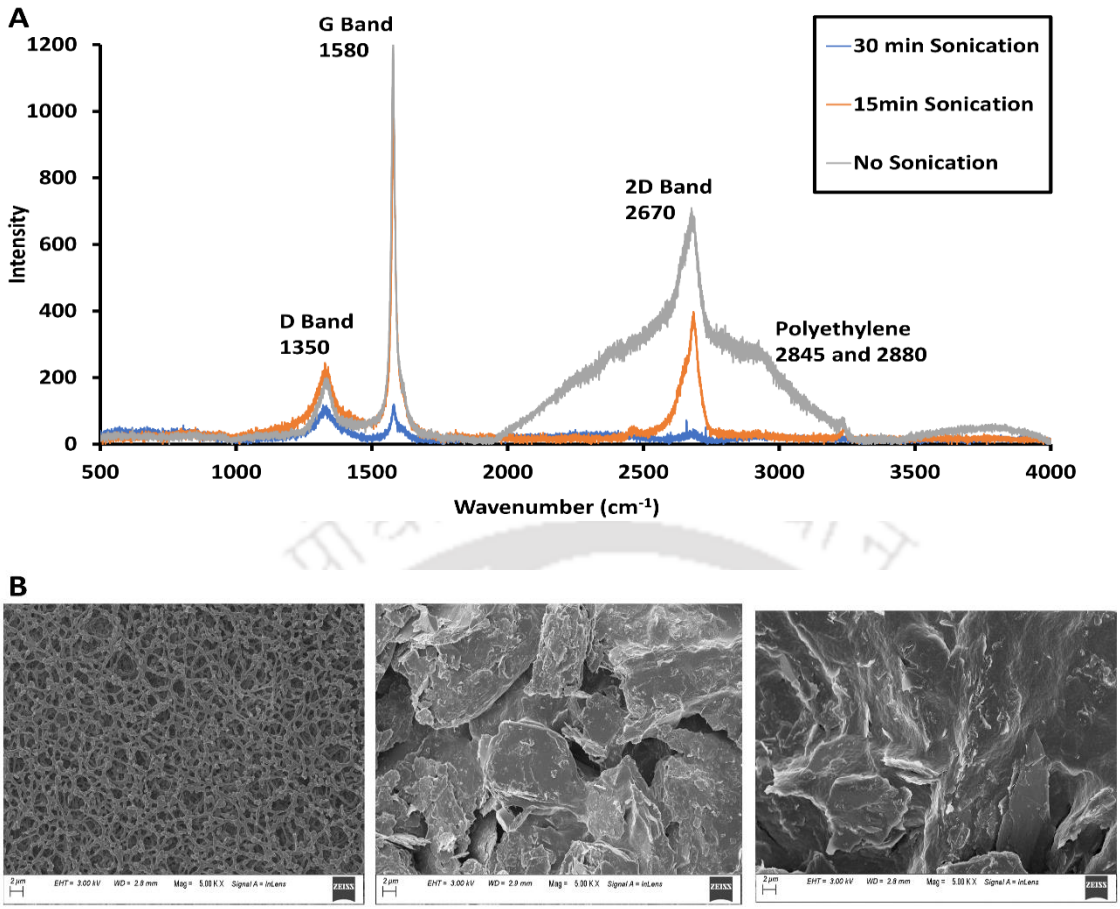

Figure 6.3: (A) Raman spectra of conductive ink at different periods of sonication. (B) FESEM from left to right: plain nitrocellulose, screen printed graphite electrode (no sonication) and screen-printed graphite electrode at 30 min sonication.

Electrode Type	D/G Ratio
No Sonication	0.1283
15 Min	0.1774
30 Min	0.707

Table 6.1: D/G ratio data extracted from the Raman spectrum of conductive ink captured at different period of sonication.

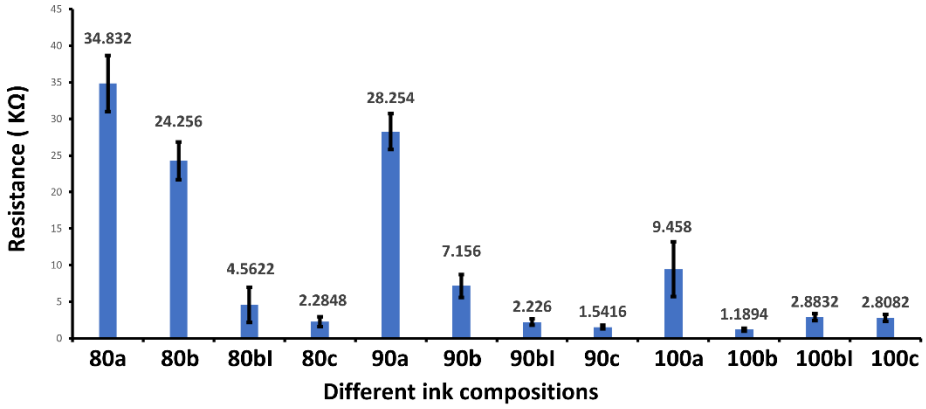

80a: Graphite (no sonication)+80% PEG
80b: Graphite (sonicated)+80% PEG
80bI: Graphite (sonicated)+80% PEG + Iron nanoparticles
80c: Graphite (no sonication)+80% PEG + SWCNT

90a: Graphite (no sonication)+90% PEG
90b: Graphite (sonicated)+90% PEG
90bI: Graphite (sonicated)+90% PEG + Iron nanoparticles
90c: Graphite (no sonication)+90% PEG + SWCNT

100a: Graphite (no sonication)+100% PEG
100b: Graphite (sonicated)+100% PEG
100bI: Graphite (sonicated)+100% PEG + Iron nanoparticles
100c: Graphite (no sonication)+100% PEG + SWCNT

Figure 6.4: Resistance measurements of different composition of conductive ink.

6.3.2 Platform selection

The screen-printing images of conductive ink on various platforms is shown in figure 6.5. The PVDF membrane was not a good surface for the printing due to its high hydrophobicity, which hampered the ink adherence to the membrane. The printing characteristics were better in the nitrocellulose membrane in comparison to Whatman paper. The reason may be attributed to the high hydrophilic nature of the paper. Hence, an attempt was made to make the platform partially hydrophobic using 0.5% AKD. The printing was better on the as prepared hydrophobic Whatman paper in comparison to non-hydrophobic one, even though it was not as good as plain nitrocellulose membrane. Like PVDF membrane, the printing on hydrophobic nitrocellulose membrane was also poor for similar reason. The electrical permittivity of nitro cellulose membrane on functionalization results in 1-3% reduction depending on the type of functionalized material. This makes nitrocellulose an ideal candidate in terms of permittivity. Other properties like cohesion and hydrophobicity also matters equally. So, the plain nitrocellulose membrane was selected for further printing studies.

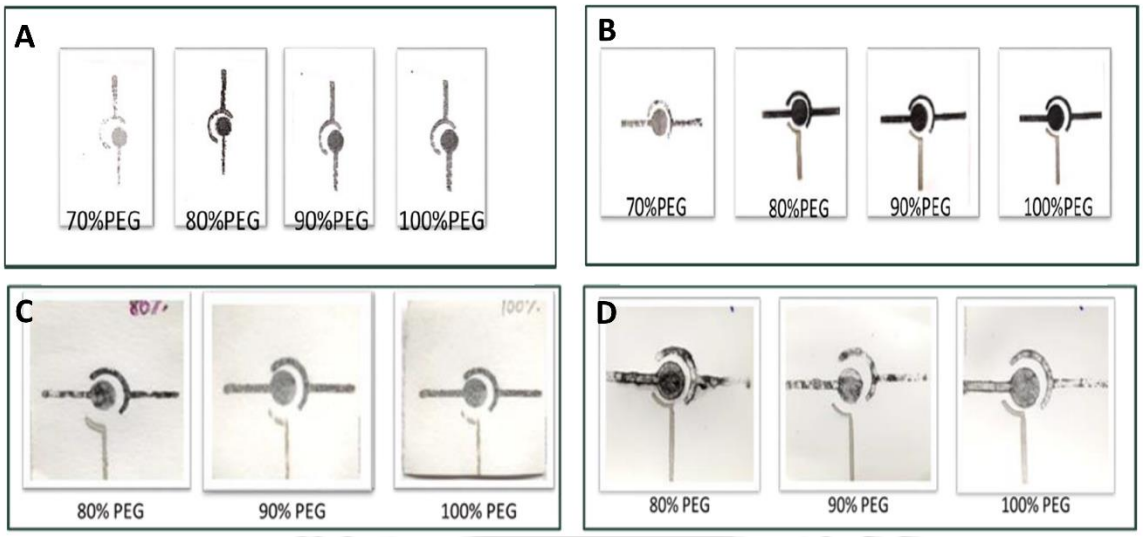

Figure 6.5: Different PEG compositions of conductive ink printed on (A) Whatman paper, (B) nitrocellulose membrane, (C) AKD treated Whatman paper, and (D) AKD treated nitrocellulose membrane.

6.3.3 Screen printing technique optimization

SPE when manually prepared generally yields inconsistent electrode performance. Hence the complete process was streamlined by considering every factor which could affect the printing consistency. The only factor which was difficult to maintain consistently was the applied pressure while printing with a squeeze. The following factors greatly affected the SPE performance:

1. Number of layers of print
2. Time space between printing of layers
3. The angle of Squeeze while printing
4. Number of iterations of printing with same aliquot of conductive ink
5. Distance between each of the electrodes

Increase in number of layers of the electrodes led to the change in the resistance, which decreased till 5 layers of printing, following which no further significant increase in the resistance was observed (Figure 6.6 A). Increase in number of layers for electrode printing

resulted in the filling up of the gaps which were present due to the mesh used during the SPE generation. Similarly, the resistance was analysed for the control and reference electrode (Figure 6.6 B). For the Ag/ AgCl paste, which was used for printing reference electrode, no significant change in resistance of the electrodes with respect to the number of layers was observed. Carbon ink that was used in the generation of counter electrodes had least resistance with a single layer. The time difference between printings of each layer was also studies and was found that the instant printing of the layers had the best yield with least resistance exhibited by the electrode (Figure 6.6 C). The angle of squeeze dictates the pattern of flow of the graphite and the clay present in the conductive ink. An angular squeeze position allows little clay particles to pass through the mesh of the wooden frame. An angle of 15^0 to 30^0 was the best angle for holding the squeeze to print (Figure 6.6 D).

Number of layers of electrodes than can be printed with a single aliquot of conductive ink was also measured (Figure 6.6 E) and was observed that up to 10 layers can be printed in a single aliquot. The distance between each of the electrodes is also very important as the membrane creates impedance of its own in the 3 electrode SPEs printed. Hence resistance measurements were taken at different distance of the electrodes (Table 6.2). The distance of 0.1mm between the RE-WE and CE-WE and a distance of 1cm between RE-CE gave the highest conductance measurement. All the resistance measurements were was calculated for the SCPs by Kelvin technique which is a method of measuring the sheet resistance by four probe.

6.3.4 Response characteristic of the aptasensor

CV and EIS studies were performed to analyse the functioning of the SPEs and its performance as an electrochemical sensor. The initial characterisation of the electrode was performed at 50 mVs^{-1} by tracing the behaviour of the potassium ferricyanide as a redox indicator. The SPEs exhibits anodic peak at 0.35V and a cathodic peak at -0.16 V. A shift in both the peaks was observed on immobilization with cT21 with anodic peak at 0.2V and a cathodic peak at -0.14 V (Figure 6.7 A). The redox peak current decreased with increase in the concentrations of cTnT. The reason has been attributed to the interference of the charge transfer on the surface of the electrode caused by the negatively charged ssDNA aptamer, cT21.

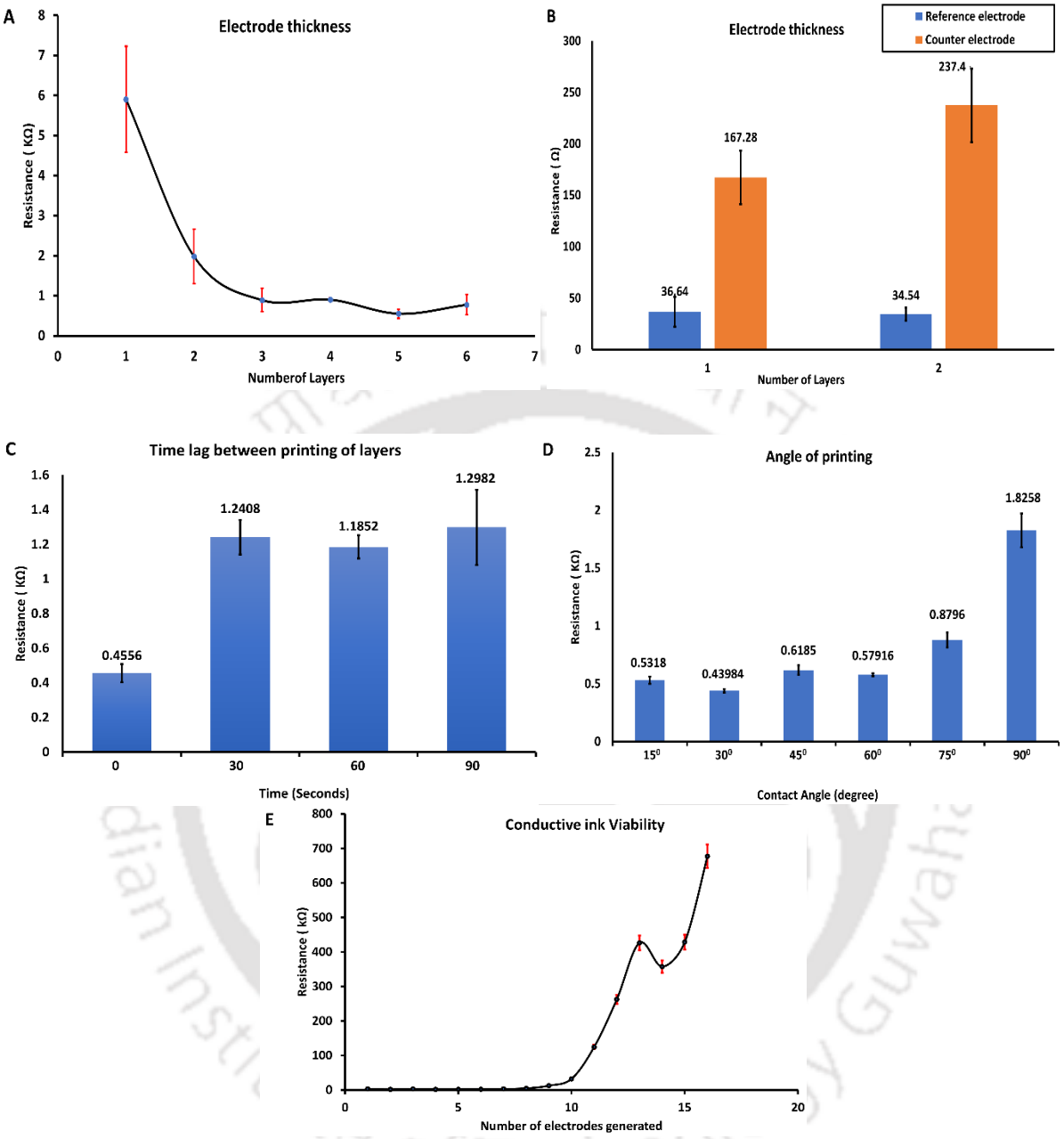

Figure 6.6: Resistance measurements for different screen-printing technique: (A) Number of layers that can be printed to generate working electrodes with least resistance. (B) Number of layers that can be printed to generate reference and counter electrodes with least resistance. (C) Incubation time after printing each layer of working electrode. (D) Study of the effect of the contact angle of the squeeze while screen printing. (E) Study of resistance behaviour of same aliquot of conductive ink in terms of number of layers of prints made on the nitrocellulose membrane.

The current reduction was more or less the same till 1nM cTnT concentration following which then the reduction occurred linearly till 100 nM (Figure 6.7 B). The linear region of the biosensor on the basis of the CV experiments was 1 nM to 100 nM (Figure 6.8). The LOD was calculated in the linear region. In the linear range the curve follows the equation y = -1.8982x +206.37. The LOD was 280.03 pM.

Electrode No.	RE- WE	RE- CE	CE- WE	Max current
E45	3mm	3mm	2mm	39µA
E46	1mm	2mm	1mm	75µA
E47	1mm	2mm	1mm	83µA
E40	1mm	2mm	0.1mm	85µA
E50	0.5mm	2mm	0.25mm	60µA
E48	0.25mm	2mm	0.5mm	59µA
E36	0.2mm	2mm	1.2mm	75µA
E44	0.2mm	1mm	0.1mm	516µA
E43	0.1mm	2mm	1mm	855µA
E42	0.1mm	2mm	1mm	131µA
E39	0.1mm	2mm	1mm	106µA
E41	0.1mm	2mm	0.1mm	132µA
E49	0.1mm	1mm	0.1mm	495µA

Table 6.2: The distance between each of the electrodes and their respective current outputs.

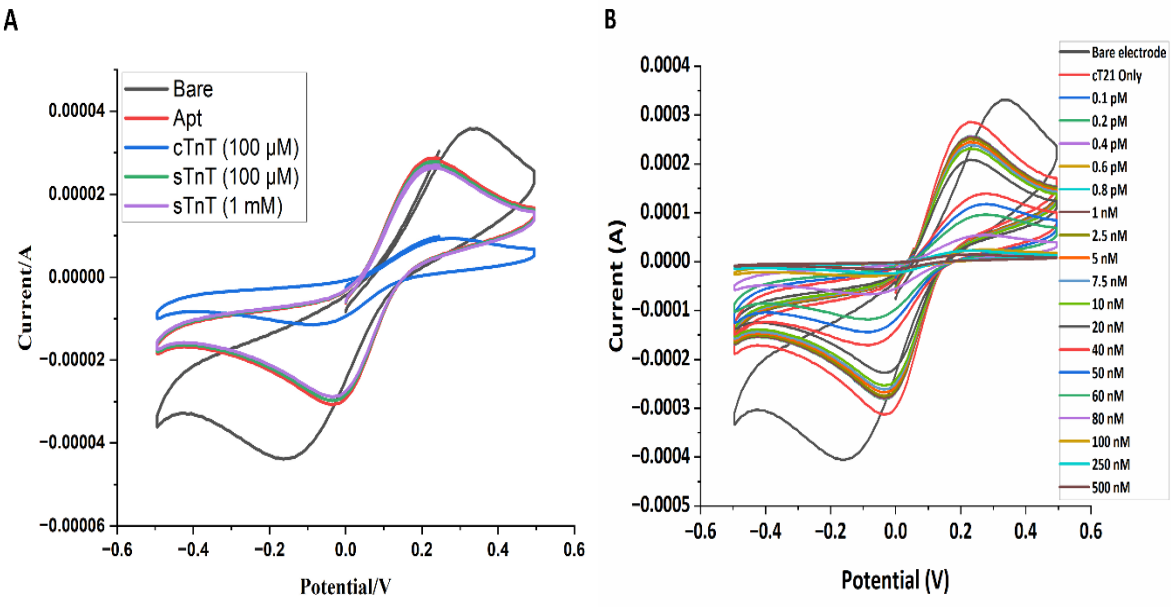

Figure 6.7: (A) CV spectra of bare SPE, at different fabrication steps and in presence of the control protein sTnT. (B) CV peak current values of SPE at different concentrations of cTnT.

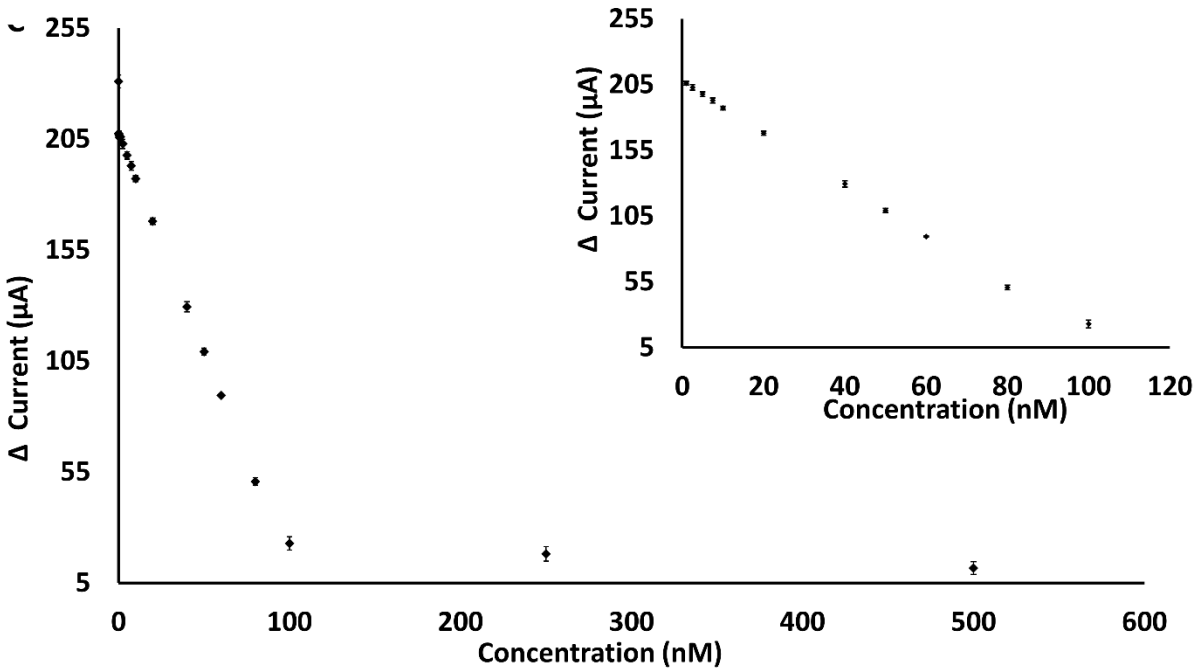

Figure 6.8: Response curve of the decreasing peak current values with increasing cTnT concentration and the linear range used for calculating the LOD of the sensor.

Impedance was also measured for the SPEs because it is one of the highly sensitive techniques for studying the adsorption process on the surface of the electrode. The impedance increased with increasing cTnT concentration as seen in the 1/Nyquist plots

(Figure 6.9). There was trend of increasing impedance signal from 1 nM to 20 nM. At concentrations of higher than 20 nM there is saturation in the impedance signal. Hence the EIS method was not suitable for LOD calculation.

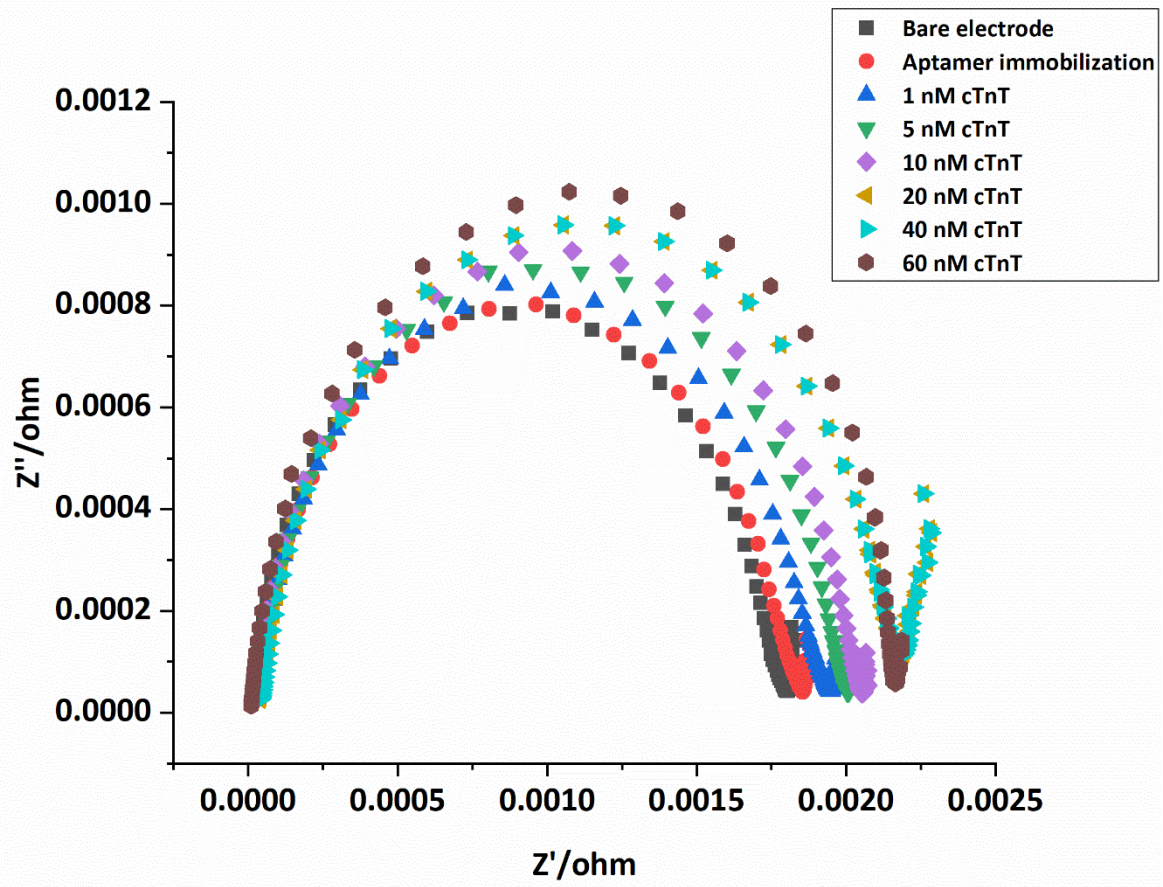

Figure 6.9: 1/Nyquist plots on the response of the generated cT21-SPEs toward cTnT concentration.

6.4 Conclusion

Herein, a disposable paper based electrochemical biosensing platform for cTnT detection has been developed using the aptamer cT21 as biorecognition element. The screen printed electrodes (SPE), prepared by a pencil led (graphite) conductive ink, were printed on a nitrocellulose membrane and the compositions in the electrode were optimized to achieve its best performance. The parameters considered for the optimization of the SPEs were thickness of the working electrode, distance between the electrodes, time lag between printing of electrode layers. The cT21 aptamer was physically adsorbed on the SPE and performance of the developed sensor was successfully analysed by CV and EIS. The LOD of

the sensor, discerned from the cyclic voltammetry experiment, was 280.03 pM and the linear detection range was 1 nM to 100 nM. The impedance spectroscopy studies also revealed similar pattern of increase in impedance with the increasing concentrations of cTnT. The fabricated sensor could detect cTnT at a clinically significant much lower level. Notably, the cTnT levels in any healthy individual are < 5 nM.

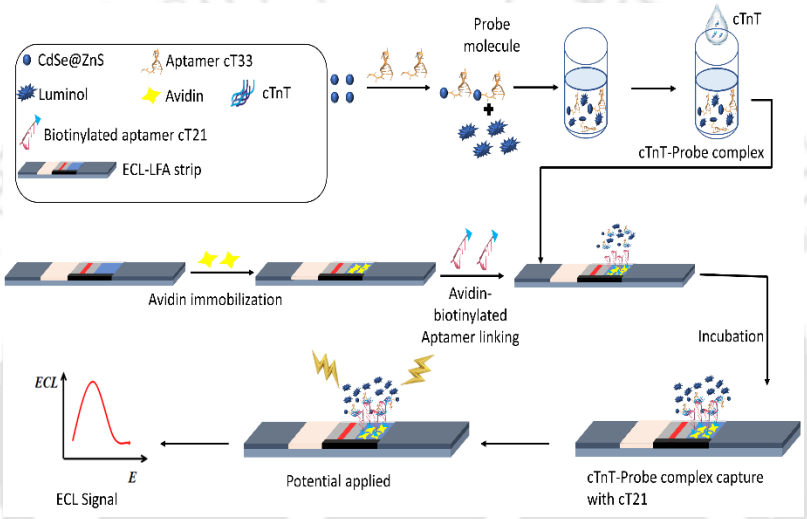

Chapter 7

Electrochemiluminescence-Based LFA Assay for cTnT Detection

Chapter 7

Electrochemiluminescence-Based LFA Assay for cTnT Detection

7.1 Overview

Electrochemiluminescence (ECL) is an electrochemical reaction-based luminescence phenomenon where a charged species is generated at the electrode interface due to a potential-induced chemical reaction, which results in the formation of an excited state of ECL luminophore (Bachu et al., 2020). Upon return of the luminophore to the ground state, luminescent radiation in the visible region is emitted. The ECL, in short, is a combination of chemiluminescence and electrochemistry. The ECL mainly occurs in two ways: annihilation reaction and co-reactant reaction. Most initial sensor-based works were limited to annihilation reaction using ruthenium compounds as luminescent probes. The invention of co-reactant reactions enhanced the prospect of the sensor-based ECL for practical utility, as revealed by the surge of sensor-based publications (> 75%) and patents following the year 2009. The first ECL bioassay, performed for oxalate ion detection, was reported in the 1990s. Eventually, several platforms and materials for ECL assays were explored, such as quantum dots (Bard et al., 2002) and various other nanoparticles and nanomaterials (Ding et al., 2002). Quantum dots exhibit strong ECL peaks in the presence of certain co-reactants like $K_2S_2O_8$ and H_2O_2. Hence, these fluorescent nanoparticles were adopted to develop biosensors following signal enhancement and quenching phenomena (Zou et al., 2004, Ding et al., 2006, Jhe et al., 2007, Jiang et al., 2007).

Luminol is the most widely used co-reactant as it produces a strong anodic peak at λ_{425nm} in alkaline conditions (Chen et al., 2011). The only disadvantage of luminol is that the ECL intensity at physiological pH is very weak and requires reagents that generate oxygen free radicals to enhance the ECL emission (Lin et al., 2008). Gold nanoparticles are explored as a catalyst to enhance the ECL signal to mitigate these plaguing problems (Zhang et al., 2014). The usage of gold nanoparticles reduces the problem only to a certain extent. Later on, it was observed that a combination of the quantum dots and luminol exhibits very good electrocatalytic behaviour. Hence in the current work, lumidot were used as a luminescent probe as it eliminates the need for unstable H_2O_2 and offers a stable and enhanced ECL signal (Dong et al., 2014).

Chromatographic papers have been intensively studied to create a biosensor support platform for point-of-care testing (POCT). These are cost-effective, biocompatible, and bio-degradable materials and allow passive fluids diffusion through capillary channels in microfluidic devices, obviating the need for an external energy source. Paper platforms are growingly explored to develop lateral flow assays (LFA) based biosensors in research and commercial paradigms. LFAs are POCT devices, which are low-cost system widely used for the quantitative and qualitative detection of target analytes. It relies on the capillary movement of the sample through the test strip and is convenient to design for developing a portable device.

The current chapter describes an ECL-LFA strip where cTnT is detected by exploring aptamer-protein-aptamer sandwich assay. CdSe@ZnS quantum dots, commercially known as lumidot, are catalysts to enhance the ECL signal. A DC voltage supply device has been coupled to the system to provide the potential for the specially designed LFA strips equipped with a two-electrode system to induce the ECL reaction.

7.2 Experimental methods

7.2.1. Materials

ssDNA aptamer (cT33) and 5' biotinylated cT21 aptamer were procured from IDT technologies (USA). KCl, NaCl, NaH_2PO_4, Na_2HPO_4, H_2O_2 (~50 w/v%), methanol (99.9%), and Streptavidin were purchased from HiMedia Laboratories Pvt. Ltd. Alkyl ketene dimer 1840 (AKD) was purchased from Flourish Paper and Chemicals Limited (Mumbai, India). For the generation of lateral flow assay (LFA) platform, Whatman Grade 1 Filter paper, and Lumidot were purchased from Sigma Aldrich (USA). Nitrocellulose blotting membrane (0.45µm) was purchased from HiMedia Laboratories Pvt. Ltd. Blotting membrane was purchased from Bio-Rad laboratories. Finally, a potential generating device (12V transformer), a general-purpose diodes 1N4007, Capacitors, resistors, LM7805 voltage controller, Multimeter were purchased from electronics dealers from Guwahati, Assam.

7.2.2 Docking studies

The aptamers cT12, cT21, cT22 and cT33 exhibited best binding affinities to the target as revealed from the studies described in chapter 5. Four docking studies were performed for cTnT and the aptamers in patch dock web server. The aptamer cT12, cT21, cT22 and cT33 pdb files were generated for docking by adopting the procedure explained in the chapter 3. The cTnT protein pdb file was downloaded from the RSCB PDB server. The docking results were downloaded and then analysed in VMD. In VMD one aptamer and one docked complex was uploaded to verify the binding regions of the aptamers with the protein. The aptamers binding at different regions of the target proteins were selected for ECL_LFA sensor.

7.2.3 DC voltage supply device

A DC voltage supply device was installed to provide a required potential to the LFA platform. The step-down transformer produces 12 V at its output that fed into full-wave bridge rectifier, which converts the AC voltage into DC voltage. To reduce fluctuations for a steady voltage, the 1µF capacitor was connected to the rectifier. The voltage regulator IC LM7809 controls the 12V DC input from the 1µF and produced 9V volt output. The output voltage was stored in the 0.1µF capacitor. The 9V voltage output was divided using a voltage divider circuit comprising two equal value resistors. The voltage divider enables the user to obtain a voltage in the range from -4.5V to +4.5V. Using the potentiometer, the voltage can be selected between -4.5V to +4.5V. To measure the value of the output voltage before it is fed into the device, a DC voltammeter was used. The circuit fabrication design is illustrated in the figure 7.1.

7.2.4 LFA platform design

Paper based LFA platform was prepared initially by designing the dimensions of the platform in adobe illustrator CS6 (Version 2020). Platforms with different dimensions of length and width were tested in order to minimize the time required for the solution to travel from one end to the other through capillary action. The capillary action was made directional by creating a base platform with AKD modified chromatography paper No 1. The paper was

dipped in a 1% (w/v) AKD solution in n-heptane. The paper was then heated on a hot plate at 100 °C for 5 minutes and then allowed to cure for 30 minutes at 60 ℃ prior uses. This hydrophobic paper was used as the back pad upon which the LFA platform was constructed. The blotting membrane was utilized as absorbent pad and sample pad. A Whatman filter paper grade-1 was cut and saturated with 0.1M KCl solution to make the conjugate release pad which aids conduction between both the electrodes. Nitrocellulose membrane (0.4 µM) was used as the stage to create test zones. The LFA strips were prepared by cutting sample pad (1cm x 0.3mm), conjugate pad (1cm x 0.3mm), nitrocellulose membrane (1.5cm x 6.5cm), and absorbent pad. The electrodes had a geometrical surface area of 1cm x 0.3mm. The entire set up was glued one upon other with the help of a starch-based adhesive. The order of the membrane layers from bottom to top was chromatography paper < Nitrocellulose membrane < Whatman paper < Blotting membranes. There was a 2mm overlap between each of the layers of the LFA. The LFA platform designed is illustrated in the scheme 7.1.

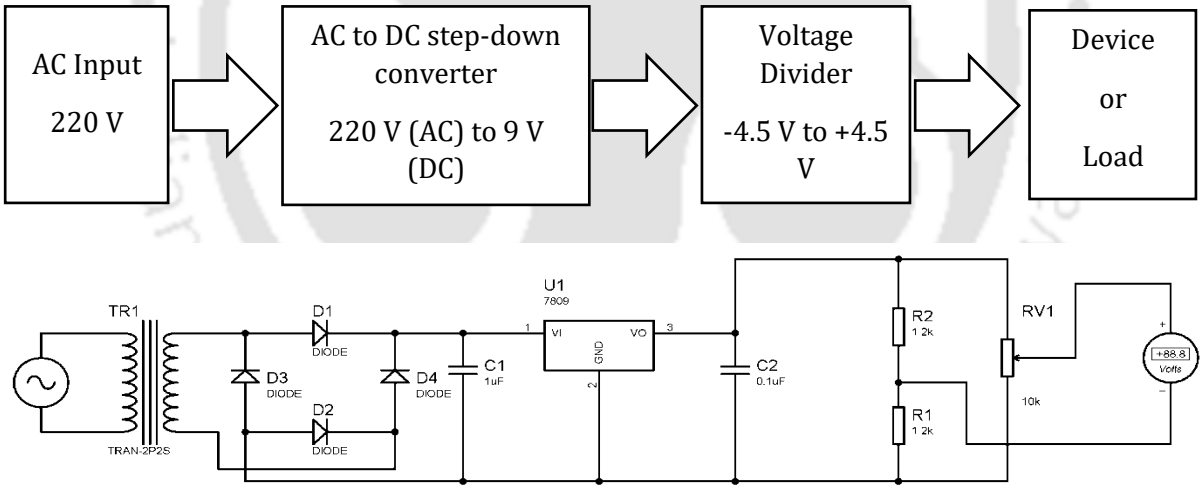

Figure 7.1: Circuit design of the DC voltage supply device fabricated for potential generation.

7.2.5 Fabrication of LFA

The generated LFA platforms were immobilized with aptamers by exploiting avidin-biotin chemistry. The strong physical absorption of avidin on nitrocellulose membrane is well documented (Tang et al., 2019). Streptavidin was directly adsorbed on to the nitrocellulose

membrane by drop casting and then incubating in a hot air oven at 37^0 C for 1hr. Once the streptavidin is immobilized onto the LFA strips, the streptavidin was then linked to the biotinylated cT21 aptamer. Scheme 7.2 illustrates the ECL-LFA strip generated and all its components.

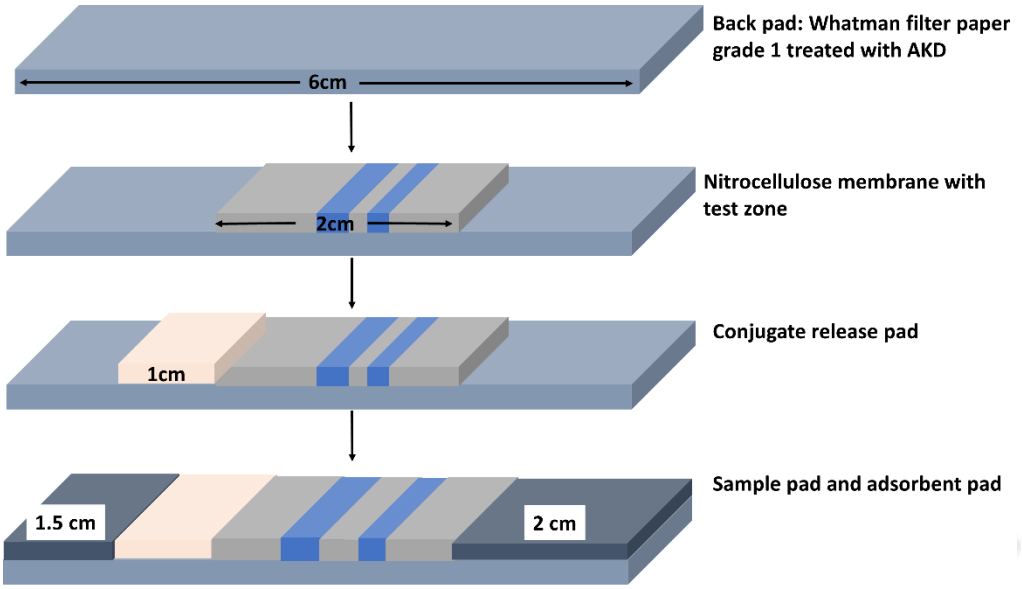

Scheme 7.1: Schematic representation of the LFA strip designed for the ECL sensor. The nitrocellulose membranes were screen printed with Ag/AgCl ink as reference ink and Carbon ink as working electrode by adopting the screen-printing procedure mentioned in chapter 6.

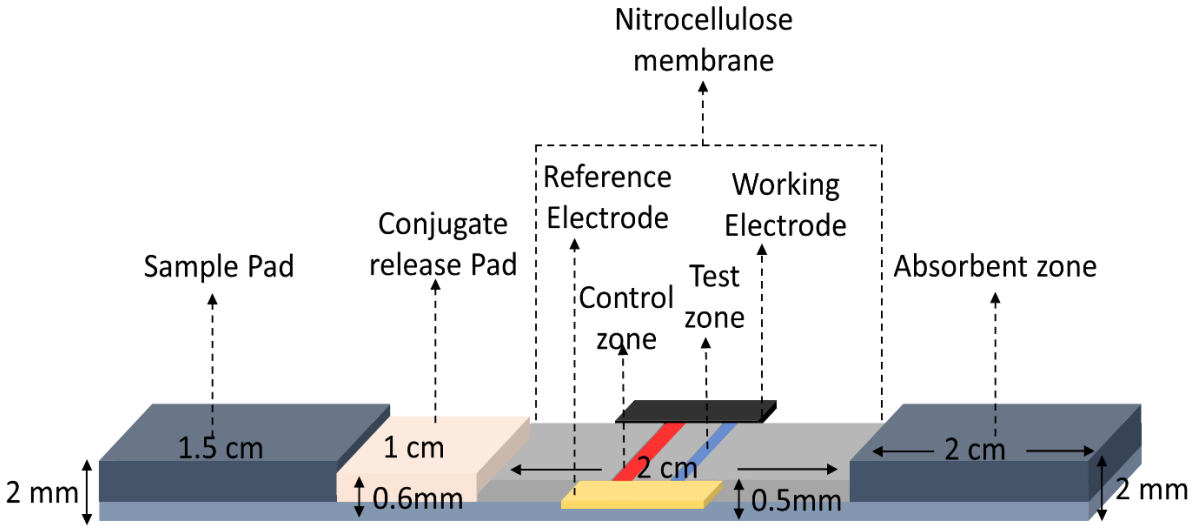

Scheme 7.2: ECL-LFA strip developed and all its components.

7.2.6 Characterization of luminol and lumidot

Luminol ECL is a very weak luminescence in neutral conditions without the aid of co-reactants like boric acid or H_2O_2 and metal nanoparticles. The addition of the co-reactants or the metal nanoparticles results in an enhancement in the ECL signal. The catalytic effect of lumidot over luminol was reported by dong et al (2014) in a thrombin ECL sensor. The lumidot, luminol and the combination of the both were characterized by fluorescence and UV-Visible spectroscopy

7.2.7 Electrochemical characterization of luminol and lumidot

Cyclic voltammetry (CV) was performed on Zahner Zennium electrochemical workstation (Zahner-elektrik, Germany) in the potentiostat mode in a three-electrode configuration. Ag/AgCl (3 M NaCl), platinum wire (Pt) and gold electrode were used as reference, auxiliary and working electrodes, respectively. All the measurements were taken in the electrolyte solution containing 10 mM $K_3Fe(CN)_6/K_4Fe(CN)_6$ (1:1) and 0.1 M KCl in PBS. The CV measurements were carried out in a potential range of -2 V to 2 V with amplitude of 10 mV. The slew rate was set at 100 mV/s. All the experiments were performed at RT in a dust free condition.

7.2.8 Aptamer lumidot linking

The lumidot and the aptamer cT33 were linked to each other by EDC-NHS chemistry. Lumidot (CdSe@ZnS) was spread and dried on an Eppendorf tube cap and mixed with 0.1 M Phosphate buffer (pH 7.4) with 10 mM EDC and 5 mM NHS. The solution was incubated for 1 hr. The unreacted EDC was quenched with 2-mercaptoethanol. Finally, 5 µM of the aptamer (cT33, N13) was introduced into the above solution and incubated at 4^0 C overnight. Fluorescence and UV- Visible spectra of the individual solutions and the aptamer-lumidot solution were recorded.

7.2.9 Set up for ECL-LFA detection of cTnT

cTnT solution was added to the ECL buffer solution (table 3.8 in appendix) which contains the lumidot linked to cT33 aptamer. The reaction buffer was incubated for 5 min at 37^0 C.

The reaction buffer concoction was added onto the sample of the LFA strip and the concoction was allowed to flow through. After duration of 15min with the aid of the DC voltage supply device a potential of 0.6 V was applied and the ECL signal response was captured.

7.2.10 statistical analysis of data

All the LFA experiments were performed in triplicates, and the resultant images were capture in a Nikon L830 Coolpix camera in dark conditions. The distance between the camera and the LFA strip was maintained constant with the aid of a tripod. Following which the captured images were processed and transformed into Red, Green, Blue (RGB) values through image J software to measure the pixel intensity of the individual colour. The obtained RGB values were statistically interpreted by calculating the mean of the data with their standard deviation (SD). The limit of detection (LOD) was calculated from the slope of the calibration curve for the cTnT detection by using the relation, LOD= Limit of blank (LOB) + 1.65 X SD of lowest concentration, where LOB = Mean of blank + 1.65 X SD of blank.

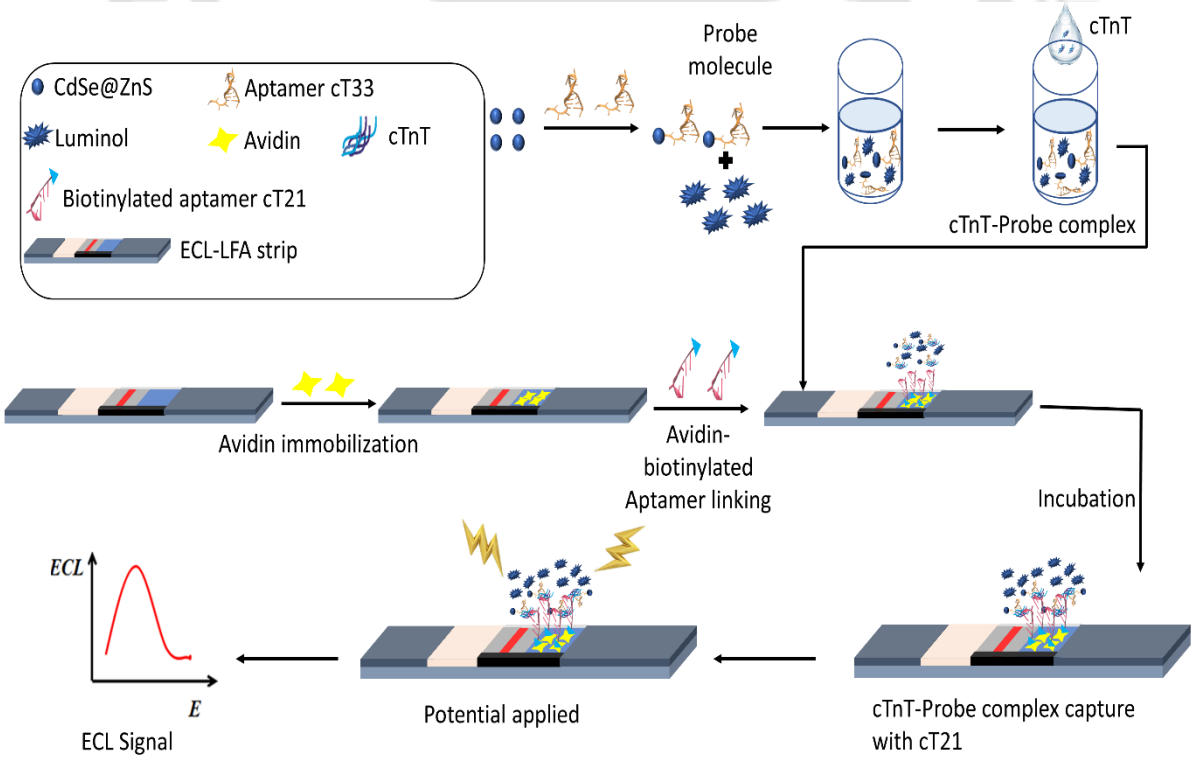

Scheme 7.3: Schematic representation of the steps involved in the ECL-LFA assay.

7.3 Results and Discussion

The objective of the current ECL-LFA work is to develop POC-based rapid detection of cTnT for AMI diagnosis. A microfluidic ECL-LFA device has been designed and fabricated to detect cTnT on the basis of Electrochemiluminescence response signal. The LFA is made on a backpad made up of AKD modified grade 1 Whatman filter paper. The AKD modification makes the backpad hydrophobic and ensures the capillary flow in forward and not in downward direction. The blot membrane is used as the sample pad as it receives the reaction buffer +cTnT solution and the sample pad filters the reaction buffer and aids the flow of this reaction buffer concoction. The reaction buffer consists of luminol solution and aptamer cT33, which is conjugated with lumidot. The conjugation is achieved through EDC-NHS chemistry. The cT33 lumidot complex acts as a biorecognition element which binds specifically to cTnT. The lumidot functions like a catalyst enhancing the ECL intensity.

The reaction buffer concoction flows from the sample pad to the conjugate pad which is a reservoir of dehydrated KCl solution, which make the reaction buffer conductive and enables the ECL reaction to occur on application of potential. The reaction buffer mixes with KCl and then flows into the nitrocellulose membrane. The nitrocellulose membrane consists of the test zone which is immobilized with cT21 aptamer which is the capture molecule. The cT21 aptamer captures the cTnT-cT33-lumidot complex. A potential is applied and the lumidot by resonance energy transfer oxidizes luminol resulting in the emission of an anodic ECL signal. The ECL intensity is proportional to the concentration of cTnT present in the solution.

7.3.1 Aptamers selection for ECL-LFA

Docking studies were performed to find out two aptamers which binds to cTnT in a symbiotic pattern. Four aptamers cT12, cT21, cT22, cT33 were developed against cTnT. cT21 has the best binding affinity among the four aptamers. Hence, cTnT-cT21 complex is docked against the other 3 aptamers. All the three complexes are visualized in VMD. The cT22 had same interaction region as cT21 (amino acid number 196 to 261) and was not considered for further study as the motivation behind the study was to identify an aptamer which complements cT21 and binds to a different region of the cTnT protein. cT12 and cT33

interacts with the amino acid sequence 122-179 and 131-190, respectively of the cTnT protein. Among cT33 and cT12, cT33 has the betted binding affinity. Hence cT21 and cT33 aptamers were chosen for aptamer-protein sandwich assay. The binding regions of different aptamers with cTnT are illustrated in the figure 7.2.

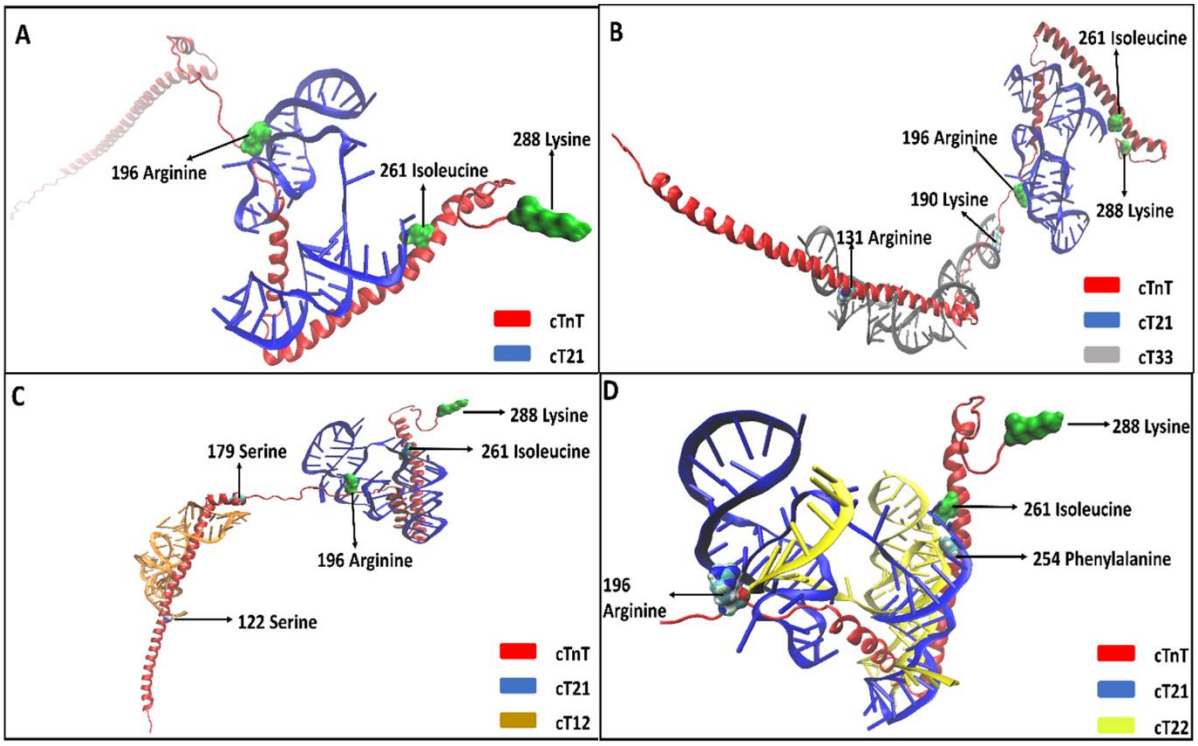

Figure 7.2: aptamer-protein docking interactions. (A) cT21 interaction with cTnT protein, (B) cT21 and cT33 interaction with cTnT, (C) cT21 and cT12 interacting with cTnT, (D) cT21 and cT22 interaction with cTnT.

7.3.2 Dimensional optimization LFA strip

The micro-fluid displacement in the proposed LFA strip is occurred through capillary forces. For the fluid to gain sufficient capillary forces to move through the microfluidic channel, the dimensions of the platform were optimized. To this effect, different widths of the LFA strips were crafted and examined the time required for the liquid to flow through the strips. Smaller the width higher was the flow rate. However, a minimum of 3mm width between the electrodes was required to ensure their contactless operations and to keep space for aptamer immobilization. Hence, width of 3mm was finalized for the LFA strip generation which has a flow rate of 0.83 ml/min. Various quantity of reaction buffer was introduced

into the strip and the volume at which the sample pad is filled with reaction buffer and has no overflow is selected as the sample quantity. The quantity required was 150 µl. The absorbent pad increases the capillary force by absorbing the excess fluid.

The length of the absorbent pad and the fluid that can be injected into the LFA strip are proportional. The length of the absorbent pad was also optimized to 2cm x 3mm as at this dimension the absorbent pad gets saturated. The ECL-LFA strips designed for the current study is illustrated in figure 7.3.

7.3.3 Characterisation of luminol and lumidot

The fluorescence behaviour of both Luminol and lumidot independently and in their mixture were recorded. The purpose of the UV-Visible absorbance spectroscopy and the fluorescence spectroscopy was to understand the individual behaviour of both luminol and lumidot and also their behaviour in the presence of each other. Two peaks were observed for luminol at λ_{305nm} and λ_{355nm} in UV-visible absorption spectra ranging from $\lambda_{300\text{-}400nm}$. The lumidot in an absorption spectrum of $\lambda_{250\text{-}500nm}$ exhibits a peak at λ_{260nm}. The mixture of luminol + lumidot solution results in the increase in the peak intensity of both luminol and lumidot peak. Figure 7.4B shows the fluorescent emission spectra of the luminol (1 mM), lumidot (6 µM) and their mixture with same concentration. The maximum fluorescence emission peaks of luminol and lumidot were at ~λ_{425nm} and at λ_{580nm}, respectively.

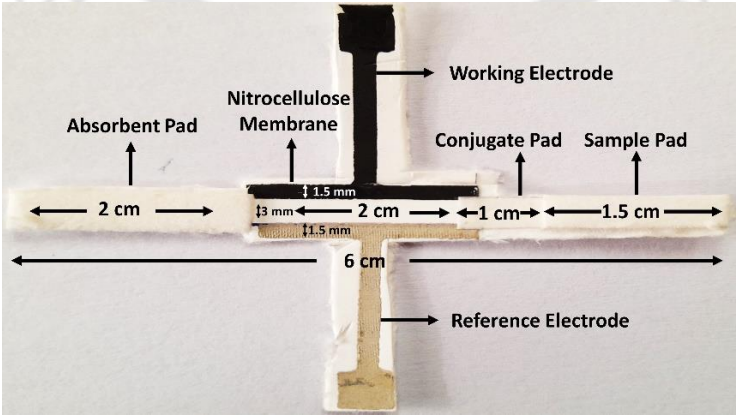

Figure 7.3: image of the ECL-LFA for detection of cTnT.

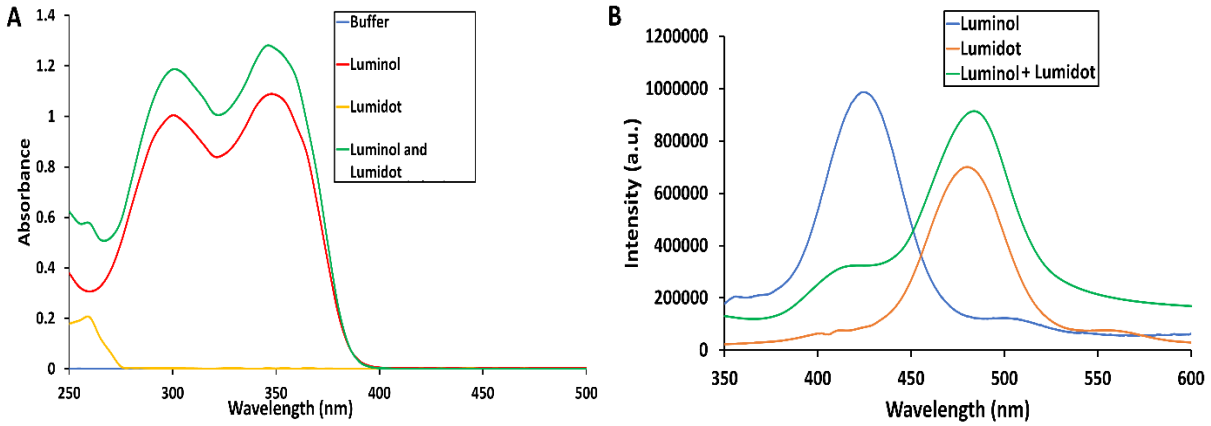

Figure 7.4: (A) UV-vis absorption spectra of luminol, lumidot, luminol + lumidot. (B) Fluorescence spectra of luminol, lumidot, luminol+ lumidot.

The overlap of the emission peaks of the mixture with same concentration as the individual samples, implies the occurrence of resonance energy transfer (RET) between the two molecules. Also, in the case of the mixture the emission at λ_{425nm} decreased drastically while the emission at λ_{580nm} increased significantly indicating the RET occurrence between luminol and lumidot which plays a key role in the ECL of Luminol in presence of lumidot without addition of H_2O_2 or any other co-reactant.

7.3.4 Electrochemistry of luminol and lumidot

CV studies were performed to analyse the effect of luminol solution in the presence of lumidot as catalyst. The bare gold electrode in the potassium ferricyanide solution yields a characteristic peak at a potential of 0.4 V; when the solution was replaced with luminol solution, an anodic peak at 1.4 V and a cathodic peak at 0.15 V were detected. The intensities of these peaks increased by 25% in the presence of lumidot further established the catalytic effect of lumidot on luminol (Dong et al., 2014). Visible CV peaks of lumidot were not observed as it was in the solution and not immobilized on the electrode surface. The aim of this experiment was to establish that the lumidot can enhance the ECL peak even when it was in the solution and not on the electrode surface.

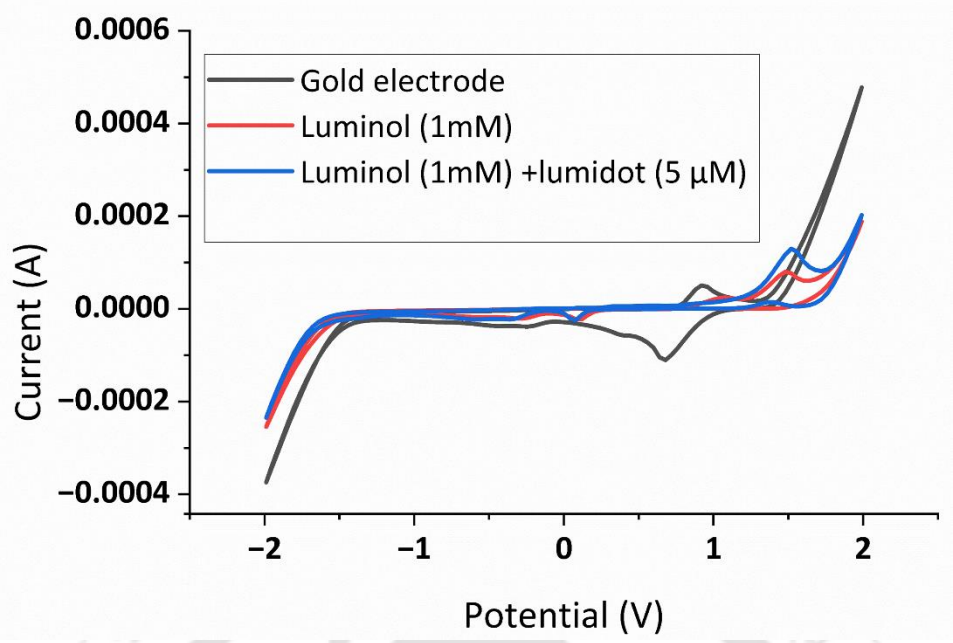

Figure 7.5: CV spectra of gold electrode bare, in presence of luminol and luminol+ lumidot.

7.3.5 Detection of cTnT using ECL-LFA strips

The ECL-LFA strips were connected to the DC voltage supply device. The cTnT was added to the aptamer cT33-lumidot solution and then the generated mixture was loaded into the sample pad. The cT33-lumidot-cTnT complex travelled from the sample pad of the LFA strip into the nitrocellulose membrane where the cT33-lumidot-cTnT complex was capture by cT21 aptamer. The unbound cT33-lumidot travels through the strip and was not captured in the strip. After an incubation time of 15 min, the potential was applied and the ECL luminescence was captured. The cT33-lumidot-cTnT complex reaches the nitrocellulose membrane in 3 min. However, to avoid any false positive result, an incubation time of 15 min was adopted as these results in the reaching of the cT33-lumidots into the absorbent pad. The intensity of the blue colour developed was varying depending upon the concentration of cTnT. The emission of the ECL luminescence was the indication of the presence of cTnT in the given sample.

7.3.6 Quantitative detection of cTnT

The cTnT was quantified by capturing the images of the ECL luminescence. The ECL was generated by the RET between luminol and lumidot. The entire reaction is depicted in the

scheme 7.4. The images were cropped and only the ECL luminescence portion of the image was select for the generation of a calibration curve. First the images were processed in Image J software and the RGB values were determined. In most of the cases the red colour was absent or negligible. The green colour intensity varied from 2 to 30 with no specific pattern. Blue colour increased with the increased concentrations of cTnT. This is because of the luminol luminescence. The luminol luminescence is weak in the absence of a catalyst but in presence of lumidot the luminescence increased exhibiting a proportional behaviour between the increased concentration of lumidot and luminol luminescence. The experiments were done in triplicates and the mean and SD was also calculated to determine the LOD of the ECL-LFA platform.

The LOB and the LOD of the ECL-LFA strip were calculated. The LOB was 42.55 pM and the LOD was found to be 42.71 pM. The linear range was observed from 100 pM to 10nM. The LOD was at 10 µM as at this concentration the blue intensity was ~255 which is the maximum intensity. Any further increase in the concentration of cTnT yields similar result. The curve (Figure 7.6) exhibits a dual behaviour the equation to calculate the cTnT levels can be divided into two regions. Till concentration of 10 nM the equation is y = 21.429ln(x) + 107.63 which exhibits a logarithmic behavior and from 10 nM till its saturation at 10 µM the response curve follows another logarithmic behaviour with an equation y = 12.638ln(x) + 144.75.

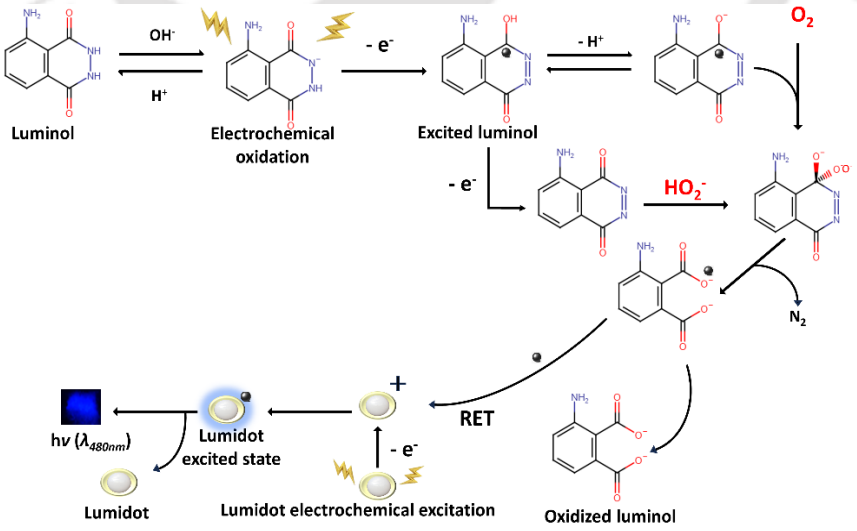

Scheme 7.4: Reaction scheme of the ECL generation reaction occurring between luminol and lumidot on electrochemical oxidation of both the species.

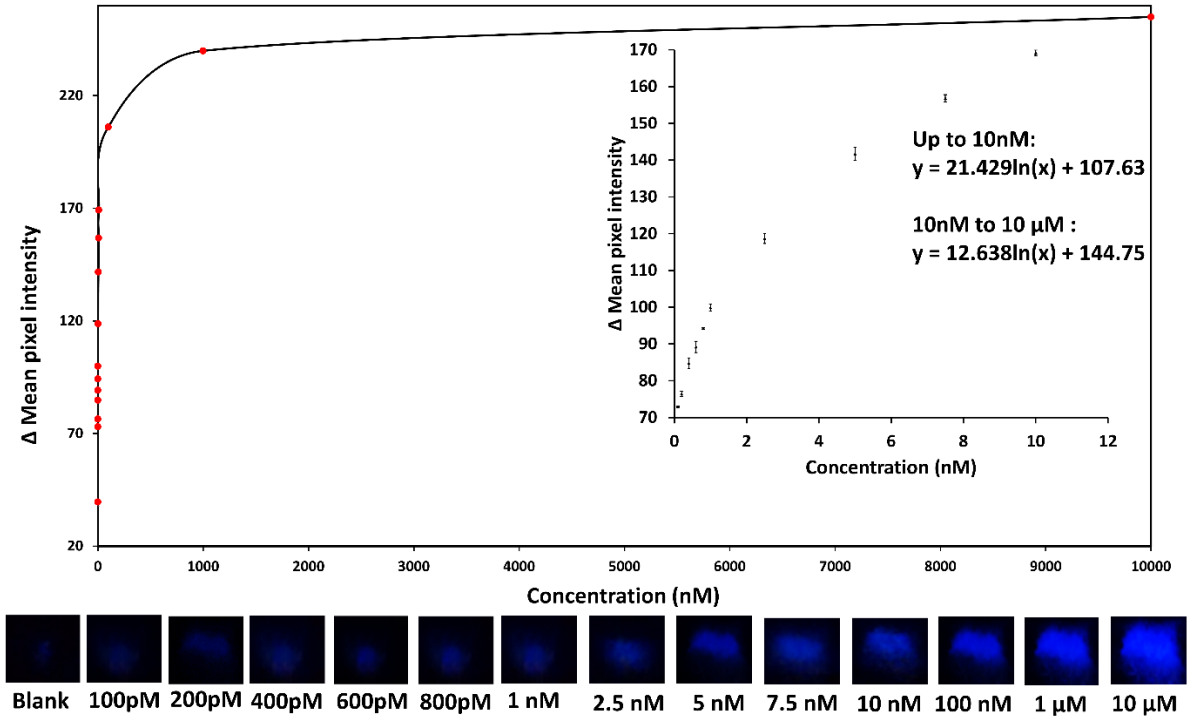

Figure 7.6: The ECL response plot derived from the mean pixel intensity of luminol in presence of varying concentrations of cTnT (1pM to 10 µM).

7.4 Conclusion

cTnT is generally referred to as gold standard biomarker for AMI. A new approach to detect cTnT through LFA was designed which functions on the principle of ECL. A modified paper based LFA strip was devised by the method of screen printing. The printed strip was transformed into a 2-electrode system for ECL based detection using was silver/silver chloride ink as reference electrode and carbon ink as the working electrode. Metal nanoparticles called, lumidot, which are known to have catalytic effect over luminol was tagged on to the aptamer cT33, which was the probe molecule. With the help of the avidin-biotin chemistry a capture probe cT21 was immobilized on the LFA strip to capture the cTnT-probe complex. A DC voltage supply device was built to supply the potential to the LFA strip. The ECL-LFA strips were able to detect very low levels of cTnT in the ECL based sensors. The LOD of the system was 42.71 pM. The ECL-LFA strip proposed in this chapter is able to detect complete diagnostic spectrum of cTnT levels from 14nM which is the minimum basal concentration of cTnT (99th percentile) to the extreme value of 10 µM which is observed in the case of a very large AMI and myocarditis. Most of the previous works till date detect

cTnT in pM to fM levels. The physiologically significant range of cTnT is from 5 nM to 10 µM. The sensors developed till date fail to detect cTnT above 285 nM which does not cover the complete physiological range.

Sensor platform	LOD	Range	Reference
Electro chemical (Thin film transistor micro device)	285 nM	Not available	Agarwal et al., 2018
ECL (Photomultiplier tube and charged coupled device)	8.57pM	14.28 – 14.28 pM	Yang et al., 2017
Electro chemical	3.5 fM	0.028 – 285.7 pM	Sharma and Jang., 2019
ECL (LFA based POCT)	42.71 pM	0.1 – 10000 nM	Current Work
Electrochemical (Screen printed electrodes)	280.03 pM	1 – 100 nM	Thesis Chapter 6

Table 7.1: A comparison of performance of various aptamer-based sensors developed to detect cTnT.

Conclusions and Future directions

The aim of the present work is to develop an aptasensor for MI using cTnT as a biomarker for the ailment. As a first step, an aptamer database “Aptabase" (https://www.iitg.ac.in/proj/aptabase/) was created by mining different aptamers available in the literatures to develop a general understanding on the nucleic acid aptamers and to offer a resourceful and interactive aptamer database to global aptamer scientists. The database provides some critical information about the aptamers, including general and specific targets, lengths, affinity to targets, buffer compositions, and GC content (%), and sequences. It could be regularly updated with the login facility offered to admin and aptamer developers, a feature that empowers the developers to add, refine and correct their data entry on demand without any need for coding skills. Additionally, a Google Analytics has been included to count the website users to analyze the interest traffics. However, the database should also be equipped with more plugins and widgets to further enhance the user experience. Some of the plugin like 2D and 3D structure generator and G-quadruplex finder needs to be included for future versions of the database.

In the next work, an in-silico ensemble method for 3D modelling of ssDNA Aptamers was formulated. This study identified the GC content, GC bond percentage, and G:C ratio as limiting factors in predicting secondary structures by different web applications. These findings prompted us to conclude that Guanine residues play a key role in the algorithms used by these applications for generating secondary structures and linked tertiary structures of the aptamers. The study also illuminates the relationship between secondary structure generation applications and RNA Composer, which generated 3D structures with 100% similarity for the same sets of aptamer candidates when the structures were generated from the same ct files. However, the predicted secondary structures differed in different applications. The dissimilarity of the algorithms used in the applications is the principal reason for the observed facts. It emphasizes the need for an improved algorithm to yield accurate structures. Understanding the guanine residues' role may help create an improved algorithm. The 3D aptamer structures could be classified into different categories based on their 3D conformation and adopted a dynamic ensemble strategy that filters out the secondary structure generation applications, which need to be harnessed for generating the 3D aptamer structure. "RNA Structure” and “UNA Fold” web applications work best for hairpin and stemloop structures, while “RNA fold” works best for helical chains and “Vector

builder" works best for globular structures. The ensemble method presented here provide precise information only if all the ensemble tools are accurate. However, currently the secondary structure generation tools need further improvement. One potential approach is to use artificial intelligence and machine learning tools to predict better secondary structures.

Prior developing the aptasensor platforms, the cTnT proteins along with the control protein, sTnT were successfully cloned, expressed and characterized. Following which a modified SELEX approach called a c-SELEX was designed and performed to develop specific aptamer against cTnT. Four specific aptamer candidates cT12, cT21, cT22, cT33 were identified, among which cT21 and cT33 were selected for the current studies based on the binding energy values with the target. The c-SELEX procedure task could be completed in a week making it quick, requires less instrumentation and allows the complete protein to interact with the aptamer library. The efficiency of the c-SELEX method, however, needs to be validated with different targets to establish it as a general tool to develop aptamer for diverse applications.

The first aptasensor developed in the current work was based on a disposable paper-based screen printed electrochemical platform with cT21 as recognition element and cTnT as the biomarker. The LOD (280.03 pM) and detection range (1nM to 100nM) offered by the aptasensor falls under the clinical range of 14 nM to 10,000nM. The proof-of-concept conceived through the work thus, has a great potential to develop as an MI aptasensor device for POC applications. The current procedure for fabricating the aptasensor, however, can be further simplified by incorporating an automated screen-printing technique to construct the SPEs. Moreover, the conductive ink used in the current study needs improvement in terms of conductivity as it exhibits significant electrical resistance. The effect of heat on led powder and PEG during the process of preparing the ink should be investigated to achieve a best composite for the function. Further, an alternative method, such as SAM, for coupling the aptamer with the electrode may improve the sensitivity of the detection system.

The second aptasensor was an ECL-based LFA platform for detection of cTnT. Metal nanoparticles, lumidots were harnessed for the catalytic activity to yield luminescence. The

characteristic features on this detection platform consist of dual aptamer sandwich assay where one aptamer is used as a capture molecule and the other is tagged with lumidot. The ECL-LFA strips were highly sensitive and capable of detecting cTnT within it's clinically relevant range. The LFA device developed through this study may be translated into a product of commercial interest with some improvements, such as coupling with a camera-integrated device such as, smart phone to capture the pixel response to further analyse with suitable custom-made software loaded in the device for quantitative detection of the cardiac biomarker for diagnosis of MI.

Bibliography

Agarwal, Dilip., Kumar, Kandpal., Manoj, Surya., Sandeep, G., 2018. Characterization and detection of cardiac Troponin-T protein by using 'aptamer' mediated biofunctionalization of ZnO thin-film transistor. Applied surface science 0169-4332. https://doi.org/10.1016/j.apsusc.2018.10.086.

Antczak, M., Popenda, M., Zok, T., Sarzynska, et al., (2016) New functionality of RNAComposer: An application to shape the axis of miR160 precursor structure, Acta Biochimica Polonica, 63(4), pp. 737–744. doi:10.18388/abp.2016_1329.

Apache.org. Available at: https://httpd.apache.org/.

Ashaduzzaman, Md., Antony, Aswathi Anto., Murugan, N, Arul., Swapneel, Deshpande., et al., 2015. Studies on an on/off-switchable immunosensor for troponin T. Biosensors and Bioelectronics 73 (2015)100–107. http://dx.doi.org/10.1016/j.bios.2015.05.055.

Ataide, Vanessa, N., Mendes, Leticia, F., Gama, Lillia, I, L, M., et al., 2020. Electrochemical paper-based analytical devices: ten years of development. Anal. Methods, 2020, 12, 1030. DOI: 10.1039/c9ay02350j.

Bachu, Vinay., Goswami, Pranab., 2020. Bioelectrochemiluminescence as an analytical signal of extreme sensitivity. Advance materials and techniques for biosensors and bio analytical applications, CRC press.

Bachu, Vinay., Deware, L., Kumar, A., Mili, M., Goswami, P. (2021) Aptabase: An aptamer databse, Website: https://www.iitg.ac.in/proj/aptabase/index.html.

Bard, Allen, J., Luttmer, J, D., 1997. Photo-Induced Electrogenerated Chemiluminescence and Up-Conversion at Semiconductor Electrodes. J. electrochem. Soc.

Bartley, J.P., Brown, T. and Lane, A.N. (1997) Solution conformation of an intramolecular DNA triplex containing a nonnucleotide linker: Comparison with the DNA duplex, Biochemistry, 36(47), pp. 14502–14511. doi:10.1021/bi970710q.

Bhalla, Nikhil., Jolly, Pawan., Formisano, Nello., Estrela, Pedro., 2016. Introduction to biosensors. Essays Biochem 30 June 2016; 60 (1): 1–8. doi: https://doi.org/10.1042/EBC20150001.

Biesecker, G., Dihel, L., Enney, K., Bendele, R, A., 1999. 'Derivation of RNA aptamer inhibitors

of human complement C5', (December 1998), pp. 219–230.

Bordbar, Mohammad Mahdi, Azarmidokht Sheini, Pegah Hashemi, Ali Hajian, and Hasan Bagheri. 2021. "Disposable Paper-Based Biosensors for the Point-of-Care Detection of Hazardous Contaminations—A Review" Biosensors 11, no. 9: 316. https://doi.org/10.3390/bios11090316.

Bradford, M, M., 1976. Rapid and sensitive method for the quantization of microgram quantities of protein utilizing the principle of protein-dye binding. Anal Biochem. 72, 248–254 (1976).

Burg, M., Floege, Jurgern., Ostendorf, Tammo., Jannsen, Uld., et al., 1999. 'Novel Approach to Specific Growth Factor Inhibition in Vivo Antagonism of Platelet-Derived Growth Factor in', 154(1), pp. 169–179.

Byrne B, Stack E, Gilmartin N, O'Kennedy R., 2009. Antibody-based sensors: principles, problems and potential for detection of pathogens and associated toxins. Sensors (Basel). 2009;9(6):4407-45. doi: 10.3390/s90604407. Epub 2009 Jun 5. PMID: 22408533; PMCID: PMC3291918.

Candiano, G., Bruschi, M., Musante, L., Santucci, L., Ghiggeri, G. M., et al., 2004. Blue silver: a very sensitive colloidal Coomassie G-250 staining for proteome analysis. Electrophoresis. 25, 1327-33 (2004).

Chen, X. M., B. Y. Su, X. H. Song, Q. A. Chen, X. Chen, and X. R. Wang., 2011. "Hydroxylamine-o-sulfonic acid as an efficient coreactant for luminol chemiluminescence for selective and sensitive detection." TrAC Trends Anal. Chem.(Reference Ed.) 30 (2011): 665-676.

Chin, C. D., Linder, V., Sia, S. K., 2007. Lab-on-a-chip devices for global health: past studies and future opportunities. Lab Chip.7, 41–57 (2007).

Cho, E. J., Lee, J. W., Ellington, A. D., 2009. Applications of aptamers as sensors. Annu. Rev. Anal. Chem (Palo Alto Calif). 2, 241-264 (2009).

Choi, K. H., Park, M. W., Lee, S. Y., Jeon, M. Y., Kim, M. Y., et al., 2006. Intracellular expression of the t-cell factor-1 rna aptamer as an intramer. Mol. Cancer Ther. 5, 2428–2434 (2006).

Chua, J. H., Chee, R. E., Agarwal, A., She, M. W. & Zhang, G. J., 2009. Label-free electrical detection of cardiac biomarker with complementary metal-oxide semiconductor-compatible silicon nanowire sensor arrays. Anal. Chem. 81, 6266–6271 (2009).

Collinson, P.O., Garrison, L., Christenson, R.H., 2015. Cardiac biomarkers - A short biography. Clin. Biochem. 48, 197–200. doi:10.1016/j.clinbiochem.2014.11.014.

Daar, A. S., Thorsteinsdottir, H., Martin, D. K., Smith, A. C., Nast, S., et al., 2002. Top ten biotechnologies for improving health in developing countries. Nat. Genet. 32, 229–232 (2002).

De Moraes, A. & Kubota, L., 2016. Recent Trends in Field-effect transistors-based immunosensors. Chemosensors 4, 20 (2016).

de Vasconcelos, E, A., Peres, Newton, G., Pereirs, Cintya, O., da Silva, Valdinete, L., et al., 2009. Potential of a simplified measurement scheme and device structure for a low cost label-free point-of-care capacitive biosensor. Biosens. Bioelectron. 25, 870–876 (2009).

Di, Ya., Wang, Peng., Xu, Shufeng., Tian, Qi., et al., 2020. 'Design , Bioanalytical , and Biomedical Applications of', 7(October), pp. 1–15. doi:10.3389/fmed.2020.00456.

Ding, Zhifeng, Bernadette M. Quinn, Allen J. Bard., et al., 2002. "Electrochemistry and electrogenerated chemiluminescence from silicon nanocrystal quantum dots." Science 296, no. 5571 (2002): 1293-1297.

Ding, Shou-Nian., Xua, Jing-Juan., Chen, Hong-Yuan., 2006. Enhanced solid-state electrochemiluminescence of CdS nanocrystals composited with carbon nanotubes in H_2O_2 solution. Chem. Commun., 2006, 3631-3633. DOI https://doi.org/10.1039/B606073K.

Ding, F., Gao, Y. and He, X., 2017. 'Bioorganic & Medicinal Chemistry Letters Recent progresses in biomedical applications of aptamer-functionalized systems', Bioorganic & Medicinal Chemistry Letters, 27(18), pp. 4256–4269. doi:10.1016/j.bmcl.2017.03.032.

Ding, Ruiyu., Cheyong, Yi Heng., Ahamed, Ashiq., Lisak, Grzegorz., 2021. Heavy Metals Detection with Paper-Based Electrochemical Sensors. Anal. Chem. 2021, 93, 1880−1888. https://dx.doi.org/10.1021/acs.analchem.0c04247.

Do, C, B., Woods, D, A., Batzoglou, S., 2006. CONTRAfold: RNA secondary structure prediction without physics-based models, Bioinformatics, 22(14), pp. 90–98.

doi:10.1093/bioinformatics/btl246.

Dong, Wei., Shen, Huai-ben., Liu, Xiu-Hua., Li, Ming-Jing., et al., 2010. CdSe/ZnS quantum dots based fluorescence quenching method for determination of paeonol. Spectrochimica Acta Part A 78 (2011) 537–542. doi:10.1016/j.saa.2010.11.023.

Duerschmied, D., Merhi, Y. and Tanguay, J., 2009. 'Inhibition of von Willebrand factor-mediated platelet activation and thrombosis by the anti-von Willebrand factor A1-domain aptamer ARC1779', (April), pp. 1155–1162. doi:10.1111/j.1538-7836.2009.03459.x.

Elgrishi, Noémie, Kelley, J., Rountree, Brian, D., McCarthy., Eric, S, Rountree., et al., 2018. "A practical beginner's guide to cyclic voltammetry." Journal of chemical education 95, no. 2 (2018): 197-206.

Ellington, A. D., Szostak, J. W, 2015. In vitro selection of RNA molecules that bind specific ligands. Nature. 346, 818-822 (1990).

Famulok, M., Blind, M., Mayer, G., 2001. Intramers as promising new tools in functional proteomics. Chem. Biol. 8, 931–939 (2001).

Famulok, M., Verma, S., 2002. In vivo-applied functional RNAs as tools in proteomics and genomics research. Trends Biotechnol. 20, 462–466 (2002).

Fedoraproject.org. Your Operating System, fedora. Available at: https://fedoraproject.org/.

Fonseca, R. A. S., Ramos-Jesus, J., Kubota, L. T. & Dutra, R. F., 2011. A nanostructured piezoelectric immunosensor for detection of human cardiac troponin T. Sensors 11, 10785–10797 (2011).

G Eyetech Study., 2002. Preclinical and phase 1A clinical evaluation of an anti-VEGF pegylated aptamer (EYE001) for the treatment of exudative age-related macular degeneration. Retina. 22, 143-152 (2002).

Garbett, N. C., Ragazzon, P. A., Chaires, J. B. Circular dichroism to determine binding mode and affinity of ligand–DNA interactions. Nat. Protoc. 2, 3166-3172 (2007).

Gaze, D, C., Collinson, P, O., 2008. Multiple molecular forms of circulating cardiac troponin: analytical and clinical significance. Ann. Clin. Biochem. 45, 349–355. doi:10.1258/acb.2007.007229.

Giddings, J, C., Keller, R, A., 1965. Advances in Chromatography. Marcel Dekker, Inc.: New York, (1965).

Gomes, A, V., Potter, J, D., Szczesna-Cordary, D., 2002. The role of troponins in muscle contraction. IUBMB Life 54, 323–333. doi:10.1080/15216540216037.

Gomes-Filho, S., Dias, A., Silva, M., Silva, B. & Dutra, R., 2013. A carbon nanotube-based electrochemical immunosensor for cardiac troponin T. Microchem. J. 109, 10–15 (2013).

Gordon, A, M., Homsher, E., and Regnier, M., 2000. Regulation of contraction in striated muscle. Physiol. Rev. **80**, 853–924.

Guo, Lei., Yang, Zhen., Zhi, Shaotao., Feng, Zhu., et al., 2017. Sensitive detection of cardiac troponin T based on superparamagnetic bead labels using a flexible micro-fluxgate sensor. RSC Adv. 7, 52327–52336 (2017).

Grant Sheila, A., Pierce, Mary, E., Lichlyter, Darcy, J., Grant, David, A., 2005. Effects of immobilization on a FRET immunosensor for the detection of myocardial infarction. Anal Bioanal Chem (2005) 381: 1012–1018. DOI 10.1007/s00216-004-2976-4.

Gupta, R., Mohan, I., Narula, J., 2016. Trends in Coronary Heart Disease Epidemiology in India. Ann. Glob. Heal. 82, 307–315. doi:10.1016/j.aogh.2016.04.002.

Hamada M, Yamada., K., Sato K, Frith., M. C., Asai., K. (2011) CentroidHomfold-LAST : accurate prediction of RNA secondary structure using automatically collected homologous sequences, 39(May), pp. 100–106. doi:10.1093/nar/gkr290.

Hernandez, J., 2023. An In-Depth Overview of Apache Web Server', https://www.sumologic.com/blog/apache-web-server-introduction/#:~:text=Apache is the web server, help create dynamic web content.

Hofacker, I, L., Fontana, W, Stadler., Bonhoeffer. L.S, Tacker., M, Schuster, P., 1994. Fast Folding and Comparison of RNA Secondary Structures, 188, pp. 167–188.

Hsueh, Hsiao-Ting., Lin, Chih-Ting., 2015. An incremental double-layer capacitance of a planar nanogap and its application in cardiac-troponin T detection. Biosensors and Bioelectronics 0956-5663. http://dx.doi.org/10.1016/j.bios.2015.12.105.

Humphrey, W., Dalke, A. and Schulten, K. 1996. VMD: Visual Molecular Dynamics, 14, pp.

33–38.

IBM.com, 2022. LAMP vs . MEAN : Available at: https://www.ibm.com/cloud/blog/lamp-vs-mean#:~:text=LAMP and MEAN are popular,grade web and mobile apps.

Ilgu, M., Yan, S., Khounlo, R., Lamm, M., Hamilton M, N., 2019. Common secondary and tertiary structural features of aptamer–ligand interaction shared by RNA aptamers with different primary sequences, Molecules, 24(24), pp. 1–12. doi:10.3390/molecules24244535.

Ireson, C. R., Kelland, L. R., 2006. Discovery and development of anticancer aptamers. Mol. Cancer.Ther. 5, 2957-2962 (2006).

Ito, T., Ueno, Y., Komatsu, Y., Matsuda, A., 2003. Synthesis, thermal stability and resistance to enzymatic hydrolysis of the oligonucleotides containing 5-(n-aminohexyl)carbamoyl-2′-omethyluridines. Nucleic Acids Res. 31, 2514–2523 (2003).

Jacobs, M., Panneer Selvam, A., Craven, J.E. et al., 2014. Antibody- Conjugated Gold Nanoparticle-Based Immunosensor for Ultra-Sensitive Detection of Troponin-T. Jala 19, 546–554. doi:10.1177/2211068214538971.

Jarvis, T. C., Davies, D. R., Hisaminato, A., Resnicow, D. I., Gupta, S., et al., 2015. Non-helical DNA Triplex Forms a Unique Aptamer Scaffold for High Affinity Recognition of Nerve Growth Factor. Structure. 23, 1293-1304 (2015).

Jeddi, I., Saiz, L., 2017. “Three-dimensional modeling of single stranded DNA hairpins for aptamer-based biosensors,” Sci. Rep., no. January, pp. 1–13, 2017, doi: 10.1038/s41598-017-01348-5.

Jenison, R. D., Gill, S. C., Pardi, A., Polisky, B., 1994. High-resolution molecular discrimination by RNA. Science. 263, 1425-1429 (1994).

Jiang, Hui, and Huangxian Ju., 2007. "Electrochemiluminescence sensors for scavengers of hydroxyl radical based on its annihilation in CdSe quantum dots film/peroxide system." Analytical chemistry 79, no. 17 (2007): 6690-6696.

Jie, Guifen, Bo Liu, Hongcheng Pan, Jun-Jie Zhu, and Hong-Yuan Chen., 2007. "CdS nanocrystal-based electrochemiluminescence biosensor for the detection of low-density lipoprotein by increasing sensitivity with gold nanoparticle amplification." Analytical

Chemistry 79, no. 15 (2007): 5574-5581.

Kakoti, A., Goswami, P., 2013. Heart type fatty acid binding protein: Structure, Function and biosensing applications for early detection of myocardial infarction. Biosens. Bioelectron. 43, 400–411. doi: 10.1016/j.bios.2012.12.057.

Kakoti, A. and Goswami, P. (2017) Multifaceted analyses of the interactions between human heart type fatty acid binding protein and its specific aptamers, Biochimica et Biophysica Acta - General Subjects, 1861(1), pp. 3289–3299. doi:10.1016/j.bbagen.2016.08.011.

Katus, H, A., Looser, S., Hallermayer, K., Rempis, A., 1992. others, Development and In Vitro Characterization of a New Immunoassay of Cardiac Troponin T, Clinical Chemistry, Volume 38, Issue 3, 1 March 1992, Pages 386–393, https://doi.org/10.1093/clinchem/38.3.386.

Kaur, H., Bruno, John, G., Kumar, Amit., et al., 2020. 'T h e r a n o s t i c s Aptamers in the Therapeutics and Diagnostics Pipelines', 8(15). doi:10.7150/thno.25958.

Ke, C., Gupta, R., Xavier, D., Prabhakaran, D., Mathur, P., Kalkonde, Y. V, … Suraweera, W., 2015. Articles Divergent trends in ischaemic heart disease and stroke mortality in India from 2000 to 2015: a nationally representative mortality study. https://doi.org/10.1016/S2214-109X(18)30242-0.

Kemp, M., Donovan, J., Higham, H., Hooper, J., 2004. Biochemical markers of myocardial injury. Br. J. Anaesth. 93, 63–73. doi:10.1093/bja/aeh148.

Kimoto, M., Yamashige, R., Matsunaga, K., Yokoyama, S., Hirao, I., 2013. Generation of high affinity DNA aptamers using an expanded genetic alphabet. Nat. Biotechnol. 31, 453-457 (2013).

Kool, E.T., 1997. Preorganization of DNA: Design principles for improving nucleic acid recognition by synthetic oligonucleotides. Chem. Rev. 97, 1473–1488 (1997).

Kraemer, S., Vaught, J. D., Bock, C., Gold, L., Katilius, E., 2011. From SOMAmer-based biomarker discovery to diagnostic and clinical applications: a SOMAmer-based, streamlined multiplex proteomic assay. PLos One. 6, e26332 (2011).

Kretsinger, R. H., 1980. Structure and evolution of calcium-modulated proteins. CRC Crit. Rev. Biochem. **8**, 119–174.

Kricka, L.J., Fortina, P., 2009. Analytical ancestry: "Firsts" in fluorescent labelling of nucleosides, nucleotides, and nucleic acids. Clin. Chem. 55, 670–683 (2009).

Krishnan, M.N., 2012. Coronary heart disease and risk factors in India e On the brink of an epidemic ? Indian Heart J. 64, 364–367. doi:10.1016/j.ihj.2012.07.001.

Kumar, Sreeniwas, A., Sinha, Nakul., 2020. Cardiovascular disease in India: A 360 degree overview. medical journal armed forces India 76 (2020) 1-3. https://doi.org/10.1016/j.mjafi.2019.12.005.

Kwak, H., Hwang, I., Kim, J. H., Kim, M. Y., Yang, J. S., et al., 2009. Modulation of transcription by the peroxisome proliferator-activated receptor δ-binding RNA aptamer in colon cancer cells. Mol. Cancer Ther. 8, 2664–2673 (2009).

Laemmli, U, K., 1970. Cleavage of structural proteins during the assembly of the head of bacteriophage T4. Nature. 227, 680–685 (1970).

Lee, Jennifer, F., Hasselberth, Jay, R., Meyers, Lauren, Ancel., Ellington, Andrew., 2004. 'Aptamer Database', 32, pp. 95–100. doi:10.1093/nar/gkh094.

Li, Y., Mui, S., Brown, J. H., Strand, J., Reshetnikova, L., Tobacman, L. S., and Cohen, C., 2002. The crystal structure of the C-terminal fragment of striated-muscle alpha-tropomyosin reveals a key troponin T recognition site. Proc. Natl. Acad. Sci. U.S.A. **99**, 7378–7383.

Li, W., Li, M., Ge, S. G., Yan, M., Huang, J. D., et al., 2013. Battery-triggered ultrasensitive electrochemiluminescence detection on microfluidic paper-based immune device based on dual signal amplification strategy. Anal. Chem. Acta, 767, 66-74 (2013).

Li, X, J., Nie, Z, H., Cheng, C, M., Goodale, A, B., Whitesides, G, M., et al., 2010**.** Paper-based electrochemical ELISA. Proc. Micro Total Analysis Systems. 14, 1487-1489 (2010).

Li, X., Tian, J., Garnier, G., Shen, W., 2010. Fabrication of paper-based microfluidic sensors by printing. Colloids Surf. B. 76, 564-570 (2010).

Liu, Y., Yobas, L., 2014. Label-free specific detection of femtomolar cardiac troponin using an integrated nanoslit array fluidic diode. Nano Lett. 14, 6983–6990. doi:10.1021/nl5032524.

Li, B. R., Chen, C. C., Kumar, U. R. & Chen, Y. T., 2014. Advances in nanowire transistors for biological analysis and cellular investigation. Analyst 139, 1589–1608 (2014).

Lin, Zhenyu., Chen, Jinhua., Chen, Guonan., 2008. An ECL biosensor for glucose based on carbon-nanotube/Nafion film modified glass carbon electrode. Electrochimica Acta Volume 53, Issue 5, 1 January 2008, Pages 2396-2401. https://doi.org/10.1016/j.electacta.2007.09.063.

Linux.com. Why use Linux ?', pp. 1–7. Available at: https://www.linux.com/what-is-linux/.

Liu, J. T. et al., 2011. Surface plasmon resonance biosensor with high anti-fouling ability for the detection of cardiac marker troponin T. Anal. Chim. Acta 703, 80–86 (2011).

Livi, P. Chee, R. E., Agarwal, A., She., 2015. Monolithic integration of a silicon nanowire field-effect transistors array on a complementary metal-oxide semiconductor chip for biochemical sensor applications. Anal. Chem. 87, 9982–9990 (2015).

Mabey, D., Peeling, R. W., Ustianowski, A., Perkins, M. D., 2004. Diagnostics for the developing world. Nat. Rev. Microbiol. 2, 231–240 (2004).

Macek, K., Becvarova, H., 1971. Papers ready for use plates, and flexible sheets for chromatography. Chromatogr. Rev.15, 1–28 (1971).

McCaskill, J, S., 1990. The equilibrium partition function and base pair binding probabilities for RNA secondary structure, Biopolymers, 29(6–7), pp. 1105–1119. doi:10.1002/bip.360290621.

Malica, L., Kirk, A. G., 2006. Integrated miniaturized optical detection platform for fluorescence and absorption spectroscopy. Sensors and Actuators A: Physical.135 (2),515-524, (2006).

Manning, P, Edward., Tardiff, C, Jill., and Schwartz, D, Steven., 2011. A Model of Calcium Activation of the Cardiac Thin Filament. 2011 American Chemical Society 50, 7405−7413. dx.doi.org/10.1021/bi200506k | Biochemistry 2011.

Marangoni, K., Neves, A. F., Rocha, R. M., Faria, P. R., Alves, P. T., 2015. Prostate-specific RNA aptamer: promising nucleic acid antibody-like cancer detection. Sci. Rep. 5, 12090 (2015).

Martinez, A. W., Phillips, S. T., Whitesides, G. M., 2010. Diagnostics for the developing world: microfluidic paper-based analytical devices. Anal. Chem. 82, 3–10 (2010).

Martinez, O., Bellard, E., Golzio, M., Mechiche-Alami, S., Rols, M. P., et al., 2014. Direct validation of aptamers as powerful tools to image solid tumor. Nucleic Acid Ther. 24, 217-225 (2014).

Mattos, A. B., Freitas, T. A., Kubota, L. T. & Dutra, R. F., 2013. An o-aminobenzoic acid film-based immunoelectrode for detection of the cardiac troponin T in human serum. Biochem. Eng. J. 71, 97–104 (2013).

Mayilo, S., Kloster, M. A., Wunderlich, M. & Lutich, A., 2009. Long-range fluorescence quenching gold nanoparticles in a sandwich immunoassay for cardiac troponin T. Nano Lett 9, 4558–4563 (2009).

MAYNARD, S.J., 2000. Troponin T or troponin I as cardiac markers in ischaemic heart disease. Heart 83, 371–373. doi:10.1136/heart.83.4.371.

Meex, Steven, J, R., Vroemen, H, M, Wim., de Boer, Douwe., Streng, S, et al., 2018. Elevated Cardiac Troponin T in Skeletal Myopathies. Journal of the American College of Cardiology. https://doi.org/10.1016/j.jacc.2018.05.017.

Melancon, M. P., Zhou, M., Zhang, R., Xiong, C., Allen, P., et al., 2014. Selective uptake and imaging of aptamer- and antibody-conjugated hollow nanospheres targeted to epidermal growth factor receptors overexpresses in head and neck cancer. ACS Nano. 8, 4530-4538 (2014).

Memoriam, I., 2008. Background to the discovery of troponin and Setsuro Ebashi ' s contribution to our knowledge of the mechanism of relaxation in striated muscle 369, 43–48. doi:10.1016/j.bbrc.2007.11.185.

Mendis, S., Thygesen, K., Kuulasmaa, K., Giampaoli, S., Ma, M., 2011. World Health Organization definition of myocardial infarction : 2008 – 09 revision 139–146. doi:10.1093/ije/dyq165.

Mi, Song, K., Lee, Su., Ban, C., 2012. 'Aptamers and their Biological Applications', Sensors, 22, pp. 612–631. doi:10.1016/j.aca.2013.11.041.

Mincu, N.-B., Lazar, V., Stan, D., Mihailescu, C.M., Iosub, R., et al., 2020. Screen-Printed Electrodes (SPE) for In Vitro Diagnostic Purpose. Diagnostics 2020, 10, 517. https://doi.org/10.3390/diagnostics10080517

Moreira, F, T, C., Dutra, R, A, F., Noronha, J, P, C., Cunha, A, L., Sales, et al., 2011. Artificial antibodies for troponin T by its imprinting on the surface of multiwalled carbon nanotubes: Its use as sensory surfaces. Biosens. Bioelectron. 28, 243–250 (2011).

Müller-Bardorff, Margit., Hallermayer, Klaus., Schroder, Angelika., Ebert, Christoph., et al., 1997. Improved troponin T ELISA specific for cardiac troponin T isoform: assay development and analytical and clinical validation. Clinical Chemistry, Volume 43, Issue 3, 1 March 1997, Pages 458–466, https://doi.org/10.1093/clinchem/43.3.458.

Munje, Rujuta, D., Jacobs, Michael., Muthukumar, Sriram., Prasad, Shalini., 2013. Novel approach for electrical tuning of nano-textured zinc oxide surfaces for ultra-sensitive troponin-T detection. The Royal Society of Chemistry 00, 1-3. DOI: 10.1039/C5AY02052B.

Ng, E. W., Adamis, A. P., 2006. Anti-VEGF aptamer (pegaptanib) therapy for ocular vascular diseases. Ann. N. Y. Acad. Sci. 1082, 151-171 (2006).

Niemeyer, C. M., 2002. The developments of semisynthetic DNA-protein conjugates. Trends Biotechnol. 20, 395–401 (2002).

Nimjee S', White R., Becker R., Sullenger B., 2017. Aptamers as Therapeutics, Annual Review of Pharmacology and Toxicology, 57, pp. 61–79. doi:10.1146/annurev-pharmtox-010716-104558.

Oberthur, Dominik., Achenbach, John., Gabdulkhakov, Azat., Buchner, Klaus., et al., 2015. 'Crystal structure of a mirror-image', pp. 1–11. doi:10.1038/ncomms7923.

Ohtsuki, I., 1999. Calcium ion regulation of muscle contraction: the regulatory role of troponin T. Mol. Cell. Biochem. 190, 33–8.

Oracle.com (India). What is a database, ACM SIGMOD Record. doi:10.1145/983055.983058.

Oracle Corporation. 'MySQL 50 Reference Manual, p. What is MySQL. https://www.oracle.com/mysql/what-is-mysql/#:~:text=MySQL is a relational database management system,-Databases are the&text=The database structure is organized,offers a flexible programming environment.

Ornatska, M., Sharpe, E., Andreescu, D., Andreescu, S., 2011. Paper Bioassay Based on Ceria Nanoparticles as Colorimetric Probes. Anal. Chem. 83, 4273-4280 (2011).

Parekh, P., Kamble, S., Zhao, N. X., Portier, B. P. and Zu, Y. L., 2013. Immunotherapy of CD30-expressing lymphoma using a highly stable ssDNA aptamer. Biomaterials. 34, 8909-8917 (2013).

Peeling, R. W., Holmes, K. K., Mabey, D., Ronald, A., 2006. Rapid tests for sexually transmitted infections (STIs): the way forward. Sex. Transm. Infect. 82, 1–6 (2006).

Pelton, R., 2009. Bioactive paper provides a low-cost platform for diagnostics. Trends Anal. Chem. 28, 925–942 (2009).

PHP.net. Downloads Documentation Get Involved Help. Available at: https://www.php.net/.

PhpMyAdmin. Bringing MySQL to the web About Latest Posts in Developers Blogs. Available at: https://www.phpmyadmin.net/.

Potyrailo, R. A., Murray, A. J., Nagraj, N., Pris, A. D., Ashe, J. M., et al., 2015. Towards maintenance-free biosensors for hundreds of bind/release cycles. Angew. Chem. Int. Ed. Engl. 54, 2174-2178 (2015).

Prabhakaran, D., Jeemon, P., 2016. Global Burden of Cardiovascular Disease Cardiovascular Diseases in India 1605–1620. Circulation. doi:10.1161/CIRCULATIONAHA.114.008729.

Radha Shanmugam, N., Muthukumar, S., Chaudhry, S., Anguiano, J. & Prasad, S., 2017. Ultrasensitive nanostructure sensor arrays on flexible substrates for multiplexed and simultaneous electrochemical detection of a panel of cardiac biomarkers. Biosens. Bioelectron. 89, 764–772 (2017).

Radom, F., Jurek, P. M., Mazurek, M. P., Otlewski, J., Jeleń, F., 2013. Aptamers: molecules of great potential. Biotechnol. Adv. 31, 1260-1274 (2013).

Ramzaeva, N., Rosemeyer, H., Leonard, P., Muhlegger, K., Bergmann, F., et al., 2000. Oligonucleotides functionalized by fluorescein and rhodamine dyes: Michael addition of methyl acrylate to 2'-deoxypseudouridine. Helv. Chim. Acta. 83, 1108–1126 (2000).

Robertson, D. L., Joyce, G. F., 1990. Selection in vitro of an RNA enzyme that specifically cleaves single stranded DNA. Nature. 344, 467-468 (1990).

Roccaro, Aldo, M., Sacco, Antonio., Purschke, Werner, G., Moschetta, Michele et al., 2014. 'therapy', 9(1), pp. 118–128. doi:10.1016/j.celrep.2014.08.042.SDF-1.

Ruckman, J., Green, Louis, S., Beeson, Jim., Waugh, Sheela., et al., 1998. '2 ¯-Fluoropyrimidine RNA-based Aptamers to the 165-Amino Acid Form of Vascular Endothelial Growth Factor (VEGF 165)', 273(32), pp. 20556–20567. doi:10.1074/jbc.273.32.20556.

Ruigrok, V. J. B., van Duijn, E., Barendregt, A., Dyer, K., Tainer, J. A., et al., 2012. Kinetic and stoichiometric characterization of streptavidin-binding aptamers. ChemBioChem. 13, 829–836 (2012).

S Techies. Introduction to PHP. doi:10.1201/9781003308669-1.

Hamid, M Z., Hitam, A, A., Rahim M, Z, A., 2020. The assessment of three dimensional modelling design for single strand DNA aptamers for computational chemistry application', Biophysical Chemistry, 267(September), p. 106492. doi:10.1016/j.bpc.2020.106492.

Santosh, B., Yadava, P, K., 2014. Nucleic acid aptamers: Research tools in disease diagnostics and therapeutics, BioMed Research International, 2014. doi:10.1155/2014/540451.

Sato, K., Kato, Y., Hamada, M., Tatsuya, A., Asai, K., 2011. 'IPknot : fast and accurate prediction of RNA secondary structures with pseudoknots using integer programming', Bioinformatics, 27(13), pp. 4–7. doi:10.1093/bioinformatics/btr215.

Schoetzau, T., Langner, J., Moyroud, E., Roehl, I., Vonhoff, S., et al., 2003. Amino modified nucleobases: Functionalized nucleoside triphosphates applicable for selex. Bioconjugate Chem. 14, 919–926 (2003).

Schwoebel, Frank., Eijk, Lucas, T, van., Zboralski, Dirk., Sel, Simone., 2013. 'Brief Report The effects of the anti-hepcidin Spiegelmer NOX-H94 on in fl ammation-induced anemia in cynomolgus monkeys', 121(12), pp. 2311–2315. doi:10.1182/blood-2012-09-456756.

Seelam, P, P., Mitra, A., Sharma, P., 2019. 'Pairing interactions between nucleobases and ligands in aptamer:ligand complexes of riboswitches: Crystal structure analysis, classification, optimal structures, and accurate interaction energies', Rna, 25(10), pp. 1274–1290. doi:10.1261/rna.071530.119.

Shanmugam, N, R., Muthukumar, S., Selvam, A, P., Prasad, Shalini., 2016. Electrochemical nanostructured ZnO biosensor for ultrasensitive detection of cardiac troponin-T. Nanomedicine 11, 1345–1358. doi:10.2217/nnm-2016-0048.

Sharma, Abhinav., Jang, Jaesung., 2019. Flexible electrical aptasensor using dielectrophoretic assembly of graphene oxide and its subsequent reduction for cardiac biomarker detection. Scientific reports (2019) 9:5970. https://doi.org/10.1038/s41598-019-42506-1.

Sheldon, R., 2023. https://www.techtarget.com/searchdatacenter/definition/Debian.

Shim, Joon, S., Browne, Andrew, W., Ahn, Chong, H., 2009. Thirteenth International Conference on Miniaturized Systems for Chemistry and Life Sciences 978-0-9798064-2-1/μTAS2009.

Silva, B, V, M., Rodriguez, B, A, G., Sales, G, F., Sotomayor, M, T., Dutra, R, F., 2016. An ultrasensitive human cardiac troponin T graphene screen-printed electrode based on electropolymerized-molecularly imprinted conducting polymer. Biosens. Bioelectron. 77, 978–985 (2016).

Stoltenburg, R., Nikolaus, N., Strehlitz, B., 2012. Capture-SELEX: Selection of DNA Aptamers for Aminoglycoside Antibiotics. J. Anal. Methods. Chem. 2012, 415697 (2012).

Sun, H., Zu, Y. A., 2015. Highlight of Recent Advances in Aptamer Technology and Its Application. Molecules. 20, 11959-11980 (2015).

Szczesna, D., and Potter, J, D., 2002. The role of troponin in the Ca2C- regulation of skeletal muscle contraction. Results Probl. Cell Differ. **36**, 171–190.

Takeda, S., 2005. Crystal structure of troponin and the molecular mechanism of muscle regulation 54, 35–41. doi:10.1093/jmicro/dfi006.

Takeda, S., Yamashita, A., Maeda, K., Maéda, Y., 2003. Structure of the core domain of human cardiac troponin in the Ca(2+)-saturated form. Nature 424, 35–41. doi:10.1038/nature01780.

Tang, Rui, Hua., Liu, Li, Na., Zhang, Su, Feng., He, Xiao, Cong., et al., 2019. A review on advances in methods for modification of paper supports for use in point-of-care testing. Microchim Acta (2019) 186: 521. https://doi.org/10.1007/s00604-019-3626-z.

Tennilä, T., Antopolsky, M., Azhayev, A., Azhayeva, E., 2008. Peptide-oligonucleotide conjugates form stable and selective complexes with antibody and DNA. Bioconjugate Chem. 19, 1361–1367 (2008).

Thiviyanathan, V., Gorenstein, D, G., 2012. Aptamers and the next generation of diagnostic

reagents. Proteomics Clin Appl. 6(0), 563–573, (2012).

Thodima, V., Pirooznia, M. and Deng, Y., 2006. 'RiboaptDB : A Comprehensive Database of Ribozymes and', 6, pp. 1–6. doi:10.1186/1471-2105-7-S2-S6.

Tobacman, L, S., 1996. Thin filament-mediated regulation of cardiac contraction. Annu. Rev. Physiol. **58**, 447–481.

Tuerk, C., Gold, L., 1990. Systematic evolution of ligands by exponential enrichment: RNA ligands to bacteriophage T4 DNA polymerase. Science. 4968, 505-510 (1990).

Tung, C. H., Stein, S., 2000. Preparation and applications of peptide-oligonucleotide conjugates. Bioconjugate Chem. 11, 605–618 (2000).

Tutorialspoint. SQL - Tutorials. https://www.tutorialspoint.com/sql/index.htm.

Ubuntu.com. Ubuntu. Available at: https://ubuntu.com/.

Ulrich, H. and Wrenger, C., 2009. 'Disease-Specific Biomarker Discovery by Aptamers'. Cytometry Part A . 75A: 727-733, 2009. doi:10.1002/cyto.a.20766.

Van, den, Hurk, R., Evoy, S., 2015. A review of membrane-based biosensors for pathogen detection. Sensors (Switzerland), 15(6), 14045–14078. https://doi.org/10.3390/s150614045.

Wang, Jingkun., Fang , Yizhen., Li, Peihua.,Lin, Huayue., et al., 2017. Evaluation of a newly developed chemiluminescence immunoassay for detecting cardiac troponin T. J Clin Lab Anal. 2018;32:e22311. https://doi.org/10.1002/jcla.22311.

Williams, B, A, R., Chaput, J, C., 2000. Synthesis of peptide-oligonucleotide conjugates using a heterobifunctional crosslinker. In Current Protocols in Nucleic Acid Chemistry; John Wiley.

World Health Organization. World Health Report, 2015. Geneva, Switzerland.

World Health Organization. World Health Report, 2021. Geneva, Switzerland.

Wu, A, H, B., Feng, Y., Moore, R., Apple, F, S., et al., 1998. Characterization of cardiac troponin subunit release into serum after acute myocardial infarction and comparison of assays for troponin T and I. Clin Chem 44, 1198–1208.

Wu, Y., Xue, P., Hui, K, M., Kang, Y., 2014. A paper-based microfluidic electrochemical immune device integrated with amplification-by-polymerization for the ultrasensitive multiplexed detection of cancer biomarkers. Biosens Bioelectron. 52, 180-187 (2014).

Xiong, X, L., Lv, Y, F., Chen, T., Zhang, X, B., Wang, K, M., 2014. Nucleic acid aptamers for living cell analysis. Annu. Rev. Anal. Chem (Palo Alto Calif). 7, 405-426 (2014).

Yager, P., Edwards, T., Fu, E., Helton, K., Nelson, K., et al., 2006. Microfluidic diagnostic technologies for global public health. Nature. 442, 412–418 (2006).

Yang, Q., Goldstein, I. J., Mei, H. Y., Engelke, D. R., 1998. DNA ligands that bind tightly and selectively to cellobiose. Proc. Natl. Acad. Sci. U S A. 95, 5462-5467 (1998).

Yang, S., Barbu-Tudoran, L., Orzechowski, M., Craig, R., et al., 2014. Three-dimensional organization of troponin on cardiac muscle thin filaments in the relaxed state. Biophys. J. 106, 855–864. doi:10.1016/j.bpj.2014.01.007.

Yang, Xiaolin., Zhao, Ying., Sun, Lijuan., Qi, Honglan., et al., 2017. Electrogenerated chemiluminescence biosensor array for the detection of multiple AMI biomarkers. Sensors and Actuators B: Chemical 0925-4005. https://doi.org/10.1016/j.snb.2017.10.108.

Yetisen, A, K., Akram, M, S., Lowe, C, R., 2013. Paper-based microfluidic point-of-care diagnostic devices. Lab Chip.13, 2210-2251 (2013).

Zakov S., Goldberg Y., Elhadad M., Ziv-Ukelson., M. 2011. 'Rich parameterization improves RNA structure prediction', Journal of Computational Biology, 18(11), pp. 1525–1542. doi:10.1089/cmb.2011.0184.

Zhang, Y., Lai, B, S., Juhas, M. 2019. 'Recent advances in aptamer discovery and applications', Molecules, 24(5). doi:10.3390/molecules24050941.

Zhang, Y., Xiong, Y. and Xiao, Y. 2022. '3dDNA: A Computational Method of Building DNA 3D Structures'.

Zhang, L., Xiong, Y., Xiao, Y., 2022. "3dDNA: A Computational Method of Building DNA 3D Structures," 2022.

Zhang, Huai-Rong., Mei-Sheng, Wu., Jing-Juan, Xu., Hong-Yuan, Chen., 2014. "Signal-on dual-potential electrochemiluminescence based on luminol–gold bifunctional nanoparticles for telomerase detection." Analytical chemistry 86, no. 8 (2014): 3834-3840.

Zhao, W., van der Berg, A., 2008. Lab on paper. Lab Chip. 8, 1988–1991 (2008).

Zheng, Q., Lavis, D, L., 2017. Development of photostable fluorophores for molecular imaging. Cur. Opin. Chem. Bio. 39:32–38, (2017).

Zou, Guizheng., Ju, Huangxian., 2004. Electrogenerated Chemiluminescence from a CdSe Nanocrystal Film and Its Sensing Application in Aqueous Solution. Analytical Chemistry 2004 76 (23), 6871-6876. DOI: 10.1021/ac049012j.

Zuker, M., 2003. 'Mfold web server for nucleic acid folding and hybridization prediction', 31(13), pp. 3406–3415. doi:10.1093/nar/gkg595.

Zuker, M. and Stiegler, P. 1981. 'Optimal computer folding of large RNA sequences using thermodynamics and auxiliary information', Nucleic Acids Research, 9(1), pp. 133–148. doi:10.1093/nar/9.1.133.

Zulkeflee, M., 2020. "Biophysical Chemistry The assessment of three-dimensional modelling design for single strand DNA aptamers for computational chemistry application," Biophys. Chem., vol. 267, no. September, p. 106492, 2020, doi: 10.1016/j.bpc.2020.106492.

Publications in refereed journals

Publications in refereed journals

Patent

A modified syringe for detection of various enzymes for various instrument free detection. Inventors: Pranab Goswami, Naveen Kumar Singh, **Vinay Bachu,** Phurpa Dema Thungon. Patent Application No. 201831030902 Dated 17.08.2018.

Book Chapter

ADVANCE MATERIALS AND TECHNIQUES FOR BIOSENSORS AND BIOANALYTICAL APPLICATIONS. ISBN (printed version): 9780367539658. **Chapter 11:** Bio-electrochemiluminescence as analytical signal of extreme sensitivity, pages 421-462 (2020) **Vinay Bachu**, Pranab Goswami.

Database

Vinay Bachu, Lazmy Deware, Ayush Kumar, Pooja Rani Kuri, Malaya Mili, Naveen Kumar Singh, & Pranab Goswami. **Aptabase: An aptamer database**, October 24 (2021): www.iitg.ac.in/proj/aptabase

Journal Publications

Vinay Bachu, Kangkana Barman, Pranab Goswami. Analysis on the in-silico ensemble methods for 3D modelling of ssDNA aptamers. Biophysical chemistry journal, 303, December 2023, 107111. https://doi.org/10.1016/j.bpc.2023.107111.

Lightson Ngashangva, **Vinay Bachu**, Pranab Goswami: Development of new methods for determination of bilirubin. Journal of Pharmaceutical and Biomedical Analysis 09/2018; 162., DOI: 10.1016/j.jpba.2018.09.034.

Priyanki Das**, Vinay Bachu**, Lepakshi Barbora, Arup Dutta, Mrinal Kumar Sarma, Pranab Goswami. Passive fuel delivery and efficient anoxic condition in anode improve performance of methanol biofuel cell. Applied Energy Journal. https://doi.org/10.1016/j.apenergy.2021.117824.

Phurpa Dema Thungon, Pooja Rani Kuri, **Vinay Bachu**, Pranab Goswami. Silk-fibroin film as enzyme stabilizing material and optical signal transducer for developing alcohol oxidase-based μPAD methanol biosensor. Biosensors and Bioelectronics: X, 2022.

Lightson Ngashangva, Bahaa A Hemdan, Mohamed Azab El-Liethy, **Vinay Bachu**, Shelley D Minteer, Pranab Goswami. Emerging bioanalytical devices and platforms for rapid detection of pathogens in environmental samples. Micromachines 2022, 13(7), 1083; https://doi.org/10.3390/mi13071083.

Manuscripts under review:

Vinay Bachu, Lazmy Deware, Ayush Kumar, Malaya Mili, Pooja rani Kuri, Naveen Kumar Singh Pranab Goswami*. “A new aptamer database “Aptabase” with user interactive interface”.

Vinay Bachu, Malaya Mili, Arup Dutta, Phurpa Dema Thungon, Pranab Goswami. Electrochemiluminescence-based lateral flow assay for detection of cardiac troponin T using aptamers developed through a c-SELEX technique.

Phurpa Thungon, Torsha Kundu, **Vinay Bachu**, Pranab Goswami. "Silk-Hydrogel-Immobilized Gold-Nanocluster-Seeded Catalase Protein as a Pre-Plasmonic Probe for Colorimetric Peroxide Sensing".

Vinay Bachu, Lekhashree, Pranab Goswami. Conductive ink-based Electrochemical Paper Platform for cardiac Troponin T Detection.

Vinay Bachu, Pooja Rani Kuri, Malaya Mili, Naveen Kumar Singh, Pranab Goswami. Recent Advances on Aptamer Development and Their Biomedical Applications.

Appendix

Copyright Permissions

Cardiac biomarkers — A short biography

Author: Paul O. Collinson,Lisa Garrison,Robert H. Christenson

Publication: Clinical Biochemistry

Publisher: Elsevier

Date: March 2015

Order Completed

Thank you for your order.

This Agreement between Vinay Bachu ("You") and Elsevier ("Elsevier") consists of your license details and the terms and conditions provided by Elsevier and Copyright Clearance Center.

Your confirmation email will contain your order number for future reference.

License Number	5612410570938
License date	Aug 19, 2023

Printable Details

Licensed Content

Licensed Content Publisher	Elsevier
Licensed Content Publication	Clinical Biochemistry
Licensed Content Title	Cardiac biomarkers — A short biography
Licensed Content Author	Paul O. Collinson,Lisa Garrison,Robert H. Christenson
Licensed Content Date	Mar 1, 2015
Licensed Content Volume	48
Licensed Content Issue	4-5
Licensed Content Pages	4

Order Details

Type of Use	reuse in a thesis/dissertation
Portion	figures/tables/illustrations
Number of figures/tables/illustrations	1
Format	both print and electronic
Are you the author of this Elsevier article?	No
Will you be translating?	No

About Your Work

Title	Aptasensing cardiac troponin-T (cTnT) for point of care detection of myocardial infarction
Institution name	Indian Institute of technology Guwahati
Expected presentation date	Aug 2023

Additional Data

Portions	Fig 1

TH-3269_156106040

Requestor Location

Requestor Location	Vinay Bachu No. 47, 2nd main, Eshwara layout J P Nagar 7th Phase, Bengaluru Bengaluru, Karnataka 60062 India Attn: IIT Guwahati

Price

Total	0.00 USD

Tax Details

Publisher Tax ID	GB 494 6272 12

Total: 0.00 USD

CLOSE WINDOW ORDER MORE

TH-3269_156106040

A Model of Calcium Activation of the Cardiac Thin Filament

Author: Edward P. Manning, Jil C. Tardiff, Steven D. Schwartz
Publication: Biochemistry
Publisher: American Chemical Society
Date: Aug 1, 2011

PERMISSION/LICENSE IS GRANTED FOR YOUR ORDER AT NO CHARGE

This type of permission/license, instead of the standard Terms and Conditions, is sent to you because no fee is being charged for your order. Please note the following:

- Permission is granted for your request in both print and electronic formats, and translations.
- If figures and/or tables were requested, they may be adapted or used in part.
- Please print this page for your records and send a copy of it to your publisher/graduate school.
- Appropriate credit for the requested material should be given as follows: "Reprinted (adapted) with permission from {COMPLETE REFERENCE CITATION}. Copyright {YEAR} American Chemical Society." Insert appropriate information in place of the capitalized words.
- One-time permission is granted only for the use specified in your RightsLink request. No additional uses are granted (such as derivative works or other editions). For any uses, please submit a new request.

If credit is given to another source for the material you requested from RightsLink, permission must be obtained from that source.

BACK CLOSE WINDOW

TH-3269_156106040

Multiple molecular forms of circulating cardiac troponin: analytical and clinical significance

Author: David C Gaze, Paul O Collinson

Publication:
Annals of Clinical Biochemistry: An international journal of biochemistry and laboratory medicine

Publisher: SAGE Publications

Date: 2008-07-01

Gratis Reuse

Permission is granted at no cost for use of content in a Master's Thesis and/or Doctoral Dissertation, subject to the following limitations. You may use a single excerpt or up to 3 figures tables. If you use more than those limits, or intend to distribute or sell your Master's Thesis/Doctoral Dissertation to the general public through print or website publication, please return to the previous page and select 'Republish in a Book/Journal' or 'Post on intranet/password-protected website' to complete your request.

BACK CLOSE WINDOW

Characterization of cardiac troponin subunit release into serum after acute myocardial infarction and comparison of assays for troponin T and I

Author: Wu, Alan H B; Feng, Yue-Jin
Publication: Clinical Chemistry
Publisher: Oxford University Press
Date: 1998-06-01

Order Completed

Thank you for your order.

This Agreement between Vinay Bachu ("You") and Oxford University Press ("Oxford University Press") consists of your license details and the terms and conditions provided by Oxford University Press and Copyright Clearance Center.

Your confirmation email will contain your order number for future reference.

License Number	5612430482790
License date	Aug 19, 2023

Printable Details

Licensed Content

Licensed Content Publisher	Oxford University Press
Licensed Content Publication	Clinical Chemistry
Licensed Content Title	Characterization of cardiac troponin subunit release into serum after acute myocardial infarction and comparison of assays for troponin T and I
Licensed Content Author	Wu, Alan H B; Feng, Yue-Jin
Licensed Content Date	Jun 1, 1998
Licensed Content Volume	44
Licensed Content Issue	6

Order Details

Type of Use	Thesis/Dissertation
Requestor type	Educational Institution/Non-commercial/ Not for-profit
Format	Print and electronic
Portion	Figure/table
Number of figures/tables	1
Will you be translating?	No

About Your Work

Title	Aptasensing cardiac troponin-T (cTnT) for point of care detection of myocardial infarction
Institution name	Indian Institute of technology Guwahati
Expected presentation date	Aug 2023

Additional Data

Portions	Fig 2

TH-3269_156106040

Requestor Location

Requestor Location	Vinay Bachu No. 47, 2nd main, Eshwara layout J P Nagar 7th Phase, Bengaluru Bengaluru, Karnataka 60062 India Attn: IIT Guwahati

Price

Total	0.00 USD

Tax Details

Publisher Tax ID	GB125506730

Total: 0.00 USD

CLOSE WINDOW ORDER MORE

TH-3269_156106040

Marketplace

Order Confirmation

Thank you for your order. You will receive a confirmation email with details about your order.

This is not an invoice. Please go to manage account to access your order history and invoices.

CUSTOMER INFORMATION

Payment by invoice: You can cancel your order until the invoice is generated by contacting customer service.

Billing Address

Vinay Bachu
No. 47, 2nd main, Eshwara layout
J P Nagar 7th Phase, Bengaluru
Bengaluru, Karnataka 60062
India

+91 8277240262
vinayb.bachu@gmail.com

Customer Location

Vinay Bachu
No. 47, 2nd main, Eshwara layout
J P Nagar 7th Phase, Bengaluru
Bengaluru, Karnataka 60062
India

PO Number (optional)

N/A

Payment options

Invoice

ORDER CONFIRMATION

Confirmation Number: 1387917

Order Date: 19-Aug-2023

1. Analytical methods : advancing methods and applications

0.00 USD

Article: A novel approach for electrical tuning of nano-textured zinc oxide surfaces for ultra-sensitive troponin-T detection

Order License ID	1387917-1	**Publisher**	RSC Pub
ISSN	1759-9660	**Portion**	Image/photo/illustration
Type of Use	Republish in a thesis/dissertation		

LICENSED CONTENT

Publication Title	Analytical methods : advancing methods and applications	**Rightsholder**	Royal Society of Chemistry
Article Title	A novel approach for electrical tuning of nano-textured zinc oxide surfaces for ultra-sensitive troponin-T detection	**Publication Type**	Journal
		Start Page	10136
		End Page	10144
		Issue	24
		Volume	7
Author/Editor	Royal Society of Chemistry (Great Britain)		
Date	01/01/2009		
Language	English		
Country	United Kingdom of Great Britain and Northern Ireland		

REQUEST DETAILS

TH-3269_156106040

Portion Type	Image/photo/illustration	Distribution	Worldwide
Number of Images / Photos / Illustrations	1	Translation	Original language of publication
Format (select all that apply)	Print, Electronic	Copies for the Disabled?	No
Who Will Republish the Content?	Academic institution	Minor Editing Privileges?	No
		Incidental Promotional Use?	No
Duration of Use	Life of current edition	Currency	USD
Lifetime Unit Quantity	Up to 499		
Rights Requested	Main product		

NEW WORK DETAILS

Title	Aptasensing cardiac troponin-T (cTnT) for point of care detection of myocardial infarction	Institution Name	Indian Institute of technology Guwahati
		Expected Presentation Date	2023-08-31
Instructor Name	Prof. Pranab Goswami		

ADDITIONAL DETAILS

Order Reference Number	N/A	The Requesting Person/Organization to Appear on the License	Vinay Bachu (Indian Institute of Technology Guwahati)

REQUESTED CONTENT DETAILS

Title, Description or Numeric Reference of the Portion(s)	Fig 1	Title of the Article/Chapter the Portion Is From	A novel approach for electrical tuning of nano-textured zinc oxide surfaces for ultra-sensitive troponin-T detection
Editor of Portion(s)	Munje, Rujuta D.; Jacobs, Michael; Muthukumar, Sriram; Quadri, Bilal; Shanmugam, Nandhinee Radha; Prasad, Shalini	Author of Portion(s)	Munje, Rujuta D.; Jacobs, Michael; Muthukumar, Sriram; Quadri, Bilal; Shanmugam, Nandhinee Radha; Prasad, Shalini
Volume / Edition	7		
Page or Page Range of Portion	10136-10144	Issue, if Republishing an Article From a Serial	24
		Publication Date of Portion	2015-12-21

Total Items: 1

Total Due: 0.00 USD

Accepted: Marketplace Permissions General Terms and Conditions and any applicable Publisher Terms and Conditions

TH-3269_156106040

Studies on an on/off-switchable immunosensor for troponin T

Author:
Md. Ashaduzzaman,Aswathi Anto Antony,N. Arul Murugan,Swapneel R. Deshpande,Anthony P.F. Turner,Ashutosh Tiwari

Publication: Biosensors and Bioelectronics

Publisher: Elsevier

Date: 15 November 2015

Order Completed

Thank you for your order.

This Agreement between Vinay Bachu ("You") and Elsevier ("Elsevier") consists of your license details and the terms and conditions provided by Elsevier and Copyright Clearance Center.

Your confirmation email will contain your order number for future reference.

License Number	5612420746778
License date	Aug 19, 2023

Printable Details

Licensed Content

Licensed Content Publisher	Elsevier
Licensed Content Publication	Biosensors and Bioelectronics
Licensed Content Title	Studies on an on/off-switchable immunosensor for troponin T
Licensed Content Author	Md. Ashaduzzaman,Aswathi Anto Antony,N. Arul Murugan,Swapneel R. Deshpande,Anthony P.F. Turner,Ashutosh Tiwari
Licensed Content Date	Nov 15, 2015
Licensed Content Volume	73
Licensed Content Issue	n/a
Licensed Content Pages	8

Order Details

Type of Use	reuse in a thesis/dissertation
Portion	figures/tables/illustrations
Number of figures/tables/illustrations	1
Format	both print and electronic
Are you the author of this Elsevier article?	No
Will you be translating?	No

About Your Work

Title	Aptasensing cardiac troponin-T (cTnT) for point of care detection of myocardial infarction
Institution name	Indian Institute of technology Guwahati
Expected presentation date	Aug 2023

Additional Data

Portions	Fig 1

TH-3269_156106040

Requestor Location

Requestor Location	Vinay Bachu No. 47, 2nd main, Eshwara layout J P Nagar 7th Phase, Bengaluru Bengaluru, Karnataka 60062 India Attn: IIT Guwahati

Price

Total	0.00 USD

Tax Details

Publisher Tax ID	GB 494 6272 12

Total: 0.00 USD

CLOSE WINDOW ORDER MORE

TH-3269_156106040

Elevated Cardiac Troponin T in Skeletal Myopathies Skeletal TnT Cross-Reactivity and/or Cardiac TnT Expression?

Author:
Wim H.M. Vroemen,Douwe de Boer,Alexander S. Streng,Alma M.A. Mingels,Steven J.R. Meex

Publication: Journal of the American College of Cardiology
Publisher: Elsevier
Date: 17 July 2018

Order Completed

Thank you for your order.

This Agreement between Vinay Bachu ("You") and Elsevier ("Elsevier") consists of your license details and the terms and conditions provided by Elsevier and Copyright Clearance Center.

Your confirmation email will contain your order number for future reference.

License Number	5612421118473
License date	Aug 19, 2023

Printable Details

Licensed Content

Licensed Content Publisher	Elsevier
Licensed Content Publication	Journal of the American College of Cardiology
Licensed Content Title	Elevated Cardiac Troponin T in Skeletal Myopathies Skeletal TnT Cross-Reactivity and/or Cardiac TnT Expression?
Licensed Content Author	Wim H.M. Vroemen,Douwe de Boer,Alexander S. Streng,Alma M.A. Mingels,Steven J.R. Meex
Licensed Content Date	Jul 17, 2018
Licensed Content Volume	72
Licensed Content Issue	3
Licensed Content Pages	3

Order Details

Type of Use	reuse in a thesis/dissertation
Portion	figures/tables/illustrations
Number of figures/tables/illustrations	1
Format	both print and electronic
Are you the author of this Elsevier article?	No
Will you be translating?	No

About Your Work

Title	Aptasensing cardiac troponin-T (cTnT) for point of care detection of myocardial infarction
Institution name	Indian Institute of technology Guwahati
Expected presentation date	Aug 2023

Additional Data

Portions	Figure 1

TH-3269_156106040

Requestor Location

Requestor Location	Vinay Bachu No. 47, 2nd main, Eshwara layout J P Nagar 7th Phase, Bengaluru Bengaluru, Karnataka 60062 India Attn: IIT Guwahati

Price

Total	0.00 USD

Tax Details

Publisher Tax ID	GB 494 6272 12

Total: 0.00 USD

CLOSE WINDOW ORDER MORE

TH-3269_156106040

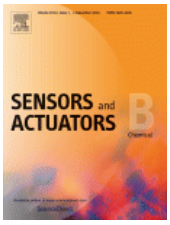

Electrogenerated chemiluminescence biosensor array for the detection of multiple AMI biomarkers

Author: Xiaolin Yang,Ying Zhao,Lijuan Sun,Honglan Qi,Qiang Gao,Chengxiao Zhang
Publication: Sensors and Actuators B: Chemical
Publisher: Elsevier
Date: March 2018

Order Completed

Thank you for your order.

This Agreement between Vinay Bachu ("You") and Elsevier ("Elsevier") consists of your license details and the terms and conditions provided by Elsevier and Copyright Clearance Center.

Your confirmation email will contain your order number for future reference.

License Number	5612401077228
License date	Aug 19, 2023

Printable Details

Licensed Content

Licensed Content Publisher	Elsevier
Licensed Content Publication	Sensors and Actuators B: Chemical
Licensed Content Title	Electrogenerated chemiluminescence biosensor array for the detection of multiple AMI biomarkers
Licensed Content Author	Xiaolin Yang,Ying Zhao,Lijuan Sun,Honglan Qi,Qiang Gao,Chengxiao Zhang
Licensed Content Date	Mar 1, 2018
Licensed Content Volume	257
Licensed Content Issue	n/a
Licensed Content Pages	8

Order Details

Type of Use	reuse in a thesis/dissertation
Portion	figures/tables/illustrations
Number of figures/tables/illustrations	1
Format	both print and electronic
Are you the author of this Elsevier article?	No
Will you be translating?	No

About Your Work

Title	Aptasensing cardiac troponin-T (cTnT) for point of care detection of myocardial infarction
Institution name	Indian Institute of technology Guwahati
Expected presentation date	Aug 2023

Additional Data

Portions	Scheme 1

TH-3269_156106040

Requestor Location

Requestor Location	Vinay Bachu No. 47, 2nd main, Eshwara layout J P Nagar 7th Phase, Bengaluru Bengaluru, Karnataka 60062 India Attn: IIT Guwahati

Price

Total	0.00 USD

Tax Details

Publisher Tax ID	GB 494 6272 12

Total: 0.00 USD

CLOSE WINDOW ORDER MORE

Permission to reuse content from an article published by Portland Press:

- If the content that you are seeking to re-use is in a Portland Press article that is published open access under a CC BY licence NO permissions are required, although you must cite the published article and credit the authors when you re-use it (or part of it).
- If the article you are seeking to re-use is published open access under any other type of licence (e.g. CC BY NC-ND) or a Portland Press license to publish then please complete a re-use permission-request form via copyright.com.
- To find out what licence the article is published under look for the copyright line on the published article, which can be found underneath the abstract or full text, depending on what view you are seeing for the article. Where there is no creative commons license attached, please complete a re-use permission request form via copyright.com.
- **FOR AUTHORS:** if you are a named author on the article you wish to re-use then you will not need to seek any permissions except for re-use of non-open access papers that involves commercial re-selling or bulk distribution. For the latter, please visit copyright.com.

LinkedIn

YouTube

Biochemical Society Membership

EXPLORE

Publishing Life Cycle

Biochemical Society Events

About Portland Press

Portland Press

Registered address *– First Floor, 10 Queen Street Place, London EC4R 1BE*
Mailing address *– 1 Naoroji Street, London WC1X 0GB*

Portland Press Tel
+44 (0)20 3880 2795
Portland Press Company no. 02453983

Biochemical Society Tel
+44 (0)20 3880 2793
Email: editorial@portlandpress.com

Biochemical Society Company no. 00892796
Registered Charity no. 253894
VAT no. GB 523 2392 69

TH-3269_156106040

CCC Marketplace

Order Confirmation

Thank you for your order. You will receive a confirmation email with details about your order.

This is not an invoice. Please go to manage account to access your order history and invoices.

CUSTOMER INFORMATION

Payment by invoice: You can cancel your order until the invoice is generated by contacting customer service.

Billing Address

Vinay Bachu
No. 47, 2nd main, Eshwara layout
J P Nagar 7th Phase, Bengaluru
Bengaluru, Karnataka 60062
India

+91 8277240262
vinayb.bachu@gmail.com

Customer Location

Vinay Bachu
No. 47, 2nd main, Eshwara layout
J P Nagar 7th Phase, Bengaluru
Bengaluru, Karnataka 60062
India

PO Number (optional)

N/A

Payment options

Invoice

ORDER CONFIRMATION

Confirmation Number: 1387910

Order Date: 19-Aug-2023

1. Analytical methods : advancing methods and applications

0.00 USD

Article: Electrochemical paper-based analytical devices: Ten years of development

Order License ID	1387910-1	**Publisher**	RSC Pub
ISSN	1759-9660	**Portion**	Image/photo/illustration
Type of Use	Republish in a thesis/dissertation		

LICENSED CONTENT

Publication Title	Analytical methods : advancing methods and applications	**Rightsholder**	Royal Society of Chemistry
Article Title	Electrochemical paper-based analytical devices: Ten years of development	**Publication Type**	Journal
Author/Editor	Royal Society of Chemistry (Great Britain)	**Start Page**	1030
Date	01/01/2009	**End Page**	1054
Language	English	**Issue**	8
Country	United Kingdom of Great Britain and Northern Ireland	**Volume**	12

REQUEST DETAILS

Portion Type	Image/photo/illustration	**Distribution**	Worldwide

TH-3269_156106040

Number of Images / Photos / Illustrations	1	Translation	Original language of publication
Format (select all that apply)	Print, Electronic	Copies for the Disabled?	No
Who Will Republish the Content?	Academic institution	Minor Editing Privileges?	No
Duration of Use	Life of current edition	Incidental Promotional Use?	No
Lifetime Unit Quantity	Up to 499	Currency	USD
Rights Requested	Main product		

NEW WORK DETAILS

Title	Aptasensing cardiac troponin-T (cTnT) for point of care detection of myocardial infarction	Institution Name	Indian Institute of technology Guwahati
Instructor Name	Prof. Pranab Goswami	Expected Presentation Date	2023-08-31

ADDITIONAL DETAILS

Order Reference Number	N/A	The Requesting Person/Organization to Appear on the License	Vinay Bachu (Indian Institute of Technology Guwahati)

REQUESTED CONTENT DETAILS

Title, Description or Numeric Reference of the Portion(s)	Fig 1	Title of the Article/Chapter the Portion Is From	Electrochemical paper-based analytical devices: Ten years of development
Editor of Portion(s)	Ataide, Vanessa; Mendes, Let?cia; Gama, Lillia; Araujo, William; Paixao, Thiago Regis Longo Cesar	Author of Portion(s)	Ataide, Vanessa; Mendes, Let?cia; Gama, Lillia; Araujo, William; Paixao, Thiago Regis Longo Cesar
Volume / Edition	12		
Page or Page Range of Portion	1030-1054	Issue, if Republishing an Article From a Serial	8
		Publication Date of Portion	2020-01-01

Total Items: 1

Total Due: 0.00 USD

Accepted: Marketplace Permissions General Terms and Conditions and any applicable Publisher Terms and Conditions

TH-3269_156106040